554A

BEHAVIOR OF SINGLE PILE AND PILE GROUP IN OVERCONSOLIDATED CLAY UNDER RELATIVELY LOW FREQUENCY LOADING

By

M. W. O'Neill, G. W. Blaney, and G. L. Muster,II

December, 1982

Fugro-Gulf, Inc.

University of Houston

This report is bound in two parts. The first part contains the basic report and Appendices A and B (References and Notations). The second part contains Appendices C - G, which provide detailed documentation of the soil properties, instruments, test records, and data reduction procedure.

In some places manufacturers' names have been used to provide descriptions of instruments that are as specific as possible. This in no way constitutes an endorsement of these instruments by either Fugro-Gulf, Inc., or the University of Houston.

This report reflects the views of the authors, who are responsible for the facts and accuracy of the information contained herein. The contents do no necessarily reflect the official view of Fugro-Gulf, Inc., or the University of Houston.

Michael W. O'Neill
Geoffrey W. Blaney
Gordon L. Muster, II

December 15, 1982

TABLE OF CONTENTS

List of Figures

List of Figures (Cont'd)

List of Figures (Cont'd)

List of Figures (Cont'd)

List of Figures (Cont'd)

List of Figures (Cont'd)

List of Figures (Cont'd)

List of Figures (Cont'd)

List of Tables

List of Tables (Cont'd)

SUMMARY

Dynamic load tests were conducted on a single pile and a group of nine piles by applying quasi-harmonic vertical and horizontal loads at the level of the pile heads, which were capped. The piles were 10.75 in. (273 mm) diameter, closed-ended steel piles which penetrated 44 feet (13.4 m) below grade and which had a 0.365 in. (9.27 mm) wall. The soil was a saturated, overconsolidated clay. Prior to the dynamic tests, the single pile and pile group had been subjected to static vertical load tests, so that their behavior was well-understood. Both the piles and soil were instrumented, primarily with seismic type instrumentation.

The tests were modeled mathematically with three different types of models: (1) DRIVE and SPASM, discrete element programs that require the input of unit load transfer curves and externally estimated radiation damping; (2) PILAY/RIGDF, a program suite that uses plane strain theory to estimate linear complex stiffness functions for the soil at various elevations; and (3) KPILE, a program for simulation of horizontal motion that is similar to PILAY/RIGDF but which does not use a plane strain asssumption.

Comparisons of measurments and predictions indicated that both DRIVE (vertical response program) and PILAY/RIGDF were capable of modeling vertical behavior of the single pile under loadings that were below those that produced static failure. Damping inputs for DRIVE were reasonably accurately developed from an analysis of the pile driving data; however, empirical modifications had to be made to the static unit load transfer curves to affect a close comparison with the measurements.

Vertical behavior of the nine-pile group could not be modeled reasonably with either DRIVE or PILAY/RIGDF, apparently because wave interference produced dynamic group effects that could not be rationally replicated in the programs, which are single-pile models. On the other hand, horizontal behavior of the group was modeled reasonably well by PILAY/RIGDF, a single pile program suite, because the fundamental frequency of the group under horizontal loading was well below the frequency at which the first wave interference should appear.

Horizontal behavior of the single pile was predicted accurately below system resonance by SPASM with calculated static unit load transfer inputs. Although a very pronounced peak in deformation occurred at resonance, the magnitude of response at the peak was predicted to be too large by PILAY/RIGDF. It is speculated that PILAY/RIGDF's failure to consider radiation damping due to surface waves produced this effect.

Some degree of nonlinearity was produced in all of the tests; however, limitations on the availability of vibrating equipment, coupled with the high capacity of the piles, prevented the tests from producing significant failures in the soil.

CHAPTER 1. INTRODUCTION

PURPOSE OF THE STUDY

The study reported herein is concerned with the behavior of a full-sized driven pile and a group of full-sized driven piles in overconsolidated clay under high-amplitude and relatively low frequency dynamic loading at the heads of the piles. "Relatively low frequency" is understood to mean in the context of this report that the frequency of loading was in the range of the fundamental frequency of the pile or group and not in the range of higher harmonics. The behavior of the piles was studied both experimentally and analytically, and the experimental and analytical results were compared.

The primary purpose of the study was to determine whether typical existing mathematical models could replicate single pile or group pile behavior when the single pile or pile group was loaded harmonically at the pile head. Secondly, the effect of load amplitude and resultant soil nonlinearty was studied, primarily by experimental means. The final purpose was to provide fundamental, clearly documented data describing the response of full-sized piles to dynamic loading as a basis for testing future mathematical models.

SCOPE OF THE STUDY

Full-scale experiments were conducted on a single 10.75 in. (273 mm) diameter carbon steel pipe pile and a square-matrix (3 x 3 x 3 - diameter spacing) group of similar piles, each driven closed-ended with a flush boot plate to a depth of approximately 44 ft (13.4 m) in a deposit of very stiff, overconsolidated, saturated clay. The single pile and pile group, which was rigidly capped, had been subjected previously to static vertical (compression and uplift) tests to failure. All piles were subsequently retapped prior to beginning the present series of tests.

Both vertical and lateral harmonic loadings were applied with inertial mass vibrators attached to caps on the piles. The frequency of

the applied loads was restricted to a range of approximately 1.3 Hz to 90 Hz by the loading equipment available. The nominal load amplitudes varied from approximately 400 to 600 lb (1.78 to 2.67 kN) (lateral load on the single pile); 400 to 8,000 lb (1.78 to 35.6 kN) (vertical load on the single pile); 4,000 to 12,000 lb (17.8 to 53.4 kN) (lateral load on the group); and 4,000 to 40,000 lb (17.8 to 178 kN) (vertical load on the group). The maximum nominal applied loads (double amplitude, without load amplification factors) were about 4.5 percent of the static vertical capacity of the single pile and 2.7 percent of the static vertical capacity of the pile group. The maximum lateral load applied to the single pile produced a single amplitude displacement of approximately one inch (25 mm) at the point of load application (about 7 ft (2.1 m) above the soil surface), which was the safe limit for the vibrators. Actual loads varied considerably from nominal loads in many tests because of system compliance.

The load amplitudes employed were not sufficient to permit the soil surrounding the piles to fail, since provision of such high load amplitudes was beyond the safe range of economically available vibrating equipment. However, they were sufficient to produce measureable nonlinear effects, which were useful in assessing the mathematical models.

The range of applied frequencies in each case encompassed the primary mode resonant frequency of the pile-soil system being tested. The applied frequency values are representative of most frequency components of seismic waves on stiff soil sites and of vibratory frequencies produced by machine loadings. They are somewhat higher than the frequencies produced by water wave loadings; however, the test results should provide some insight into water wave loading response as well. The applicability of results from pile-head loading to problems of soil-induced (seismic) loading were not the objective of this study.

All tests were conducted with the pile caps suspended about 3 ft (0.9 m) above the soil surface, and the soil surface was kept flooded in order to model underwater soil response; for example, pumping of particulate matter from the gap that forms between a laterally loaded pile and the soil. The piles were instrumented with accelerometers, strain gages (vertical mode only) and slow-response (static) pore water pressure

cells in order to measure responses at the pile head and several levels below the soil surface. Soil instrumentation consisted of surface geophones (velocity transducers), subsurface geophones, and slow-response pore water pressure transducers.

During each vibration test, data were recorded in digital form for selected pile and soil instruments on magnetic tapes using exploration geophysics recording equipment. These tapes were then processed using digital signal processing techniques to arrive first at power spectral density functions for each instrument and, finally, transfer functions between applied load and instrument force or displacement over a selected range of frequencies. Such transfer functions, also referred to herein as "spectra," were also obtained from the mathematical models employed. The experimental results were compared with the analytical results by superimposing graphically the transfer functions and by observing effects obtainable from the transfer functions, such as normalized mode shape envelopes and phase.

The four major classes of mathematical models for computing the response of single piles to dynamic loading are:

1) structural analogies,
2) discrete element models,
3) continuum models, and
4) finite element models.

These models are discussed in Chapters 2 and 5.

The analytical algorithms selected for this study included one from each major class of models, except the first.

While numerical algorithms have also been developed recently to permit direct analysis of dynamic interaction of piles within groups, analysis of dynamic group pile behavior was limited in this study to the use of single pile models in which the inputs were altered to soften soil response in the manner measured or calculated for static loading, which is the present (1982) state-of-the-practice approach to dynamic modeling of pile groups.

ORGANIZATION OF REPORT

Copious amounts of data and analytical output were generated during the course of the study. Only selected representative data records could be processed within the time and budgetary constraints. The results of the analytical studies are presented in summary form and compared with the representative processed data in this report. Unprocessed data are stored on digital tapes archived at the Department of Civil Engineering of the University of Houston and can be made available to study sponsors who wish to continue the study in greater detail. Processing the tapes involves spectral analysis of the time domain digital data, statistical computations and computation and plotting of transfer functions. Future processing will require the use of the DCASS5 software package described in Chapter 5 and Appendix G of this report or a similar program. DCASS5 was written for and debugged on a VAX 11/780 digital computer and utilizes DIGICON library routines for manipulating data.

This report presents, in order, a summary description of previous analytical and experimental studies of the dynamic response of piles, a detailed description of the geotechnical conditions at the test site, a review of the pile installation and earlier static load test results, documentation of the experimental procedures, a detailed description of the analytical study to model pile behavior, presentations of the analytical and experimental results, comments, conclusions and recommendations. References, notation and supporting data are provided in Appendixes A-G. Appendixes C-G are bound separately from the main report.

CHAPTER 2. BACKGROUND

GENERAL

The principal problem of characterizing pile foundations for purposes of conducting a dynamic analysis of the superstructure is that of determining pile-head impedance functions, or stiffness and damping parameters. Impedance functions may depend on such factors as frequency, direction and amplitude of loading; genesis of the loading (structure generated, as a vibrating machine foundation, or soil generated, as during a seismic event); energy transmissibility of the soil; material hysteresis of the piles; density of the soil and piles; geometry of the piles; the presence and spacing of neighboring piles if the pile is part of a group or cluster; and stress-strain characteristics of the soil. The last factor includes material hysteresis (internal damping) and properly should account for the alterations that pile installation make of the in-situ soil properties.

Impedance functions are normally computed in four modes: axial response to axial loading, lateral deflection due to lateral force loading, rotation due to moment loading, and a cross or coupled mode relating lateral deflection to moment loading or rotation to lateral force loading. Once the impedance functions are calculated, the necessary mode shapes and natural frequencies can be obtained for the superstructure. The process may be an iterative one since pile loadings influence the computed impedance functions in a nonlinear system and because pile loadings cannot be determined until the superstructure has been analyzed.

The problem of determining impedance functions is too complex to be solved entirely by empirical methods. However, an entirely analytical approach may not be justified either in practice because it is presently not possible to account for the effects of pile installation on soil behavior. Similarly, loading may produce geometric nonlinearities (e.g., gap zone formation and soil wash-out during lateral vibration) that are difficult to model. Consequently, a dual analytical and experimental approach to solving the fundamental problem is necessary. This is the approach taken in the present study.

A brief review of the technical literature is in order to place the present study in context. The review is subdivided into experimental and analytical studies, since most prior work has involved only one aspect of the problem.

EXPERIMENTAL STUDIES

Existing Data

Experimental studies are described first since they generally precede serious analytical studies chronologically. One of the first systematic studies of foundation response to vibratory loading was reported by Tschebotarioff and Ward (92) in 1948. This study, which was primarily oriented toward prediction of the fundamental frequency of vertically loaded block-type foundations, utilized both full-scale and model test data in sand and clay, including data for pile-supported blocks foundations. Regression analysis of the experimental data led to the following simple equations to compute vertical natural frequency, f_n:

$$f_n = (p)^{-0.5} f_{nr} \qquad (2\text{-}1)$$

$$f_{nr} = (1/2\pi)(k'g/(1 + W_s/W_v))^{0.5} \qquad (2\text{-}2)$$

in which, for pile systems, p, a pressure term, is the total weight of the vibrator, pile cap (foundation block), piles, and soil between the piles divided by the total cross-sectional area of the pile system including the soil between the piles, and f_{nr} is the "reduced natural frequency." The k' term represents a modulus of subgrade reaction for the soil, g is the acceleration due to gravity, W_v is the weight of the soil presumed to be vibrating in phase with the foundation, and W_s is the weight of the vibrator, foundation block, and piles. The term f_{nr} is in units of $F^{0.5}/LT$, so that the pressure term p must be chosen in units corresponding to those used to compute f_{nr}.

The concepts proposed in Ref. 92 prevailed for many years and continue to be used by some designers even today.

Significant full-scale vertical harmonic and free vibration tests were conducted in the next two decades in conjunction with specific foundation design problems (4, 22, 46, 83). Tests described in the above references include tests in both clay and sand and include tests on groups of piles and a few free lateral vibration tests. Each had rather limited instrumentation because the principal aim of the tests was to establish values of resonant frequency and damping, which could be accomplished by measuring only the pile-head loads and displacements. Stevens (89) reviewed many of these tests and proposed a new set of simplified design equations for vertical response of single piles:

$$f_n = (1/2\pi)(k_1 k_2/m\ (k_1 + k_2))^{0.5} \tag{2-3}$$

$$\delta_{ww} = (F_o^2((k_1 + k_2)^2 + c^2\omega^2)/ \\ ((k_1 k_2 - (k_1 k_2 m\omega^2))^2 + c^2\omega^2(k_2 - m\omega^2)^2)^{0.5} \tag{2-4}$$

In the above equations k_1 = static stiffness of the embedded portion of the pile; k_2 = static stiffness of the freestanding portion of the pile = $(AE)_{pile}/L_f$, where L_f = freestanding length; m = mass of the structure vibrating in phase with the pile head; c = total damping of the system; ω = circular frequency of the applied load; δ_{ww} = axial displacement amplitude (single); f_n = natural frequency; and F_o = applied force.

Application of Eq. (2-4) to several tests involving freestanding pipe and H-piles yielded computed c values (as percentages of critical system damping) of 8 to 38 percent. The lower damping values were probably influenced by the effect of the low damping in the freestanding portion of the pile. Two other significant observations were made by Stevens: (1) progressive settlement occurred in piles in clay or sand whenever the static component of load was approximately half of the static capacity under relatively small amplitude resonant harmonic loads, and (2) the total damping ratio in a four-pile group was slightly less than that in a single pile. The latter comparison was obtained from tests in which a significant part of the piles' lengths were cased off from the soil and in which the piles were driven through stiff clay

and tipped in a very dense sand, causing them to act as end bearing piles.

More recent studies by Chon (16, 75) have indicated that friction piles in sand undergoing lateral harmonic excitation have natural frequencies and damping that increase as the pile diameter increases and natural frequencies that decrease as the static load bias is increased. The latter observation was also noted by Stevens for axial vibrations, which is evidence that the static load on a pile influences soil stiffness by creating soil stresses in the nonlinear range.

Novak and Grigg (57) and Petrovski and Jurukovski (68) observed a similar effect in large model piles and full scale piles, respectively, in sand when the magnitude of the dynamic component of load was increased.

Linear continuum models (described later) were found to yield accurate solutions in Refs. 57 and 75 for lateral excitation as long as the soil modulus was back-computed from static lateral load tests using a static elastic solid approach (e.g., 68) and static load values approximating the static bias during vibratory loading.

Reference 57 notes that the best comparisons between computed (linear continuum) and measured vertical response of piles in sand was obtained when the shear wave velocity of the soil v_s input into the model was equal to $0.7(v_s)$ measured along the pile shaft and $2(v_s)$ measured in the soil beneath the pile tip. Baka and Stokoe (5) observed good correlation for model piles in sand between measured and predicted vertical response from a linear continuum model when length-to-diameter ratios exceeded 20, in which surface wave effects not modeled by the continuum theory presumably are not important.

Group action in a 2 x 2 pile group (57) was found to be modeled adequately by setting

$$k_G = k_1/\Sigma\alpha \tag{2-5}$$

and

$$C_G = C_1/\Sigma\alpha, \tag{2-6}$$

where k and c are the stiffness and damping components of pile-head impedance, respectively; subscripts G and 1 refer to the group and the single pile, respectively; and α is a two-pile static interaction factor for the mode of (axial or fixed-head lateral) motion being considered (68). The term $\Sigma\alpha$ is the sum of all possible two-pile interaction factors considering each pile successively as the active pile divided by the number of piles in the group. Reference 4 also recommends the use of Eqs. (2-5) and (2-6) for purely vertical or horizontal motion but to use direct sums of stiffness and damping when computing rocking stiffness and damping for a pile group. This method was found to give fairly good results when compared to tests of free vertical and lateral vibrations conducted on a 2 x 2 pile group of concrete-filled step taper piles in stiff clay spaced at 3 butt diameters on centers and on single piles, where measured damping ratios were between 16 and 38 percent, and no strong trend could be observed between damping ratios in single piles and in pile groups or between horizontal and vertical modes of motion.

Novak and Howell (59) also tested single piles and a 2 x 2 group in silty fine sand under forced vibrations in torsion. Again, acceptable linear continuum solutions were obtained when v_s values back-computed from static torsion tests were used.

The susceptibility of driven piles in initially loose, saturated sand to liquefaction was studied in full-scale by Scott, et al. (84). Local liquefaction was found to occur under relatively small harmonic loads forced through resonance. System damping was observed to be approximately only 3 percent of critical, possibly due to the fact that the natural frequency of the pile was lower than the natural frequency of the sand layer.

The literature is relatively replete with reports of harmonic load tests of model piles, particularly under low amplitude lateral loading (e.g., 1, 26, 70, 71, 72, 73, 81, 95). These tests, conducted both in clay and sand, all indicate that low damping ratios can be expected in laterally loaded piles relative to those in axially loaded piles.

Valeria and Oteo (95) conducted model tests of a pile group in loose sand in which the piles were instrumented for bending moment. Long-term, low-amplitude loading of the piles at their resonant frequency caused a four-fold increase in deflection and a lowering of the point of maximum moment as compared to short-term loading.

Prevost, et al. (72, 73) have modeled the response of single piles and pile groups to lateral harmonic loading in dense and loose dry and saturated sand in a centrifuge. Nonlinear response was exhibited, as evidenced by the reduction of natural frequency as dynamic load amplitude was increased. These piles, which were also instrumented with strain gages, revealed that bending was prevalent in only the upper 30 percent of the piles, even at resonance. Damping was found to decrease with increasing soil density and to be relatively independent of frequency. However, stiffness was found to be more dependent on frequency than was predicted by linear continuum theory. The authors attributed this effect to wave reflections from the centrifuge bucket.

Additional insights into the behavior of piles under dynamic loading have been developed through observation of in-service foundations. Diaz (20) found good agreement between predictions using the linear continuum approach (without corrections for group action) and measured response for a generic compressor founded on complex groups of drilled shafts and short and long driven piling in clay stratigraphies in all modes but torsion. Comparisons were made at the operating frequency of the compressor (which produced secondary frequencies and couples), which was considerably below the fundamental frequency of the foundation in every mode.

Richart and Woods (77) have reported on the response of a pile-supported auto shredder that was undergoing considerable vibratory motion. The operating frequency of the shear hammer was four times the frequency of the shredder and coincided with the natural rocking frequency of the pile foundation. The study emphasized the need for accurate determination of exciting frequencies of all components of the loading system and consideration of all possible modes of foundation response in the design process.

Cook and Vandiver (18) have reported on the dynamic response of a large-diameter, single-pile marine structure in relatively normal sea states in normally consolidated clay soils in the Gulf of Mexico. Calculations of pile response from a dynamic finite element program required that hysteretic soil damping of about 0.6 percent of critical be used to affect good comparisons between measurements and predictions.

Response of widely spaced long pipe piles supporting a deep water marine terminal in dense silty fine sand near Honshu to far field seismic loading was recently reported by Ueda and Shirashi (94). Response was measured under seismic events ranging up to 7.4 in Richter magnitude. These investigators used a relatively simple lumped mass model, in which pile-soil interactions were represented by single linear springs and dashpots. The authors were able to compute relatively accurate superstructure response when total damping in the range of 3 to 4 percent of critical was employed.

The degradation of soils surrounding cyclically loaded piles and rate of loading effects have been considered in Refs. 7, 8 and 43. Matlock (43) has observed only minor soil degradation around laterally loaded piles in soft saturated clays below a soil stress level of approximately 72 percent of the static ultimate capacity of the soil. Similarly, Holmquist and Matlock (cited in Ref. 62) have demonstrated that significant degradation of axial pile capacity does not occur in soft clays until the applied shear stress becomes approximately equal to the shear strength of the soil, provided reversals in the direction of load do not occur. For two-way cyclic loading, only about one-half of the soil's shear strength can be sustained. While these observations were made based on model tests with slow rates of loading relative to the resonant frequency of the pile-soil system, they are consistent with Stevens' observation that near-resonant loading produces continual plunging of axially loaded piles at about half the static capacity. Bea, et al. (7, 8) have analyzed large numbers of axial and lateral load tests in which piles were subjected to transient loads at widely varying load rates. They concluded that a gain in axial or lateral capacity for piles in clay of about 10 percent per log cycle of time can be expected. Furthermore, the net effect of high loading rates and cyclic degradation

results in a soil state that produces higher dynamic than static capacities provided the cyclic load magnitude does not exceed about 70 percent of the ultimate static capacity of the pile in either mode.

Need for Further Experiments

The preceding review indicates a substantial lack of data on dynamic performance of full-scale laterally loaded piles in clay. Additionally, those full-scale and model test data that are available generally contain insufficient information to validate properly existing mathematical models.

In order to evaluate existing models, the response of piles (displacement, velocity, acceleration, or stress) to loading amplitude and frequency at several levels below the surface should be measured for comparison with predicted mode shapes. Incorrect modeling can produce fortuitously correct values of f_n and δ_{ww}, but incorrect combination of f_n, δ_{ww}, and mode shape. In-situ soil shear or Young's moduli and the variation of such moduli, as well as material damping, with depth and strain level are also desirable information. Static test records that indicate low amplitude static stiffness are also useful in investigating dynamic model performance. These data are generally missing in the literature for tests on piles in clay, and a need exists for conducting tests in which these data are available.

Data could not be found on the dynamic response of full-scale, vertically or laterally loaded groups of friction piles in clay, in which the loading conditions were controlled, and no well-documented, full-scale controlled tests on groups larger than 2 x 2 in soil of any kind were evident. Since piles are often used in groups, acquisition of further documentation on the performance of pile groups under dynamic loading seems essential in order to give insights into their behavior under seismic, vibrating machine, and wave loading.

Finally, although appreciable experimental data relating to the dynamic behavior of single, axially loaded piles in clay exists, additional data are desirable to establish a statistically significant data base.

The full-scale test program described in this report is aimed at filling the needs described above.

ANALYTICAL STUDIES

Four classes of analytical models to solve problems involving response of piles to dynamic loading can be identified. (Specifically excluded from this discussion are models for studying exclusively pile drivability, which are beyond the scope of this study.) These classes are:

1) structural analogies,
2) discrete element models,
3) continuum models, and
4) finite element models

These models are described in general terms briefly in the following sections.

Structural Analogies

Structural analogies generally involve replacement of the piles in a foundation system with springs, masses, and dashpots and conducting the solution for pile-head response using standard techniques of vibrational analysis for small numbers of degrees of freedom (14, 19, 82, 83, 87). Pile stiffness is generally evaluated from static analogies (e.g., equivalent column in the vertical mode or beam-on-elastic-foundation in the lateral mode). System damping is usually arbitrarily prescribed as a percentage of critical damping, or damping is disregarded entirely. Some algorithms allow for inclusion of an in-phase soil mass to model soil damping effects (14).

Structural analogy models are characterized by their relative simplicity and consequent attractiveness to structural designers. They are especially utilitarian for modeling structures supported on complex groups of piles (19, 83, 87). They suffer the limitations that relatively minimal soil characterization is employed, that the methods for obtaining spring and dashpot constants are not predicated on the best theoretical considerations, and that they are limited to linear response. Structural analogies will not be considered further in this report.

Discrete Element Models

Discrete element models are more fundamental than structural analogies. The pile is modeled by replacing the continuous system with a series of discrete, rigid elements with flexible connections, which properly model pile flexibility, either laterally or axially. The soil is modeled by some type of independently derived Winkler spring, located at each pile element, which may either be linear, nonlinear, or nonlinear-hysteretic. The soil spring, in some algorithms, is placed in parallel with a viscous dashpot, which simulates damping.

Several versions of the discrete element model use a coefficient of subgrade reaction approach to develop soil spring constant values (24, 65, 78). Others use elastic halfspace theory to compute uncoupled stiffness and damping constants for each element (27, 30). Nonlinearity is introduced in the model described in Ref. 30 by reducing the shear modulus of the soil based upon the mean shear strain amplitude in the soil using a procedure proposed by Hardin and Drnevich (29).

Kagawa and Kraft (35) have proposed a discrete element model for lateral response in which nonlinear soil stiffness is modeled by uncoupled lateral force-resistance curves ("p-y curves") developed from finite element modeling of seismically induced pile motion. Numerous other algorithms employ lateral soil force-resistance curves specified a-priori by the user, including pioneering techniques developed by Penzien, et al. (66) and Tucker (93). The former algorithm permits the specification of hysteretic behavior and also allows for the input of moving suports in order to simulate seismic loading. Recent algorithms are more efficient and accept more generalized soil properties than was characteristic of earlier solutions (3, 7, 40, 44, 45). At least one axial version of this model also exists (25).

Discrete element algorithms are characterized by decoupled soil stiffness behavior, radiation damping that is arbitrarily specified by prescribing external dashpot constants, and time-domain solutions when nonlinearity is involved. The latter characteristic makes most versions of this model relatively cumbersome for handling linear problems. The discrete element model also is unable to account for dynamic pile-soil-pile coupling in pile groups.

Continuum Models

Continuum models generally utilize discretization processes for piles similar to those in the discrete element models, but the soil response is represented by stiffness and damping functions determined by a more or less rigorous treatment of the soil as a vibrating medium capable of dissipating energy through radiation. Approximate or exact coupling of soil response is also employed, through which pile-soil-pile interaction maybe properly represented and solutions to group response obtained. Soil response is constrained to be linear, at present, in the continuum model, so that hysteretic damping is either neglected or prescribed arbitrarily as an external damping factor. The linearity limitation, however, permits solutions to be developed in the frequency domain, such that considerably less effort is required to obtain pile-head impedance functions than is required in the time domain discrete element solutions.

Assumptions prevalent in many algorithms include those of plane strain pile and soil motion for determining soil stiffness and damping functions and energy radiation away from the piles in horizontal layers. The plane strain assumption requires that the soil stiffness go to zero as the frequency of motion approaches zero. In practical algorithms, (e.g., 54) soil stiffness and damping for low frequencies are assumed to equal stiffness and damping at some arbitrary low frequency. References 52 and 61 provide excellent overviews of the continuum model.

Some continuum algorithms (e.g., 15, 95) utilize a static Mindlin equation solution (68) to develop soil stiffness and add in-phase soil mass to the masses of the pile elements and additional arbitrarily specified damping. This approach, while rigorously invalid for dynamic loading, circumvents the need for plane strain assumptions and can be extended to the prediction of group behavior.

Novak and his associates developed the first continuum solutions for single piles in homogeneous and layered elastic media (50, 51, 54) for harmonic, aseismic axial and lateral loading at the pile head. These solutions were extended to permit a stepwise decrease in elastic moduli with increasing radial distance from the pile (60), and to torsional loading (58, 59), including inferences for torsional response

in pile groups. Ettouney and Janover (23) have recently extended the continuum solution to battered piles and have found that the effects of battering are most pronounced at low frequencies.

Explicit modeling of groups of piles under dynamic pile-head loading, considering pile-soil-pile interaction, is a recent endeavor. Prior to the late 1970's, the prevailing practice was to compute the impedance functions for single piles, to sum these functions over the various piles, and to then reduce the resulting sum by applying static interaction or "softening" factors (4, 50), as suggested in Eqs. (2-5) and (2-6). Investigation of the practice described here was a subject of the experimental and analytical studies for this research project. Recent analytical studies, described subsequently, indicate that this approach may be erroneous in ideal materials and for geometrically perfect groups.

Continuum group models include "dynamic Mindlin" solutions (17) and procedures that extend the horizontally propagating wave solution into the group domain (36, 47, 48, 86, 98). The latter solution is highly efficient for concentric circular pile groups of the type used by the offshore oil and gas industry.

Finite Element Models

A number of studies have been conducted in which the dynamic response of piles has been simulated using the finite element method. Blaney, et al. (13) produced solutions for lateral frequency dependent impedance functions that were analytically consistent for frequencies down to zero. The model used was one in which the pile was modeled by rigid links to produce the proper shear stiffness and in which the far field soil response was modeled by a boundary integral method.

Kagawa and Kraft (32, 33, 34) have used an equivalent linear finite element solution to determine nonlinear dynamic p-y curves for later discrete element analysis. Kagawa and Kraft concluded that, in long piles, as the ratio of pile stiffness to soil stiffness increases, the effective soil subgrade modulus approaches its static value. Good agreement between finite element and simplified models using dynamic p-y curves under seismic excitation were observed.

Angelides and Roesset (2) and Dobry, et al. (21) have used the finite element method to study the fundamental properties of laterally vibrating pile-soil systems. Kuhlemeyer (37, 38, 39) has developed conclusions similar to Blaney, et al., that plane strain continuum modeling does not produce correct impedance functions at low frequencies but that the impedance function values below a dimensionless frequency, a_0 (defined later), of 0.3 can be reasonably approximated by those computed for $a_0 = 0.3$. A complete, approximate solution for vertical pile-head displacements of single piles in a linear elastic soil medium is given in terms of a_0, pile length-to-radius ratio, and mass ratio in Ref. 39. That reference also discusses approximate use of the solution in pile groups.

Wolf and Von Arx (100, 101) have used the finite element method directly in the analysis of group behavior in both vertical and battered piles. Results of their study are given later in this report.

Effects of Pile Cap Embedment

The preceding discussion has applied only to groups of freestanding piles, in which the pile cap, or substructure connecting the piles to the superstructure, is not in contact with the soil. When the cap contacts the soil, conventional practice (4) is to treat the cap as a buried or partially buried footing, to determine footing stiffness and damping from continuum or finite element solutions, and to add such stiffness and damping to the values computed for the piles. Solutions for footing stiffness may be found in several references, including Refs. 10 and 97 (horizontal and rocking motion), 56 (vertical motion) and 96 (torsion).

Discussion of Basic Phenomena

Most of the basic soil dynamics text books in use today (e.g., 6, 69, 76, 102) contain very little material pertaining to the response of piles. Simplified analytical schemes are given in Refs. 69 and 76, but these schemes largely exclude the results of analytical modeling reviewed in the previous sections. The analytical solutions are simply too recent to have found their way into classroom texts. However, excellent cohesive overviews of the state-of-the-art in the dynamic

behavior of piles can be found in Refs. 3, 61, 74, 79, 80 and 99. These overviews conclude in general that radiation damping is high in the vertical mode and low in the horizontal (coupled sliding and rocking) and torsional modes, as is the case for footings. Continuum models that use plane strain soil reactions are accurate for small displacements, especially in the vertical mode, as the assumption of horizontal energy propagation and omission of surface wave phenomena seem to be relatively satisfactory.

Single Piles. At least four recent studies (2, 21, 32, 49) have focused on the possible compatibility of continuum and finite-element-type solutions and discrete element solutions for single laterally loaded piles. Nogami and Novak (49) determined that the Winkler assumption that is characteristic of the discrete element model yields reasonably accurate solutions only when the forcing frequency is much greater than (at least twice) the natural frequency of the pile-soil system in elastic soils. Otherwise, significant coupling occurs in the soil.

Dobry, et al. (21), in comparing linear finite element and subgrade reaction (discrete element) solutions, determined that in long piles, $[(L/D)(E_p/E_s)^{-0.25} > 5]$ displacement response varies little with frequency at above twice the natural frequency of the pile-soil system, implying that discrete element solutions might be valid for that case. For $(L/D)(E_p/E_s)^{-0.25} < 5$ (short piles) the displacement response is frequency dependent at all frequencies. Results were found to be relatively independent of the Poisson's ratio of the soil.

Angelides and Roesset (2) have noted that the continuum and finite element models fail to replicate gaps that form between a laterally loaded pile and the soil but that discrete element models can do so. Existing discrete element models can also consider displacement-dependent stiffness and hysteresis (material nonlinearity) but the stiffness and hystersis functions are derived from static tests, or are estimated. Angelides and Roesset used the soil element model of Blaney, et al. (13), incorporating an iterative linearization technique to model nonlinear soil behavior, where the constitutive properties of the soil elements were established using a realistic soil profile. The same soil data were used to establish nonlinear p-y curves (43), and the

finite element and discrete element solutions were compared at low frequency loading. Higher soil stiffness was obtained in the finite element model, which was attributed principally to gapping that was modeled in the discrete element model but not in the finite element model. The nonlinear finite element solution also showed that radiation damping and stiffness typically decrease with increasing pile-head force level, but that the damping ratio (defined as $c_{uu}/2k_{uu}$) increases with increasing pile-head force as a net effect of increasing hysteretic damping and decreasing radiation damping.

Kagawa and Kraft (32) showed that the discrete element solution and finite element solution for single piles excited by motion at the base of the pile agreed well as long as the p-y curves contained dynamic modification effects (34) and loading was restricted to amplitudes that do not produce gapping between the pile and soil.

Group Piles. At this point some elaboration on the dynamic response of groups of round piles is in order, since the phenomenon of dynamic interaction of piles within a group is of concern. Only the response of vertically oriented piles will be considered here.

In the vertical mode of loading Nogami (47, 48) has obtained linear continuum solutions for both rigid and flexible piles in uniform soils and soils in which the shear modulus increases parabolically with depth. Rigid pile solutions in homogeneous soils are summarized in Fig. 2.1, in which the real and imaginary components of complex stiffness for small groups for two spacings are divided by their respective components for single piles. Complex stiffness K* is defined by Eqs. (2-7) and 2-8):

$$F(t) = K^*\delta(t) \tag{2-7}$$

$$K^* = k_r + ik_i \tag{2-8}$$

F is the exciting harmonic pile-head force amplitude, δ is pile-head displacement amplitude, i is $(-1)^{0.5}$; and k_r and k_i are the real (Re) and imaginary (Im) components of the complex stiffness, respectively. The real component is most strongly associated with stiffness and the imaginary component is most strongly associated with damping.

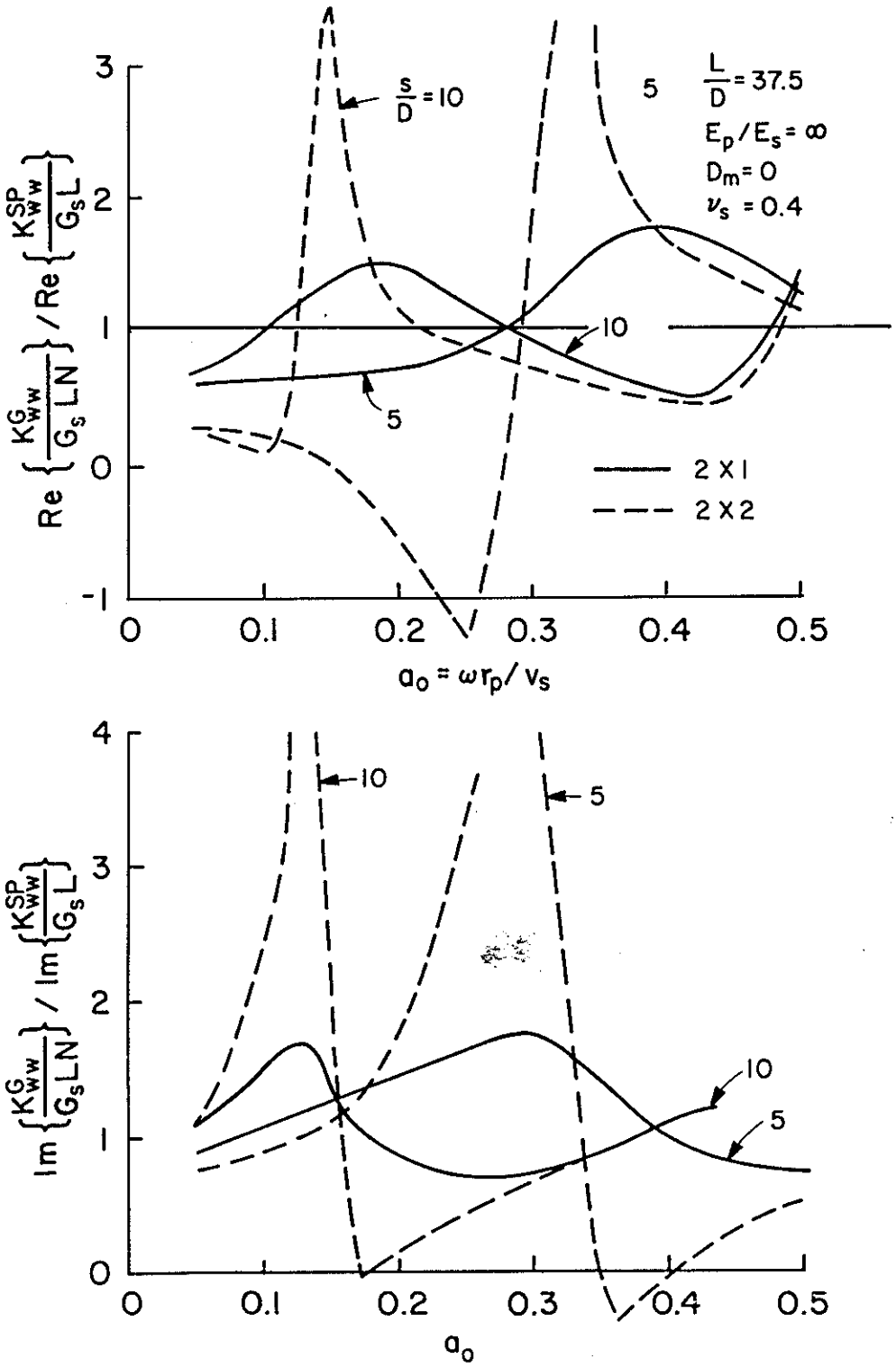

Fig. 2.1. Complex Stiffness and Damping Functions for Rigid-Pile Groups (48).

In Fig. 2.1 complex stiffness has been normalized by the product of soil shear modulus (G_S), pile length (L), and number of piles (N). The superscript G refers to "group," SP refers to "single pile" and the subscript ww refers to uncoupled axial behavior. Group stiffness is either greater or less than that for a single pile, depending on the S (pile spacing) to diameter (D) ratio, N, and forcing frequency, which is described in dimensionless form in Fig. 2.1, where r_p = pile radius, and v_S = shear wave velocity of the soil. Note that r_p/v_S is the time required for a soil shear wave to travel a distance equal to the pile radius. Material damping for the pile and soil is zero for this case.

$Re(K^G)$ (i.e., group stiffness) increases when the imposed pile motion is out of phase with shear waves arriving from neighboring piles and decreases when the two motions are in phase. In the 2-pile group at S = 10 D antiphase motion occurs at $a_0 \approx 0.20$ and in-phase motion occurs at $a_0 \approx 0.40$. When the spacing is reduced to 5D, the first anitphase peak occurs at $a_0 \approx 0.40$.

$I_m(K^G)$ (i.e., group damping) is more complicated than stiffness. In general, damping peaks and troughs lead corresponsding stiffness peaks and troughs by $a_0 \approx 0.1$. Figure 2.1 does not include the effects of hysteretic damping in the soil or the piles, which may be significant for widely spaced piles.

Stiffness and damping in the larger (2 x 2) group are seen to vary more significantly with a_0 than they do in a simple 2 x 1 group. This behavior is due to the superposition effects that occur as a result of shear waves produced by several piles influencing a given pile.

Figure 2.2 shows a similar solution by Nogami (48), but in which pile flexibility, material damping (5 percent of critical), and soil nonhomogeneity in the form of a parabolically increasing shear modulus are considered. Figure 2.2 is specific to a loose sand or normally consolidated clay soil profile and to the specified pile stiffness and geometry. The results are displayed in terms of the pile-head impedance functions k and c, directly, where G_S and v_S are taken as average values along the embedment depth of the piles. Note that $k_{ww} = k_r$ and $c_{ww} = k_i/2ik_{ww}$ in Eq. (2.8).

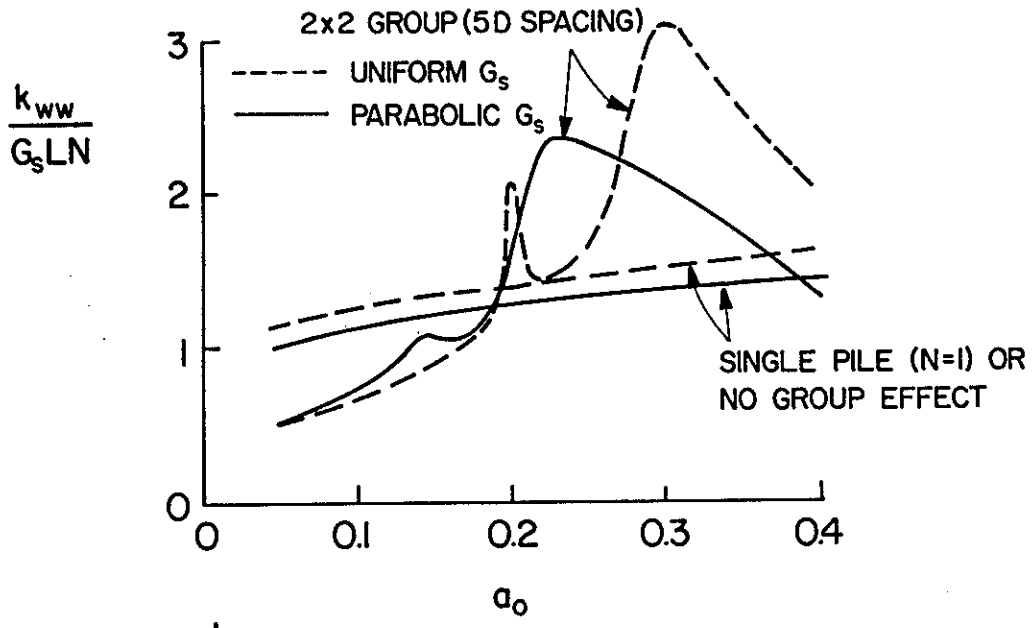

$\frac{L}{D}$ = 25 E_p = 5000 KSI ν_s = 0.4 D_n = 0.05

G_s = 30,000 (100z) 0.5 psf (Z = depth)

COMPLEX STIFFNESS AND a_o USE MEAN G_s AS REFERENCE VALUES

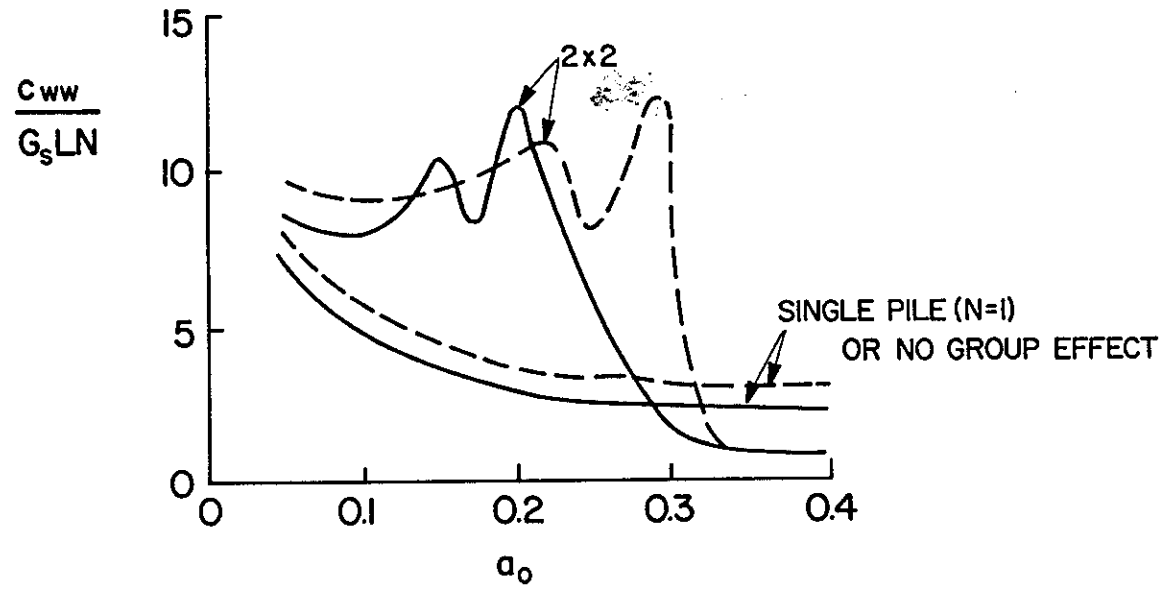

Fig. 2.2. Complex Stiffness and Damping Functions for Flexible-Pile Groups (48) (1 lb = 4.45 N; 1 K = 4.45 kN; 1 ft = 0.305 m).

Pile flexibility affects the group behavior somewhat, most notably in the presence of initial peaks in the stiffness functions, which represent the first antiphase interference of diagonal piles. The second peak, which is more pronounced than the first, represents interference in adjacent piles and occurs at $a_o \approx (2)^{0.5}$ times the value of a_o corresponding to the diagonal pile interference. Diagonal pile interference does not appear in the solution for rigid piles. Nogami also obtained solutions for 4 x 4 square matrix groups of flexible piles and found that the first peak becomes more pronounced and shifts downward in frequency (by $a_o \approx 0.04$) from that shown in Fig. 2.2, as more piles at wider spacings become involved. The effect of soil nonhomogeneity is also to produce downshifts in stiffness and damping peaks.

Sheta and Novak (86) have modeled the soil surrounding each individual pile in the group as being radially (as well as vertically) inhomogeneous. The presence of a weakened zone around individual piles, in which the modulus of the weakened soil is 0.2 to 0.5 times that of the undisturbed soil and the radial thickness of the weakened zone is one pile radius, increases both stiffness and damping in 2-pile groups spaced closer than about 10 D. The increase in stiffness over radially homogeneous soil is slight (10 percent or less) for friction piles, while the increase in radiation damping is up to 100 percent. This observation leads to the general conclusion that, if pile installation results in weakened zones around piles, that the displacements in a small, vertically loaded group would likely be less dependent on the frequency of the applied load than suggested by Figs. 2.1 and 2.2, which assume the soil to be radially homogeneous.

Kaynia and Kausel (36) have recently demonstrated that the analysis of dynamic response of pile gorups can be treated by using a superposition technique analogous to that proposed by Poulos (68) for statically loaded piles. In any mode of loading (vertical, horizontal translation, rotation about a horizontal pile-head axis, and horizontal translational-rotational coupling), dynamic interaction between two generic piles, i and j, can be determined in principle from Eq. (2-9):

$$\delta_j = I_{\delta i}(a_o = 0) \qquad (2\text{-}9)$$

where δ_j is the dynamic displacement of the head of Pile j, δ_i ($a_o = 0$) is the static displacement of the head of Pile i under the amplitude of dynamic load applied to the pile head, P_o, and I is a complex interaction factor that depends on a_o, relative soil-pile stiffness (E_s/E_p), L/D, and S/D. If the impedance functions for a single, isolated pile, k and c, are known, then P_o can be calculated from Eq. (2-10) (76):

$$P_o = \frac{F_o\ (k^2 + c^2\omega^2)^{0.5}}{((k - m\omega^2)^2 + c^2\omega^2)^{0.5}} \qquad (2\text{-}10)$$

where F_o is the amplitude of the harmonic load assumed to exist on one pile and m is the mass supported by one pile.

Interaction factors, I_{wzFz}, for vertical motion in a linear homogeneous soil are given in Fig. 2.3 for a particular set of parameters. The equation given below the figure summarizes the calculation of dynamic vertical displacement amplitude of one pile in a group when that pile and all neighboring piles are subjected to a unit dynamic force F_o at the pile heads. That equation could be used directly to predict the displacement response spectra in the various piles of a flexibly capped group in which the loads are equally distributed to the piles and may be used, along with appropriate boundary conditions, to fourmulate the displacment response spectrum for a rigidly capped group. The applicability of interaction factors to pile systems with properties other than those shown is uncertain.

Kaynia and Kausel also found that radiation damping generally increases with foundation size. They developed interaction factors for the other loading modes that have not been reproduced here.

One of the studies most clearly defining lateral group effects is that of Wolf and Von Arx (101). A particular solution, in which two-pile soil response functions were developed from finite element solutions using toroidal elements with a circumferential Fourier expansion, is shown for a rigidly capped group in Fig. 2.4. The soil is a homogeneous, linear viscoelastic medium, and coupling between vertical and horizontal motion is included.

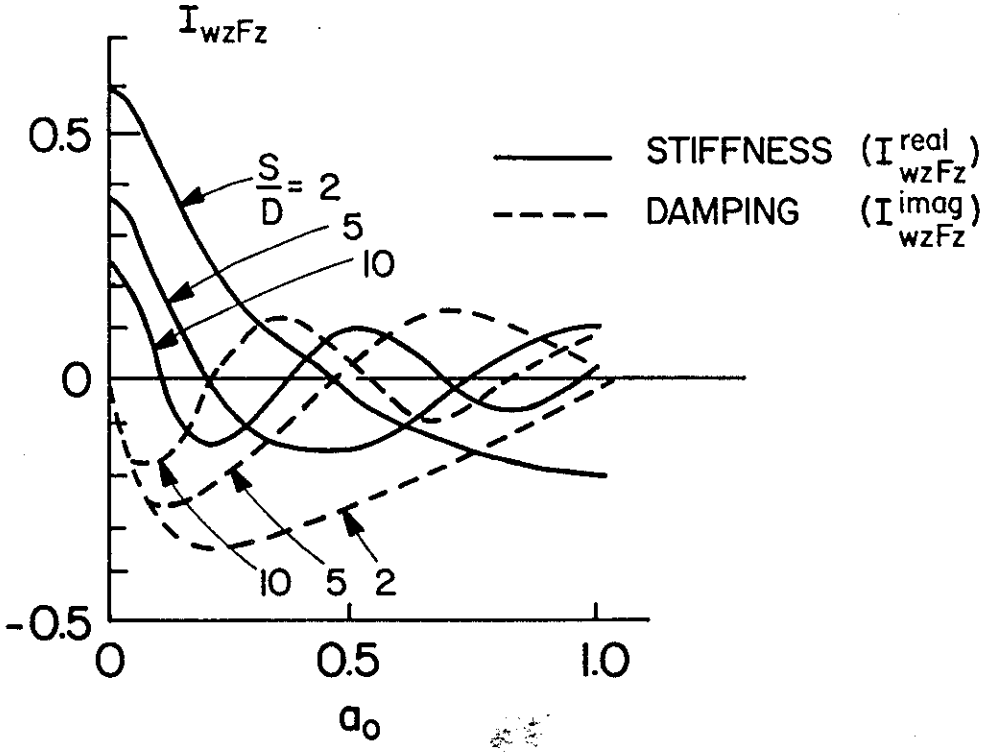

$$\delta^{l}_{wj} = (k + ia_o c)^{l}_{j} + \sum_{\substack{i=1 \\ i \neq j}}^{N} (I^{real}_{wzFz,i} + ia_o I^{imag}_{wzFz,i})\, \delta_{wi} \quad (a_o = 0)$$

EQUAL UNIT LOADS ON PILES 1-N

$\frac{L}{D}$ = 15 ; ρ_s/ρ_p = 0.7 ; $E_s/E_p = 10^{-3}$ (uniform soil)

Fig. 2.3. Dynamic Interaction Factors for Vertical Loading (36).

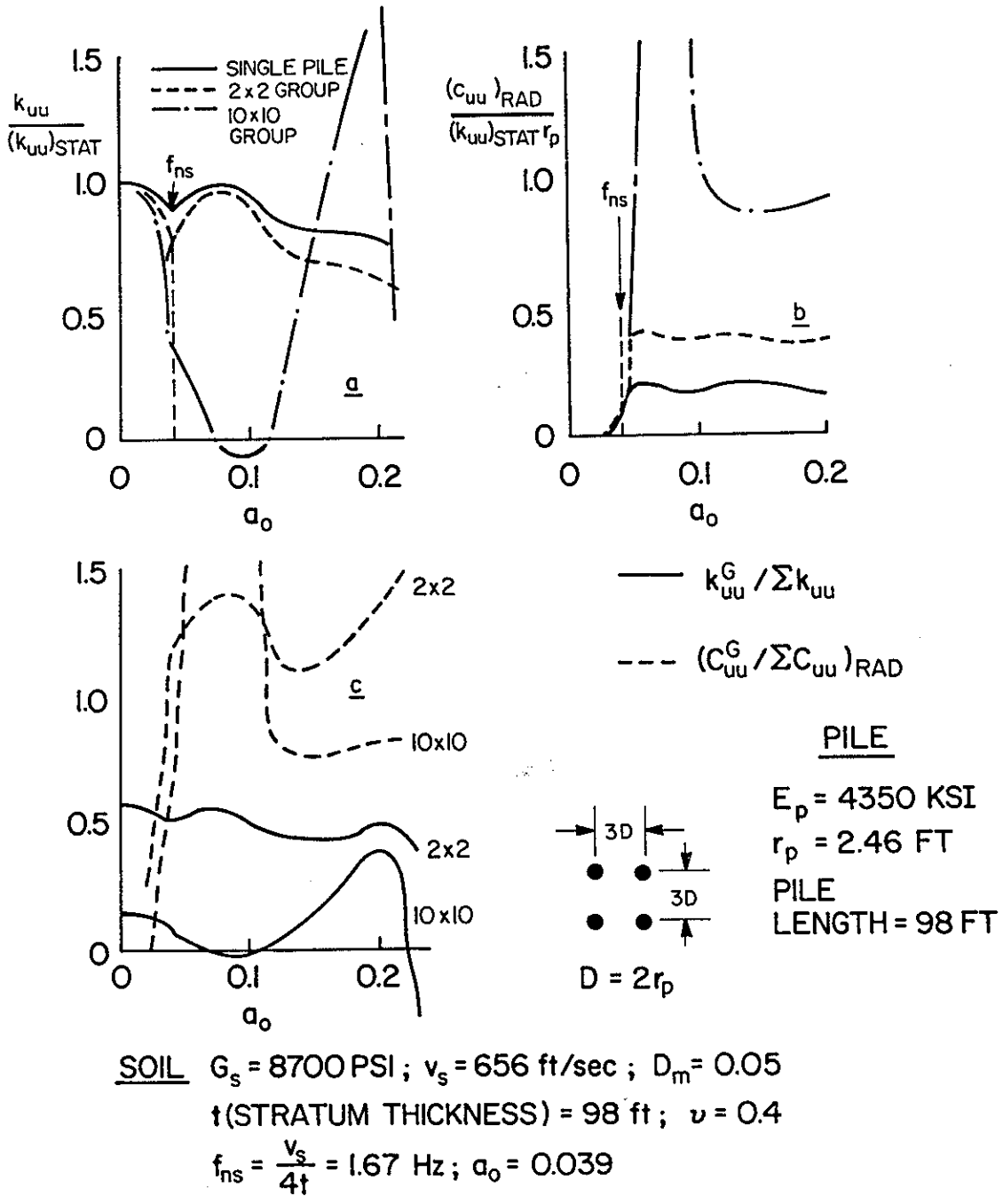

Fig. 2.4. Complex Stiffness and Damping Functions for a Laterally Loaded Flexible-Pile Group (101) (1 ft = 0.305 m; 1 in. = 25.4 mm; 1 k = 4.45 kN).

Figure 2.4, which includes effects of pile flexibility and material damping D_m = 5%, indicates that up to a frequency equal to about one-half of the natural shear frequency, f_{ns}, of the soil layer in which the piles are embedded, horizontal stiffness k_{uu} is approximately constant, and that radiation damping $(c_{uu})_{rad}$ is approximately zero. The latter effect was also noted by Dobry, et al. (21). This approximation is seen to be less valid as the size of the group increases. Large variations in stiffness and damping occurred near f (= $\omega/2\pi$) = f_{ns}; however, above f ≈ 3 f_{ns} horizontal stiffness and damping become more nearly constant for square groups up to 10 x 10 in size.

For a 2 x 2 group, group stiffness was found to be about 0.5 times the sum of single pile stiffnesses between a_o = 0 and a_o = 0.2, while the ratio of group damping to single pile damping increased rapidly until f ≈ f_{ns} and continued to increase, but more slowly beyond that. In any event, absolute group damping remains low below f = f_{ns}. For large groups (e.g., 10 x 10), k and c are more variable because of multiple wave interferences. The negative stiffnesses at a_o = 0.09 and 0.23 in Fig. 2.4c are due to in-phase soil-pile effects.

Wolf and Von Arx found little difference in dynamic group effects for both horizontal and vertical loading based on the pile material type (mass density and elastic modulus effects); however, slightly less group effect was evidenced for steel piles in the vertical mode than for more flexible concrete or timber piles.

In summary, the various analytical techniques predict strong frequency dependence of the group impedence functions, with increasing complexity as numbers of piles increase. Somewhat less frequency dependence occurs in small groups in the horizontal loading mode than occurs in the vertical mode. This observation suggests that single pile discrete element solutions cannot be rigorously used in general along with static interaction factors to compute the response of a group pile. However, it may be possible to compute the approximate response in this fashion for small groups of laterally loaded pile groups at relatively low frequencies and for vertically loaded pile groups on a site specific basis.

STRATEGY FOR PRESENT PROJECT

The state-of-the-art in the mathematical modeling of piles and pile groups under harmonic loading has advanced significantly in recent years, as evidenced by the preceding literature review. Relatively less research has been performed on full-scale piles in real geological materials, however. Inadequate full-scale data exist to permit assessment of the mathematical models under in-service conditions. Questions concerning effects that are difficult to model, including pile-soil gap formation and cyclic soil degradation, stiffness and damping nonlinearities produced by loading the piles, initial spatial variations of soil modulus within the soil mass for single piles and pile groups produced by inserting the piles, and surface wave efects, among others, cannot be answered without conducting well-controlled field tests.

This study's objective was to gain insight into the dynamic response of a full-scale pile and pile group by conducting such tests in overconsolidated clay. Soil properties, loading conditions, pile geometry, and pile and soil response to loading were thorougly documented. Harmonic pile-head loadings were applied in the horizontal and vertical directions under realistic conditions (e.g., combined shear and moment at the pile head for the horizontal case) on both a single pile and a rigidly capped pile group of representative size installed by standard driving procedures. No attempt was made to obtain perfect geometry (perfectly vertical piles and exactly equal spacings in the group).

Both pile systems had been subjected to static vertical load tests to failure prior to the dynamic testing program, so that relations between static capacity and stiffness and dynamic load amplitudes and stiffness are known in the vertical mode. In addition, a post-vibration static horizontal load test was conducted on the single pile in order to assess static stiffness.

Dynamic loads were applied at increasing, then decreasing, magnitudes in an attempt to produce nonlinear response and to assess whether any permanent degradation had occurred in the soil. Loading was provided by hydraulic inertial mass or rotating mass vibrators under relatively constant programmed force amplitude conditions. (Actual forces

varied considerably with frequency, as described subsequently.) The standard method of loading was through 30 second sweeps from a high frequency to a low frequency in order to permit observation of resonance peaks in the response. About 750 total cycles of load were applied for each vertical sweep and 300 for each horizontal sweep. Discrete frequency tests were also run to establish whether any differences could be observed between the sweep response and response at a constant frequency. Constant, discrete frequency tests were also 30 seconds in length and contained the same order of magnitude of loading cycles as the sweeps. The number of load repetitions chosen to be applied during each test (sweep or discrete frequency) is representative of the order of magnitude of the number of load cycles that might occur under seismic loading or storm wave loading but is not representative of long-term vibrating machine loadings.

Soil response was also monitored in order to develop insights into wave propagation in a real soil system where the waves are produced by loading the piles. Wave propagation effects were thought by the authors to influence pile-soil-pile interaction in very large groups in a significantly different manner than is predicted by theory due to the "ground roll" or low-pass frequency soil filtering phenomenon.

State-of-the-art analytical algorithms were used to model the experimental results. Analytical results were forced to match experimental results as closely as feasible, considering the budgetary resources for the study by varying the inputs in order to infer appropriate ranges of input paramenters and their deviations form theoretical values in overconsolidated clay. Two algorithms from the discrete element class and one each from the continuum and finite element classes were selected for modeling measured behavior. Each of the algorithms is an explicit single pile model, but the discrete element and continuum models were also modified (either through input or output) to reflect softening of soil response under static group loading or, arbitrarily in some cases, stiffening of single pile response to reflect actual measurements.

CHAPTER 3.

GEOTECHNICAL INFORMATION

Site Location

The site of the full-scale dynamic load tests was located on the campus of the University of Houston, which is situated approximately two miles southeast of the intersection of I 45 and US 59 in Houston, Texas. See Fig. 3.1. More specifically, it was at the immediate east end of a campus building known as the Band Annex. Topographically, the site is essentially flat.

Geologically, the site is situated on a series of conformable Pleistocene-aged, transported terrace deposits. The uppermost of these deposits, known locally as the Beaumont formation, extends from the surface to a depth of about 26 ft (8 m). The soils of the Beaumont formation were deposited in fresh water during the Peorian Interglacial Stage and preconsolidated by desiccation as the nearby sea withdrew during the Late Wisconsin Ice Age. The Beaumont soils classify as CH according to the Unified Soil Classification System. They contain a network of variable, closely spaced, discontinuous fissures and slickensides, particularly below a depth of 12 ft (3.7 m).

The deposit encountered below a depth of 26 ft (8 m) is the Montgomery formation, an older transported Pleistocene soil that was deposited and preconsolidated in a manner similar to the Beaumont formation. The Montgomery formation is basically a CL which extends to a depth of at least 250 ft (76 m) at the test site. It contains fewer fissures and slickensides than the Beaumont formation but contains numerous silt and sand seams, layers, and lenses. Rock is not present within at least 600 ft (180 m) of the surface.

The average total unit weights of the Beaumont and Montgomery soils are 126 pcf (19.8 kN/m^3) and 133 pcf (20.9 kN/m^3), respectively.

The water table at the test site is situated about 7.5 ft (2.3 m) below grade, as measured by pneumatic piezometers situated between the surface and a depth of 50 ft (15.3 m). Below that depth, however, a gradual decline in piezometric elevation is normally experienced in

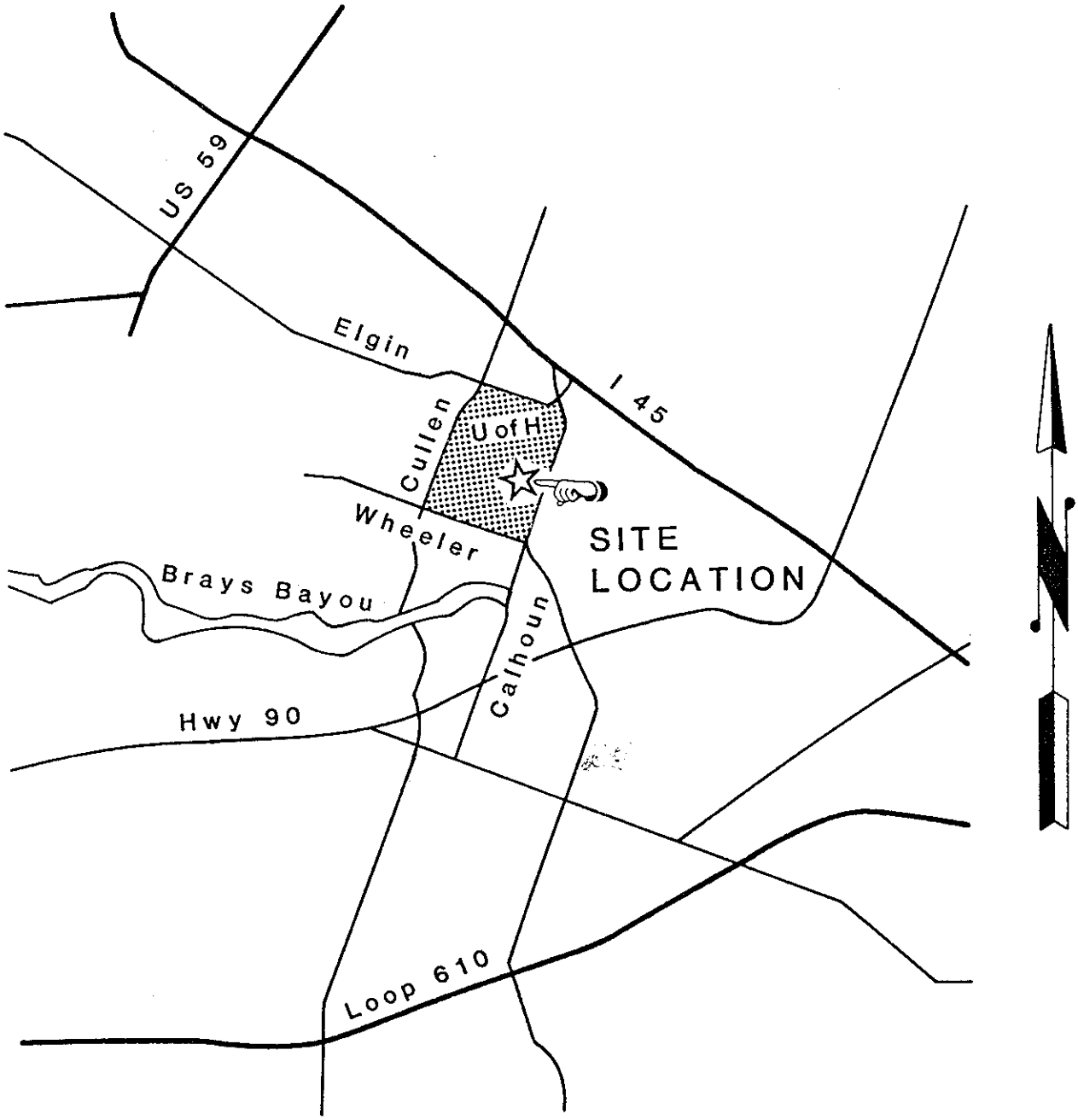

Fig. 3.1. Test Site Location.

Houston. Typical measurements taken in a sand layer at a depth of 115 ft (35 m) indicate a piezometric elevation 15 to 20 ft (4.6 to 6.1 m) below surface grade, suggesting a downward percolation of groundwater.

Site Investigation Plan

Much of the site investigation was carried out in conjunction with site characterization for the static load tests, which preceded this study. Details of that investigation are contained in Appendix C and elsewhere (41, 42). Only summaries are given in this chapter. In-situ and laboratory procedures for the earlier study included the following tests:

1. Standard penetration (SPT)
2. Quasi-static cone penetration (CPT)
3. Cross-hole (shear and compression wave)
4. Self-boring presuremeter (SBP)
5. UU triaxial
6. Normalized triaxial (42)
7. Consolidation
8. Classification

Samples for the laboratory tests (Nos. 5-8) were taken with 2.9 in. (74 mm) i.d. thin-walled sampling tubes. They remained sealed in the tubes until just prior to testing, at which time they were extruded. In-situ tests and soil sampling were accomplished in January - April, 1979, prior to the static tests.

During the present study additional thin-walled tube samples were taken, and low and high amplitude resonant column tests were conducted. A deep boring was also made and logged electronically in order to observe possible reflective interfaces in the soil mass. Field operation for these investigations were conducted in September - December, 1980, following the static tests and prior to the dynamic tests.

The locations of the in-situ tests and sample boring locations are shown in Fig. 3.2, which also indicates the location of the 9-pile test group, the single test pile and steel casings that had been placed on the site for purposes of constructing deep anchors for the static tests (63). These casings, shown in profile in Fig. 3.3 were steel, 4 ft (1.22 m) in outside diameter, and 0.5 in. (12.7 mm) thick. They were

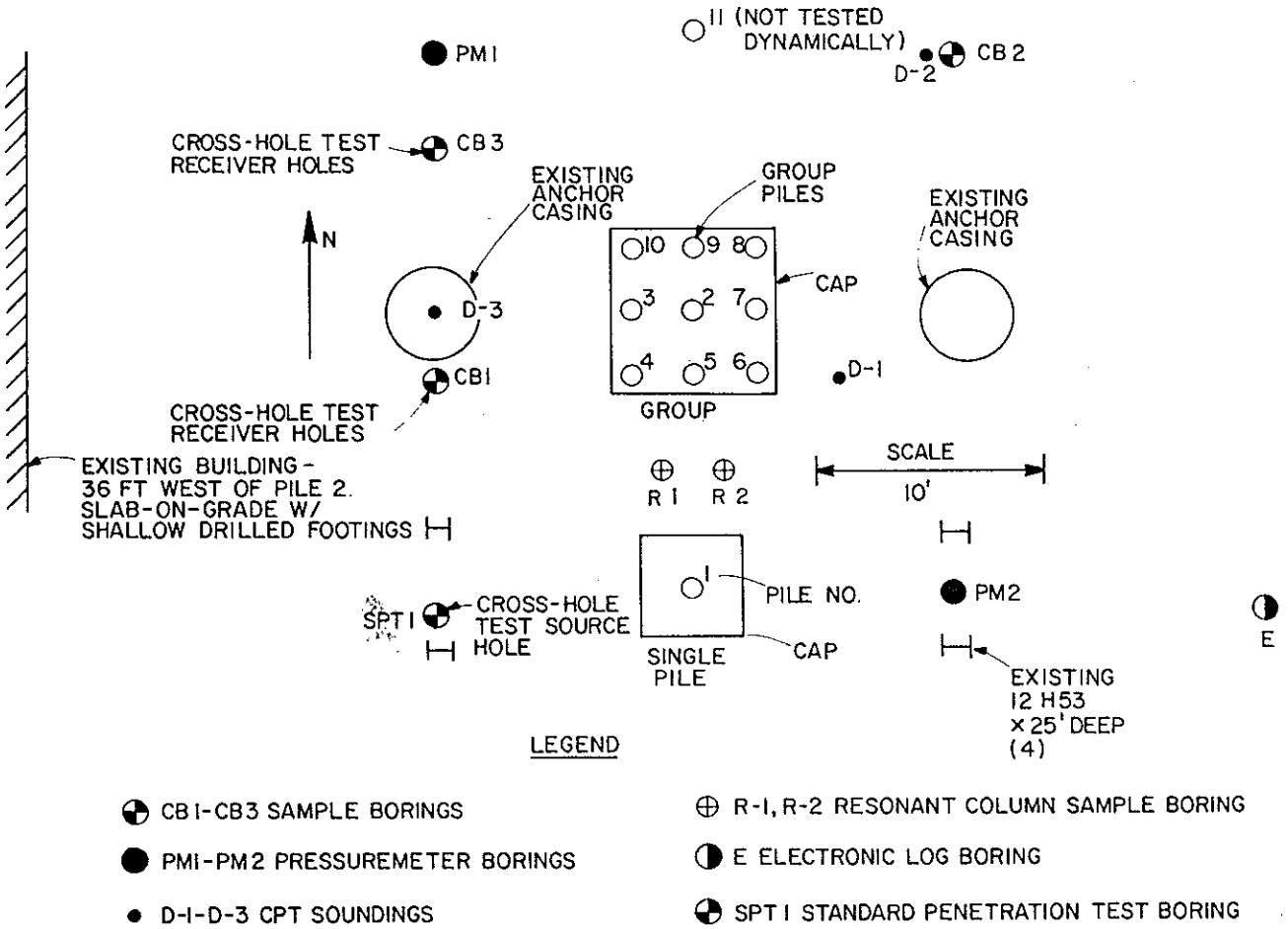

Fig. 3.2. Soil Boring and Test Locations (1 ft = 0.305 m).

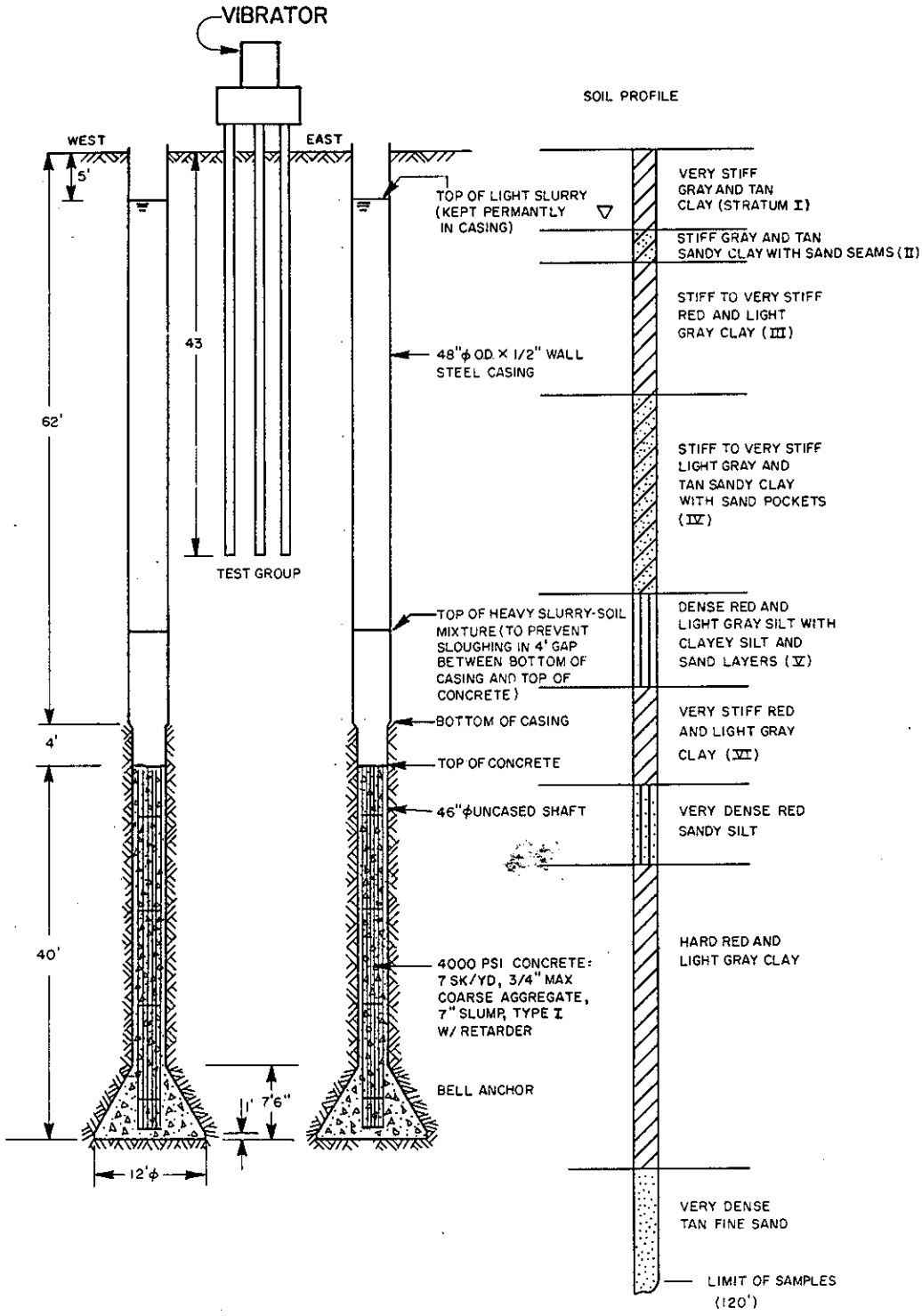

Fig. 3.3. Elevation View of Pile Group and Static Anchor Casings (1 ft = 0.305 m; 1 in. = 25.4 mm).

empty of soil to a depth of 66 ft (20 m) but were essentially full of natural groundwater. The concrete anchors for the static tests were present from 66 to about 106 ft (20 to 32 m) below grade.

General Soil Profile

The near-surface soil profile at the test site is shown in Fig. 3.3. The strata marked I, II, and III are in the Beaumont formation, while those marked IV, V, and VI and those that are unmarked are in the Montgomery formation. Figure 3.4 presents the results of the deep resistivity (resistance) and spontaneous potential logs and interpretations. Several possible reflective/refractive interfaces are noted, but in general gradation between layers occurs gradually so that strong energy returns are not expected.

Table 3.1 summarizes classification test results to a depth of 90 ft (27.5 m), and Fig. 3.5 is provided to give a general indication of soil consistency. The low SPT value at 30 ft (9.1 m) is due to the presence of a weathered very silty clay zone at the surface of Stratum IV of the Montgomery formation. The high SPT value at 39 ft (11.9 m) is due to a very sandy clay lense. Otherwise, the soil can be seen to become stronger with depth in an approximately linear manner.

A typical boring log, detailed dry unit weights and moisture contents, and void ratios are given in Appendix C.

Geotechnical Test Results

Profiles of indicated CPT tip and sleeve resistance from a Fugro-type cone are given in Fig. 3.6, and a summary plot of undrained shear strength profiles from several test methods is given in Fig. 3.7. Reference 42 presents an analysis of the differences in the indicated shear strengths. The SBP and CPT (N_C = 10) gave undrained shear strength values that were consistently higher than the UU or normalized triaxial compression tests, probably because of partial drainage. It is the authors' opinion that the profile indicated by the UU triaxial tests is most representative of the in-situ shear strength in the Beaumont formation, and the normalized triaxial profile is most representative of the shear strength in the Montgomery formation. In the latter tests, samples were consolidated isotropically until a state of normal

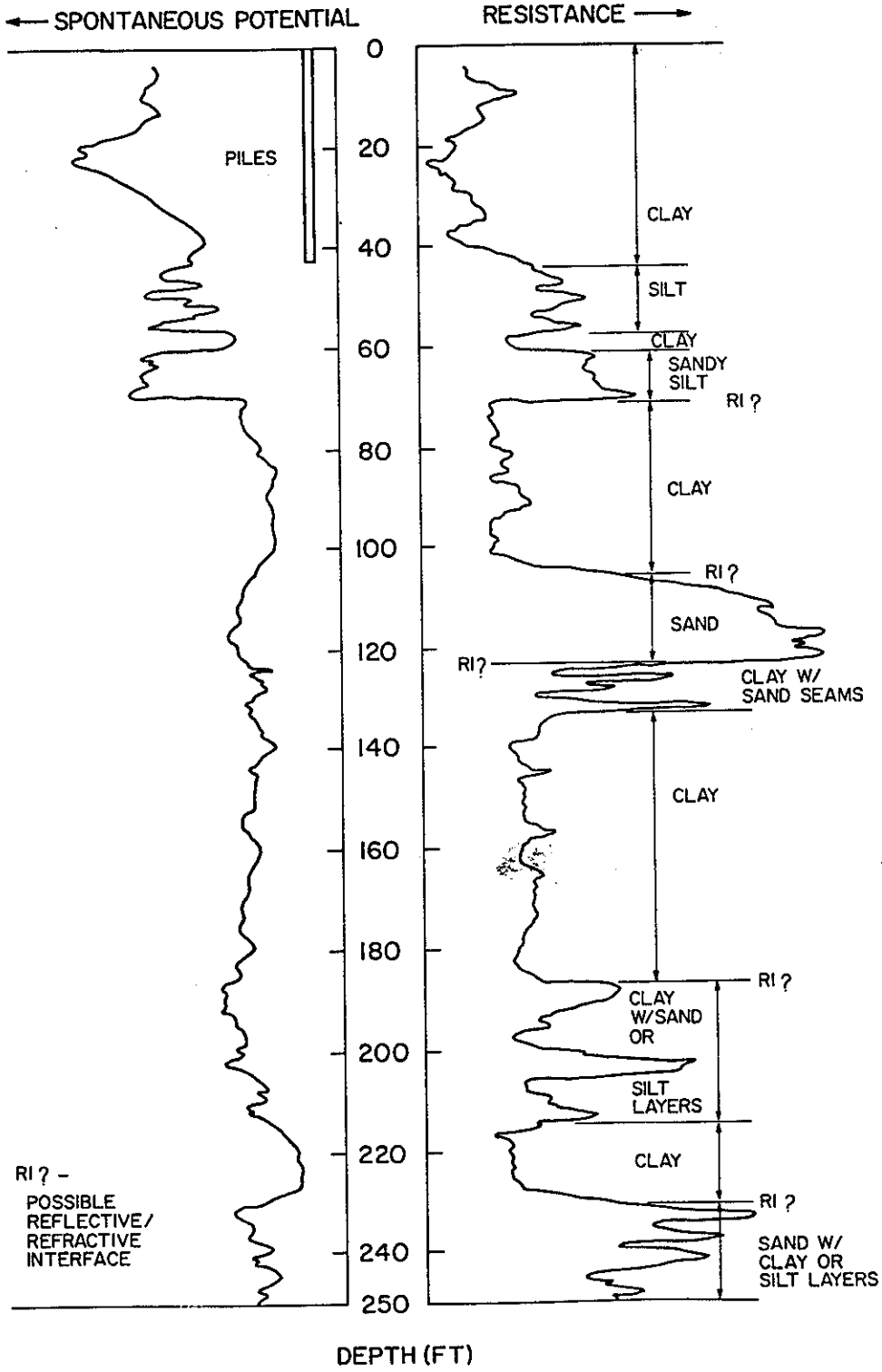

Fig. 3.4. Relative Resistivity/Spontaneous Potential Log (1 ft = 0.305 m).

Table 3.1. Summary of Index Property Tests (1 ft = 0.305 m)

Sample Interval (ft)	% Passing #200 Sieve	Specific Gravity	Liquid Limit (%)	Plastic Limit (%)	Plasticity Index (%)
0 - 2			34	13	21
2 - 4			43	13	30
4 - 6			53	15	38
6 - 8			51	15	36
			56	12	44
8 - 10		2.70			
		2.63			
		2.58			
10 - 12	63.0		35	14	21
12 - 14			52	17	35
			62	16	46
14 - 16			74	19	55
16 - 18	99.0				
18 - 20		2.67	69	26	43
20 - 22			66	26	40
22 - 24		2.72	65	25	40
			69	25	44
24 - 26			69	19	50
26 - 28	78.1		24	19	5
28 - 30	86.0		25	11	14
32 - 34		2.62	29	12	17
		2.63			
36 - 38	80.0	2.59	31	19	12
38 - 40	67.3		28	7	21
40 - 42	56.0		27	15	12
42 - 44	61.0		49	20	29
44 - 46	92.0		31	19	12
46 - 48	88.0	2.62	29	15	14
		2.59			
48 - 50	87.0		23	23	0
			28	18	10
53 - 55			23	21	2
58 - 60			26	22	4
			27	20	7
68 - 70			79	21	58
78 - 80			71	21	50
88 - 90			51	14	37

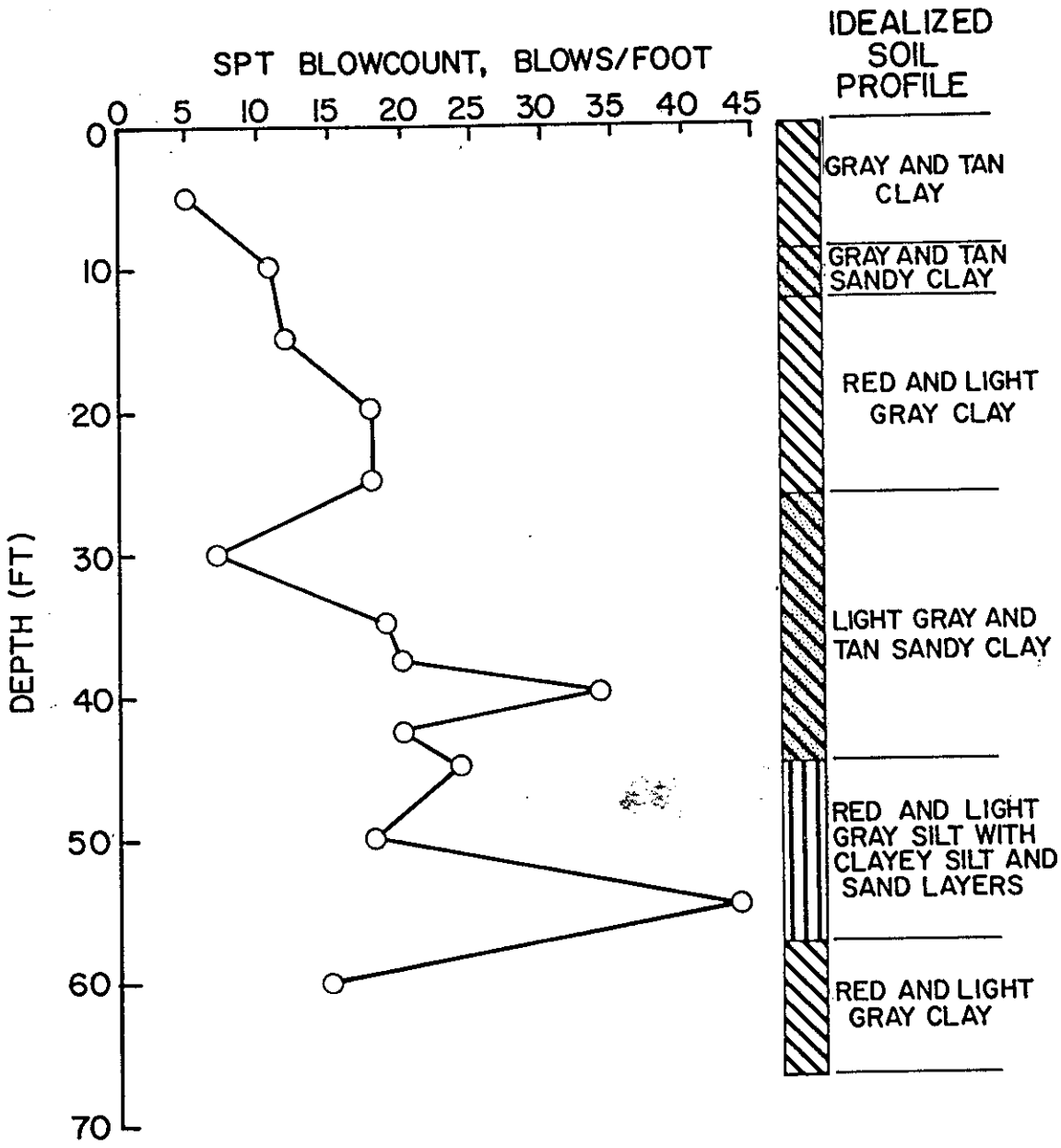

Fig. 3.5. SPT Test Results (1 ft = 0.305 m).

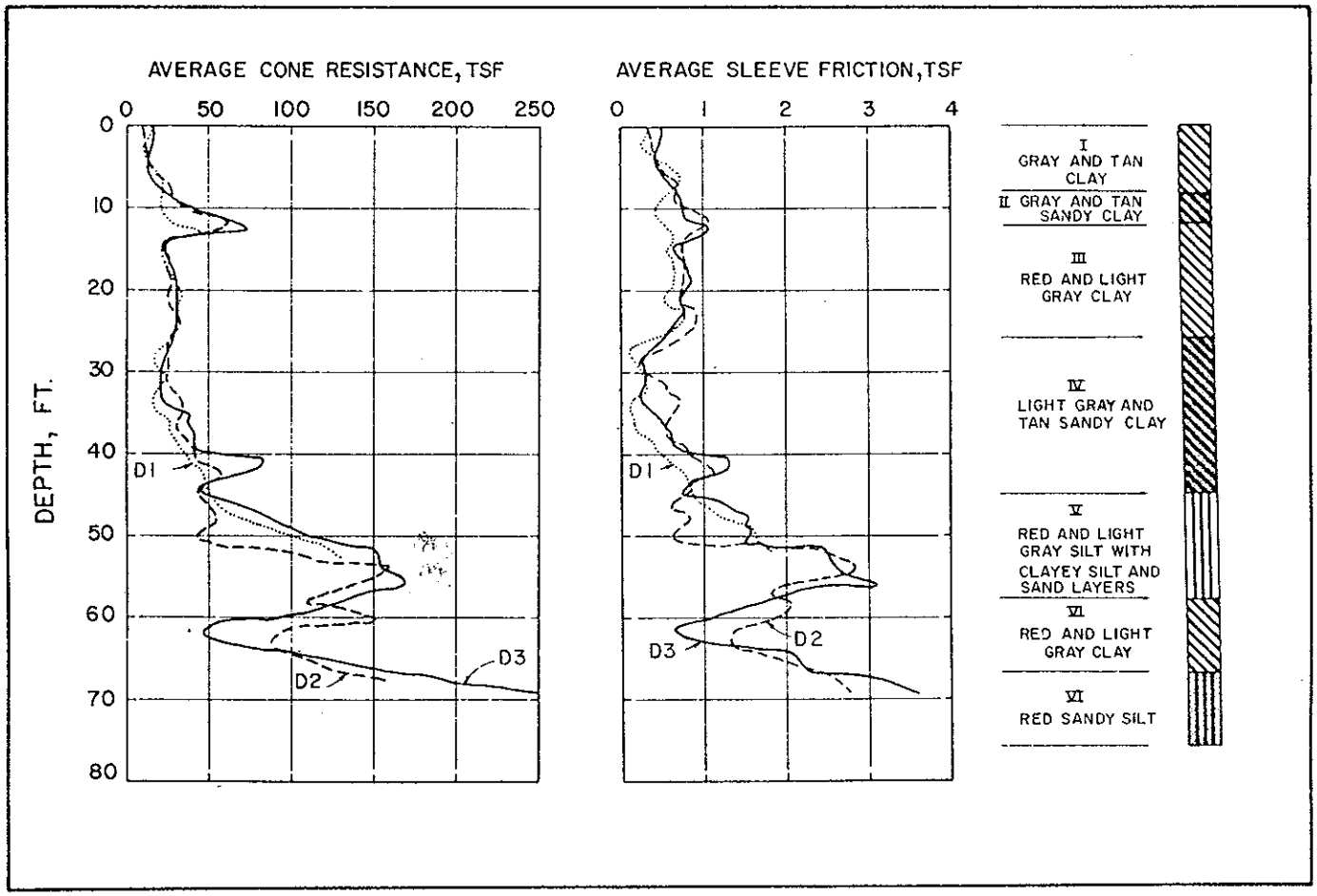

Fig. 3.6. Static Cone Penetrometer Results (Before Pile Driving) (1 ft = 0.305 m; 1 tsf = 95.8 kPa).

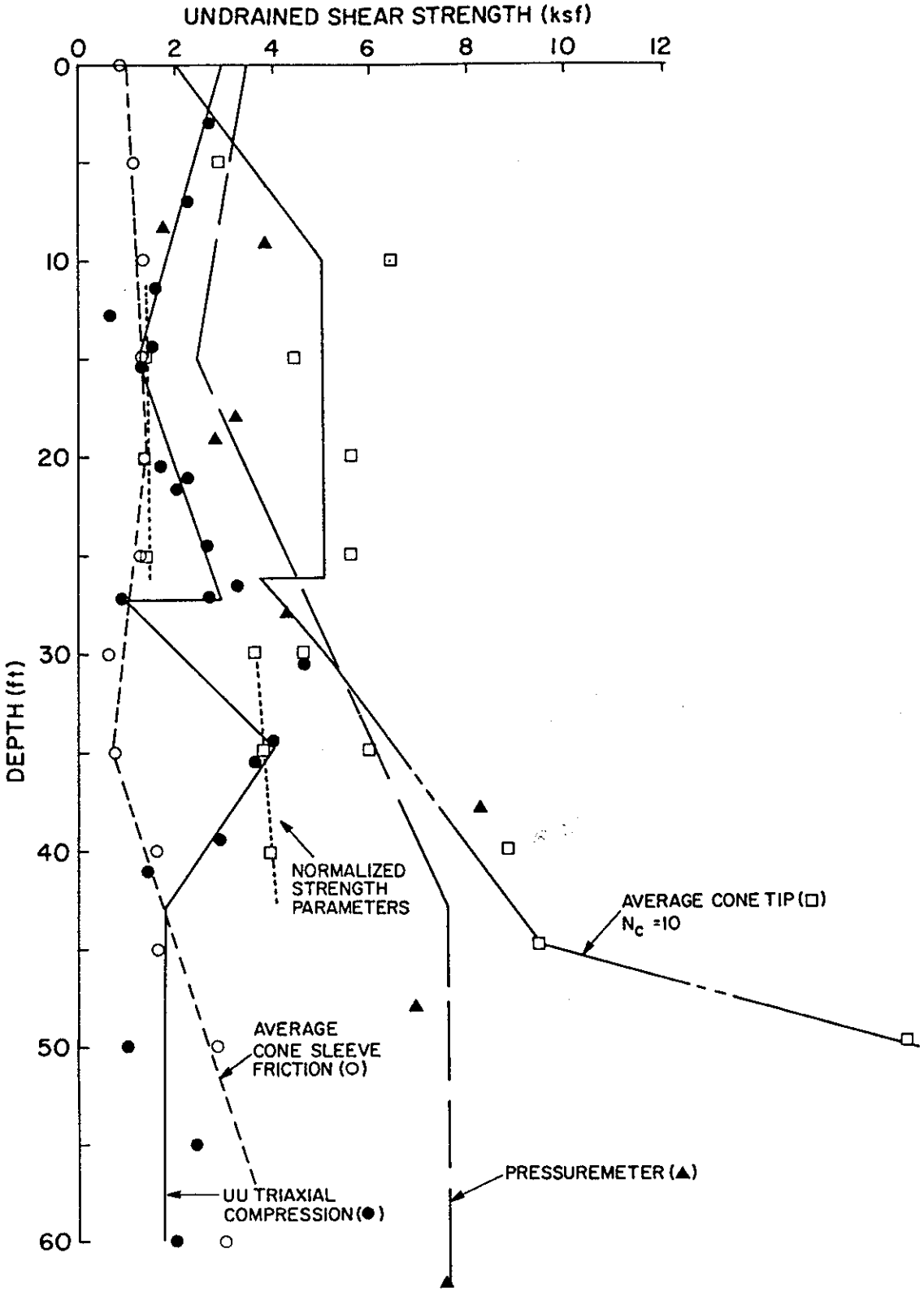

Fig. 3.7. Indicated Undrained Shear Strength Profiles (1 ft = 0.305 m; 1 ksf = 47.9 kPa).

consolidation was reached and then rebounded to a known overconsolidation ratio (OCR) equal to that computed from lab and in-situ tests (41, 42). Direct UU triaxial compression tests yield unrepresentatively low strengths below Stratum III due to excessive sample disturbance in the sandy materials.

The OCR at the test site (42) can be approximated by

$$OCR = 16\ (d)^{-0.55} \tag{3-1}$$

where d is depth in meters. Equation (3-1) is not valid above a depth of 5 meters, where the OCR exceeded 7, or below 15 meters, where the OCR was less than 3.5.

A profile of measured coefficient of earth pressure at rest (K_o) is shown in Fig. 3.8. Several triaxial samples were consolidated under K_o conditions for purposes of determining K_o. SBP and one-dimensional consolidation tests were also employed for that purpose. The indicated earth pressure coefficients exceeded 1.0 to a depth of about 30 ft (9.1 m) and appear to exceed 1.9 above a depth of 10 ft (3.1 m).

Stress-strain properties were measured by several methods, including the $\overline{CU}$ and UU triaxial compression test (direct and normalized), the SBP test, the cross-hole test, one dimensional consolidation tests, and low and high amplitude resonant column tests. Detailed stress- and pore water pressure-strain curves, failure envelopes and effective stress paths for the $\overline{CU}$ triaxial compression tests are given in Appendix C, as are data summaries from the cross-hole and one-dimensional consolidation tests.

Figure 3.9 summarizes soil Young's moduli (E) for the soil indicated by the UU triaxial, self-boring pressuremeter, and cross-hole tests. In the former tests, E was defined as the secant modulus to the laboratory stress difference - axial strain curve at 20 percent of the failure stress difference. In the SBP tests, E was computed from expanding cavity theory at the point of maximum radial stress rate. E-values were computed from measured shear modulus values in the cross-hole test, assuming a Poisson's ratio of 0.5 (i.e., $E = 3G$).

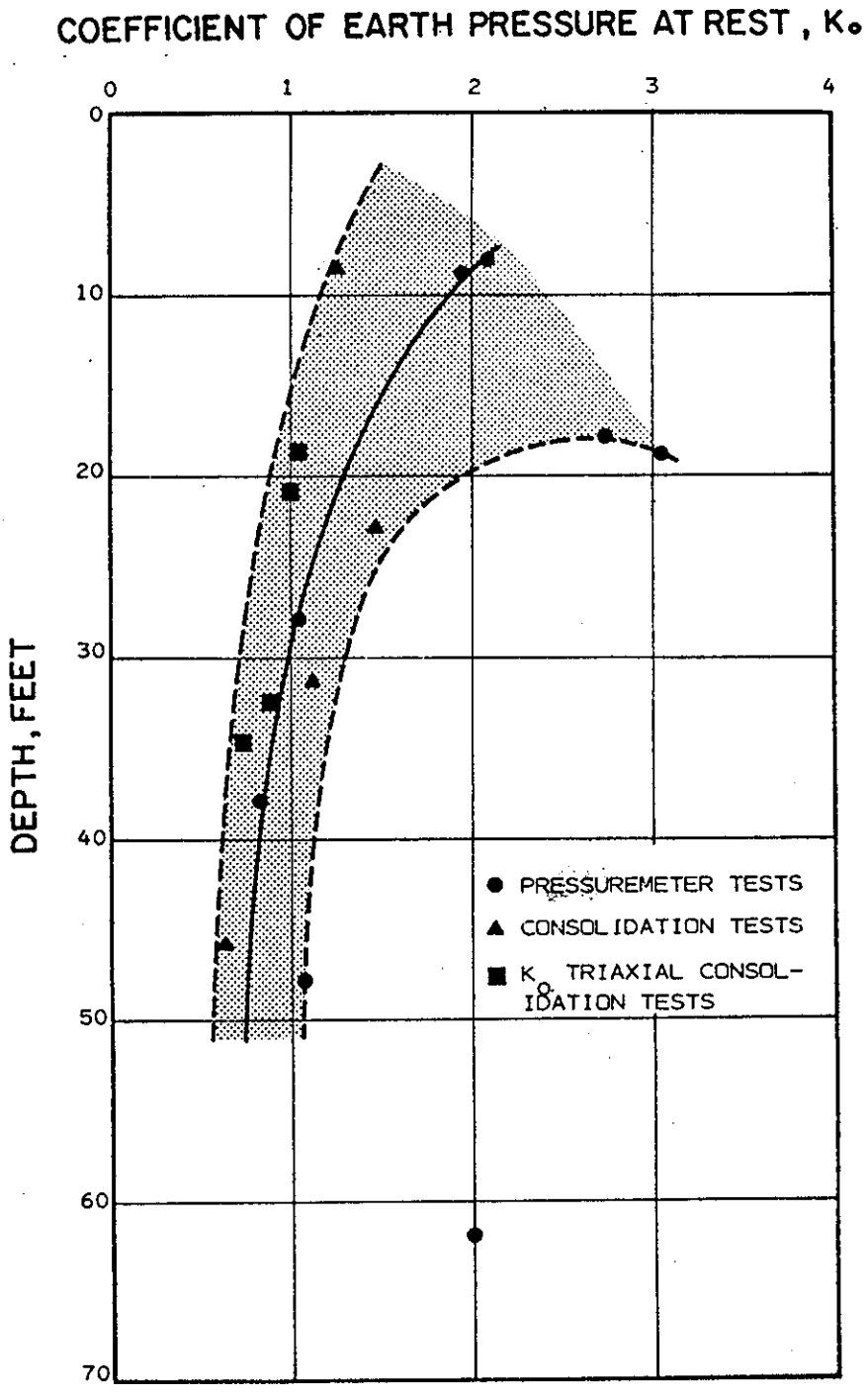

Fig. 3.8. K_o vs. Depth (1 ft = 0.305 m).

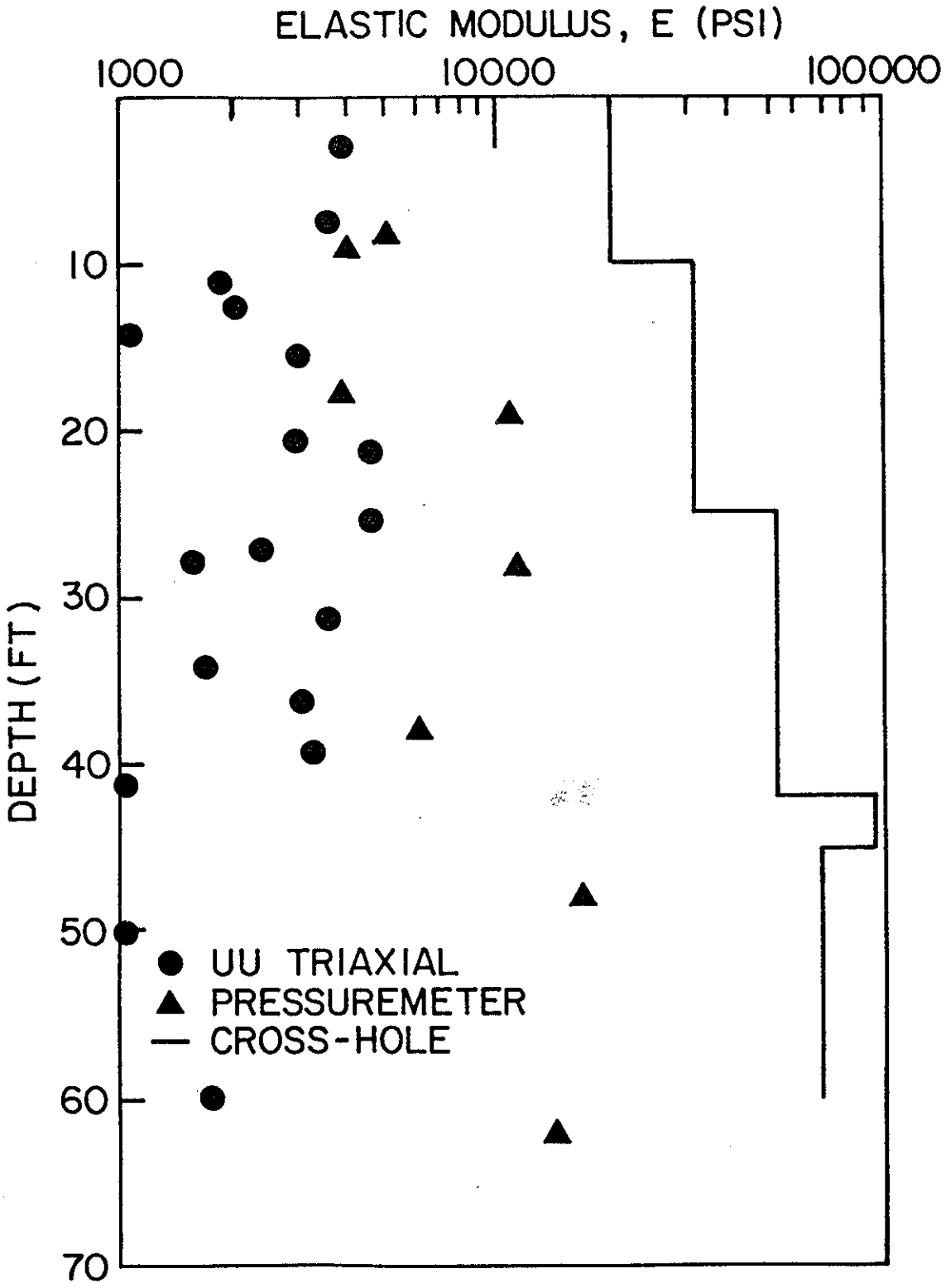

Fig. 3.9. Young's Modulus vs. Depth (1 ft = 0.305 m; 1 psi = 6.89 kPa).

Torsional resonant column tests (77) were conducted on representative samples recovered from depths of 6.8 ft (2.1 m), 16.7 ft (5.1 m), and 31.7 ft (9.7 m). Samples were excited torsionally at low shear strain amplitudes ($\leq$ 0.001%) under stepwise variable isotropic confining pressures (applied under conditions where drainage was permitted) and at various times after application of confining pressure increments. During each test the resonant frequency of the sample was measured and the shear modulus computed by using simple elasticity equations. Damping ratios for the samples were then computed during motion decay by the logarithmic decrement method (76).

The entire procedure was then repeated at successively higher shear strain amplitudes, to a maximum value of greater than 0.1%. The test sequence is summarized in Table 3.2.

Resonant column test results are summarized in Tables C.1 - C.3, and detailed graphs showing shear moduli (G) as functions of shear strain amplitude, (γ), confining pressure ($\bar{\sigma}_c$), and time of confinement (t) in Appendix C.

The shear moduli of the soil at the site were found to be influenced significantly by the magnitude of $\bar{\sigma}_c$ and to be relatively less influenced by t and γ. Figure 3.10 presents G vs. γ for t = 1000 min. for the confining pressures that most closely resulted in matches on the low γ end with G measured from crosshole tests. As can be seen, confining pressures ranging from 2 to 4 times the mean normal in-situ effective stress were necessary to produce the low-end match. This phenomenon may be due to the effects of sample disturbance and the resultant need to close seams, slickensides, and fissures before in-situ conditions are replicated. The soil also appeared to be essentially linear up to γ = 0.01% above 16.7 ft (5.1 m) and γ = 0.001% at 31.7 ft (9.7 m).

Figure 3.10 has a scale marked "u" superimposed below the γ scale. The parameter u is the lateral displacement of a 10.75 in. (273 mm) diameter pile corresponding to the γ value shown above u. γ is interpreted as the average shear strain in a horizontal plane produced by the lateral deformation u and is related to u by (34):

Table 3.2. Summary of Test Conditions for Resonant Column Tests (1 ft = 0.305 m; 1 psi = 6.89 kPa)

Sample Depth (ft)	In-Situ Vertical and Mean Effective Stresses (psi)	Effective Continuing Pressures (psi)	Shear Strain Amplitude Range (%)
6.8	5.9 (vert.) 11.0 (mean)	11.0 22.0 44.0	0.001-0.1
16.7	10.6 (vert.) 14.0 (mean)	14.0 28.0 56.0	0.001-0.1
31.7	17.3 (vert.) 17.0 (mean)	8.5 17.0 34.0 68.0	0.001-0.1

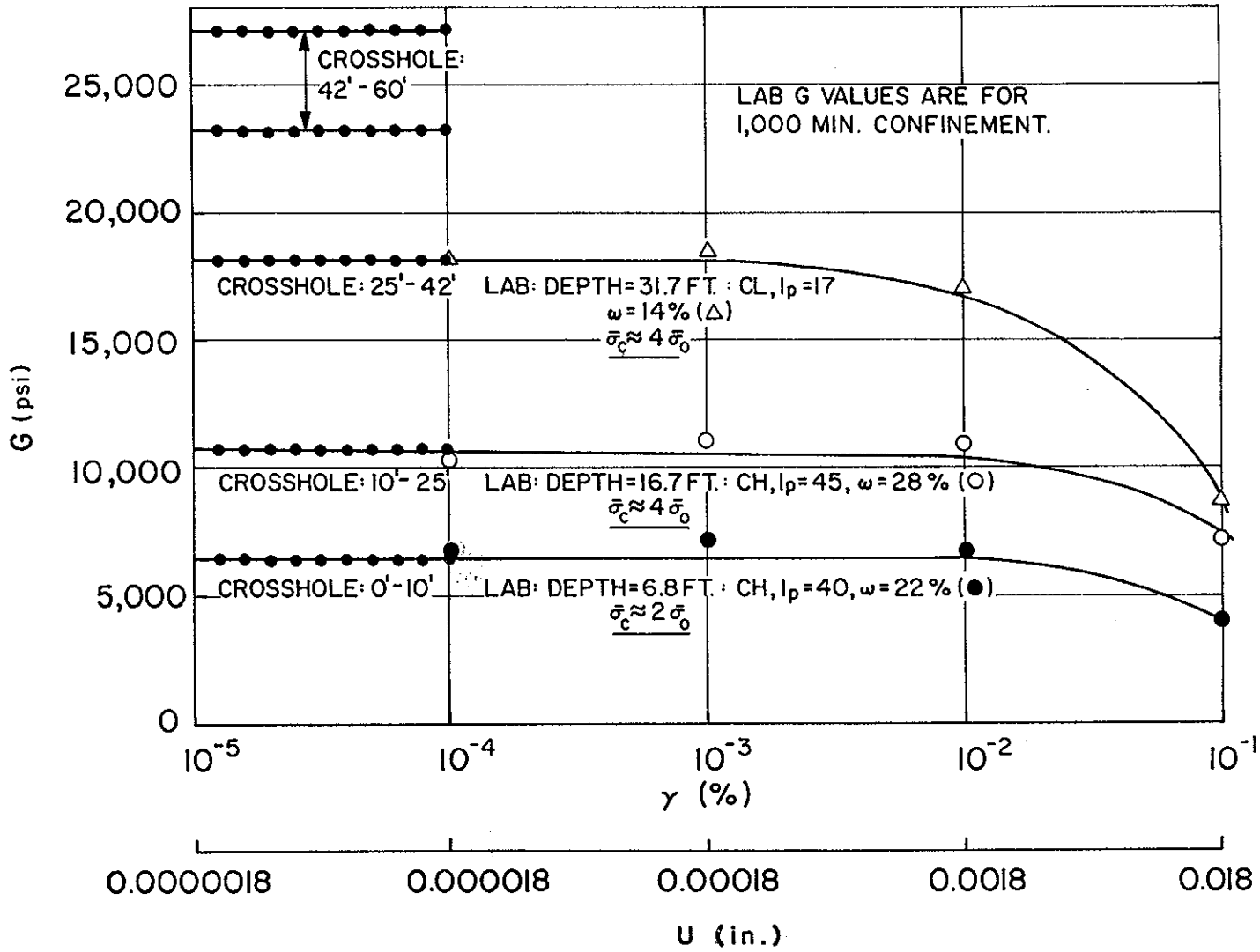

Fig. 3.10. Shear Modulus vs. Shear Strain Amplitude (1 ft = 0.305 m; 1 in. = 25.4 mm; 1 psi = 6.89 kPa).

$$u \doteq \frac{D\gamma}{0.6} \qquad (3\text{-}2)$$

where D = pile diameter.

Damping ratios appeared to be relatively independent of $\bar{\sigma}_c$ and t, as indicated by data in Appendix C. Damping ratios for t = 1000 min. are plotted as functions of γ (and u) in Fig. 3.11. Minimum damping ratios (corresponding to γ = 0.0001%) varied considerably among the samples, with the least plastic sample exhibiting the highest value (5.5%). Damping in all cases increased markedly above γ = 0.01% (u = 0.002 in.) to a value of approximately 15 % of critical at γ = 0.5%.

The low amplitude damping, D_{min}, was interpreted as being viscous and non-hysteretic. The hysteretic component, labeled D_h, was assumed to be approximately represented by $D - D_{min}$ at any given value of γ. A plot of this interpretation of hysteretic damping is presented in Fig. 3.12. D_h is seen to be insignificant ($<$ 1%) only below γ = 0.01% (u = 0.002 in.).

Figures 3.13 and 3.14 compare the resonant column test results with those from other well-documented studies, indicated on the figures. The soil at the test site appears not to be unusual. It tends to be slightly more linear and to exhibit slightly lower hysteretic damping than other soils (Fig. 3.14).

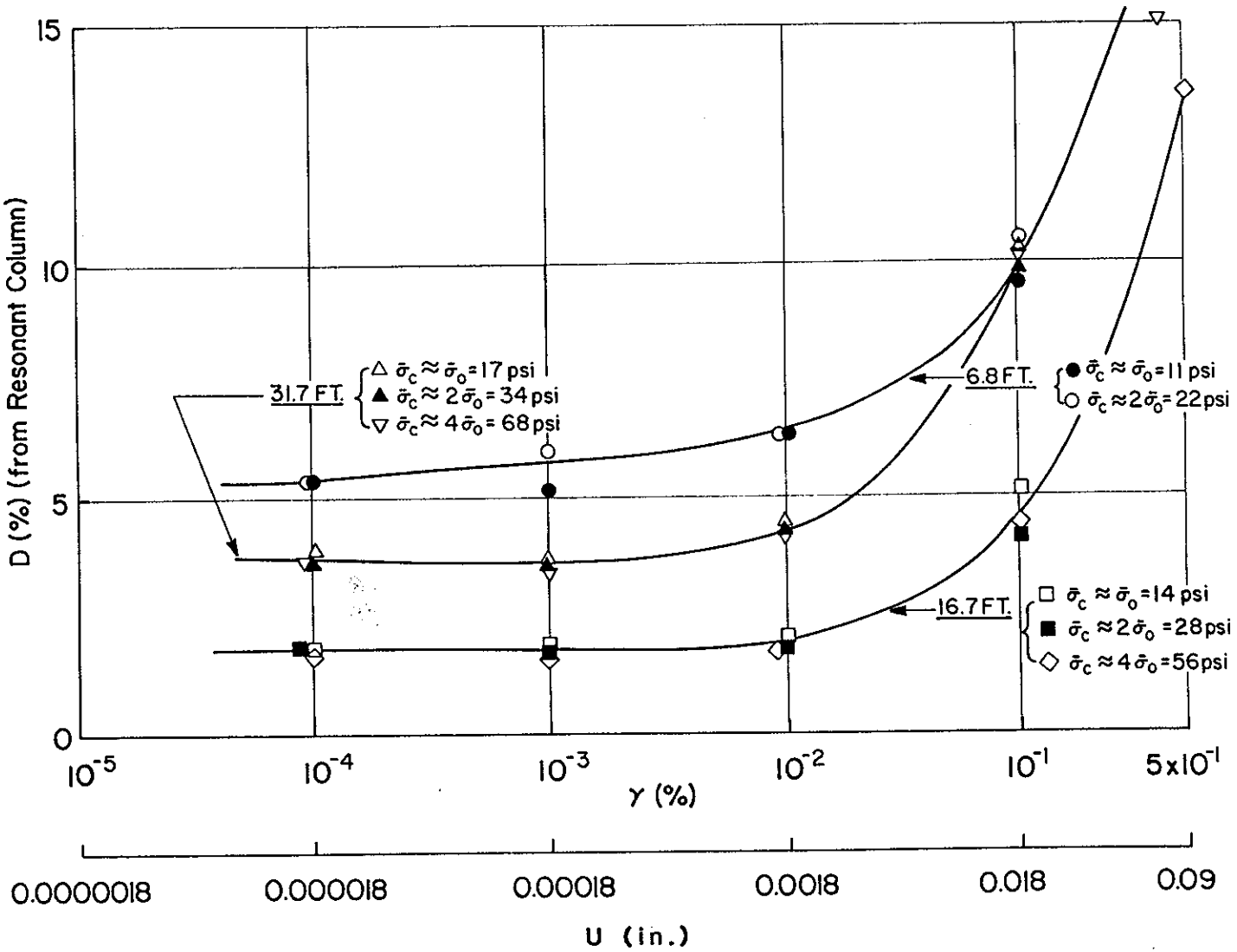

Fig. 3.11. Damping Ratio vs. Shear Strain Amplitude (1 ft = 0.305 m, 1 in. = 25.4 mm; 1 psi = 6.89 kPa).

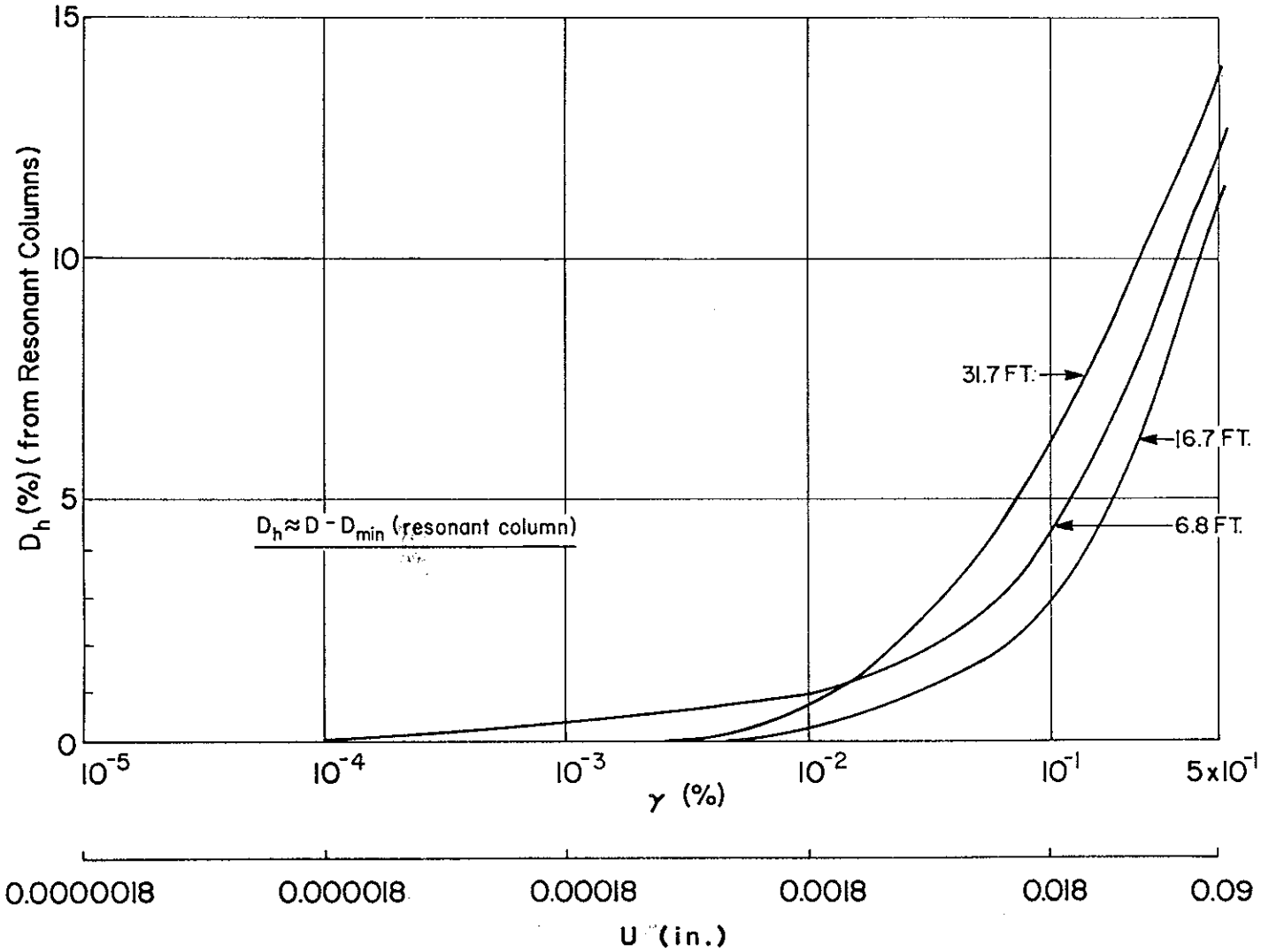

Fig. 3.12. Interpreted Hysteretic Damping vs. Shear Strain Amplitude (1 ft = 0.305 m; 1 in. = 25.4 mm).

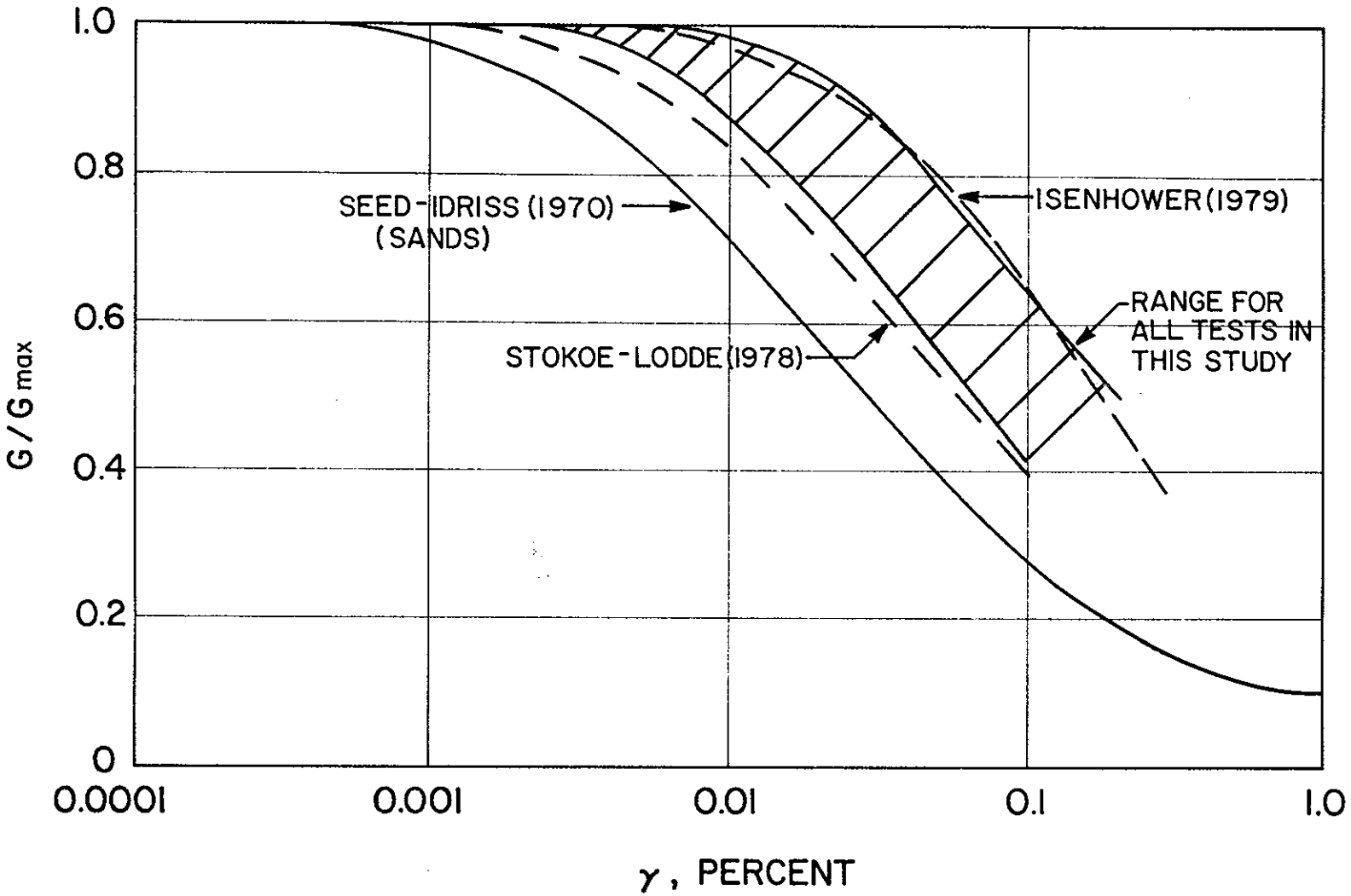

Fig. 3.13. Shear Modulus Comparisons.

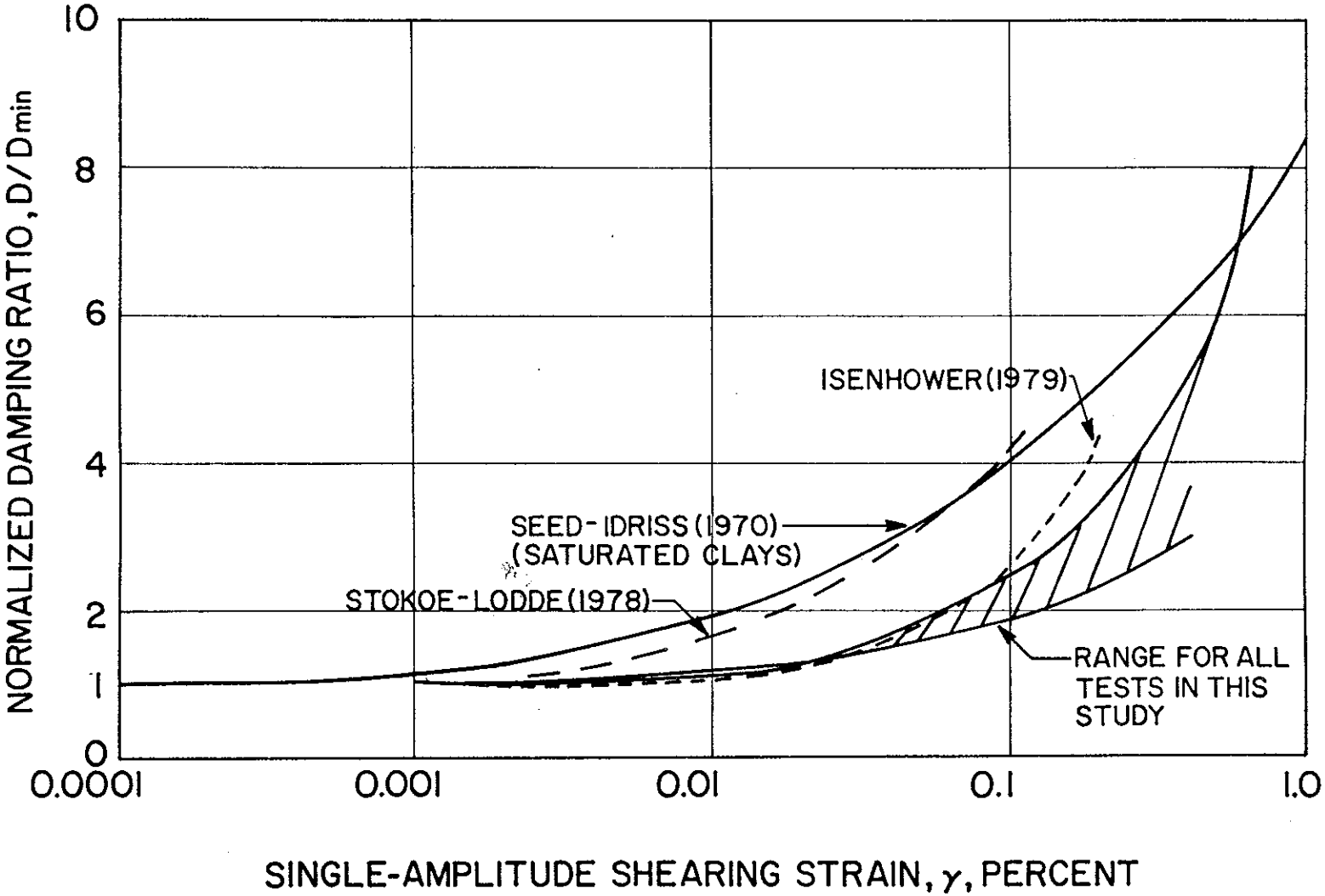

Fig. 3.14. Damping Ratio Comparisons.

CHAPTER 4. PILE INSTALLATION AND STATIC TEST SUMMARY

GENERAL

The test piles were installed in October - November 1979. All piles were impact driven with a single acting, steam operated Raymond 1S hammer, producing a rated energy of 19,500 ft-lb (26,460 m-N) per blow. Pilot holes were drilled to a depth of 10 ft (3.1 m) and to a diameter of 8 in. (203 mm) prior to driving. All piles were carbon steel pipes, 10.75 in. (273 mm) in outside diameter, with 0.365 in. (9.27 mm) thick walls, and with 1.0 in. (25.4 mm) thick boot plates cut flush with the sides of the piles. The piles had been instrumented prior to driving with internal strain gage bridges to measure axial load distributions in the piles during subsequent static vertical loading. These bridges were not designed to respond to flexural stresses.

INSTALLATION

The piles were all driven to a penetration of 42.5 ft (13.0 m) (Piles 1-3,4, and 8, as denoted in Fig. 4.1) or 43 ft (13.1 m) in the geometric pattern shown on Fig. 4.1, in the driving order 1, 2, 3, 10, 9, 8, 7, 6, 4, 5. Pore pressure response during and after installation is documented in Ref. 63. The single pile (No. 1) protruded about 3 ft (.91 m) above the ground, and the group piles protruded about 8 ft (2.4 m) above ground at the end of initial driving. Piles 1-3, 4, and 8 were restruck after short (1 hr - 4 days) set-up periods to their full 43 ft (13.1 m) penetrations. Driving records for the 10 test piles involved in the present study are given in Table 4.1. The piles were observed to drive relatively uniformly. Following installation the piles were inclinated, with the resulting geometry shown in Fig. 4.1. The pile spacing can be seen to be nonuniform, especially near the pile tips. The group piles were then capped with a massive concrete block suspended off the soil.

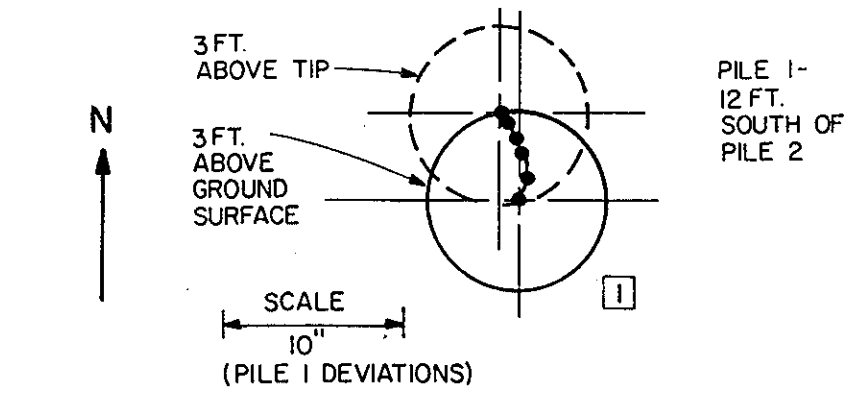

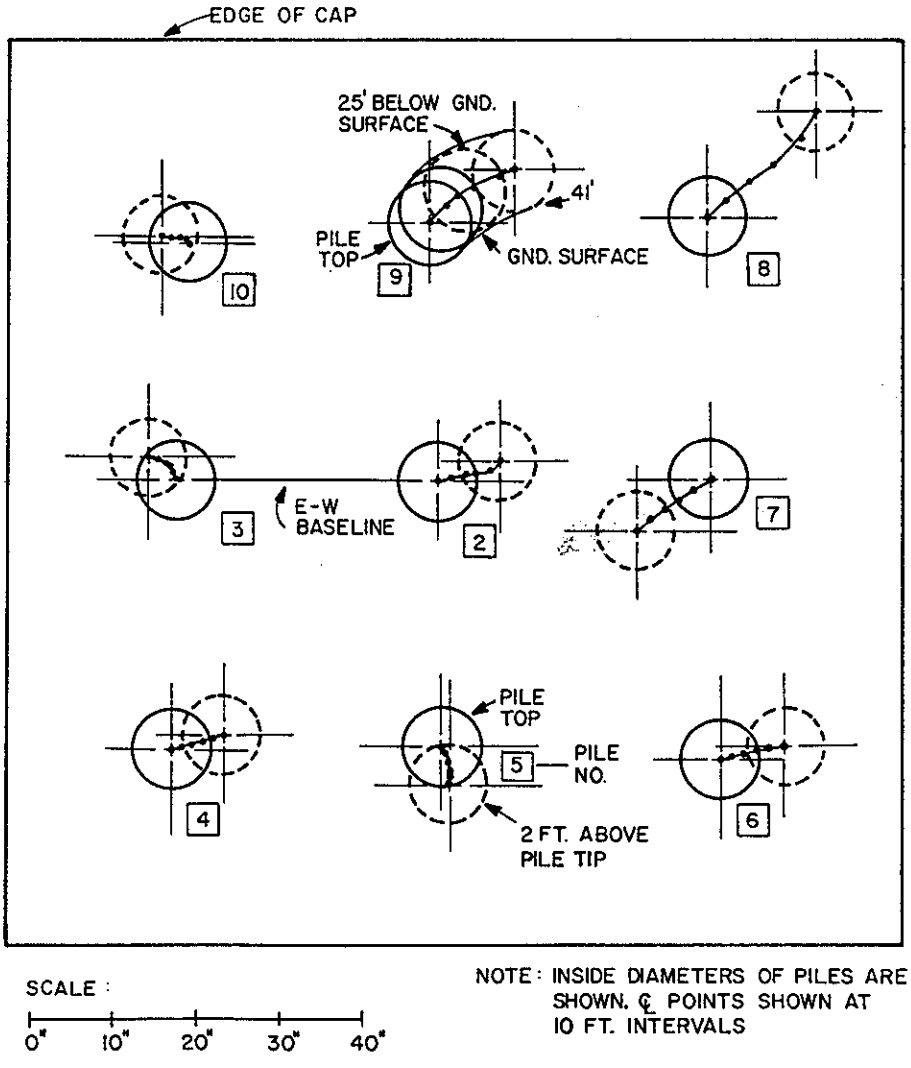

Fig. 4.1. Pile Orientations (1 ft = 0.305 m; 1 in. = 25.4 mm).

Table 4.1. Driving Records
(1 ft = 0.305 m; 1 in. = 25.4 mm)

Penetration (ft)	Pile Number									
	1	2	3	4	5	6	7	8	9	10
1										
2										
3										
4										
5										
6										
7										
8										
9										
10										
11	3		2	2	3		1	2	4	1
12	6	6	7	6	4	6	5	4	4	5
13	7	6	5	5	5	4	4	6	4	5
14	5	5	3	5	5	4	4	4	3	4
15	4	5	4	6	4	3	4	4	4	4
16	5	6	5	5	5	4	4	5	3	6
17	6	6	7	5	5	4	5	4	4	5
18	8	6	7	6	5	5	5	5	4	4
19	6	6	5	5	5	5	6	5	5	6
20	7	7	6	5	5	4	5	5	5	5
21	7	6	6	6	5	5	6	5	5	6
22	7	6	6	5	5	5	6	6	7	6
23	8	8	8	7	6	6	6	6	6	7
24	9	7	8	7	6	6	8	7	7	8
25	9	8	9	7	6	7	8	8	7	8
26	10	8	8	7	7	7	8	7	8	8
27	9	8	8	8	7	6	7	7	7	7
28	10	9	9	7	7	6	8	8	7	8
29	10	8	10	7	7	7	8	7	8	9
30	10	10	10	8	8	7	9	7	8	8
31	10	10	10	9	8	7	10	8	10	8
32	11	10	11	10	9	8	11	8	9	8
33	11	10	12	10	10	9	11	8	10	9
34	11	12	13	11	11	9	10	10	11	9
35	12	12	14	11	11	8	10	10	12	10
36	12	11	15	12	10	9	11	10	11	9
37	12	13	17	12	13	10	11	10	12	10
38	14	14	18	14	14	9	12	12	12	10
39	13	14	15	12	12	10	13	11	13	12
40	13	15	18	13	13	10	13	11	13	10
41	14	16	17	13	13	10	13	11	13	11
42	15	16	19	13	11	10	13	12	13	11
43	8/19	11/27	24	9/16	18	15	14	7/19	17	14
43+	88 (5")	74 (7")	60 (6")	89 (8")	111 (10")	* (7")	* (7")	72 (6")	* (7")	* (7")

Run Zone

Table 4.1. (Cont'd). Driving Records

NOTES. 1. Piles driven in 8"ϕ x 10 ft deep pilot holes.

2. Piles initially driven in 4-day period in October-November, 1979. Piles 1, 2, 4 and 8 were driven to 42.5 ft and restruck to 43 ft several days after initial driving. First no. at 43 ft penetration is for 42-42.5 ft and second is 42.5-43 ft restrike.

3. Piles initially driven with Raymond 1s hammer, 50 blows/minute, steam operated. Rated energy is 19,500 ft-lb/blow. Hammer cushion: 16" aluminum-micarta stack. No pile cushion.

4. Second restrike to 43+ ft penetration on 10 April 1980 with Delmag D-12 diesel hammer. No cushions. Number in parentheses indicates distance driven. * Indicates no blow count data taken.

LOAD TESTING

During November, 1979 - March, 1980, three separate static, monotonic compression tests to failure were conducted on both the single pile (Pile No. 1) and the pile group (Piles Nos. 2-10), followed by additional compression tests on subgroups comprised of Pile Nos. 2, 4, 6, 8, and 10 and 4, 6, 8, and 10. The massive cap was then removed, and single, static, monotonic uplift tests to failure were conducted on Pile Nos. 1, 2, 4, 5, and 9 individually. Results of the static compression tests are summarized in Table 4.2, and considerable detail on the pile installation, static compression tests, and static uplift tests may be found in Ref. 63. The piles behaved basically as friction piles with only minor differences in ultimate shaft resistance in uplift and compression. About 28 percent of the applied, ultimate compressive load was developed in end bearing. Average unit load transfer curves measured during initial compression loading (Test 1) of Pile No. 1 and Pile No. 11 (an isolated pile identical to Pile No. 1 not used in the present study) are shown in Figs. 4.2 and 4.3. Figure 4.2 shows mobilized shaft shear stress, f, as a function of relative pile-soil movement, z, at four levels that are designated by their depths below the ground surface. Figure 4.3 shows mobilized end bearing force, Q, vs. tip settlement, z. Figures 4.2 and 4.3 present the unit load transfer curves in two forms: one in which the residual stresses acting on the piles before load testing are neglected and one in which they are considered. One method of analyzing the dynamic response of these piles, described in Chapter 5, used the static unit load transfer curves as input. For that analysis, the curves marked "neglecting residual stresses" and "corrected" were used. Residual stress effects were not explicitly included in the dynamic analytical modeling because the algorithm used to model pile response (DRIVE) had not been investigated for its ability to handle nonzero stresses as an initial condition prior to application of dynamic loads. In any event the residual stresses are seen to be relatively small.

The average pore water pressures along the group piles at various stages of compression testing are shown in Fig. 4.4. Pore pressures generated during installation dissipated rapidly, so that by the end of the last compression test in February 1980 the pore water pressures

Table 4.2. Summary of Static Tests (1 in. = 25.4 mm; 1 k = 4.45 kN; SP = Single Pile).

Test (a)	Failure Mode	Plunging Failure Load (k) (b)	Settlement at 50% of Plunging Load (in)	Efficiency	Settlement Ratio at 50% of Plunging Load
SP 1 (15 days)	Plunging	168	0.068		
SP 11 (15 days)	Plunging	133	0.048		
9-Pile (20 days)	Plunging of Individual Piles w/ Tiping of Group	1332	0.094	0.99	1.62
SP 1 (78 days)	Plunging	187	0.080		
SP 11 (78 days)	Plunging	170	0.067		
9-Pile (82 days)	Plunging of Individual Piles	1532	0.113	0.98	1.54
SP 1 (105 days)	Plunging	177	0.080		
SP 11 (105 days)	Plunging	181	0.077		
9-Pile (110 days)	Plunging of Individual Piles	1541	0.116	0.96	1.48
5-Pile (113 days)	Plunging of Individual Piles	832	0.096	0.93	1.31
4-Pile (116 days)	Plunging of Individual Piles	661	0.085	0.92	1.19

(a) Times between pile installation and test shown in parentheses
(b) Includes cap weight and weight of loading accessories

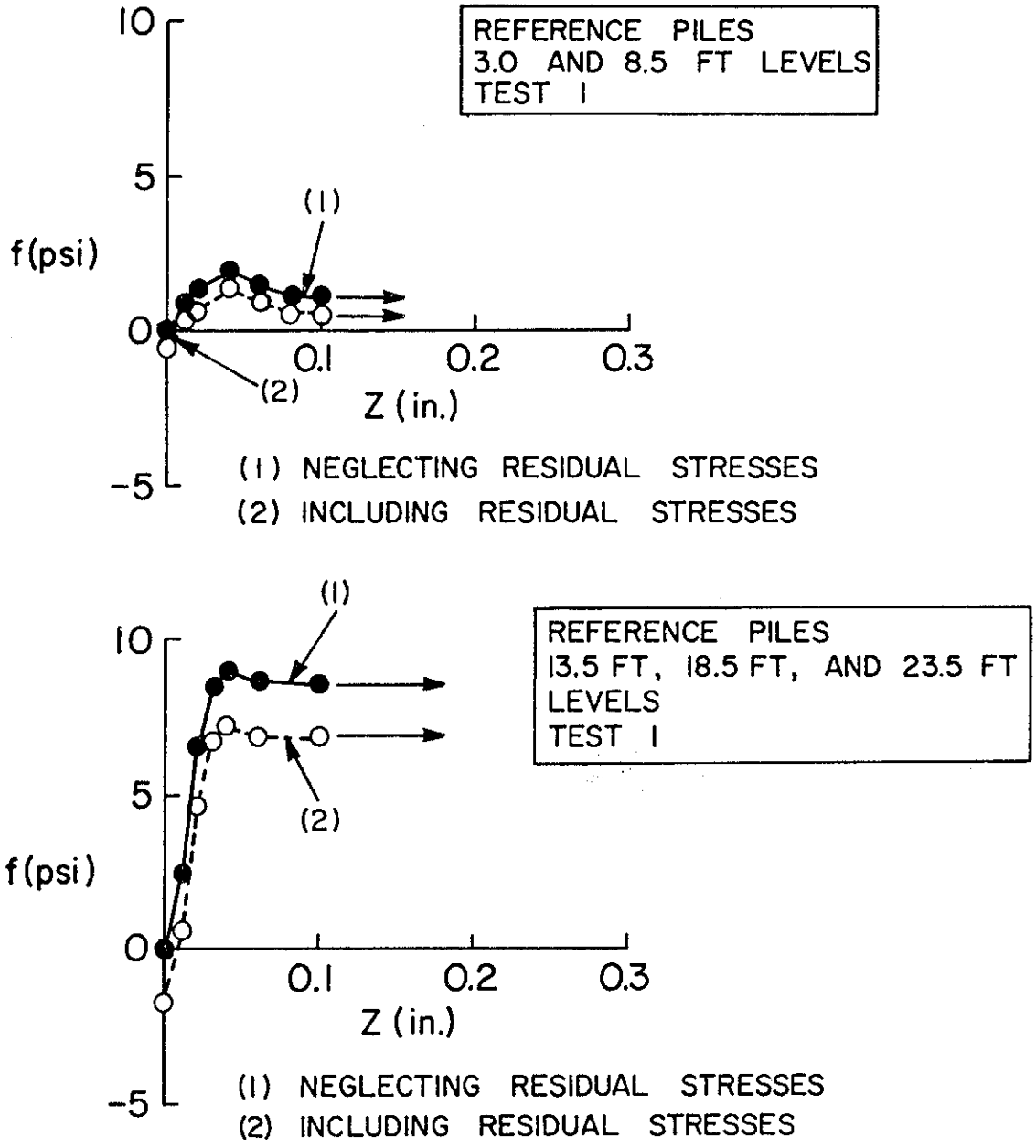

Fig. 4.2. Average Static f-z Curves for Reference Piles (1 ft = 0.305 m; 1 in. = 25.4 mm; 1 psi = 6.89 kPa).

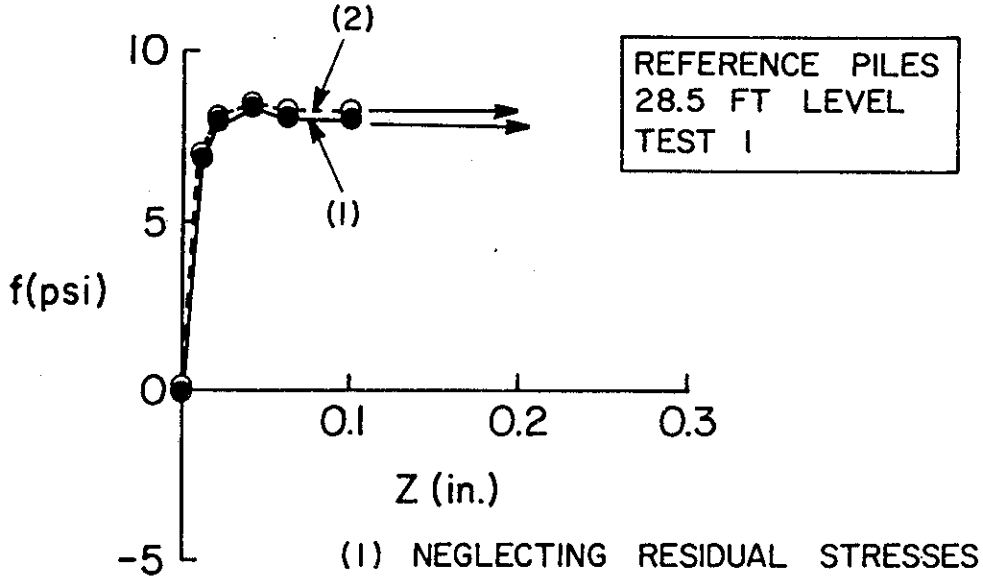

(1) NEGLECTING RESIDUAL STRESSES
(2) INCLUDING RESIDUAL STRESSES

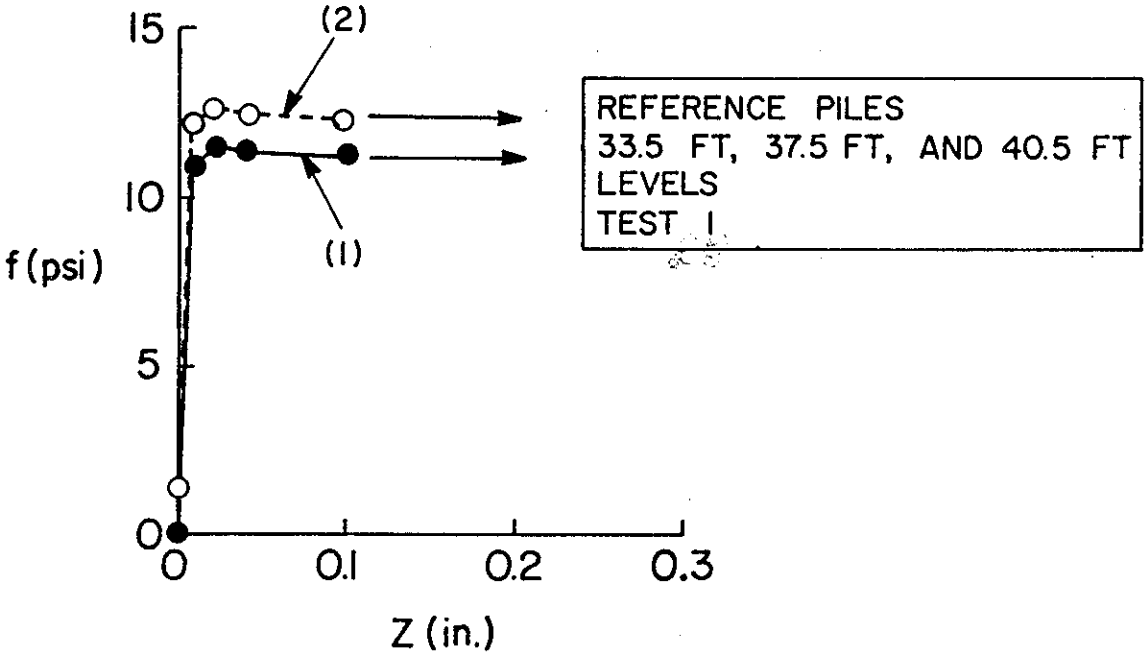

(1) NEGLECTING RESIDUAL STRESSES
(2) INCLUDING RESIDUAL STRESSES

Fig. 4.2 Continued

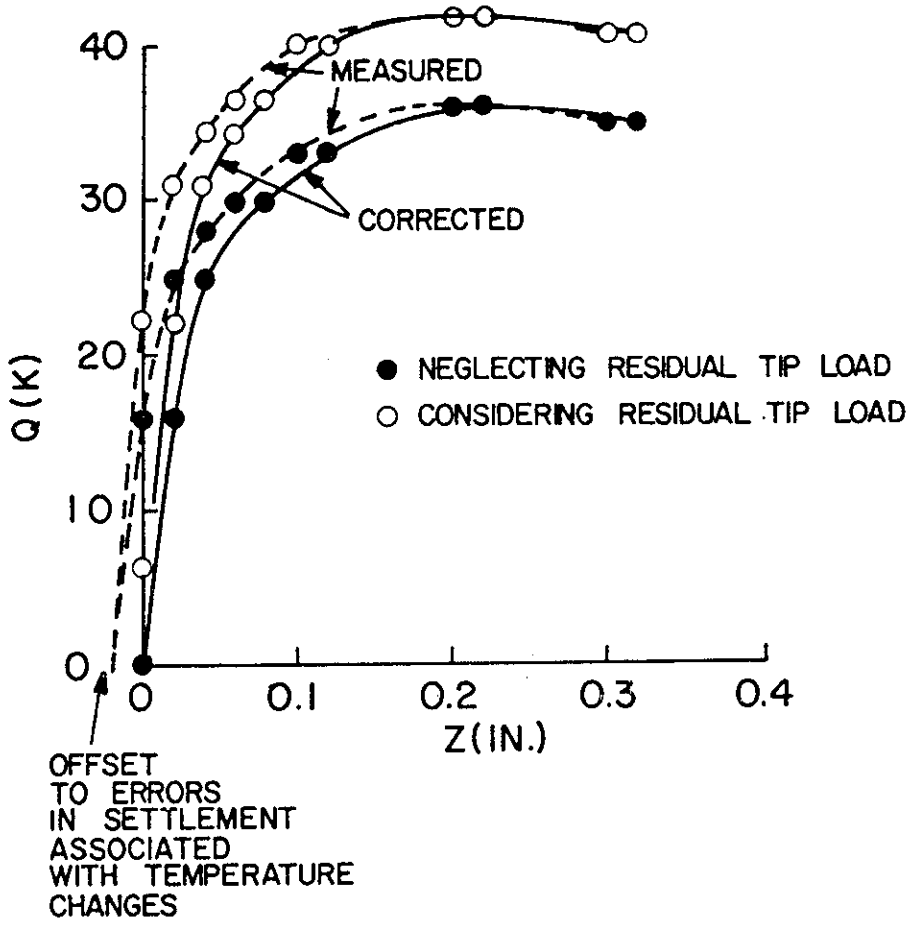

Fig. 4.3. Average Static Q-z Curves for Reference Piles (1 ft = 0.305 m; 1 in. = 25.4 mm; 1 psi = 6.89 kPa).

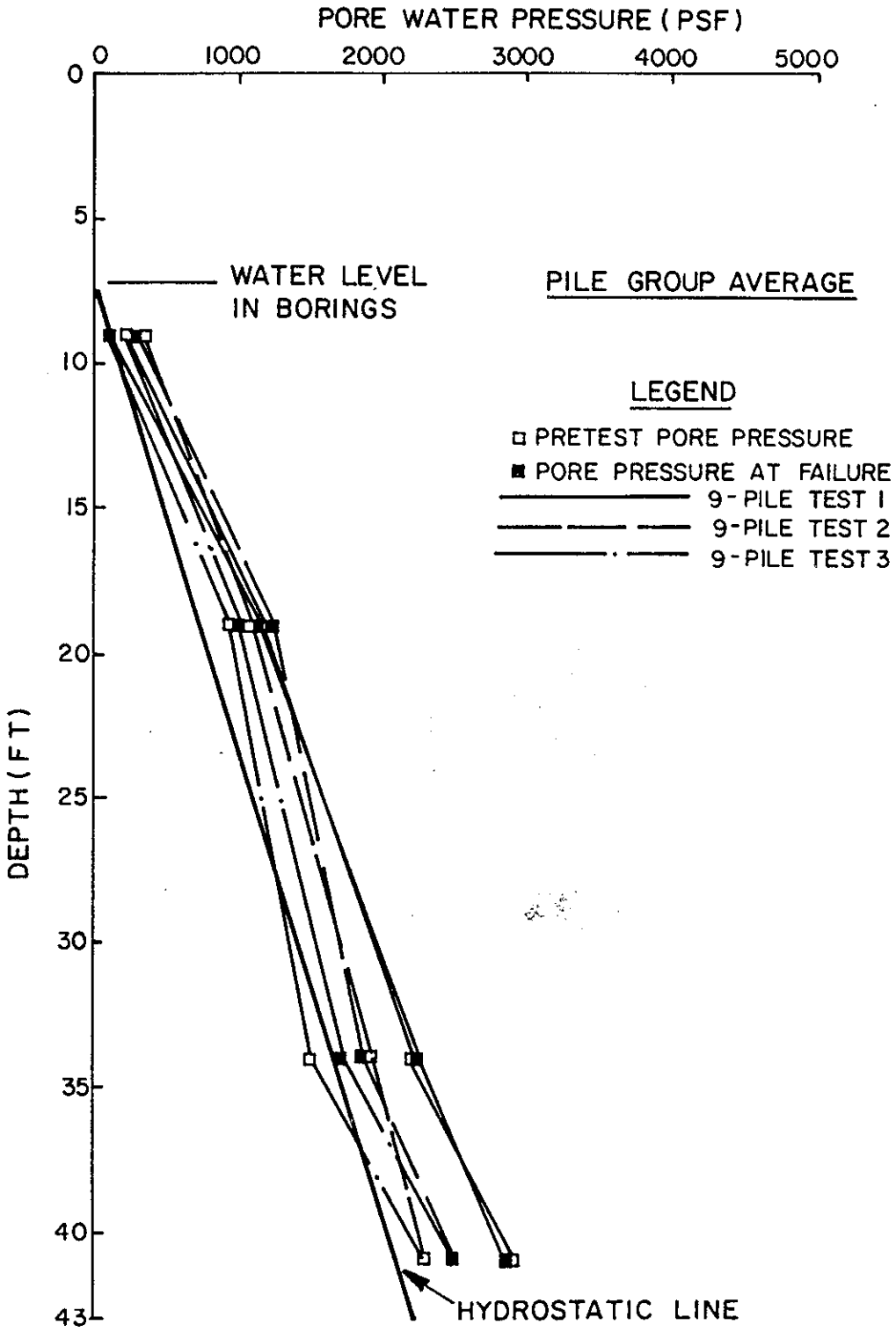

Fig. 4.4. Pore Water Pressure Profiles for Static Tests (1 ft = 0.305 m; 1 psf = 47.9 Pa).

against the piles were essentially hydrostatic. The soil exhibited very little tendency to dilate or contract during monotonic axial testing, as indicated by the small changes in pore pressure shown on Fig. 4.4.

The initial slopes of the static load-settlement curves for the first load test were as follows:

Pile No. 1: 1430 k/in. (250 kN/mm)

9-Pile Group: 8067 k/in. (1413 kN/mm)

The initial static stiffness of Pile No. 1 in uplift (following compression testing) was 2420 k/in. (425 kN/mm). No uplift tests were performed on the group. These stiffness values are valid for a plane 12 in. (305 mm) above the ground surface.

During the static tests, the following observations having possible relevance to the dynamic study were made (63):

1. Axial loads in the group were distributed relatively uniformly among the piles throughout the range of compression loading.
2. Failure in the group occurred through plunging of individual piles, not by "block action."
3. Load-settlement response was only slightly nonlinear up to relatively large percentages of ultimate load in both the group and in the single pile, which results from the shapes of the unit load transfer curves shown in Figs. 4.2 and 4.3.
4. Multiple compression loadings to failure produced degradation in ultimate shaft capacity of less than 10 percent but produced a significant increase in tip capacity in both the single piles and group piles.
5. Some rotation of the group cap in the form of pitching about an east-west axis toward the north and twisting clockwise about a vertical axis was observed in response to application of vertical load.

SECOND RESTRIKE

The procedure for conducting the uplift tests on individual group piles required removing the massive pile cap from the group. This was accomplished by cutting the piles just below the cap and removing the

cap. After the uplift tests, it was thought that pile tip-soil contact had been destroyed and the residual stress state significantly altered on the piles that had been subjected to uplift tests. Therefore, on April 10, 1980, all 10 piles were restruck again using a Delmag D-12 diesel hammer and driven approximately 6 in. (150 mm) below their elevations prior to uplift testing, resulting in piles with penetrations of 43.5 to 44 ft (13.3 to 13.4 m). Strain gages along selected piles were monitored during this restrike to provide baseline data for examining soil damping under transient loading, as described in Chapters 6 and 7. Blow counts for the second restrike are recorded below the dashed line in Table 4.1.

Approximately four months following the second restrike, the cap again was mated to the group piles by welding the pile tops to matching stubs in the cap that were left exposed when the cap was removed.

STATIC HORIZONTAL TEST

At the conclusion of the dynamic tests, a free-head lateral load test was conducted on the single pile by jacking against the pile group. The purpose of this test was to establish the initial static horizontal stiffness of the single pile. Results are shown in Fig. 4.5.

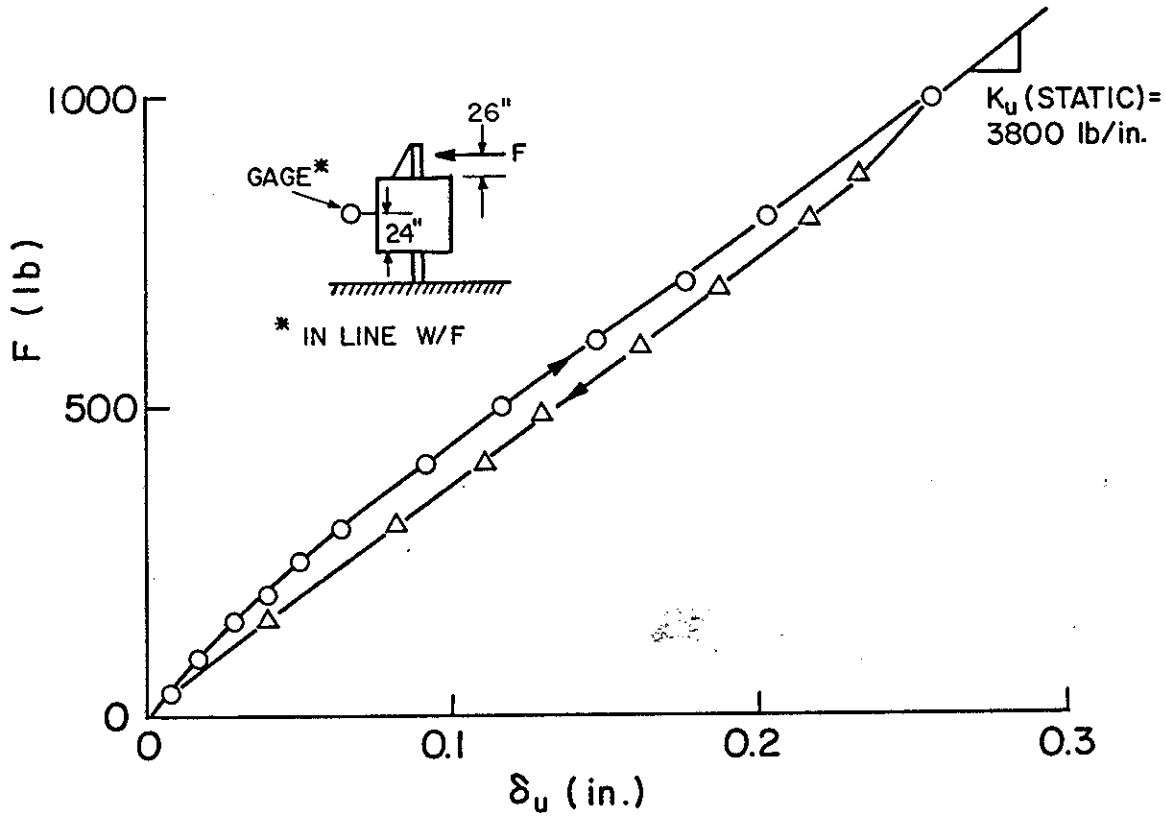

Fig. 4.5. Static Lateral Load-Displacement Curve for Pile No. 1 (1 lb = 4.45 N; 1 in. = 25.4 mm).

CHAPTER 5

EXPERIMENTAL PROCEDURES

SITE LAYOUT

The general site layout is shown in Fig. 5.1. The piles were in a shallow pool of water during all tests. In addition to the group and single test piles and anchor casings that remained from the static tests, several other major devices were installed for the dynamic tests. These devices include (1) a rail-supported steel gantry that was used for moving heavy equipment, such as vibrators; (2) an instrument trailer that housed vibrator control units, power supplies for strain gages and accelerometers, oscilloscopes for monitoring pile and ground response, amplifiers for the strain gage circuits, and a work area for field personnel; (3) a seismic data recording truck that housed binary gain and simple gain amplifiers for all instruments and a 60-channel digital tape recording system; (4) a pump for the larger of the vibrators used (vibrator provided by the U.S.A.E. Waterways Experiment Station hereafter referred to as the WES vibrator); (5) a diesel-powered generator for the WES vibrator; and (6) power signal generators for the smaller of the vibrators used (vibrators provided by the Federal Highway Administration, hereafter referred to as the FHWA vibrators). Devices (4), (5), and (6) produced high frequency vibrations that in some cases increased the noise level in recorded instrument response during the tests. In order to minimize their effects, devices (4) and (5) were placed on flatbed trailers that were supported on partially flattened tires and moved as far from the instrument locations as feasible. Device (6) was placed on timber cribbing.

Pneumatic piezometers used during the static tests had leads which were fed to a readout box located as shown.

The site was surrounded on three sides by low-rise structures with shallow foundations, as shown in Fig. 5.1. The fourth (north) side was open to a flexible base parking lot for equipment access. The presence of the nearby buildings and anchor casings may have had a small effect on the transmission of seismic waves, but analyses of the data acquired

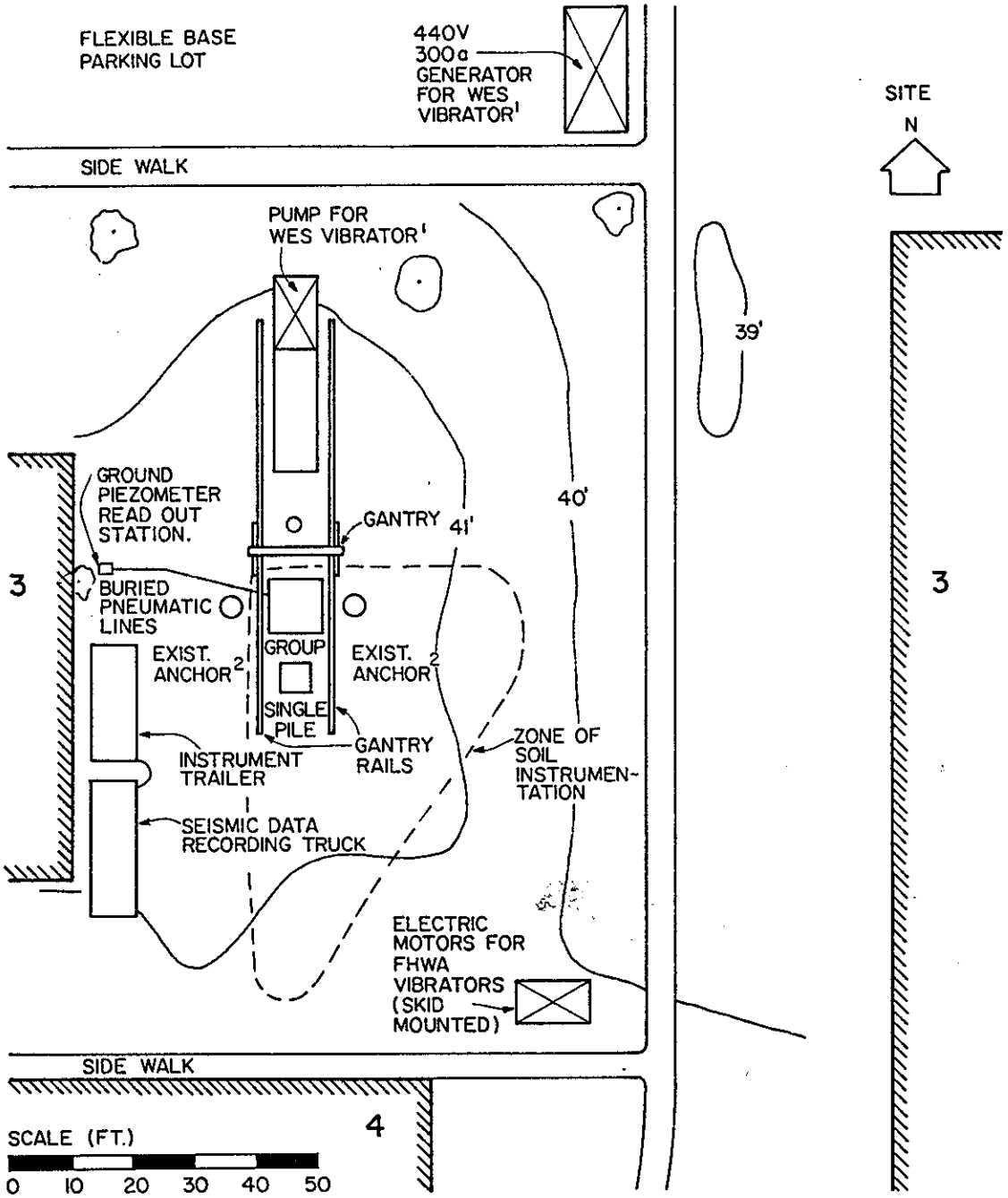

1. TRAILER MOUNTED. ISOLATED BY PARTIALLY FLATTENED TIRES.
2. 4 FT DIAMETER, WATER-FILLED, CASED HOLES, 70 FT DEEP, WITH CONCRETE FILLING TO 108 FT DEPTH (BELLED AT BASE).
3. BUILDING : STORY-AND-A-HALF, SUPPORTED BY SHALLOW CONCRETE DRILLED FOOTINGS.
4. BUILDING : SINGLE STORY , SLAB-ON-GRADE.

Fig. 5.1. General Site Layout for Dynamic Tests (1 ft = 0.305 m)

indicated that the effect was of very minor significance with regard to the response of the test piles.

Figure 5.2 is an orthographic view from the northwest of the pile group, showing the single pile with the cap in place that was used to provide mass and as an attachment for the vibrators, and the gantry being used to position a vibrator.

TRANSDUCERS

A south-north profile through Piles 1, 5, 2, and 9 is shown in Fig. 5.3. This figure indicates pictorially the locations of the various transducers employed during the tests, which are described in this section. Designators for the various transducers are given. These designators identify the various instruments in the processed data records.

Strain Gages

Axial strain gage bridges had been placed along the piles at 5 ft (1.54 m) intervals. These bridges were used to measure axial force mode shapes in the piles and were wired in a full-Wheatstone-bridge configuration that provided for multiplication of axial strain, cancellation of bending strain, and temperature compensation (63). The physical location of each gage at a typical strain gage level is depicted in Fig. 5.4. The curved tabs accommodated dummy bonded electrical resistance gages such that they were free from hoop strain, and the active (vertical) gages (not shown) were bonded directly to the inside of the pile wall about 50 mm below the tabs. The strain gage networks were exercised and calibrated in 1979, prior to installing the piles. Only the strain gages on Piles 1 (single pile), 2 (group center pile), 8 (group corner pile), and 9 (group center edge pile) were monitored during dynamic vertical loading. The data acquisition system was programmed to accommodate seven strain gage channels during any one test, with provisions that a test could be repeated, the gages switched, and a different set of seven strain gage circuits monitored. Those seven bridges (six in the case of Piles 8 and 9) indicating the highest stability were selected in each pile, so that the response of a pile along its full length could be monitored during any given test. The

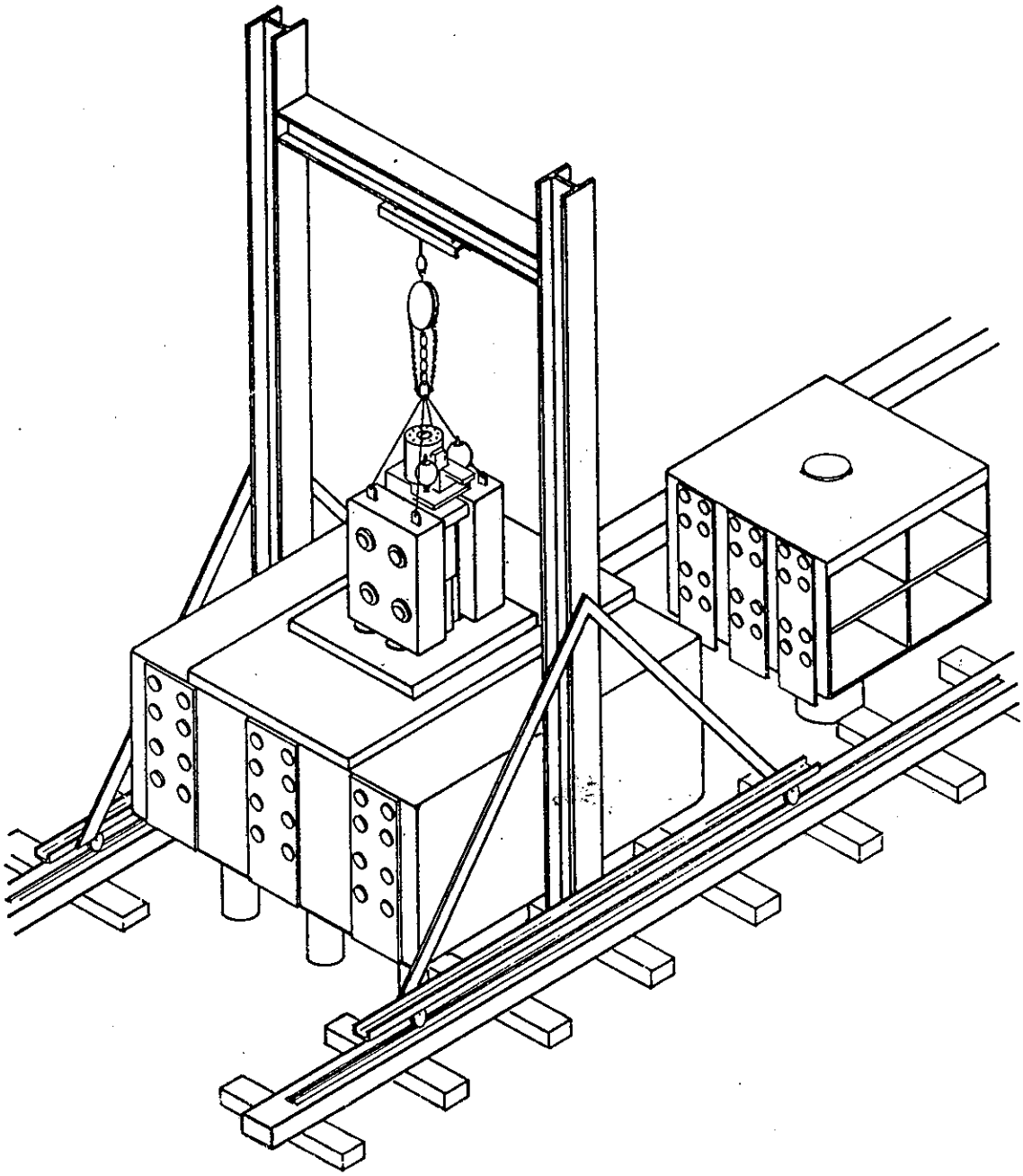

Fig. 5.2. View of Pile Caps, Vibrator, and Service Gantry.

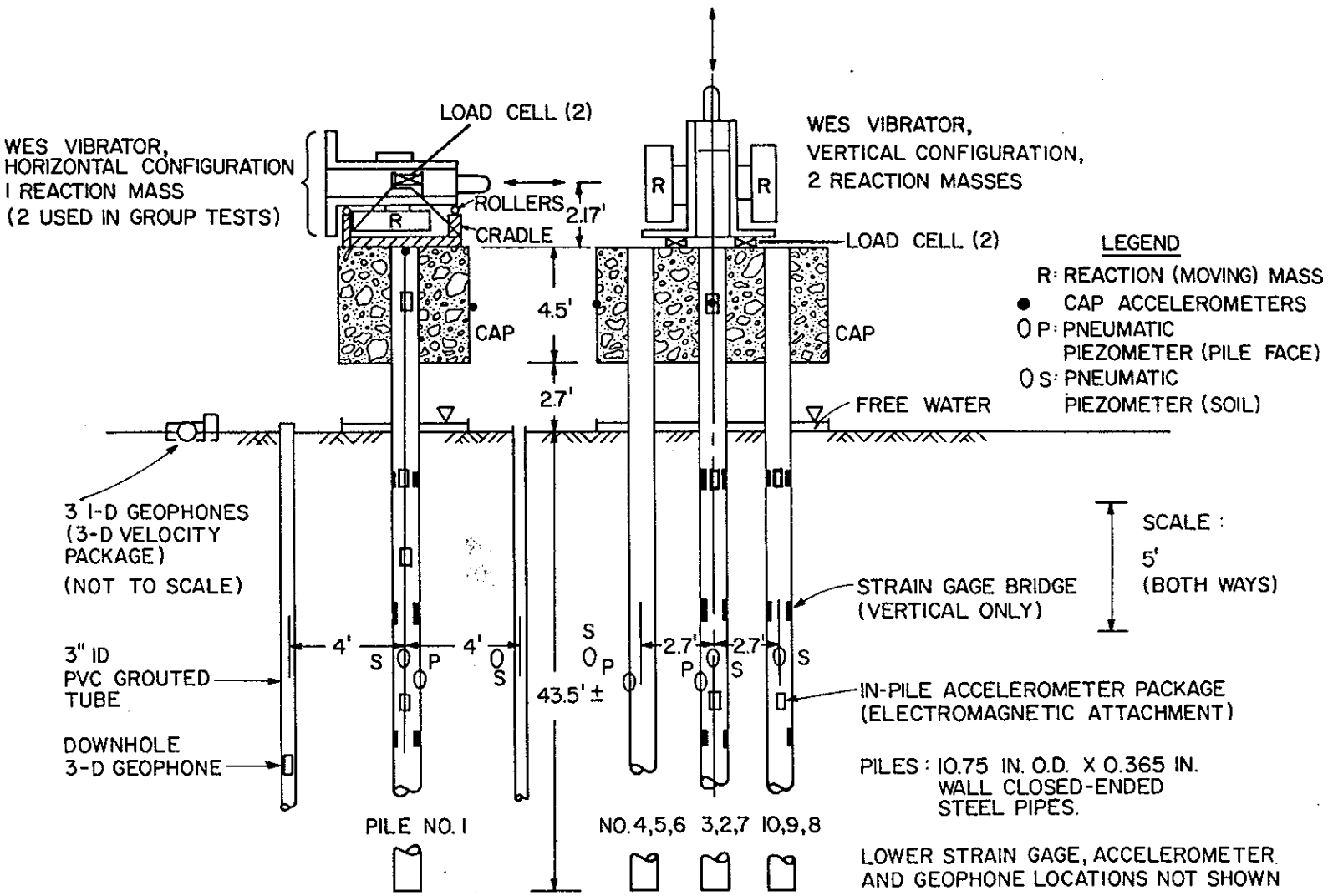

Fig. 5.3. Profile Showing Transducer Locations (1 ft = 0.305 m; 1 in. = 25.4 mm).

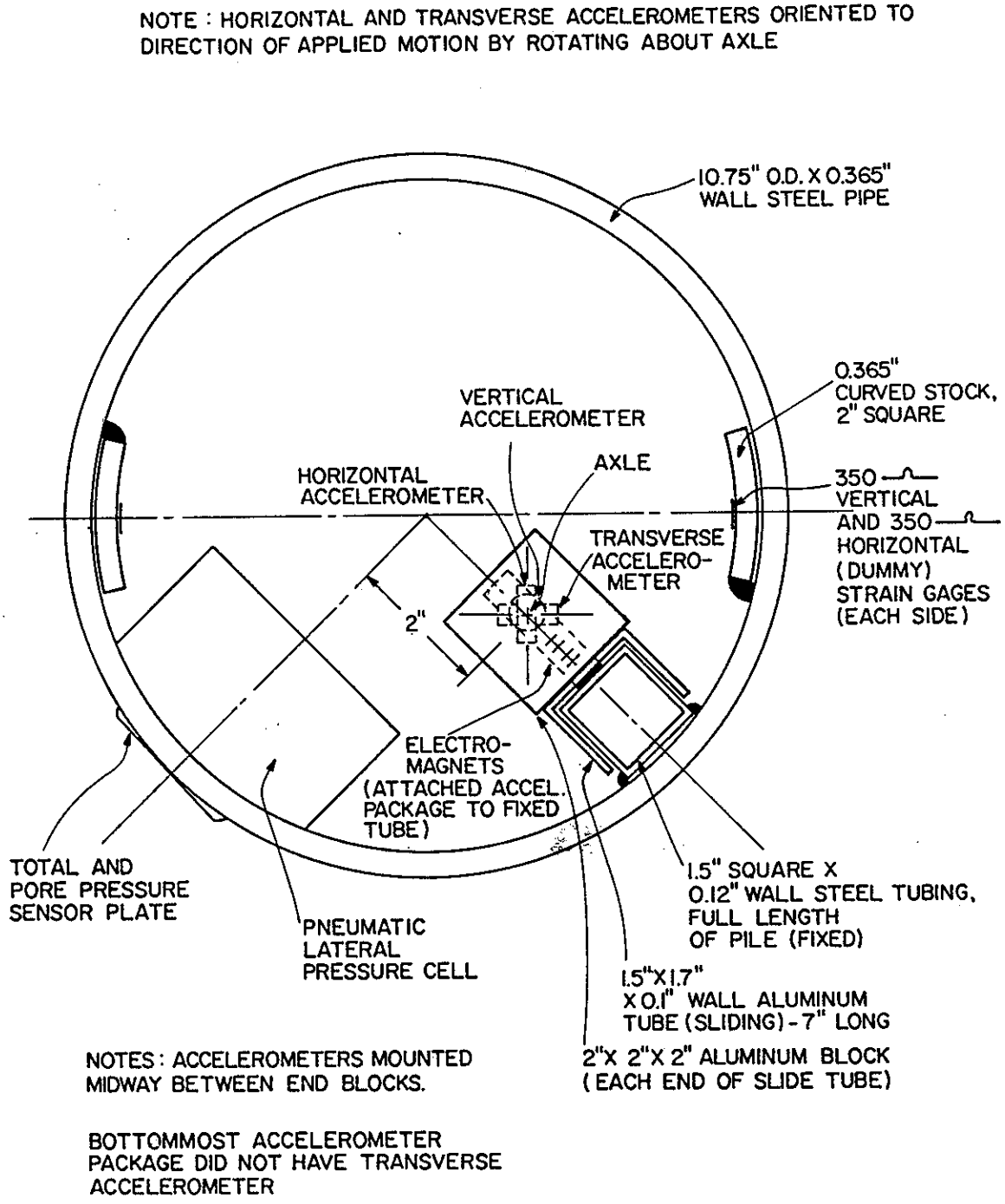

Fig. 5.4. Typical Pile Cross-Section (1 in. = 0.305 m).

designations of the strain gage bridge levels monitored during the dynamic tests and their locations relative to the soil surface are given in Table 5.1. The designations define each instrument in the DCASS 5 data processing system described later in this chapter.

Load Cells

Load cells were mounted between the vibrators and the pile caps. The load cells, which were excercised and calibrated prior to testing, are depicted in Fig. 5.3 as located on the WES vibrator (described in detail later). For the horizontally mounted vibrator (shown on the single pile in Fig. 5.3), the two load cells were attached to a cradle that was bolted to the pile cap and to shoulders on the vibrator. The vibrator itself moved on rollers atop a portion of the cradle, so that it was forced to transmit all of its load through the two load cells. In the vertical configuration (shown on the pile group in Fig. 5.3), the load cells were placed directly between the vibrator frame and steel plates epoxied to the top of the cap, so that again the vibrator transmitted its load through the load cells. The dead weights of the inertial masses was supported by air bags in the vertical configuration.

In each configuration the load cells were restrained by bolting one end to the vibrator and the other end to the cradle or cap. The load cell and vibrator configurations were reversed from the configuration shown in Fig. 5.3 when the single pile was subjected to vertical load and the group was subjected to horizontal load.

The FHWA vibrators were also used to apply some low amplitude forces. Unlike the WES vibrator, which was used as a single vibrator, the FHWA vibrators were used in pairs. For vertical testing they were placed symmetrically on the pile cap, with a bank of four small load cells wired in series between the cap and each vibrator. Each four-cell bank was read as a unit. For horizontal testing the vibrators were mounted on opposite sides of the cap, with the load cell banks bolted to plates epoxied to the sides of the group cap, which was concrete, shown in Fig. 5.2, or to the single pile cap itself, which was steel. Cap details are described later. The dead weights of the FHWA vibrators were supported by air bags during horizontal loading. In the data records the sums of the load cell or load cell bank readings are designated INF4.

Table 5.1. Strain Gage Levels Monitored During Loading
(1 ft = 0.305 m)

Pile	Level Designation	Depth Below Soil Surface (ft.)	Static Test Level Designation (Level No.)
1	P1F0	1.5	1
	P1F1	6.5	2
	P1F2	11.5	3
	P1F3	16.5	4
	P1F4	21.5	5
	P1F7	36.5	8
	P1F9	42.5	10
2	P2F1	6.5	2
	P2F2	11.5	3
	P2F5	26.5	6
	P2F6	31.5	7
	P2F8	39.5	9
	P2F9	42.5	10
8	P8F0	1.5	1
	P8F1	6.5	2
	P8F2	11.5	3
	P8F3	15.5	4
	P8F6	31.5	7
	P8F9	42.5	10
9	P9F0	1.5	1
	P9F1	6.5	2
	P9F3	16.5	4
	P9F5	26.5	6
	P9F8	39.5	9
	P9F9	42.5	10

Notes: All gages were existing full-bridge transducers installed for static tests conducted approx. 18 mos. before dynamic tests. Static calibration factors were used. All bridges were wired to sense axial strains only. Only Pile 1 was monitored during single pile tests and Piles 2, 8, and 9 during group tests.

Accelerometers

Accelerometers were attached to the caps in order to define cap motion in six degrees of freedom during loading. Accelerometers were also affixed to the piles at several levels, down to a depth of 29.5 ft (9.00 m) below the ground surface. Figure 5.4 shows how the down-pile accelerometers were attached to the piles. The down-pile accelerometers were PCB 308 B piezoelectric accelerometers (except as described later) that were placed in triaxial packages attached to aluminum tubes that slid along permanent steel tube tracks mounted inside the pile. When a package had been lowered to the required depth, it was affixed to the steel tube by electromagnets. An axle in the package permitted the two horizontal accelerometers to be oriented in the direction of and transverse to the direction of the applied load. These down-pile triaxial accelerometer packages were designated AP1 - AP4 and placed at the depths shown in Figs. 5.5 and 5.6 for the single pile and group tests, respectively. An additional designator, V, H, or T (vertical, horizontal, or transverse), follows the package number on the test records. This added designation is used for all 3-d or 2-d transducers, including geophones.

Three biaxial accelerometer packages (no transverse component), consisting of two PCB 393 B seismic accelerometers were also constructed and affixed to the piles at the lowest level at which pile acceleration measurements were attempted (29.5 ft (9.00 m) below grade). These accelerometers are more sensitive than the PCB 308 B accelerometers used at the higher elevations. They were lowered into each pile and attached to the guide tube in a manner similar to that described above for the triaxial accelerometer packages. These packages were designated AP5 - AP7.

It is observed in Fig. 5.4 that the centers of the horizontal accelerometers were 2 in. (50 mm) from the axis of the pile. This offset was assumed to be of negligible importance when interpreting horizontal data.

The cap accelerometers, shown in Figs. 5.4, 5.5, and 5.6, were also PCB 308 B piezoelectric accelerometers. They were placed singly in the positions and attitudes shown and designated AP19, AP20, and AP21

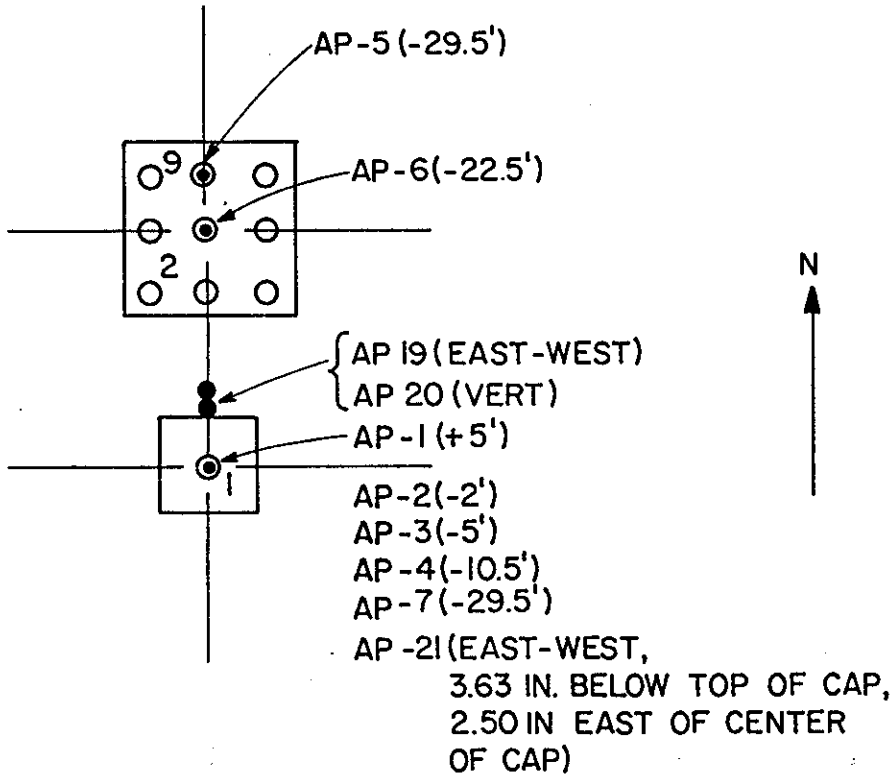

NOTES :

1. AP (ACCELEROM PACKAGE) 1-4 WERE 3-D PIEZOELECTRIC ACCELEROMETERS (HORIZONTAL : N-S; TRANSVERSE : E-W; AND VERTICAL COMPONENTS).

2. AP 5-7 WERE 2-D SEISMIC PIEZOELECTRIC ACCELEROMETERS (HORIZONTAL : N-S; AND VERTICAL COMPONENTS).

3. AP 19 AND 20 WERE 1-D PIEZOELECTRIC ACCELEROMETERS AFFIXED TO CENTROID OF NORTH FACE OF CAP, 59 IN. (1.50 M) ABOVE GROUND SURFACE

4. AP 21 WAS 1-D ACCELEROMETER AFFIXED TO INSIDE OF PILE 1 , AS INDICATED.

Fig. 5.5. Accelerometer Locations for Single Pile Tests (1 ft = 0.305 m).

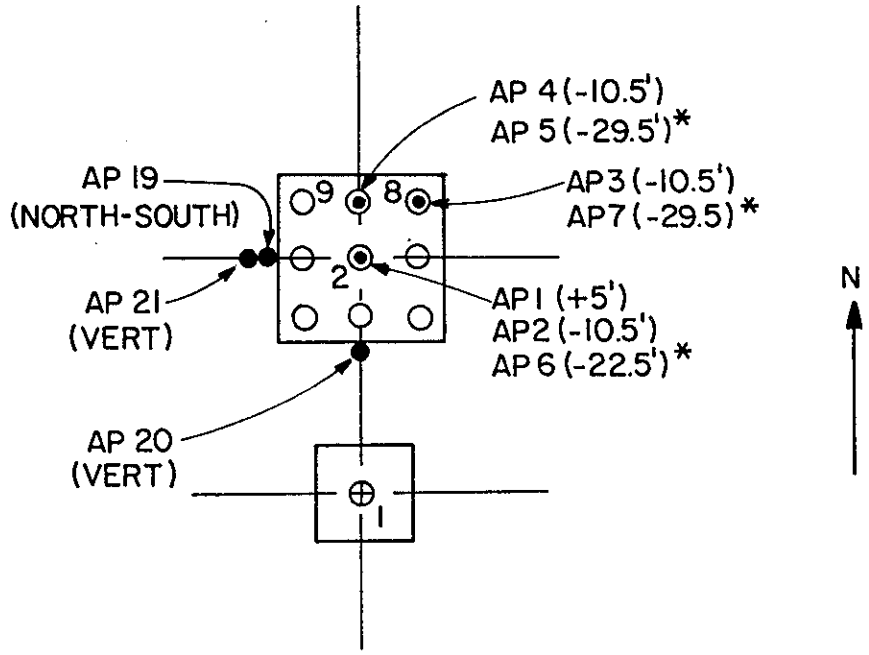

NOTES :

1. AP (ACCELEROM PACKAGE) 1-4 WERE 3-D PIEZOELECTRIC ACCELEROMETERS (HORIZONTAL : N-S; TRANSVERSE : E-W; AND VERTICAL COMPONENTS).

* 2. AP 5-7 WERE 2-D SEISMIC PIEZOELECTRIC ACCELEROMETERS (HORIZONTAL : N-S; AND VERTICAL COMPONENTS).

3. AP 19 AND 21 WERE 1-D PIEZOELECTRIC ACCELEROMETERS AFFIXED TO CENTROID OF WEST FACE OF CAP, 59 IN. (1.50 M) ABOVE GROUND SURFACE.

4. AP 20 WAS 1-D PIEZOELECTRIC ACCELEROMETER AFFIXED TO CENTROID OF SOUTH FACE OF CAP, 59 IN. (1.50 M) ABOVE GROUND SURFACE.

Fig. 5.6. Accelerometer Locations for Group Tests (1 ft = 0.305 m).

individually. These accelerometers, together with the down-pile packages in the cap, permitted measurements of cap motion in three orthogonal directions and rotations about three orthogonal cap axes.

Relevant accelerometer calibration data, obtained from the manufacturer and verified by tests in the UHCC structural mechanics laboratory using a servo-controlled MTS testing machine, are given in Appendix D. As used in the experiments, the frequency response was essentially flat (< 0.2% error) down to 20 Hz, with a very gradual rolloff below 20 Hz. The response at 10 Hz was 0.66 % below its flat value; at 4 Hz it was 4% below its flat value; at 2 Hz it was 19% below its flat value; and at 1 Hz it was 28.4% low. The frequency response has little impact on the data acquired above frequencies of 4 Hz (i.e., all relevant data for vertical tests and for horizontal group tests). In the very low frequency tests (i.e., horizontal single pile tests where relevant data were below 4 Hz), the measured amplitudes of acceleration were somewhat below the true values.

The accelerometers were used to measure accelerations directly and also to measure displacements by employing harmonic motion theory during data reduction. The acceleration amplitude values in the computed raw fast Fourier transform of the data were divided by the respective squares of the corresponding circular frequencies to obtain displacements.

Geophones

Geophones, or velocity transducers, were placed on the soil surface and in grouted PVC pipes to a depth of 29.5 ft (9.00 m) beneath the soil surface in order to obtain insights into wave transmission from the single pile and pile group into the soil. In addition, a few geophones were affixed to the outsides of the piles to provide pile response data supplementary to those data obtained from the strain gages and accelerometers.

The primary geophone transducer was the Geospace HS-10, which is a low-frequency rolloff geophone. The HS-10 geophones were placed as triaxial surface packages (Fig. 5.3), designated VP9 - VP16, at the locations shown in Fig. 5.7 (single pile tests) and Fig. 5.8 (group tests).

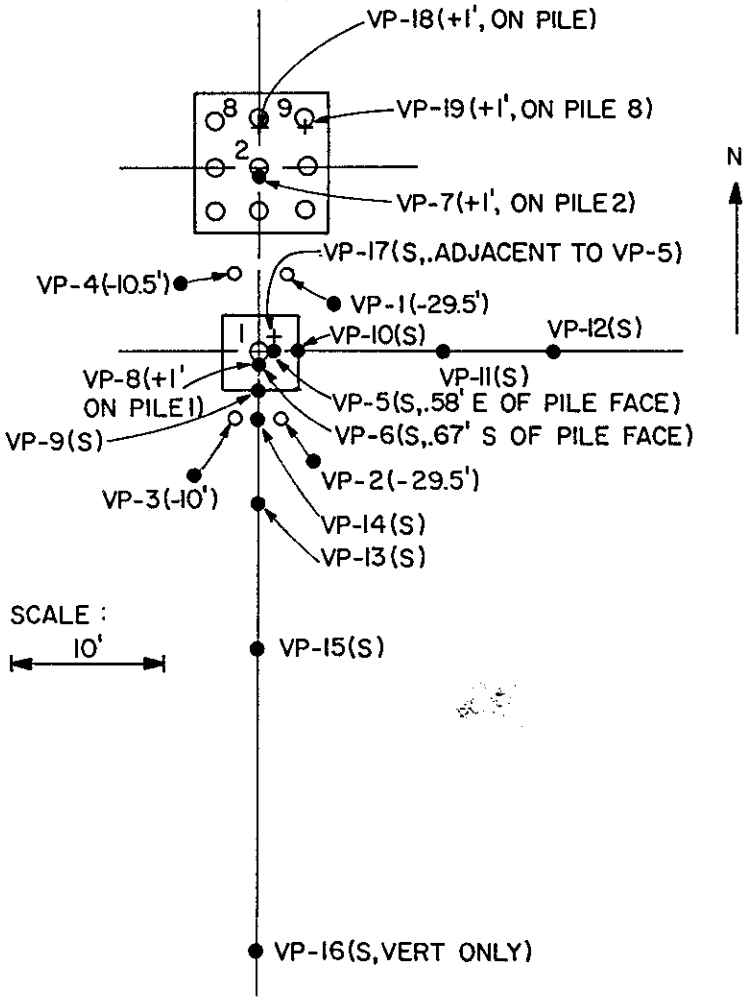

Fig. 5.7. Geophone Locations for Single Pile Tests (1 ft = 0.305 m).

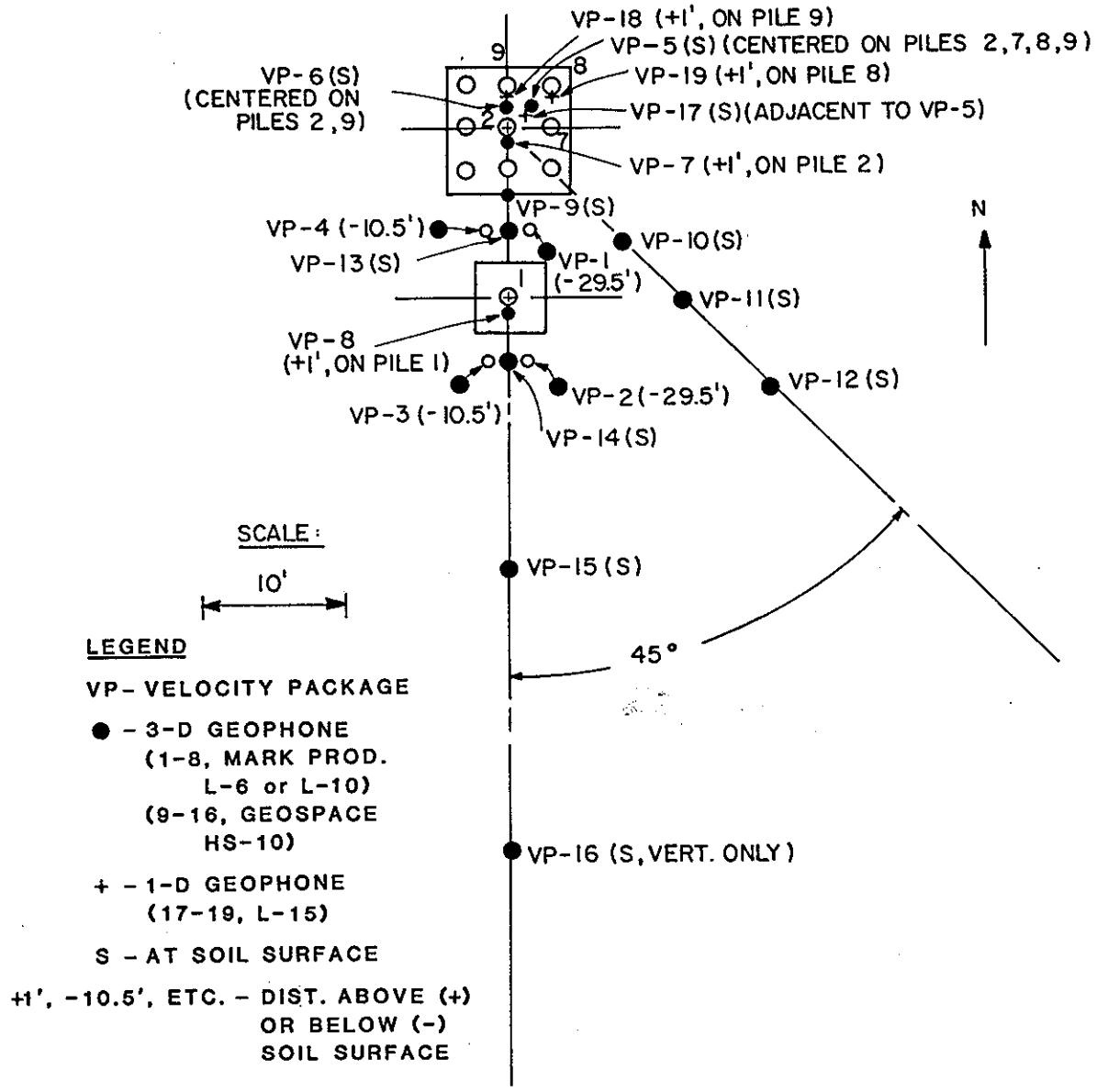

Fig. 5.8. Geophone Locations for Group Tests (1 ft = 0.305 m).

Typical calibration data for the HS-10 geophones are given in Appendix D. The natural frequency of the HS-10 is about 1.0 Hz, and only minor (10%) rolloff is observed above 1.5 Hz.

The downhole geophone packages, designated VP1 - VP4, were also triaxial packages containing geophones of digital quality. In these packages, three orthogonal geophones were placed inside a sealed aluminimum case. The downhole packages, VP1 - VP4, were lowered down grouted PVC pipes (Fig. 5.3) to the depths indicated in Figs. 5.7 and 5.8 and wedged against the pipes with mechanical wedges. Four other similar packages, VP5 - VP8, were placed either on piles or in the soil at the soil surface between piles in the group. Packages VP1 - VP8 consisted of Mark Products L-6 or L-10 geophones, which roll off at about 10 Hz. These geophones were of limited use for single pile horizontal test, in which most frequencies of interest were below 4 Hz. Manufacturers' calibrations were used for VP1 - VP8, and a typical set of calibration curves is shown in Appendix D.

Several one-directional (vertical) 4.5 Hz geophones of the Mark Products L-15 type were placed at the soil surface and on the piles within the group. These geophones were designated VP17 - VP19.

A total of 51 geophones was employed. Considering the number of load cells, strain gages, and accelerometers used and the 60-channel limitations of the data acquisition equipment, it was not possible to read all gelphone channels during every test.

Geophone (velocity) data were converted to displacements during data reduction in a manner similar to that employed in the conversion of accelerometer data, except that frequency domain velocity amplitude values were divided by the first power of the circular frequencies.

Piezometers

Several pneumatic piezometers were located in the faces of Piles 1, 2, 3, 4, and 5 at depths of 10, 35, and 42 ft (3.05, 10.7, and 12.8 m) below the soil surface, as shown schematically in Figs. 5.3 and 5.4. Additional pneumatic piezometers were situated in the soil at a depth of 9 ft (2.7 m) near the piles as shown in Fig. 5.3 (63). The soil piezometers marked S in Fig. 5.3 that appear to be on the surfaces of Piles

1, 2 and 9 are actually located 1 ft (0.3 m) west of Pile 1, midway between Piles 2 and 7, and midway between Piles 8 and 9. Other piezometers, for which data were not taken, were situated in the soil at greater depths (63). Acquisition of piezometer data was manual. An air-activated pressure gage which required about 10 seconds to stabilize was employed. Pore pressure peaks produced by dynamic impulses could not be detected with this system, which was the system used in the earlier static tests.

PILE CAP PROPERTIES

Pile caps were welded to the tops of the single test pile and the 9-pile group to accommodate the vibrators and to provide a small static load bias to the piles .

Single Pile

The cap for Pile 1 is shown conceptually in Fig. 5.9, with additional detail given in Fig. 5.10. The cap was essentially a plate steel box 5 ft (1.53 m) square in plan and 4.5 ft (1.37 m) high. The north and south quadrants of the box were filled with semi-lightweight concrete (density of 135 pcf (21.3 kN/m^3)), while the east and west quadrants remained open. This was done to produce a relatively lightweight cap that applied a vertical static load to the pile as nearly equal to the loads applied to the group piles as possibly, commensurate with maintenance of cap rigidity, in order to afford a means of comparing group and single pile response. The base of the cap was 32 in. (0.81 m) above the general soil surface. A small indentation in the ground about 4 in. (0.81 mm) deep was present around all 10 piles tested, so that the distance from the cap base to the first possible point of pile-soil contact was 36 in. (0.92 m). This was the free-standing pile length modeled mathematically (Chapter 6).

The numbered items on Fig. 5.10 are as follows:

1. 0.5 in. (12.7 mm) steel plate (2),
2. 0.375 in. (9.5 mm) steel plate (4),
3. 0.375 in. (9.5 mm) steel plate (2),

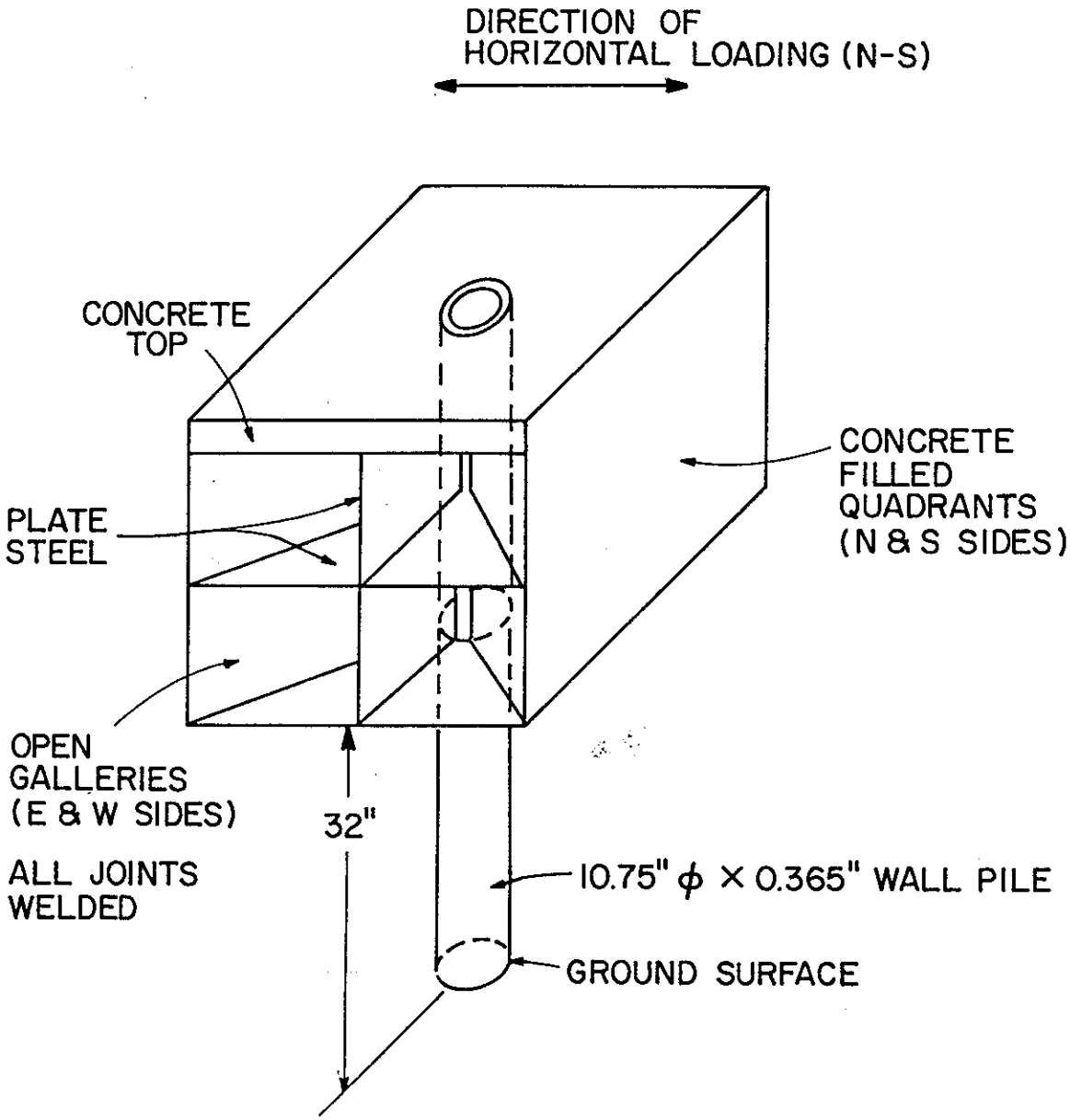

Fig. 5.9. General View of Single Pile Cap (1 in. = 25.4 mm).

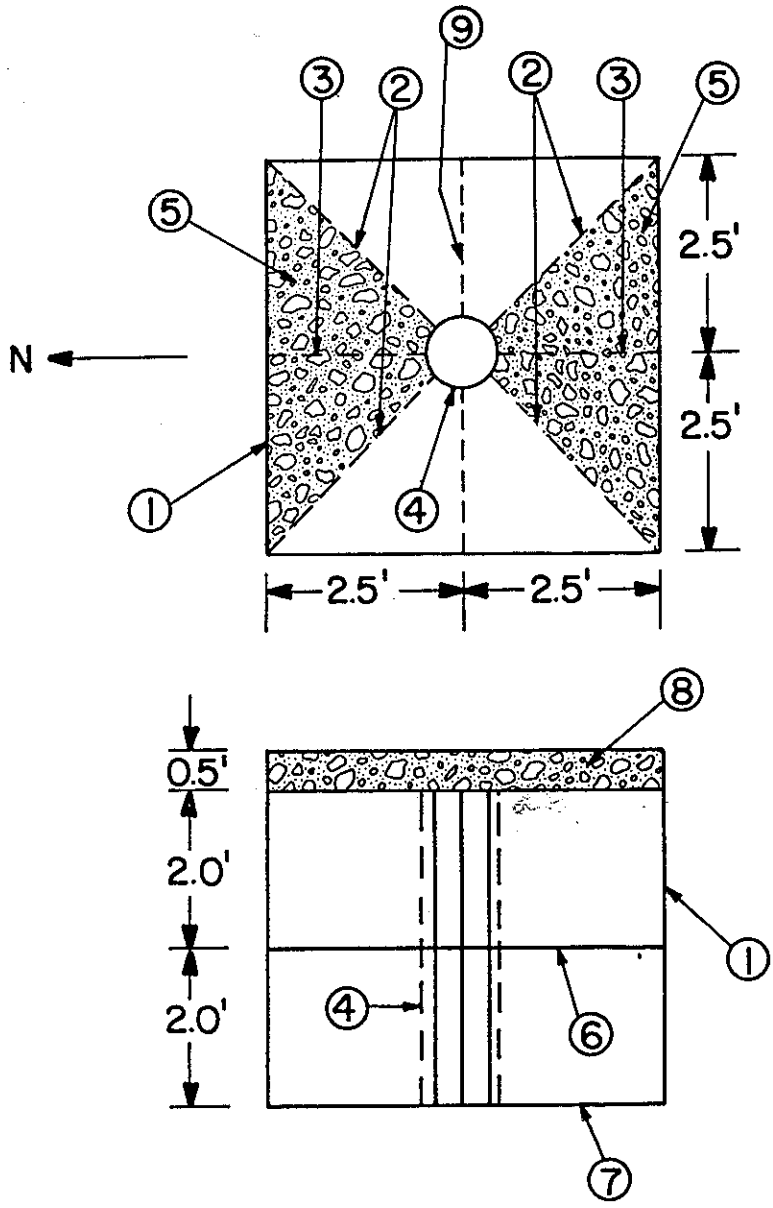

Fig. 5.10. Details of Single Pile Cap (1 ft = 0.305 m).

4. 10.75 in. (273 mm) o.d. by 0.365 in. (9.27 mm) wall steel pipe (open at top),
5. Semi-lightweight concrete filler,
6. 0.5 in. (12.7 mm) steel plate (2),
7. 0.5 in. (12.7 mm) steel plate (2),
8. Concrete surface (unit weight of 150 pcf (23.6 kN/m^3), covering entire surface,
9. 0.375 in. (9.5 mm) steel plate (2).

Figure 5.11 shows an elevation view of the cap, looking east, with the vibrators shown schematically in place. The WES vibrator is shown atop the pile cap in both the vertical and horizontal loading arrangements. The FHWA vibrators are shown affixed to the sides of the cap through the load cell banks (denoted L) for the horizontal loading case. The FHWA vibrator was not used to apply vertical loads to the single pile. Figure 5.11 gives the distances of the lines of lateral load application from points of reference on the cap and also shows generically the distance of the center of gravity (CG) above the cap base, z_c, and the distance from the CG to AP1, z_a. The quantity z_c was calculated by computing the weight and center of gravity of the cap from the data in Fig. 5.10 and all other components vibrating in phase with the cap. Static weights of the vibrators themselves were not included in the calculations of translational pile response from mathematical models (chapter 6) because they can be eliminated in mathematical models from the cap-pile-soil free body by replacement of their inertia effects with the known forces measured by the load cells. Values for cap weight, z_c, z_a, and vibrator weight (excluded from the mathematical models) are given in Table 5.2.

Although the vibrator masses can be excluded for computing translational response, they cannot be neglected for rotational response, because the moment applied to the cap through either the rollers (WES) or the load cell banks (FHWA) was not measured. Hence, mass moments of inertia of the cap-vibrator system about the cap CG, whose location was computed assuming all vibrators masses as contributing, were necessary mathematical model inputs (Chapter 6). Therefore, their values were calculated and are presented Table 5.2. The designation 0, 1, or 2 Rem

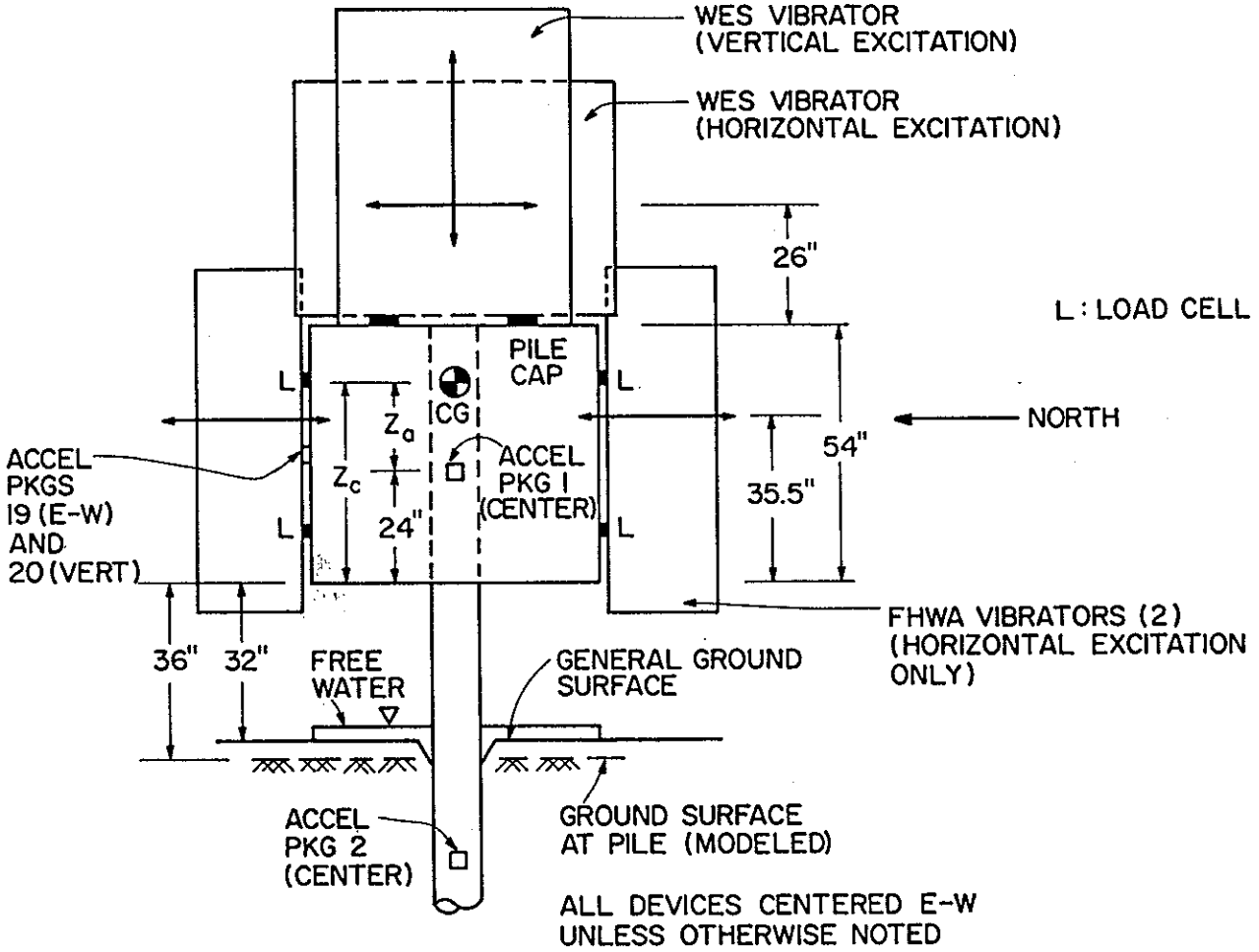

Fig. 5.11. Elevation of Single Pile Cap (1 in. = 25.4 mm).

Table 5.2. Summary Of Mass And Inertia Properties For Pile Caps And Vibrators: Analytical Studies (1 lb = 4.45 N; 1 ft = 0.305 m)

Cap/ Vibrator Case	Cap Wgt.[a] (lb.)	Vibrator Wgt.[b] (lb.)	Total Wgt. (lb.)	Wgt. Per Pile Used In Response Analyses (lb.)	Z_c (ft.)	Mass Moment Of Inertia About C.G. Of Cap ($lb\text{-}sec^2\text{-}ft$)	Z_a (ft.)
Single/ Vertical/ WES/0 Rem	12,425	5275	17,700	12,425	-	-	-
Single/ Vertical/ WES/2 Rem	12,425	16,460	28,885	12,425	-	-	-
Single/ Horizontal/ FHWA	11,825	2276	14,101	11,825	2.49	2783	0.49
Single/ Horizontal/ WES/1 Rem	13,825	11,075	24,900	13,825	4.25	4916	2.25
Group/ Vertical/ FHWA	55,440	2276	57,716	6160	-	-	-
Group/ Vertical/ WES/2 Rem	56,040	16,460	72,500	6227	-	-	-
Group/ Horizontal/ WES/2 Rem	57,440	16,460	73,900	6382	3.32	23,906	1.32

a. Values used to compute masses in analytical studies-translational modes (includes support cradle for WES vibrator).
b. Not used in computing translational mass but was used in computing rotational mass moments of inertia.

following the WES vibrator designation in Table 5.2 refers to the number of reaction masses (Rem) affixed to the vibrator for a particular test. Vibrator details are considered later in this chapter.

Pile Group

The group cap is shown in Fig. 5.12. The piles protruded through the cap, which was precast and constructed of heavily reinforced concrete. The piles were left open for access at the top. A cast-in-place concrete cover 3 in. (75 mm) thick was placed on the cast-in-place concrete to reinforce the steel vibrator mounting plates and to provide a cap equal in thickness to that of the single pile cap. All concrete in the group cap had a unit weight of approximately 150 pcf (23.6 kN/m^3).

All tests on the pile group were conducted with the vibrators mounted atop the cap, as shown in Fig. 5.13, which gives relevant dimensions. The FHWA vibrators were used in vertical and rocking tests, while the WES vibrator was used in vertical and horizontal tests.

As with the single pile cap, the vibrator masses were not included in the cap mass for purposes of modeling dynamic response, but the group mass moments of inertia were included in model computations (Chapter 6). Relevant group mass details and appropriate dimensions are given in Table 5.2.

VIBRATORS

FHWA Vibrators

The FHWA vibrators were tandem unbalanced-force counter-rotating mass units, Type RVCG-10,000, manufactured by L.A.B. Corporation. See Fig. 5.14. The load amplitude was controlled by monitoring pressure in the pneumatic system that controlled the gas eccentric fluid mass in the rotating vibrator cylinders. The frequency was controlled by controlling the frequency of a Varidyne electric motor, which powered the vibrators.

The FHWA vibrators were used in tandem, either in phase (vertical tests) or 180 degrees out of phase (rocking and horizontal tests). The phase between the two vibrators was controlled through the Varidyne using the manual controller. The controller was also capable of generating pre-programmed sweeps (continuous vibration at constant force amplitude with continuously varying frequency).

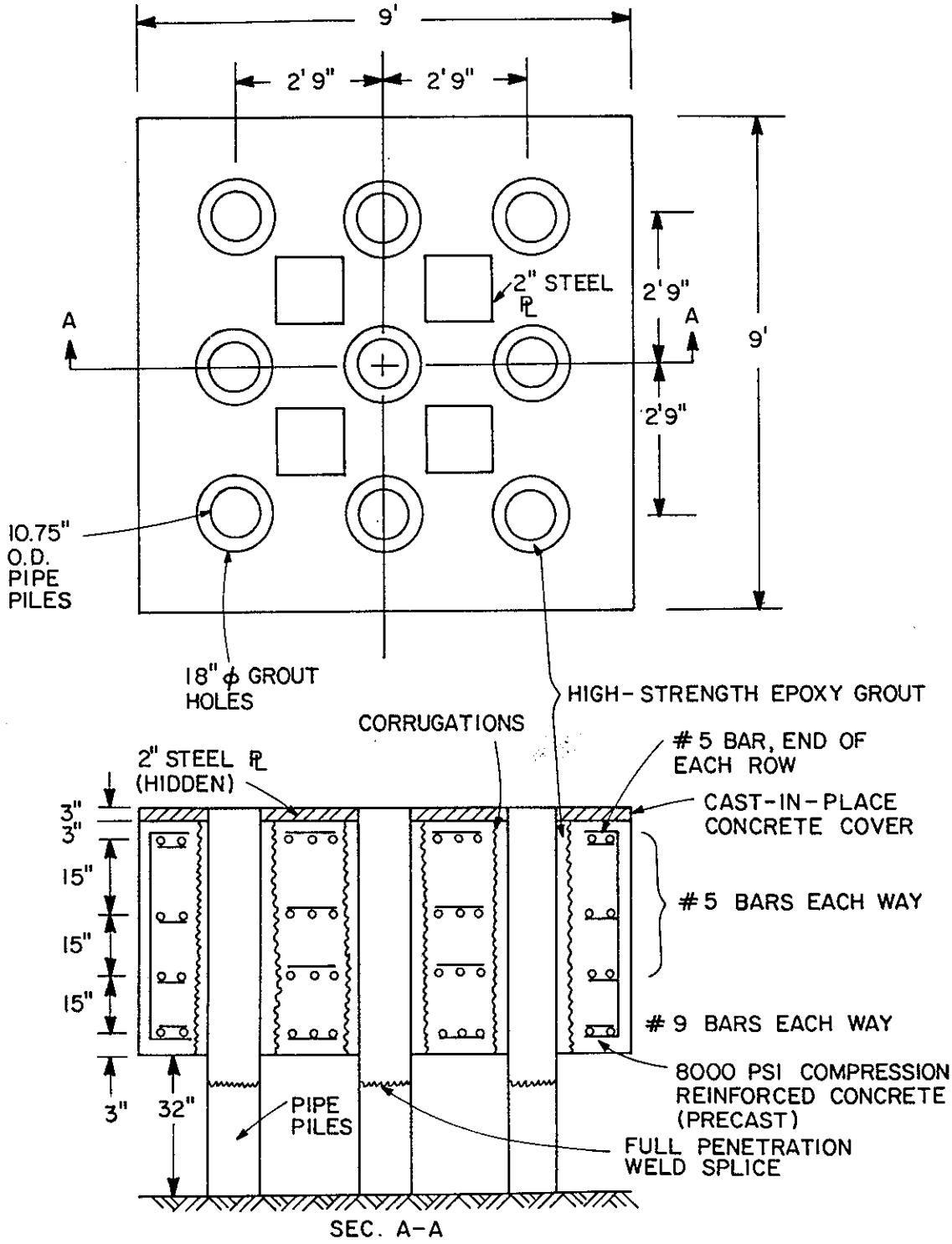

Fig. 5.12. Details of Group Cap (1 ft = 0.305 m; 1 in. = 25.4 mm; 1 psi = 6.89 kPa).

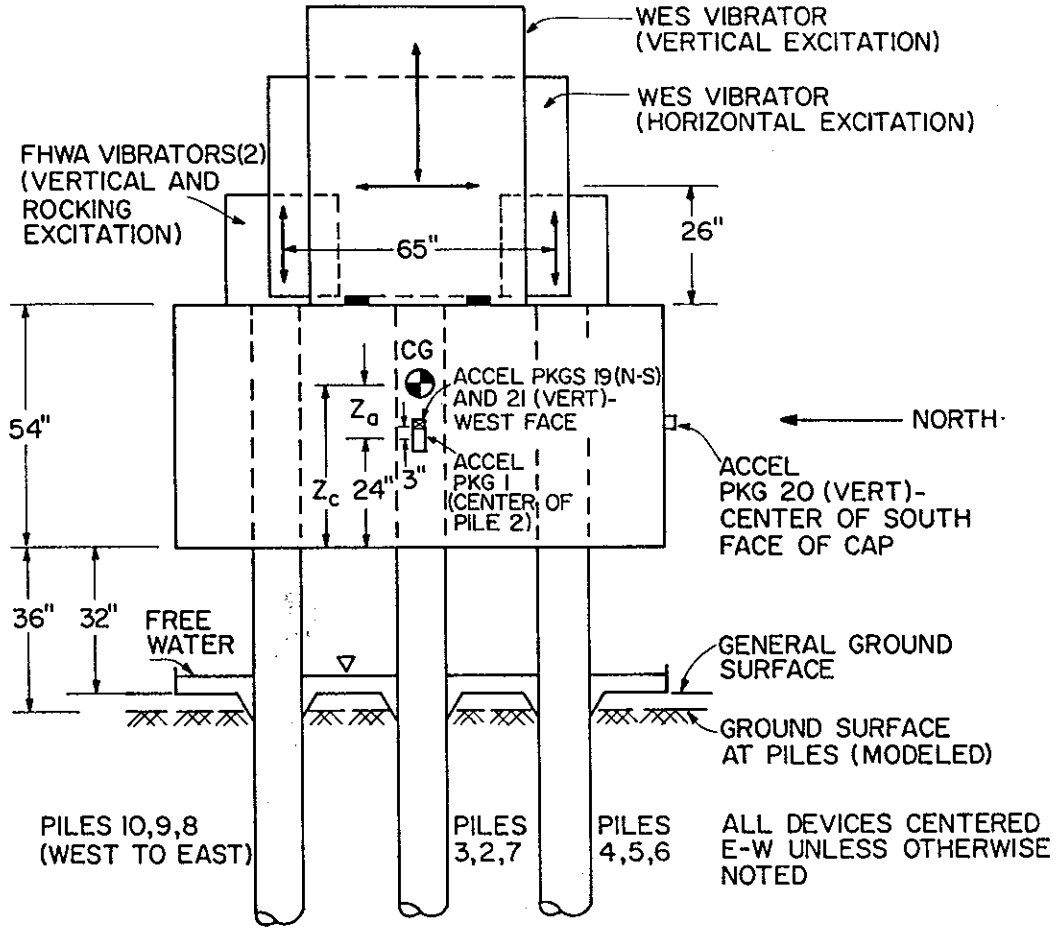

Fig. 5.13. Elevation of Group Cap (1 in. = 25.4 mm).

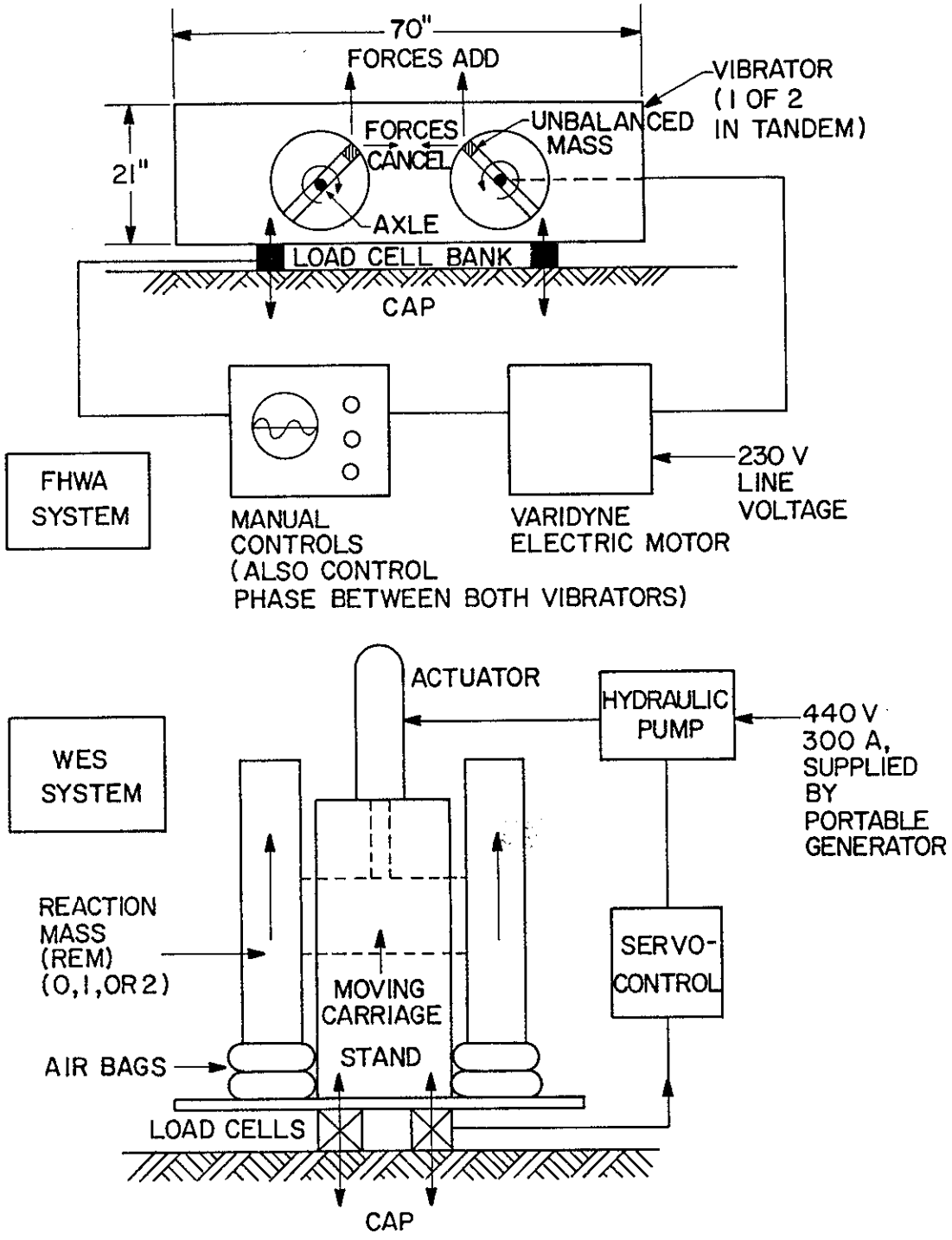

Fig. 5.14. Schematics of FHWA and WES Vibrator Operation (1 in. = 25.4 mm).

The FHWA vibrators had maximum design outputs of 10,000 lb (44.5 kN) each and were capable of applying loads in the frequency range of 1.8 to 47.5 Hz, with lower frequencies possible by manual cranking. The full force output could not be achieved below a frequency of 22 Hz. Problems with fluid mass seals prevented the application of peak design amplitudes in the present tests, requiring the use of the WES vibrator, described subsequently, for the higher load amplitudes.

Each vibrator weighed 729 lb (3.24 kN), and each load cell bank, together with the steel plate to which the load cells were mounted, weighed 409 lb (1.82 kN). The total weight of the tandem vibrators and the pair of load cell banks was 2276 lb (10.13 kN).

WES Vibrator

The WES vibrator system is depicted schematically in Fig. 5.14. It was manufactured as a one-of-a-kind instrument by personnel at the U.S.A.E. Waterways Experiment Station in Vicksburg, Mississippi. The WES vibrator was a hydraulically actuated linear inertial mass vibrator with a closed loop hydraulic and control system. In principle, the vibrator operated by moving a carriage and (if desired) reaction masses translationally at a prescribed frequency or through a sweep. The vibrator stand (stationary frame) weighed 4375 lb (19.5 kN). The reaction masses weighed approximately 5770 lb (25.7 kN) each, and the moving parts of the ram and carriage weighed 900 lb (4.01 kN). The reaction masses were detachable and the maximum load amplitude available was controlled by the number of reaction masses that were used. With both reaction masses in place, the vibrator was capable of generating a force amplitude of 50,000 lb (222.5 kN) in the frequency range of 25 to 50 Hz. Below 25 and above 50 Hz, rolloffs in force occurred: at 15 Hz, max. force = 40,000 lb (178 kN); at 10 Hz, max. force = 30,000 lb (133.5 kN); at 5 Hz, max. force = 15,000 lb (66.8 kN); at 2 Hz, max. force = 5,000 lb (22.3 kN); and at 1 Hz, max. force = 2,200 lb (9.79 kN); at 70 Hz, max. force = 30,000 lb (133.5 kN); and at 90 Hz, max. force = 15,000 lb (66.8 kN).

In Fig. 5.14 the WES vibrator is shown in the vertical loading configuration. In that mode air bags were used as shown to prevent jerk forces from damaging the actuator. These bags, which acted as soft springs, had a minor effect on system response. They were not used when the vibrator was mounted horizontally. In the vertical mode a small frame (weight of 600 lb (2.67 kN)) was affixed to the pile cap to balance the vibrator. The mass of that frame was assumed to vibrate in phase with the cap and was included in cap mass, CG, and mass moment of inertia computation.

When the vibrator was used horizontally (Fig. 5.3), the vertical balancing frame was removed, and a larger steel cradle was attached to the pile cap. This cradle was fitted with rollers for the entire vibrator to roll along, and horizontal mounts for the load cells, which were placed horizontally between the stand (stationary frame) and the cradle. This arrangement permitted essentially all of the unbalanced force generated by the vibrator to pass through the load cells. The weight of the horizontal carriage was 2000 lb (8.90 kN), which was added to the cap weight. The difference in the weight of the horizontal carriage and the vertical balance frame accounts for the differences in cap weights between horizontal and vertical tests recorded in Table 5.2.

The WES vibrator servo-control system operated by sensing load cell outputs. During a frequency sweep the load varied as the pile head stiffness changed. It was not possible for the servo-controller to respond to these changes quickly enough to produce constant force output. This necessitated the use of transfer function analysis of the sweep data, described later in this chapter. Force level variability is discussed in Chapter 7.

DATA ACQUISITION

The electronic data acquisition system is depicted schematically in Fig. 5.15. The outputs from the accelerometers, strain gages (and load cells), HS-10 geophones, and Mark-type geophones were all directed into a patch panel, which was used to select the instruments that would be read for a given test. The geophones operate on an electrical induction principle and so did not require power. The accelerometers did require small battery (d.c.) units for activation, and the strain gages and load

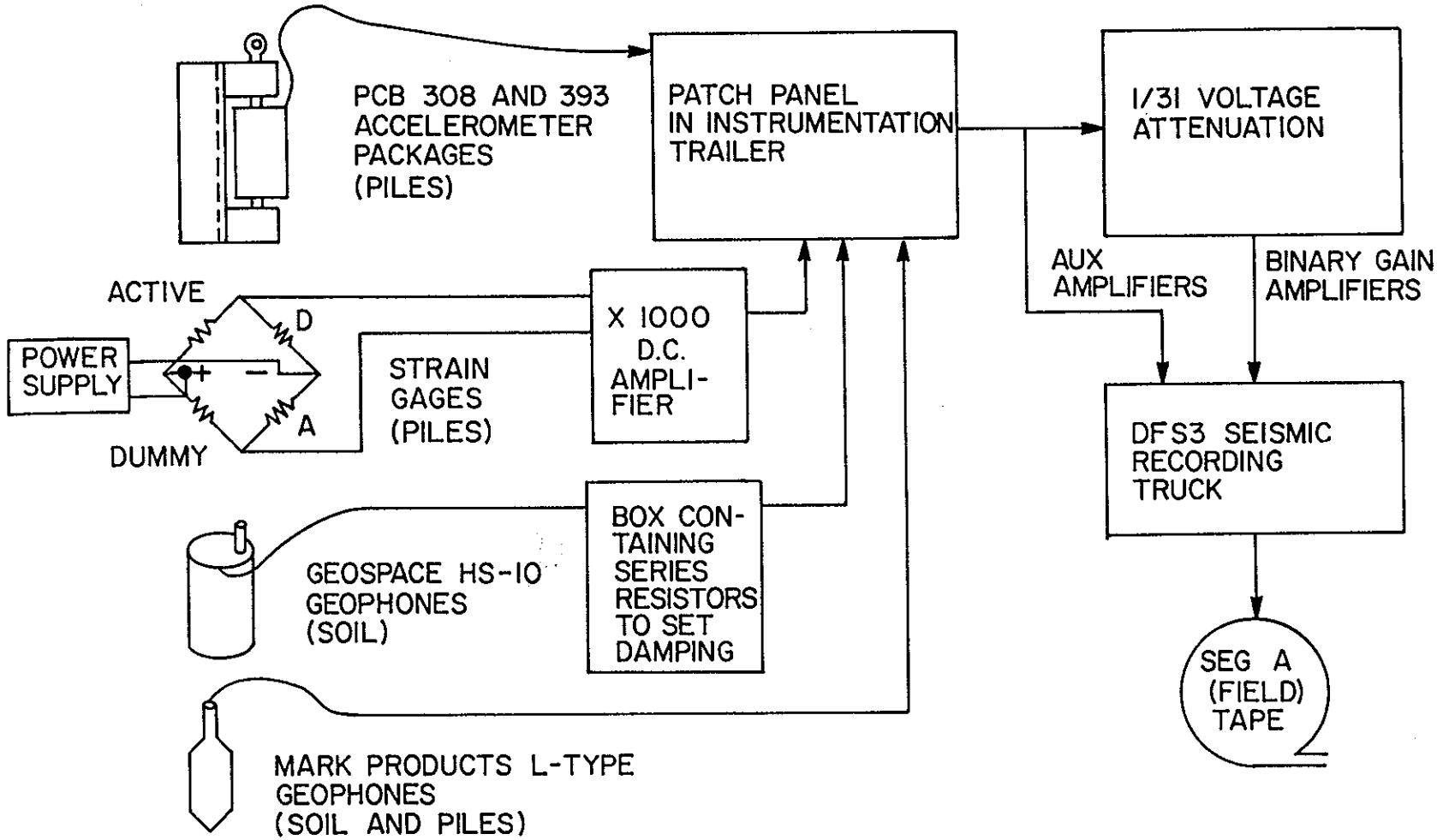

Fig. 5.15. Schematic of Data Acquisition.

cells required application of precise d.c. voltages from a power supply. The strain gage signals were post-amplified by constant gain amplifiers before feeding into the patch panel, and precision resistors were placed in the geophone circuits to provide electrical damping in order to affect flat output above the natural frequencies of the instruments.

From the patch panel 60 channels of continuous signals were fed into the data recording truck. Channels 1-48 were subjected to a 1/31 voltage attenuation and then passed through automatic binary gain amplifiers to a digital magnetic tape recorder. Channels 49-60 (termed auxiliary channels) bypassed the voltage attenuator and passed through a set of constant gain amplifiers to the digital tape recorder. The recording system was a Texas Instruments DFS3 seismic recorder that produced multiplexed field tapes in a format termed "Society of Exploration Geophysicists Format A" (or simply SEG A). Each test was assigned a "field record number" that was recorded on a header file on the tape. The record numbers are used for referencing the test data records later in this report. Four to six field test records were normally made on each magnetic tape. The notation of which instrument appeared on a given channel during any test was made manually in a field note book. Later, when the field tapes were processed into "DCASS" (FORTRAN-formatted) tapes, the channel number-instrument coupling was entered and recorded on the header for each channel. Thus, the processed (DCASS) tapes contain instrument identificantion headers, while the field tapes do not.

Since budgetary limitations prohibited processing of all the field records that were made during the course of the study, research sponsors may wish to perform further processing of field tapes on thier own. In such a case, it will be necessary to obtain copies of the field notes in order to associate data channels with instruments. These notes are archived at the UHCC Department of Civil Engineering.

In general the geophone and load cell data were placed on the auxiliary channels (49-60). The WES vibrator load cells, as recorded on the auxiliary channels, are designated AIF5 and AIF6 (independent readings for individual cells or banks) and AIF4 (sum of AIF5 and AIF6). Strain gage designation is as described previously. The binary gain

channels (1-48) were also used for redundant load cell readings (INF4), strain gages, accelerometers, and selected geophones.

Data were sampled in all tests at time intervals of 2 milliseconds, and record lengths were typically 32 seconds each, which was also the approximate length of each vibration test. This sampling procedure provided approximately 16,000 data points per channel per test, which were recorded on the field tapes. During data processing on the VAX 11/780 minicomputer system, it was found that a maximum of 8001 data points could be handled conveniently per channel, so that only every other recorded data point was used in developing processed data. The resulting time increment of four milliseconds was adequate to replicate frequency contents up to about 125 Hz.

The signal flow in the data recording truck, through the amplifiers and tape recorder, is shown in Fig. 5.16. The primary channels (1-48) went to four, 12-channel binary gain amplifier modules that automatically increased the signal gain by successive factors of 2 until a specified voltage level was achieved.

The gain level was recorded at constant intervals within the digital data series. The amplified signals were then passed through a multiplexing unit and a converter/multiplexer that formatted the multiplexed signals in SEG A, and, finally, the signals were stored in digitized form on the 9-track magnetic tape. The auxiliary channels followed a similar path, except that the binary gain amplifiers were bypassed.

Errors inherent in the amplification process were studied independently and assessed. A summary of the errors produced on an amplified signal produced by a calibrated reference signal of known output is given in Appendix D. Average errors (for all channels) were 1% or less below 100 Hz, except at 1 Hz, where the error was about 1.6%. Errors for specific channels are also given in Appendix D. Specifications for the converter/multiplexer unit are also given in Apendix D.

Finally, two suites of data were acquired manually. The first, optical measurements of pile head translation using surveyor's transits, proved unsuccessful because the transits could not be isolated from the ground vibrations produced by the vibrating piles.

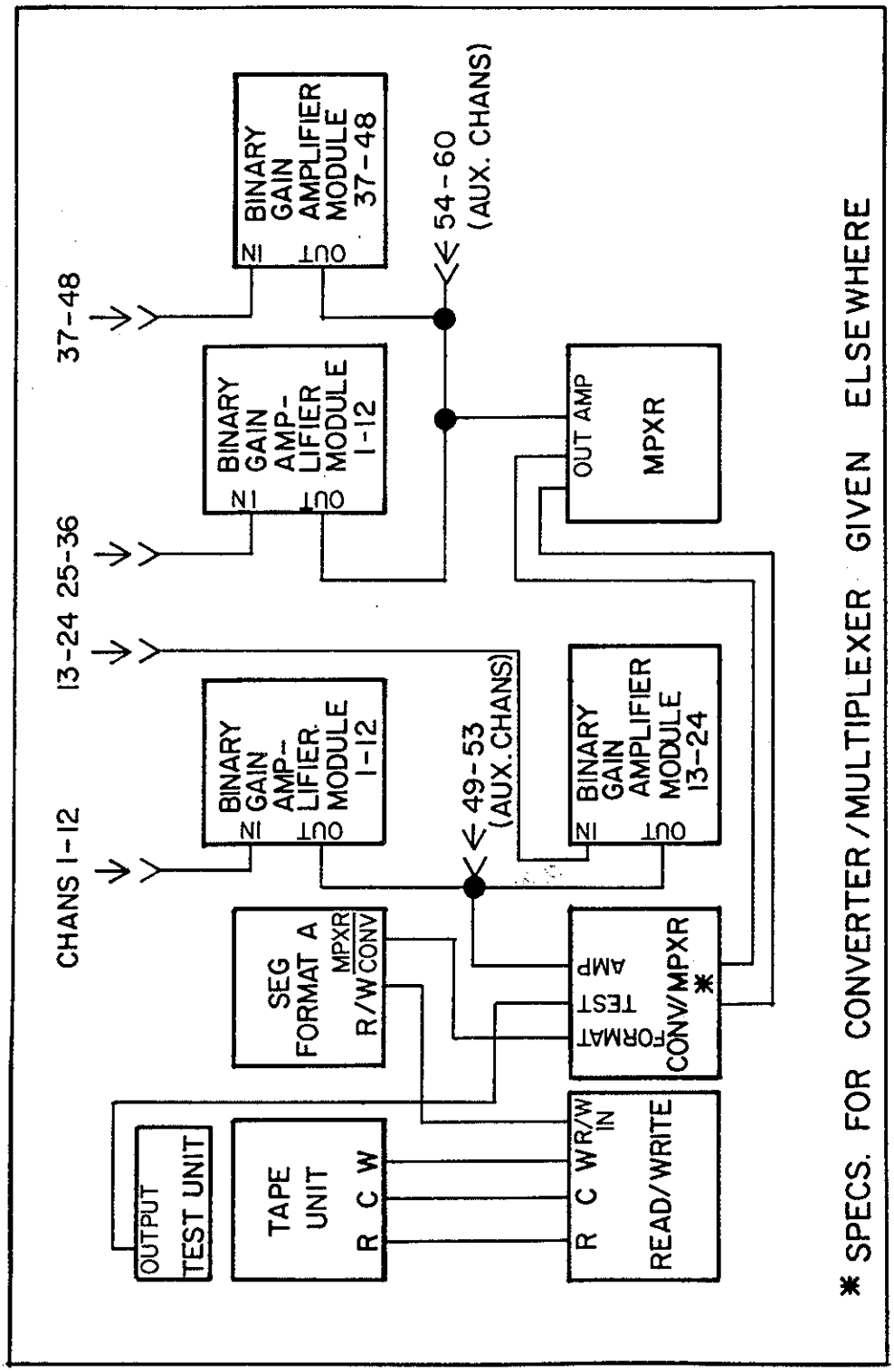

Fig. 5.16. Signal Flow in Recording Truck.

The second suite of manually acquired data were the pneumatic piezometer data. During all of the tests described subsequently, no excess pore water pressure was registered on any of the pile or soil piezometers. These piezometers and the readout equipment could resolve pressure to the nearest 0.5 psi (3.45 kPa) and were not capable of sensing transient peaks in pressure produced by dynamic loading.

DATA PROCESSING

Several steps were involved in processing the digital field, magnetic tape records. The first step, demultiplexing the records, is illustrated in Fig. 5.17. Each field record was demultiplexed on the VAX 11/780 system using a DISCO software package, which is a proprietary program of DIGICON, Inc., capable of demultiplexing data in the SEG A format. The demultiplexed records containing a sequential time series for each recorded channel were stored on a second magnetic tape, denoted a GOUT tape.

The raw GOUT tapes for selected tests were then processed using the DCASS 5 software package developed for this project. A detailed User's Guide for DCASS 5 is contained in Appendix G, and the functional operation of DCASS 5 is shown in Figs. 5.18 and 5.19.

The purpose of DCASS 5 is to convert the demultiplexed field records into functions useful to the enginer. These functions included time domain instrument response for each data channel (instrument), power spectral density (frequency domain) plots for each instrument, transfer function (response normalized by applied load over a range of frequencies) from the frequency response of one instrument (usually a load cell sum) to the output from another instrument (e.g., displacement computed from accelerometer in a pile), coherence and cross-spectra for the two spectra used in developing the transfer function, and phase between the two instruments involved in the transfer function. Certain statistical information, including autocorrelations, was also developed and printed. Principal output was in the form of machine-generated (Calcomp) plots and tape files, examples of which are in Appendix E.

The principal element of processed data that was used to characterize pile response was the frequency domain transfer function between applied load and displacement response at various points on the piles or

DISCO SEGA TO GOUT TAPE PROCESS

- CONVERT SEGA FIELD TAPE FROM SEISMIC TRUCK TO TRACE SEQUENTIAL GOUT FORMAT

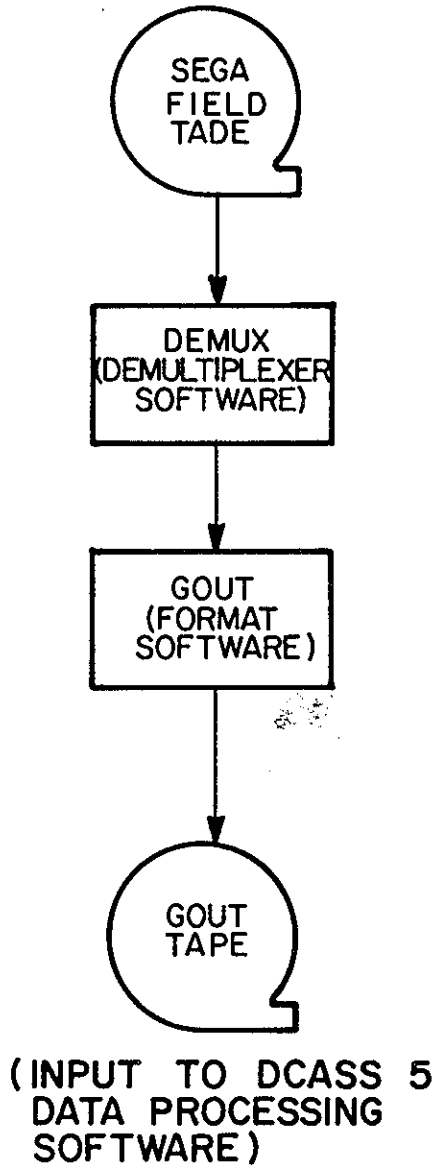

Fig. 5.17. Flow Diagram: Production of GOUT Tapes.

STANDARD DCASS 5 PROCEDURE: PASS 1

- CALIBRATE DIGITAL GOUT TAPES TO ENGINEERING UNITS AND PLOT TIME HISTORIES OF TRANSDUCERS
- PLOT SPECTRA
- COMPUTE AND LIST TIME DOMAIN STATISTICS
- GENERATE DCASS 5 RAW DATA AND FFT FORTRAN FILES (DCASS 5 RAW FFT FILE BECOMES INPUT FOR PASS 2)

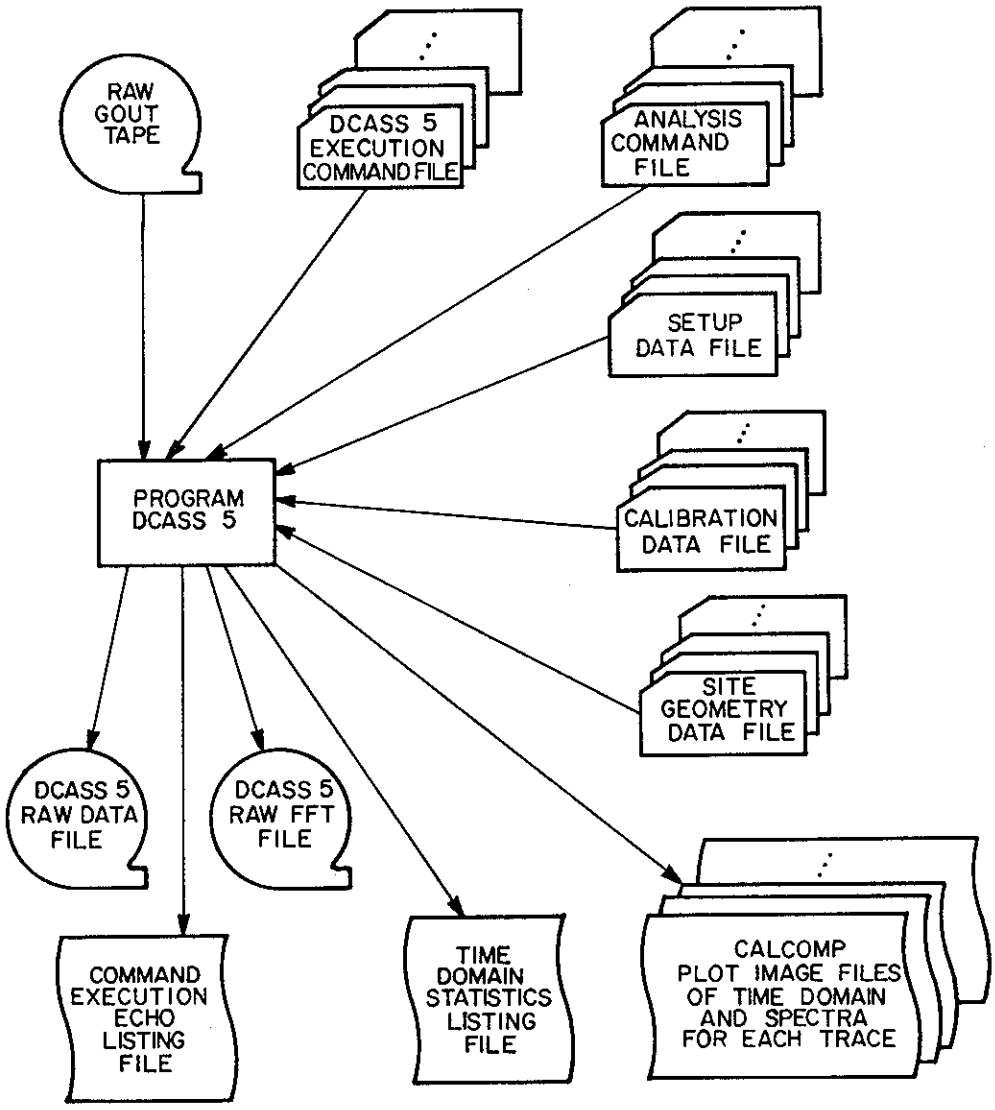

Fig. 5.18. Schematic of Inputs and Outputs for DCASS 5, Pass 1.

STANDARD DCASS 5 PROCEDURE: PASS 2

- COMPUTE AND PLOT TRANSFER FUNCTION MAGNITUDE AND PHASE
- COMPUTE AND PLOT COHERENCE FUNCTION
- COMPUTE AND PLOT AUTO AND CROSS SPECTRA

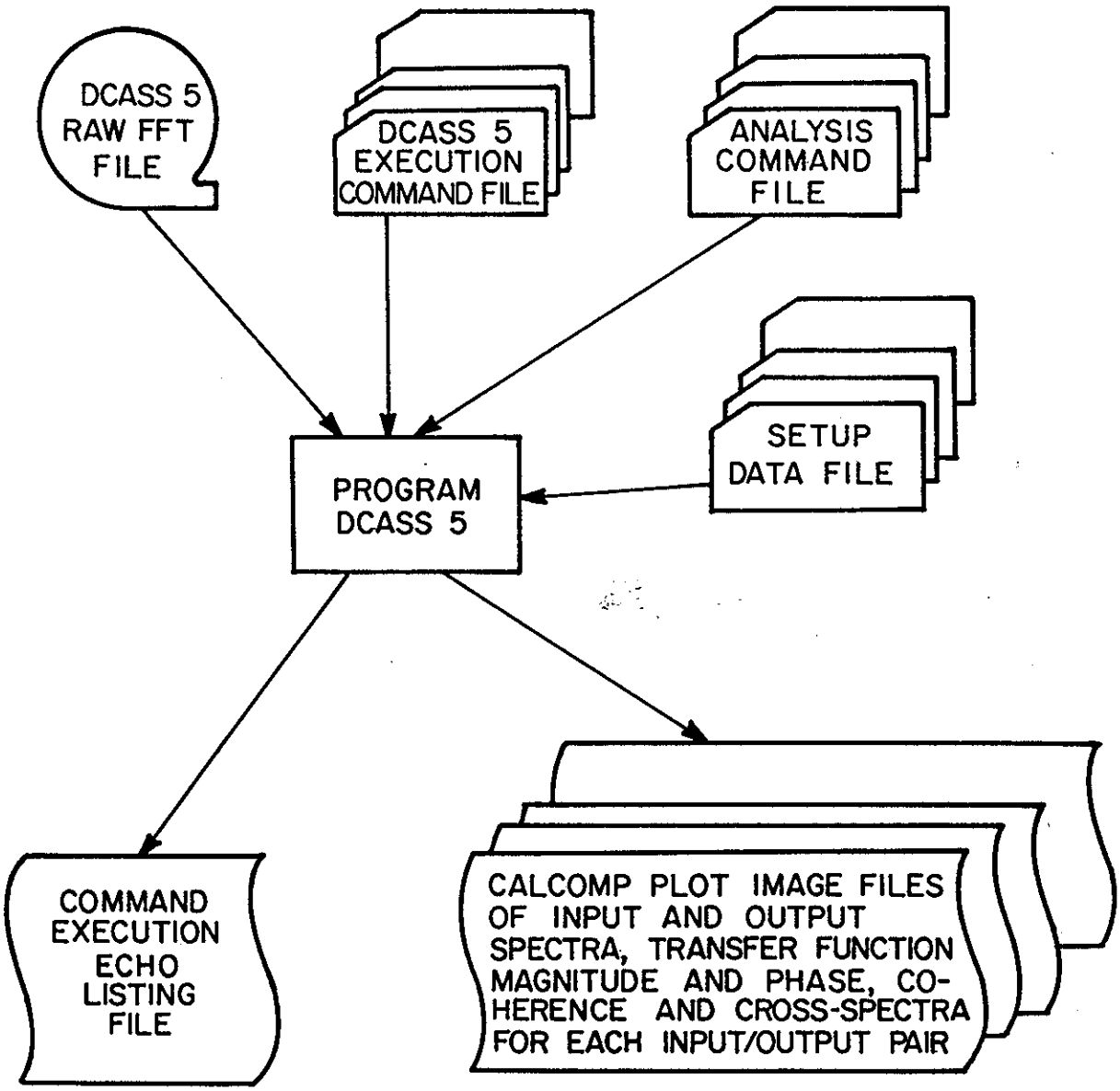

Fig. 5.19. Schematic of Inputs and Outputs for DCASS 5, Pass 2.

in the soil. The coherence functions were used to assess the quality of the transfer functions in various frequency ranges.

The above information was obtained for each processed record in two passes through DCASS 5. Pass 1, shown schematically in Fig. 5.18, involved reading the GOUT tape for the record in question; creating a geometry file that located the instruments in space; creating a calibration file, which provided voltage to engineering unit calibrations for each instrument and recording channel; and utilizing the command files shown to cause the DCASS 5 to execute the various calculations desired. The commands, along with the basic equations used in the calculations, are shown summarily in an extended table denoted Table 5.3. Further technical background on the signal processing algorithms are contained in Refs. 9, 12, and 64. An elementary overview of signal processing methods applied to problems in geotechnical engineering may be found in a paper by Skipp (88).

The output from Pass 1 includes a raw data file, a file containing the raw fast Fourier transforms (FFT) of the data, echo listings of commands, tape headers and set-up files, time domain statistics listings, and time series and power spectral density plots for each channel.

The raw FFT file (disc or tape) from Pass 1 was then read again into DCASS 5 in Pass 2, during which specified transfer functions (magnitude and phase), and coherence, were computed and output. Careful use was made of data "windowing" and related techniques in the FTT's to develop transfer functions free from side band effects. Digital filtering of the data could have been employed with DCASS 5, but filtering was not employed for the data for this study. Selected geophone response functions were manually filtered after computer processing at frequencies below the instrument resonance.

The products of the data processing procedure include GOUT tapes for records not processed by DCASS 5, and raw data tapes created by DCASS 5 (FORTRAN-formatted with headers associating instruments with data channels) and the various plots described above for the processed records.

TESTING SEQUENCE

A total of 223 sweep, steady state, and impact tests were accomplished on the single pile and the group. These tests were all

Table 5.3. Principal Commands and Equations Used in DCASS5.

Operations Performed by DCASS5 Commands

GOUT TAPE

Gout tape contains the time series of instrument output voltage levels obtained from the demultiplexed field tape. One tape contains data from several field records (tests); 60 channels per test. Note that for each field record number (FFID) on the field tape a SHOT number is generated during the demultiplex (DEMUX) process. SHOT numbers are sequential and each shot number corresponds to one FFID number.

Table 5.3. (Cont'd).

CALIBRATE COMMAND

Command Variables

(C_2 through C_5 are established by CALBDATA command from the variables CALCO (i,j) and SCALC (ICHAN) in the calibration file coresponding to the record (shot))

CALIBRATE first defines the system calibration factors;

C_2 = CALCO (2, ICHAN) = nominal analog-to-digital trace weight factor (nominal voltage per A/D bit) of DFS III recording system

C_3 = CALCO (3, ICHAN) = fractional difference from the nominal to actual trace weight factor for each recording channel

C_4 = CALCO (4, ICHAN) = trace zero offset in voltage = D.C. component of DFS III recording system response function = 0 for all traces here

C_5 = SCALC (ICHAN) = voltage per engineering unit = instrument sensitivity in volts per unit amplitude of instrument

v(j) = voltage level time series for trace ICHAN (from GOUT tape)

$FX = [C_2/(C_3 \times C_5)]$

$ZERO = C_4$ (FX) = 0 for all traces in this study

Calculations Performed

CALIBRATE computes the time series of calibrated instrument response in engineering units of the instrument amplitude;

$$x(j) = y(j)*FX - ZERO; \qquad j = 1,2,3, \ldots, NDATAT$$

where NDATAT = the number of data points on tape for each trace

Table 5.3. (Cont'd).

Command REALFFT

Command Computations

The original FAST subroutine, as written by Bergland, has been modified to calculate the normalized FFT coefficients given by

$$X(k) = \frac{1}{N}\left[\sum_{j=0}^{N-1} u(j)\, W^{kj}\right] \qquad k = 0, 1, 2, \ldots, N/2$$

where $N = 2^R$ and $u(j) = x(j) * w(j)$

$w(j)$ is the window function

Command SPECTRA

Command Computations

The spectral density function estimates are calculated by the realtion

$$G_{ij}(\omega) = \frac{2\,T}{2\pi U} \left|X(k)\right|^2 \qquad k = 0, 1, 2, \ldots, [(N/2)]$$

where

$\omega = 2\pi k/Nh$

X_k = normalized complex FFT coefficients

T = full scale segment record length in seconds

U = mean square of the data window

$$U = \frac{1}{N}\sum_{j=0}^{N-1} w_j^2$$

w_j = window shape function

SPECTRA computes $G_{11}(\omega)$, the spectrum of the input.

The spectra computed above are then smoothed as described below.

SPECTRAL SMOOTHING

The variance of spectral estimates can be reduced by smoothing in the frequency domain, which increases the band width of the spectral window. For rectangular smoothing, a revised estimate is given by

Table 5.3. (Cont'd).

$$\hat{G}_{11}(k) = \frac{1}{L} \sum_{j=1}^{L} G_{11}(k + j) \qquad k = L, 2L, 3L, \ldots, mL;$$

$$mL = n$$

$$L = (2i) + 1 \quad i = 0,1,2,\ldots$$

Similar expressions may be developed for $\hat{G}_{22}(K)$, $\hat{C}_{12}(K)$ and $\hat{Q}_{12}(K)$ where L is the number of contiguous raw estimates averaged and i = LAVE in the program. Smoothing is performed on G_{11}, G_{22}, C_{12}, and Q_{12} after spectral computations in the SPECTRA and CROSSPECTRA commands. Spectrum values $G_{ij}(k)$ correspond to frequency values

$$f = 0, L/2Nh, 3L/2Nh, \ldots, \{[2m-1)/2][L/Nh]\}$$

Given a finite length sample random wave record, the power spectral density may be obtained via the methods just described. Assuming the record was obtained from a stationary, ergodic and Guassian random wave process, the question now is what information may be obtained from the PSD function of the random wave record which will describe the process in a more convenient or usable form for design purposes.

It can be shown that the variance of the record and other properties are related to the spectrum and its various moments. The n-th moment of the spectrum is defined as

$$m_n = \int_0^{\infty} \omega^n \, 2 \, S_{xx}(\omega) \, d\omega$$

For example, the zero moment or area of the spectrial density function $S_{xx}(\omega)$ of x(t) is given by

$$m_0 = \int_0^{\infty} 2 \, S_{xx}(\omega) \, d\omega = \sigma_x^2$$

The significant wave height or the average of the one-third highest waves, denoted $H_{1/3}$, is related to the variance. Also other parameters related to wave period, length, and slope may be calculated from the spectral moments along with an additional parameter related to the spectral width.

Table 5.3. (Cont'd).

These parameters are listed below:

$H_{1/3}$ = significant one-third peak to peak value (average of the one-third highest waves)

$H_{1/10}$ = significant one-tenth peak to peak value (average of the one-tenth highest waves)

$\tilde{H}_w$ = average apparent height (2)

T_1 = Average mean period $\simeq T_{1/3}$ (significant period)

T_2 = Mean apparent zero crossing period

T_4 = Mean apparent period between peaks

ε = Spectral width parameter

where

$$H_{1/3} = 4.0(M_0)^{\frac{1}{2}}$$

$$H_{1/10} = 5.1(M_0)^{\frac{1}{2}}$$

$$\tilde{H}_w = 2.5(M_0)^{\frac{1}{2}}$$

$$T_1 = 2\pi\left(\frac{M_0}{M_1}\right)$$

$$T_2 = 2\pi\left(\frac{M_0}{M_2}\right)^{\frac{1}{2}}$$

$$T_4 = 2\pi\left(\frac{M_2}{M_4}\right)^{\frac{1}{2}}$$

$$\varepsilon = \left(1 - \frac{M_2^2}{M_0 M_4}\right)^{\frac{1}{2}}$$

T_1, T_2, T_4 and ε are appropriate for narrow band processes

Command Computations

The moments of the spectra $G_{11}(\omega)$ and $G_{22}(\omega)$ are defined by the relation

$$M_\ell = \int_0^\infty \omega^\ell \, G_{ij}(\omega) d\omega$$

and are estimated by the relation

$$M_\ell = \sum_{k=0}^{N/2-1} (2\pi k/Nh)^\ell \hat{G}_{ij}(k)$$

Table 5.3. (Cont'd).

The spectral moments are printed on the list device. The degrees of freedom in the SPECTRA and CROSSPECTRA commands for $\hat{G}_{11}(\omega)$ and $\hat{G}_{22}(\omega)$ respectively of each estimate is given by

$$\text{d.f.} = 2M$$

where M is the maximum number of segments. The normalized standard error is calculated by the relation

$$\epsilon = (1/M)^{\frac{1}{2}}$$

Command CROSSPEC

Command Computations

Raw estimates of the cross-spectrum are obtained by the relation

$$G_{12}(k) = \frac{2T}{2\pi U} X^*(k)\, Y(k) = C_{12}(k) + i\, Q_{12}(k)$$

where $C_{12}(k)$ is the one-sided coincident spectral density function and $Q_{12}(k)$ is the quadrature spectral density function

CROSSPEC also computes $G_{22}(\omega)$ for each segment of ensemble. After ensemble averaging, frequency averaging or combination final smoothed estimates will be obtained in polar form by the relations

$$|\hat{G}_{xy}(k)| = \sqrt{\hat{C}^2_{xy}(k) + \hat{Q}^2_{xy}(k)}$$

$$\hat{\theta}_{xy}(k) = \frac{360}{2\pi} \arctan[\hat{Q}_{xy}(k)/\hat{C}_{xy}(k)] \quad \text{(in degrees)}$$

Command TRANSFER

The TRANSFER command computes the magnitude of the transfer function between input and output as follows;

$$|\hat{H}_{12}(k)| = \frac{|\hat{G}_{12}(k)|}{\hat{G}_{11}(k)}$$

The transfer function phase is identical to the phase of the Crosspectrum; The coherence function is given by

$$\hat{\gamma}_{12}(k) = \frac{|\hat{G}_{12}(k)|^2}{\hat{G}_{11}(k)\hat{G}_{22}(k)}$$

Table 5.3. (Cont'd).

"WINDOW" Command

Command Variables

• IZS - Name of memory vector on which operations are performed

Calculations Performed

The WINDOW command performs the following operations

$u(j) = x(j)w(j);$ $\quad j = 1,2,3,\ldots,NDATA$

$u(j) = 0;$ $\quad j = NDATA + 1, NDATA + 2, \ldots, NDATAT$

where

$x(j)$ = the calibrated instrument response vector IZS

NDATAT = number of data points read from tape (must be power of two)

NDATA = number of non-zero data points to analyze

$w(j)$ = window function

$u(j)$ = windowed data stored in memory vector IZS

NDATA = 7500 and NDATAT = 8192 for most of the data reduction runs.

The window function type is determined by the variable IW in the FFTSIZE command. The window functions currently available include;

IW	Window Function
1	Rectangular function
2	Standard Extended Cosine Bell
	W = 10%
3	Full Cosine Bell (Hanning Window)
4	Triangular Window (Barlett Window)
5	Non-Standard Extended Cosine Bell with percentage set by user
6	Same as IW = 5, but squared

The percentage to taper each of non-zero portion of trace is determined by W. For a 100% taper, Hanning window, set W = 0.5. The window time length T is given by $T = (\Delta t)\ (NDATA)$

where Δt is the sample interval

The window functions are defined on the following sub-table and sketch.

Table 5.3. (Cont'd).

WINDOW FUNCTIONS FOR DCASS5 ANALYSIS

Window Index, IW	Shape Equation	Major Lobe Height	Highest Side Lobe (dB)	Band-width (dB)	Theoretical Roll-off (dB/octave)
1	W(t) = 1.0 for t = 0 to T	T	-13.2	0.86β	6
2	W(t) = 0.5 (1 - cos 2π5t/T) for t = 0 to T/10 and t = 9T/10 to T W(t) = 1.0 for t = T/10 to 9T/10	0.9T	-13.5	0.95β	18 beyond 5β
3	W(T) = 0.5 (1 - cos 2πt/T) for t = 0 to T	0.5T	-31.6	1.39β	18
4	W(t) = 2t/T for t = 0 to T/2 W(t) = -2t/T + 2 for t = T/2 to T	0.5T	-26.7	1.27β	12
5	W(t) = 0.5 [1 - cos $(\frac{\pi t}{WT})$] for t = 0 to WT and t = (1.0 - W)T to T W(t) = 1.0 for t = WT to (1.0 - W)T				
6	Same as IW = 5 but squared				

Table 5.3. (Co nt'd).

Common Data Windows and Their Frequency-Domain Parameters.
(From Tektronix Instr. Corp., Copyright 1975.)

Unity Amplitude Window	Shape Equation	Frequency Domain Magnitude	Major Lobe Height	Highest Side Lobe (dB)	Bandwidth (3 dB)	Theoretical Roll-Off (dB/Octave)
Rectangle 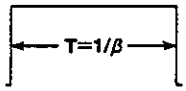	A=1 for t=0 to T	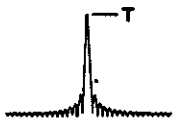	T	−13.2	0.86β	6
Extended Cosine Bell 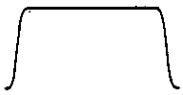	A=0.5 (1−cos 2π5t/T) for t=0 to T/10 and t=9T/10 to T A=1 for t=T/10 to 9T/10	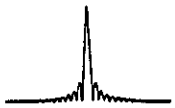	0.9 T	−13.5	0.95β	18 (beyond 5β)
Half Cycle Sine 	A=sin 2π0.5t/T for t=0 to T	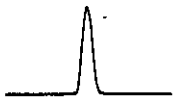	0.64 T	−22.4	1.15β	12
Triangle 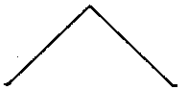	A=2t/T for t=0 to T/2 A= −2t/T + 2 for t=T/2 to T	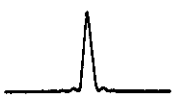	0.5 T	−26.7	1.27β	12
Cosine (Hanning) 	A=0.5(1−cos 2πt/T) for t=0 to T	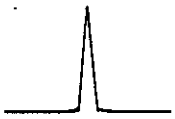	0.5 T	−31.6	1.39β	18
Half Cycle Sine^3 	A=sin^3 2π0.5t/T for t=0 to T	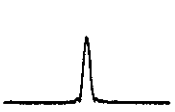	0.42 T	−39.5	1.61β	24
Hamming 	A=0.08 + 0.46 (1−cos 2πt/T)) for t=0 to T	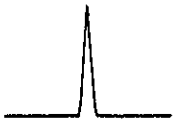	0.54 T	−41.9	1.26β	6 (Beyond 5β)
Cosine^2 	A=(0.5(1−cos 2πt/T))^2 for t=0 to T	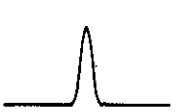	0.36 T	−46.9	1.79β	30

Table 5.3. (Cont'd).

DATASTAT COMMAND

Command Variables

The statistical calculations performed are determined by the NDSEG variable from the FFTSIZE command.

If NDSEG = 1 then only one data segment, equal to the entire record, is obtained. For this case, and the mean and mean-square are computed for the entire record. *

If NDSEG > 1 then trace is broken up into NDSEG segments. For NDSEG > 1, the mean and mean-square values are computed for each data segment.

Calculations Performed

DATASTAT computes maximum minimum and mean of the data before the data is modified.

The mean of the raw data trace, X(j), is computed as follows:

$$\bar{x} = \frac{1}{N} \sum_{j=1}^{N} x(j)$$

The estimate of the mean-square value ϕ_x is computed by the relation

$$\phi_x = \frac{1}{N} \sum_{j=1}^{N} [x(j) - \bar{x}]^2$$

* Used in present analysis

Table 5.3. (Cont'd).

The <u>average slope</u> of the data trace from beginning to end is estimated by the relation (Base line inclination)

$$\theta = \frac{(12.0)\sum_{j=1}^{N} x(j)*j}{N(N^2 - 1)} - \frac{6.0 * \bar{x}}{(N - 1)}$$

The <u>trend</u> (mean and slope) are removed from the data if IREMOV > 1 by the relation

$$x'(j) = x(j) - [\theta \cdot j] - \bar{x} + 0.5(N + 1)*\theta$$

$$j = 1,2, \ldots, N$$

The <u>mean</u> of the data is removed from the data if IREMOV = 1 by the relation (remove DC component)

$$x'(j) = x(j) - \bar{x} \qquad j = 1,2,3, \ldots, N$$

If IREMOV = 0 the data is left unchanged

accomplished between July 28, 1981, and August 20, 1981. A detailed, choronological listing of all tests is given in Appendix F. That documentation includes the field tape reel number, the FFID or "record number" of the test, the "shot number" of the test (an identification number produced when the GOUT tapes were made), the time length of the record in milliseconds, a "chan" designation that is keyed to the field notes denoting which instruments are associated with which channels for a given record, the mode of applied motion, the frequencies of motion (sweeps employed where ranges are indicated), the nominal force level applied (total of two vibrators, where the FHWA vibrators were used), the date and time of the test, and the GOUT tape number if a GOUT tape was made. The number of time series and FFT points for a given test can be determined by dividing the number in the "lgth" column by 4000. GOUT tapes could not be made from a few field records, presumably because the records had not been formatted correctly on the field tapes.

The testing sequence was essentially as given below. Table 5.4 gives a listing of the records from the tests conducted that were fully processed.

1. Very low force (< 2,000 lb (8.9 kN) single amplitude sweeps with FHWA vibrators in the vertical and rocking modes on the pile group, July 28-Aug. 6. These tests were primarily system checkout tests.
2. Group cap impact tests, Aug. 9-Aug. 10. These tests were conducted to gain some insight into the natural frequencies of the group when the cap was impacted by a 16 lb (71 N) mass dropped through a distance of about one meter. Vertical, rocking, horizontal, and torsional responses were excited. None of the impact records were fully processed because of time and budget limitations.
3. Single pile cap impact tests, Aug. 11. These tests were conducted as per the group cap impact tests and were also not fully processed.
4. Low force amplitude horizontal loading of the single pile with the FHWA vibrators, Aug. 11-Aug. 12. Several of these records were processed.

Table 5.4. Harmonic Vibration Tests and Field Record Nos. in Chronological Order (1 lb = 4.45 N)

Pile/ Test	Vibrator	Nominal Force, Single Amplitude (lb)	Frequency (Hz)	Field Record No.
GV	FHWA	660	47.5-10	371
GR	FHWA	660	46-10	372
SH	FHWA	400	10-1.8	470-476
SH	FHWA	Varied-Manually Cranked (Less Than 200)	1-3	481
SH	FHWA	"	1-3	492
SV	WES/ 0 REM	400	50-2	602
SV	WES/ 2 REM	4000	50-2	616
SV	WES/ 2 REM	4000	15	617
SV	WES/ 2 REM	4000	20	618
SV	WES/ 2 REM	4000	25	619
SV	WES/ 2 REM	8000	50-2	621
SV	WES/ 2 REM	400	50-2	623
GV	WES/ 2 REM	4000	90-40	633
GV	WES/ 2 REM	16,000	90-40	640
GV	WES/ 2 REM	16,000	72	641
GV	WES/ 2 REM	16,000	90-40	642

Table 5.4. (Cont'd). Harmonic Vibration Tests and Field Record Nos. in Chronological Order (1 lb = 4.45 N)

Pile/ Test	Vibrator	Nominal Force, Single Amplitude (lb)	Frequency (Hz)	Field Record No.
GV	WES/ 2 REM	16,000	50-2	643
GV	WES/ 2 REM	40,000	50-2	645
GH	WES/ 2 REM	4000	50-2	802
GH	WES/ 2 REM	4000	14	803
GH	WES/ 2 REM	4000	9	804
GH	WES/ 2 REM	4000	4	805
GH	WES/ 2 REM	8000	50-2	806
GH	WES/ 2 REM	4000	50-2	808
GH	WES/ 2 REM	400	50-2	815
SH	WES/ 1 REM	200	15-0.5	832
SH	WES/ 1 REM	600	15-0.5	835
SH	WES/ 1 REM	600	1.32	836
SH	WES/ 1 REM	200	15-0.5	840

Symbols: G - Group
S - Single Pile
V - Vertical Mode
R - Rocking Mode
H - Horizontal Mode

FHWA - Fed. Hwy. Admin. Vibrator
WES - Waterways Exp. Sta. Vibrator
REM - Reaction Mass (Approx. 5600 lb each)

Under frequency heading, hyphenated nos. indicate sweep from first to second value. Single nos. indicate vibrations at discrete frequency.

5. Low and high force amplitude vertical loading of the single pile with the WES vibrator, Aug. 14 and Aug. 15. Several of these records were fully processed.
6. Low and high force amplitude vertical loading of the group with the WES vibrator, Aug. 17. Several of these records were fully processed.
7. Low and high force amplitude horizontal loading of the group with the WES vibrator, Aug. 19. Several of these records were fully processed.
8. Low and high force amplitude horizontal loading of the single pile with the WES vibrator, Aug. 20. Several of these records were fully processed.

In 5-8 above, several levels of nominally increasing load amplitude were applied in order to study nonlinear soil response effects, followed by a return to a lower amplitude tested during the increasing amplitude sequence to investigate whether any permanent degradation of soil support had occurred. The principal test method was the 32-second downsweep, but loading was also applied periodically during the tests at discrete frequencies relatively near resonance in order to investigate the influence of sweeping on the response of the single pile or pile group.

The results of the various tests are presented in Chapter 7.

CHAPTER 6

MATHEMATICAL MODELING OF TESTS

GENERAL

The physical arrangements for the vertical and horizontal tests on the single pile and pile group (Figs. 5.3, 5.11, and 5.13, and Table 5.2), along with the appropriate soil characterizations (described later) were modeled with two discrete element models, entitled DRIVE and SPASM, a continuum model, entitled PILAY (in conjunction with an additional program entitled RIGDF), and a finite element program entitled KPILE. (The latter program was used only to model the horizontal response of the single pile.) Each of the programs, described in some detail in the next section, is a public domain FORTRAN-coded program intended for the solution of practical problems in pile dynamics. Their solution schemes, described in general in Chapter 2, differ appreciably, however. DRIVE (axial response) and SPASM (lateral response) and KPILE were executed on large mainframe computers (UHCC's Honeywell 66/60 and NAS AS-9000), while the PILAY/RIGDF runs were made on a PDP 11/70 minicomputer. In all probability SPASM and DRIVE could have been adapted to a minicomputer environment, but no attempt to do so was made in this study.

The various programs employed in the modeling process are described in the following section. In the final section of this chapter the specific input used in the various programs for the several tests modeled is described.

PROGRAM DESCRIPTIONS

DRIVE

Program DRIVE (25) is a discrete element algorithm that was originally written to model the axial, nonlinear response of a pile subjected to transient axial loading, such as pile driving. It has the capability also of modeling steady state dynamic loading. The DRIVE model is illustrated physically in Fig. 6.1. The pile consists of rigid rods connected by springs that represent lumped axial stiffness (AE) over an increment length h. Internal dashpots (DI) also permit specification of

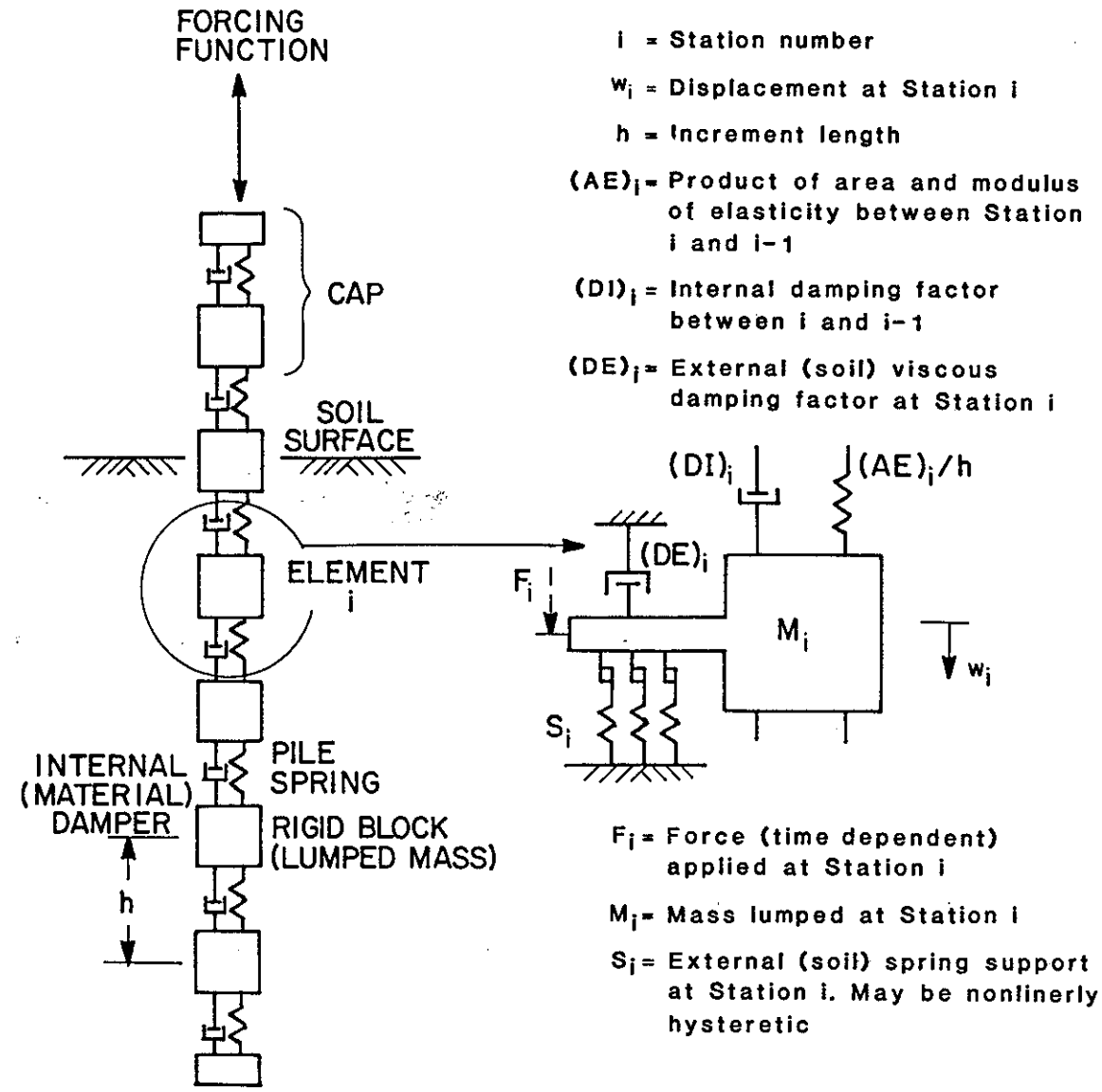

Fig. 6.1. Physical Schematic for DRIVE (25).

energy losses within the pile. Nonlinear, hysteretic, degradable soil stiffness as a function of pile movement is modeled at every element (station) in side shear and in end bearing ("f-z" curves and "Q-z" curves in side shear and end bearing respectively) by employing subelement systems of parallel linear springs, each attached to a Coulomb friction block, as depicted in Fig. 6.1. The use of the subelement soil support method is described more fully in the discussion of Program SPASM, which follows. An external dashpot (DE) is placed in series with the set of soil springs to model radiation damping. This dashpot produces soil reactions in excess of those developed in the springs in direct proportion to the element velocity and independent of frequency.

Input to DRIVE includes axial pile stiffness, AE, which can vary along the pile; internal pile damping, which was assumed to be zero for both the DRIVE and SPASM analyses; external (radiation) damping; nonlinear side resistance and end bearing vs. pile movement curves (f-z and Q-z curves); increment length, h; time step, h_t (defined later); pile mass, M (assigned to each element and may include arbitrarily any soil mass thought to vibrate in phase with the pile); and the forcing function.

The equation of motion, in implicit finite difference form for a generic element i, is

$$b_{k+1}w_{i-1,\,k+1} + c_{k+1}w_{i,\,k+1}$$

$$+ d_{k+1}w_{i+1,\,k+1} + c_k w_{i,k} + b_{k-1}w_{i-1,\,k-1}$$

$$+ c_{k-1}w_{i,\,k-1} + d_{k-1}w_{i+1,\,k-1} =$$

$$0.5\,(-F_{i,\,k-1} - F_{i,\,k+1}), \qquad (6.1)$$

where

$$b_{k+1} = (AE)_i(2h)^{-1} + (DI)_i(2h_t)^{-1}$$

$$c_{k+1} = -(AE)_i(2h)^{-1} - (AE)_{i+1}(2h)^{-1}$$

$$- (DE)_i(2h_t)^{-1} - M_i(h_t)^{-2} - (DI)_i(2h_t)^{-1}$$

$$- (DI)_{i+1}(2h_t)^{-1} - 0.5\ S_{i,\ k+1}$$

$$d_{k+1} = (AE)_{i+1}(2h)^{-1} + (DI)_{i+1}(2h_t)^{-1}$$

$$c_k = M_i(h_t)^{-2}$$

$$b_{k-1} = (AE)_i(2h)^{-1} - (DI)_i(2h_t)^{-1}$$

$$c_{k-1} = (AE)_i(2h)^{-1} - (AE)_{i+1}(2h)^{-1}$$

$$+ (DE)_i(2h_t)^{-1} - M_i(h_t)^{-2} + (DI)_i(2h_t)^{-1}$$

$$+ (DI)_{i+1}(2h_t)^{-1} - 0.5\ S_{i,\ k-1}$$

$$d_{k-1} = (AE)_{i+1}(2h)^{-1} - (DI)_{i+1}(2h_t)^{-1}$$

and where the various terms in the above expressions have been defined previously, except for h_t, which is the time increment length. Subscripts i and k refer to pile station and time increment, respectively. The units of F and AE are force (F), of DI and DE are force-time/length (FTL^{-1}), of M are force-time^2/length (FT^2L^{-1}), of h are length (L), of h_t are time (T), and of S are force/length (FL^{-1}).

A Crank-Nicholson implicit scheme is used to solve for the time histories of the deflections w and soil reactions at each element. These histories, as well as velocities and accelerations (developed from a simple routine added to DRIVE in this study), are then plotted at up to five prescribed stations along the pile. Transfer functions are then developed external to the program by plotting the amplitudes of steady state response (e.g., deflection at a pile node) against the frequency of that response. It is then relatively simple to compare these functions with those measured in the field tests in order to assess the ability of DRIVE to model pile response.

The version of DRIVE used was entitled DRIVE 7.

SPASM

Program SPASM (44, 45) is a discrete element algorithm that is similar to DRIVE but which models a vibrating, laterally loaded pile. The SPASM model is illustrated physically in Fig. 6.2. Each dot along the pile represents a station at which mass is concentrated and against which lateral nonlinear, hysteretic, degradable soil springs (inelastic supports or "p-y" curves) operate. The nonlinear soil springs consist of several linear "subelements" that can be visualized as consisting of linear parallel springs reacting against Coulomb friction blocks, as illustrated in Fig. 6.3. By engaging and disengaging the Coulomb blocks at various displacement values, defined on the elastic-plastic Q-u curves for the subelements, a complete, nonlinear, hysteretic, lateral soil reaction vs. lateral displacement relationship can be developed at each station along the pile. Figure 6.3 illustrates the loading paths on the subelements and overall load-deflection curves for symmetric two-way loading, unloading, and reloading. Any number of subelements can also be specified not to be engaged until the imposed motion exceeds the amplitude imposed on any previous cycle. The net effect of such a specification is shown in Fig. 6.2, in which formation of a gap between the pile and soil out to the characteristic knee of the nth subelement stress-strain curve is simulated. Radiation damping is modeled by assigning an external damping factor (velocity dependent reaction force) attached to each pile node.

Hence, both gapping and hysteretic damping are simulated if the lateral soil resistance curve that is input represents true soil response to lateral loading. Other important factors that are input include the flexural stiffness and mass of the pile (per increment), internal pile damping constant, external (radiation) damping constant, restraints (if any), pointwise time history of applied load, and time and length increments. It is possible to add additional mass arbitrarily to the pile mass to model soil that is vibrating in phase with the pile. (SPASM also permits loading to be applied through movement of the soil springs, thus simulating seismic loading.)

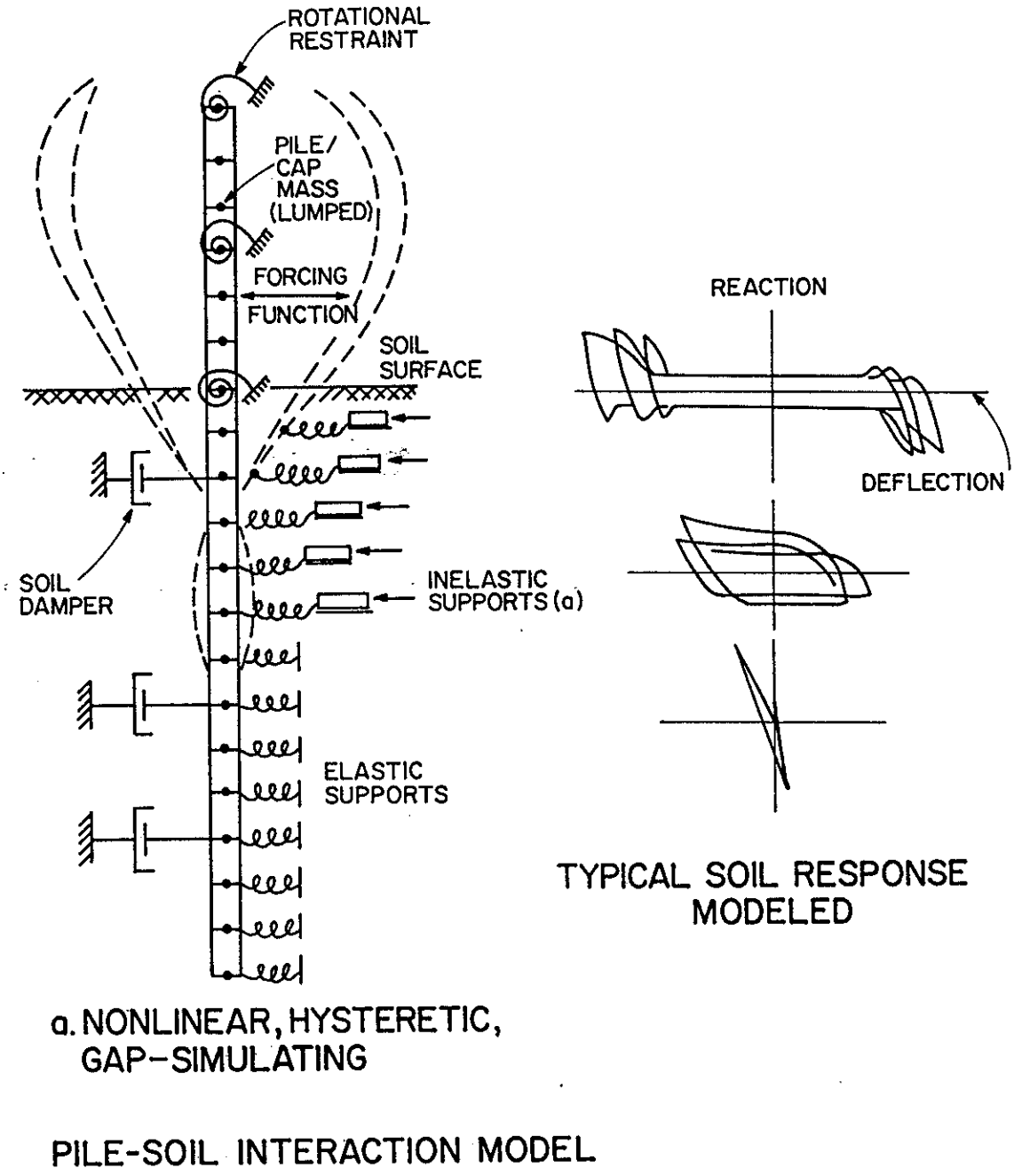

Fig. 6.2. Physical Schematic for SPASM (44).

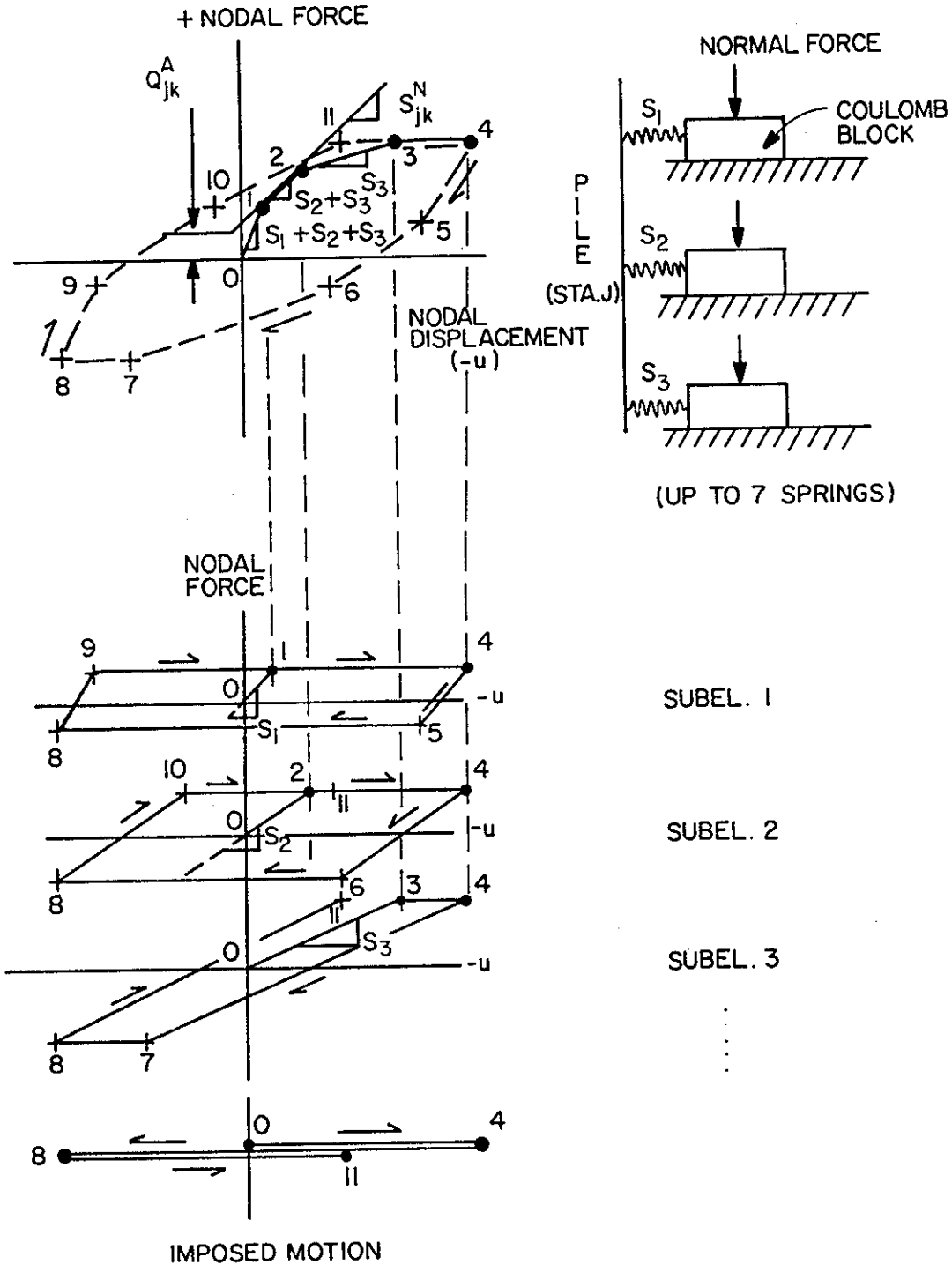

Fig. 6.3. Simulation of Hysteresis in SPASM and DRIVE.

The basic equation of motion for the pile is formulated implicitly for every node on the pile in terms of the unknown lateral nodal displacements u in the form

$$a_{k+1}u_{j-2,\,k+1} + b_{k+1}u_{j-1,\,k+1} + c_{k+1}u_{j,\,k+1}$$

$$+ d_{k+1}u_{j+1,\,k+1} + e_{k+1}u_{j+2,\,k+1}$$

$$= c_k u_{j,k} + a_{k-1}u_{j-2,\,k-1} + b_{k-1}u_{j-1,\,k-1} + c_{k-1}u_{j,\,k-1}$$

$$+ d_{k-1}u_{j+1,\,k-1} + e_{k-1}u_{j+2,\,k-1} + f_{j,\,k}, \qquad (6.2)$$

where the coefficients of the unknown deflections u are

$$a_{k+1} = F_{j-1} + \frac{D^i_{j-1}}{h_t} - \frac{h}{4} R_{j-1}$$

$$b_{k+1} = -2(F_{j-1} + F_j) - \frac{2}{h_t}(D^i_{j-1} + D^i_j)$$

$$- h^2\{T_j + \tfrac{1}{2}(T^T_{j,k+1})\}$$

$$c_{k+1} = F_{j-1} + 4F_j + F_{j+1} + \frac{1}{h_t}(D^i_{j-1} + 4D^i_j + D^i_{j+1})$$

$$+ h^2\{T_j + T_{j+1} + \tfrac{1}{2}(T^T_{j,k-1} + T^T_{j,k+1} + T^T_{j+1,k-1}$$

$$+ T^T_{j+1,k+1})\} + \frac{h}{4}(R_{j-1} + R_{j+1}) + \frac{2h^3\rho_j}{h_t^2} + \frac{h^3 D^e_j}{h_t}$$

$$+ \frac{h^3}{2}\{(S^S_j + S^N_{j,k-1}) + (S^S_j + S^N_{j,k+1})\}$$

$$d_{k+1} = -2\,(F_j + F_{j+1}) - \frac{2}{h_t}\,(D^i_j + D^i_{j+1})$$

$$- h^2\{T_{j+1} + \frac{1}{2}\,(T^T_{j+1,k-1} + T^T_{j+1,k+1})\}$$

$$e_{k+1} = F_{j+1} + \frac{D^i_{j+1}}{h_t} - \frac{h}{4}\,R_{j+1},$$

and the coefficients of the previously computed deflection are

$$c_k = \frac{4\,h^3\,\rho_j}{h_t^{\,2}}$$

$$a_{k-1} = -a_{k+1} + \frac{2\,D^i_{j-1}}{h_t}$$

$$b_{k-1} = -b_{k+1} - \frac{4}{h_t}\,(D^i_{j-1} + D^i_j)$$

$$c_{k-1} = -c_{k+1} + \frac{2}{h_t}\,(D^i_{j-1} + 4\,D^i_j + D^i_{j+1}) + \frac{2\,h^3\,D^e_j}{h_t}$$

$$d_{k-1} = -d_{k+1} - \frac{4}{h_t}\,(D^i_j + D^i_{j+1})$$

$$e_{k-1} = -e_{k+1} + \frac{2\,D^i_{j+1}}{h_t}$$

$$f_{j,k} = h^3\,\{(Q^T_{j,k-1} + Q^A_{j,k-1} + Q_j) + (Q^T_{j,k+1} + Q^A_{j,k+1} + Q_j)\}$$

$$+ h^2\,(-C_{j-1} + C_{j+1}).$$

In the above formulation j refers to a discrete pile station, and k refers to a discrete time step. Further,

F_j = flexural pile stiffness (FL^2) at Sta. j, which can vary from station to station,

D_j^i = internal pile dashpot coefficient at Sta. j (FL^2T),

D_j^e = external (soil radiation) dashpot coefficient at Sta. j (FTL^{-1}) ("soil damper" in Fig. 6.2),

h = pile increment length (L),

h_t = time increment length (T),

R = rotational restraint (external spring constant) at Sta. j (FL/RAD) (illustrated in Fig. 6.2),

$S_{j,k}^N$ = nonlinear soil spring stiffness at Sta. j and Time Step k (real) (FL^{-1}) ("inelastic supports" in Fig. 6.2),

S_j^S = fixed linear soil spring stiffness at Sta. j (FL^{-1}),

T_j = time-independent axial thrust at Sta. j. (F) (i.e., static axial load on pile),

$T_{j,k}^T$ = time-dependent axial thrust at Sta. j and Time Step k (F) (i.e., applied axial load)

$Q_{j,k}^T$ = time-dependent lateral load at Sta. j and Time Step k (F),

$Q_{j,k}^A$ = dummy lateral load to account for changes in force intercept of tangent to soil support (p-y) curve and/or the damping force caused by prescribed soil support (seismic) motion at Sta. j and Time Step k (F),

Q_j = time-independent (static) lateral load at Sta. j (F),

C_j = applied couple, if any, at Sta. j (FL/RAD),

ρ_j = concentrated mass (of pile or pile plus any in-phase soil) at Sta. j (FT^2L^{-1}).

As in DRIVE, the system of equations that results from applying Eq. (6.2) to every node, with appropriate boundary conditions, is solved using the Crank-Nicholson implicit scheme, for stability and computational speed purposes.

The outputs from SPASM were obtained in this study primarily in direct graphical form and include time histories of displacements and lateral soil reactions at each of several specified nodes. Response spectra were then developed for those nodes external to the program.

A specific version of SPASM, called SPASM 9, was used in this study.

PILAY

PILAY is an algorithm that computes pile-head impedance functions for a prismatic or step-varying pile in a layered elastic halfspace (55).

The inputs to the program are shear modulus and mass density for each horizontal soil layer described along the pile and for a layer below the tip; the Young's modulus, E; moment of inertia, I; and mass density, ρ, of the pile. The outputs are the four sets of pile-head impedance functions (stiffness (k) and damping (c)) shown in Fig. 6.4, and mode shapes and motion phase at prescribed points along the pile.

The governing differential equation for uncoupled axial harmonic motion of the pile in a linear, uniform continuum (54) is

$$w(z)\,[-\bar{\rho}\omega^2 + ic\omega + (k_{rw} + ik_{iw})] - EA\, d^2w(z)/dz^2 = 0 \qquad (6\text{-}3)$$

where

$w(z)$ = axial pile displacement (L)

$\bar{\rho}$ = mass per unit length of pile (FT^2L^{-1})

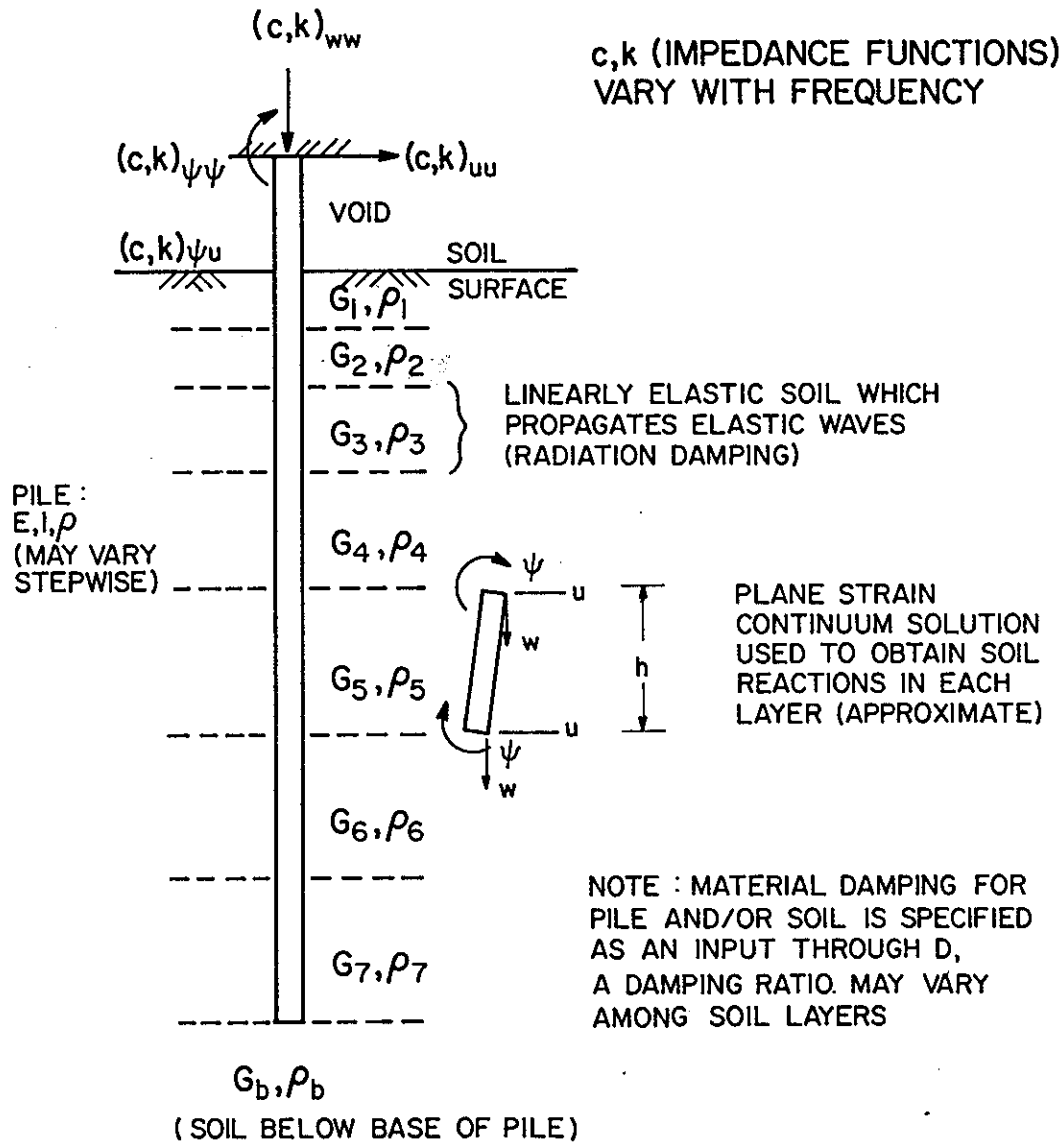

Fig. 6.4. Soil Layering System and Notation for PILAY (55).

c = coefficient of internal damping (soil or pile hysteresis) (FTL^{-1})

ω = frequency (RAD/T)

EA = axial stiffness (F)

z = depth variable (L)

i = $(-1)^{0.5}$

k_{rw}, k_{iw} = real and imaginary soil stiffness components (FL^{-1}) (See Eq. (2-8).)

The complex stiffness terms are evaluated as

$$k_{rw} = 2\pi G a_o \frac{J_1(a_o)J_o(a_o) + Y_1(a_o)Y_o(a_o)}{J_o^2(a_o) + Y_o^2(a_o)} \tag{6-4}$$

$$k_{iw} = \frac{4G}{J_o^2(a_o) + Y_o^2(a_o)} \tag{6-5}$$

where G is the soil shear modulus, $J_o(a_o)$ and $J_1(a_o)$ are Bessel functions of the first kind and order 0 and 1, respectively, and where $Y_o(a_o)$ and $Y_1(a_o)$ are Bessel functions of the second kind and order 0 and 1. These functions derive from the assumption of axially symmetric plane strain motion of the soil, which produces only horizontally propagating body waves. Surface waves are excluded. These functions are evaluated in Ref. 54.

Equation (6-3) is solved numerically in PILAY, after applying boundary conditions for a number of specified frequencies. PILAY discretizes the pile for purposes of the numerical calculations, and, where layering is specified (Fig. 6.4), changes the complex stiffness of the soil for each pile "element," based on the soil shear modulus and density at the level of the element (55).

In the horizontal mode the differential equation of harmonic motion in a linear uniform continuum is

$$EI\, d^4u(z)/dz^4 + u(z)\,[Gk_{ru} - \bar{\rho}\omega^2 + i(c\omega + Gk_{iu})] = 0 \qquad (6\text{-}6)$$

where the various parameters are as defined previously, except for the soil stiffness terms, which are

$$k_{ru} = \mathrm{Re}\,(K_u) \qquad (6\text{-}7)$$

$$k_{iu} = \mathrm{Im}\,(K_u) \qquad (6\text{-}7)$$

in which

$$K_u = 2\pi G a_o \frac{q^{-0.5} H_2^{(2)}(a_o) H_1^{(2)}(X_o) + H_1^{(2)}(X_o) H_1^{(2)}(a_o)}{H_o^{(2)}(a_o) H_2^{(2)}(X_o) + H_o^{(2)}(X_o) H_2^{(2)}(a_o)} \qquad \ldots (6\text{-}9)$$

In Eq. (6-9)

$q = (1\text{-}2\nu)/2(1\text{-}\nu)$

ν = Poisson's ratio of the soil

$X_o = a_o/(2)^{0.5}$

$H_n^{(2)}(a_o)$, $H_n^{(2)}(X_o)$ = Hankel functions of the second kind of order n (0 or 1).

These complex stiffness functions are also evaluated in Ref. 54. Horizontal body wave propagation (only) is modeled, and both translation and rotation of each pile element is allowed (Fig. 6.4).

The scheme of solution is similar to that for axial motion. Soil damping in PILAY can be contrasted to damping in DRIVE and SPASM. In

the former model radiation damping is modeled analytically, while an arbitrary empirical frequency independent damping constant is input for the latter models. Conversely, in the latter models, hysteretic damping is modeled analytically (provided the decoupled nonlinear soil resistance curves are known), while the former model uses an arbitrary frequency independent damping ratio for system hysteresis.

The complex soil stiffness functions, which are obtained assuming plane strain conditions, approach zero as the frequency approaches zero. For this reason, the impedence functions computed by PILAY for $a_0 < 0.3$ are taken to be equal to those for $a_0 = 0.3$. This low frequency approximation applied to many of the analyses made for this study.

RIGDF

Program PILAY produces only the pile-head complex impedance functions and not the spectra needed for comparison with field data. Program RIGDF (53) utilizes the PILAY impedance functions as input, along with the mass and inertial properties of the rigid mass supported by the piles (pile cap) and the amplitude and point of application of the forcing functions. Simple one- and two-degree-of-freedom vibration analysis procedures are then used to develop displacement and rotation transfer functions at the CG of the rigid mass.

In the present study the load positions, CG locations, mass and rotational properties given in Figs. 5.11 and 5.13 and in Table 5.2 were used as inputs to RIGDF in addition to the impedance functions output by PILAY. Since the PILAY/RIGDF system is linear, displacement and rotation transfer functions for the CG of the cap were developed by applying unit single load amplitudes (which resulted in non-unit moments about the CG in the horizontal case).

PILAY impedance functions were developed at the cap-pile juncture, not at the soil surface. When modeling the pile group, the single pile impedance functions from PILAY were calculated as indicated in Fig. 6.5, in which the superscript G indicates "group" and 1 indicates "single pile" (from PILAY). Symmetric spacing and vertical pile orientations were used. No group action corrections are shown.

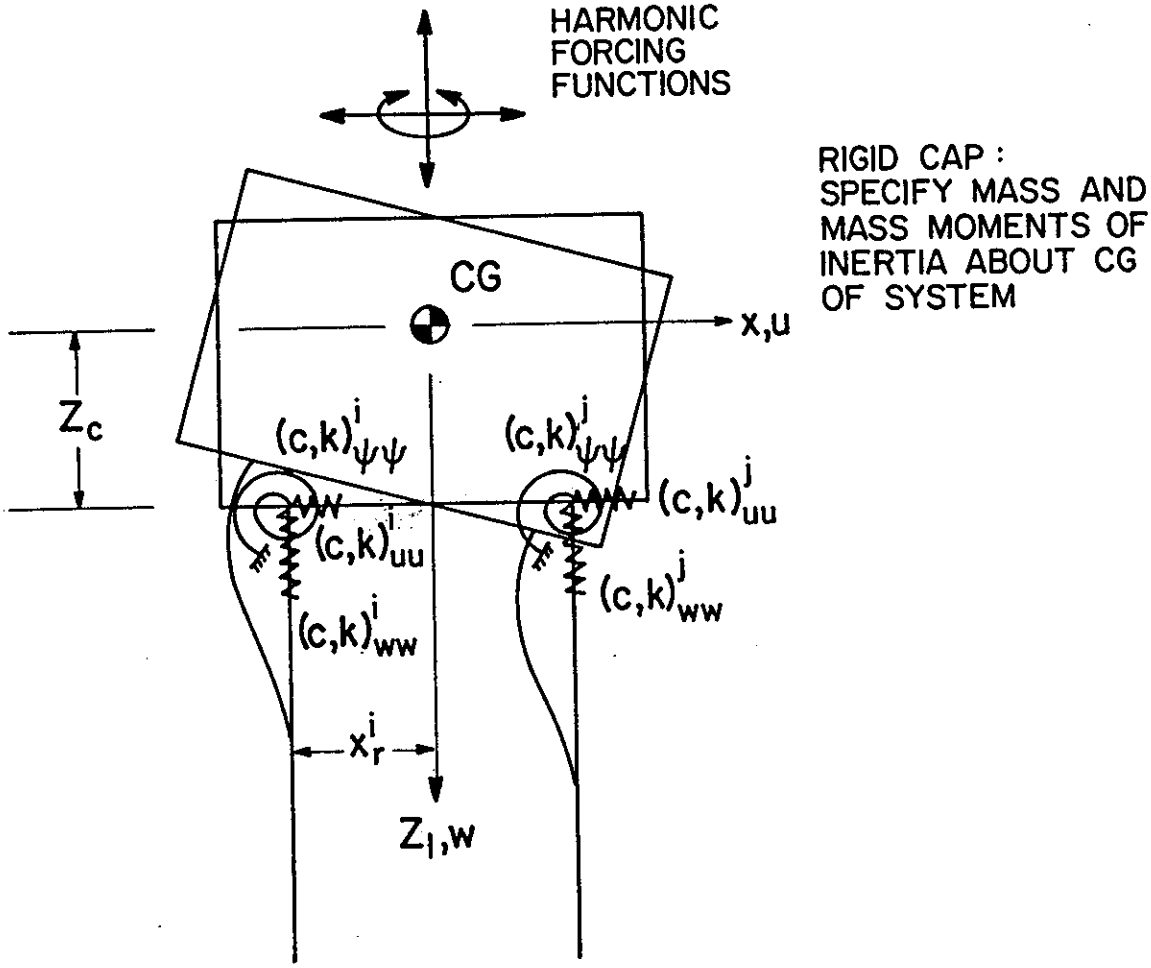

$$\mu^G_{ww} = \sum \mu^l_{ww} \qquad \mu^G_{uu} = \sum \mu^l_{uu}$$

$$\mu^G_{\psi\psi} = \sum (\mu^l_{\psi\psi} + \mu^l_{ww} X_r^2 + \mu^l_{uu} Z_c^2 - 2\mu^l_{\psi u} Z_c)$$

$$\mu^G_{\psi u} = \mu^G_{u\psi} = \sum (\mu^l_{\psi u} - \mu_{uu} Z_c)$$

μ = k or c (IMPEDANCE FUNCTIONS)

Fig. 6.5. Procedure for Assigning Stiffness and Damping Constants for RIGDF.

Group action was specified by modifying the pile head impedance functions from PILAY using approximate, but rational static-equivalent procedures. The vertical stiffness was modified for group action by letting

$$\mu_{ww}^{G} = \sum_{i=1}^{N} \mu_{ww}^{1} \Big/ \sum_{i=1}^{N} ((1 + \alpha_{ij}^{A} \ (i \neq j))/N) \qquad (6\text{-}10)$$

$$\mu_{uu}^{G} = \sum_{i=1}^{N} \mu_{uu}^{1} \Big/ \sum_{i=1}^{N} ((1 + \alpha_{ij}^{L} \ (i \neq j))/N) \qquad (6\text{-}11)$$

and letting the cross-stiffness and rotation terms remain unaltered from those shown in Fig. 6.5. In Eqs. (6-10) and (6-11) N = no. of piles in group (= 9), α_{ij} = a static 2-pile interaction factor between generic piles i and j. A refers to axial, and L refers to lateral. In practice, RIGDF solutions were obtained by setting the sums in the denominators equal to values obtained from (a) the measured results of the axial, static pile group tests (α = 1.7) (63), and (b) from a theoretical elastic halfspace solution of Poulos and Davis (α = 2.56) (68) for lateral loading.

The ww and uu damping constants for the group were adjusted exactly as shown for the stiffness terms (Eqs. (6-10) and (6-11)), according to the procedure of Ref. 55.

The coupled output spectra for horizontal loading (translation and rotation) were combined, using appropriate rotation arms, to give horizontal displacement spectra at the positions of the accelerometers in or on the caps, which were not always exactly at the CG's.

KPILE

Program KPILE (13) is a linear finite element program, in which the soil is discretized by using toroidal elements of arbitrary expansion, having 3 degrees of freedom per nodal ring. An end-on view of the rings (finite element mesh) is shown in Fig. 6.6. The toroidal elements are used only in the vicinity of the pile (the "near field") where stress

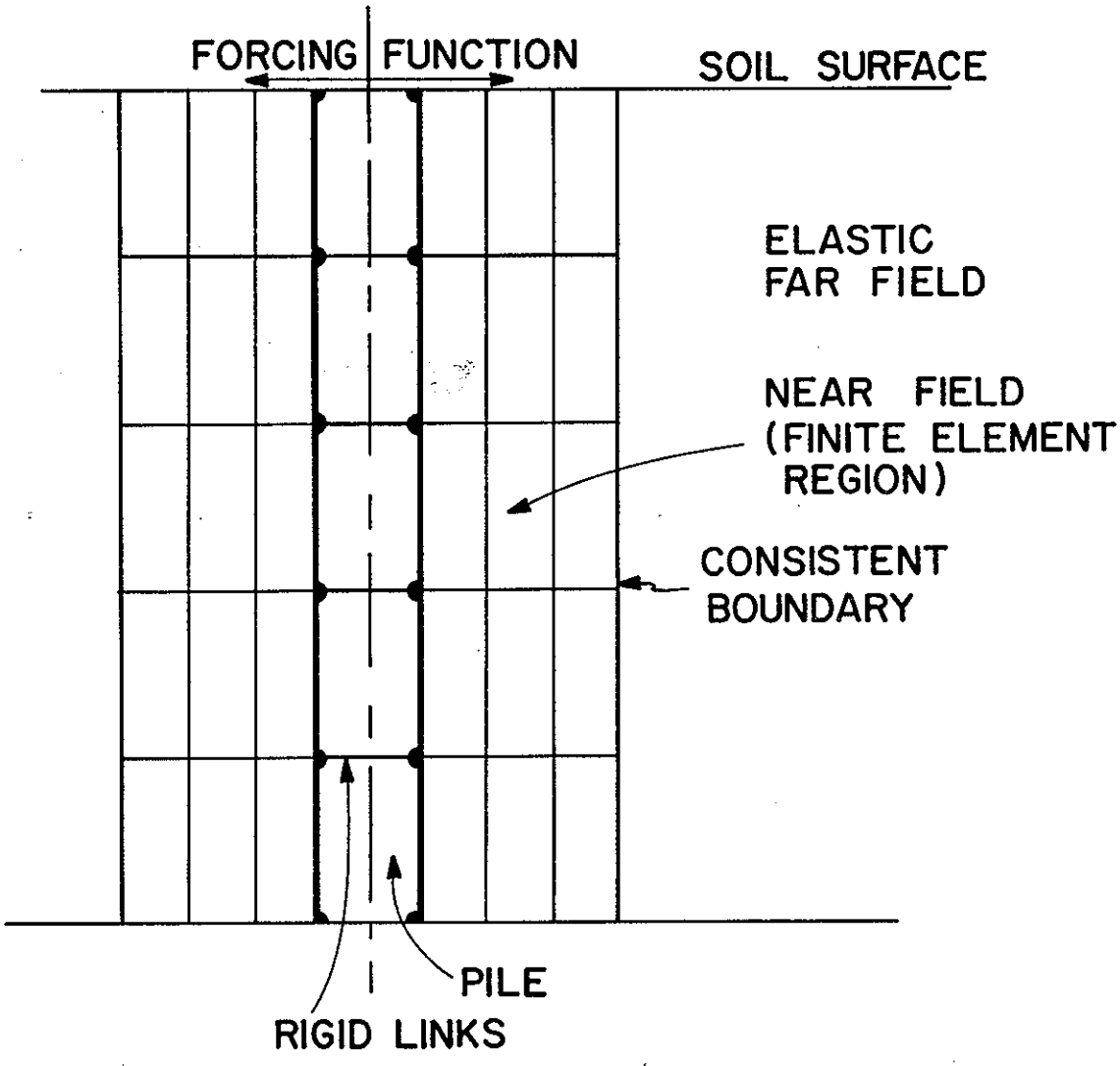

Fig. 6.6. Physical Schematic for KPILE (13).

gradients are high. The far field is represented by an energy transmitting medium that has a consistent boundary with the finite elements. The far field medium is represented mathematically by a fully populated stiffness matrix, which couples forces at the boundary nodes to displacements at all boundary nodes and obviates the need for a Winkler assumption, required in SPASM and PILAY. A Fourier expansion is used for the investigation of lateral motion. The nodes (rings) all have three degrees of freedom.

The pile is modeled in KPILE as a system of beam elements, rather than with a mesh of finite elements, in order to conserve computaion time. Rigid links (Fig. 6.6) are used to insure correct shear stiffness.

Hysteretic damping is provided for in KPILE by assigning a complex shear modulus to the soil, represented by G (1 + 2iD), where D is a prescribed damping ratio. Inputs consist of soil shear modulus and Poisson's ratio (may vary among elements), mesh geometry, pile stiffness, and frequency and amplitude of head load.

Previous studies with KPILE (13) indicate generally good agreement between KPILE and PILAY-type solutions, except that the KPILE solutions yield slightly lower stiffness.

PROGRAM INPUTS

In this section a description of the various mathematical analyses is presented along with the specific data used to characterize the piles and soil.

DRIVE

Inputs. Program DRIVE (axial excitation) was first used to simulate the restrike of Pile No. 1 that was performed on April 10, 1980. The purpose of this preliminary analysis was to use the impact driving performance to ascertain approximate values for radiation damping, assuming the validity of the measured static soil resistance curves from Figs. 4.2 and 4.3. The computed values of radiation damping then served as a basis for choosing radiation damping inputs for the

steady state analyses of the single pile and of a typical pile in the group under vertical excitation.

Pile properties for the various analytical conditions are shown in Fig. 6.7. In each analytical study (restrike, single pile harmonic loading, and group pile harmonic loading), the embedded portion of the pile was characterized in the same manner. Only the heads were idealized differently, reflecting the absence of the cap during restrike and the differences between the cap mass for the single pile and one-ninth of the cap mass for the group. Cap masses were distributed over several stations. Vibrator mass was excluded. Masses for pile increments are given in Fig. 6.7 as weights (W). No added soil masses were applied to the embedded stations in any of the analyses.

The AE of the pile was stiffened as shown by over one order of magnitude at the pile heads to reflect the increased stiffness of the caps.

Soil stiffness was modeled by inputting f-z curves in each of the five depth ranges shown in Fig. 6.7 and by a Q-z curve at the pile tip. Four sets of f-z and Q-z curves were input in all, although not each set was used for each condition shown in Fig. 6.7. These sets are tabulated in Table 6.1, in which lower case q and f refer to unit forces and upper case values refer to the lumped forces that were actually input. Set A represents the curves in Figs. 4.2 and 4.3. Set B represents the average f-z and Q-z curves measured during the first static test on the group piles (63). Use of Set B in essence satisfies Eq. (6-10). Set C is identical to Set A, except that all displacement (z) values have arbitrarily been divided by 4 to reflect possible stiffening due to impact loading of the soil. Finally, Set D is identical to Set A, but with z values divided by 12.

In Sets A and B a linear variation from zero stiffness at the soil surface to the tabulated values at the bottom of Depth Range 2 was specified to reflect known static patterns of load transfer (i.e., zero load transfer at the surfce). No further degradation was allowed in the subelements. In all other depth ranges and all other sets, the f-z curves were input uniformly over the depth ranges indicated.

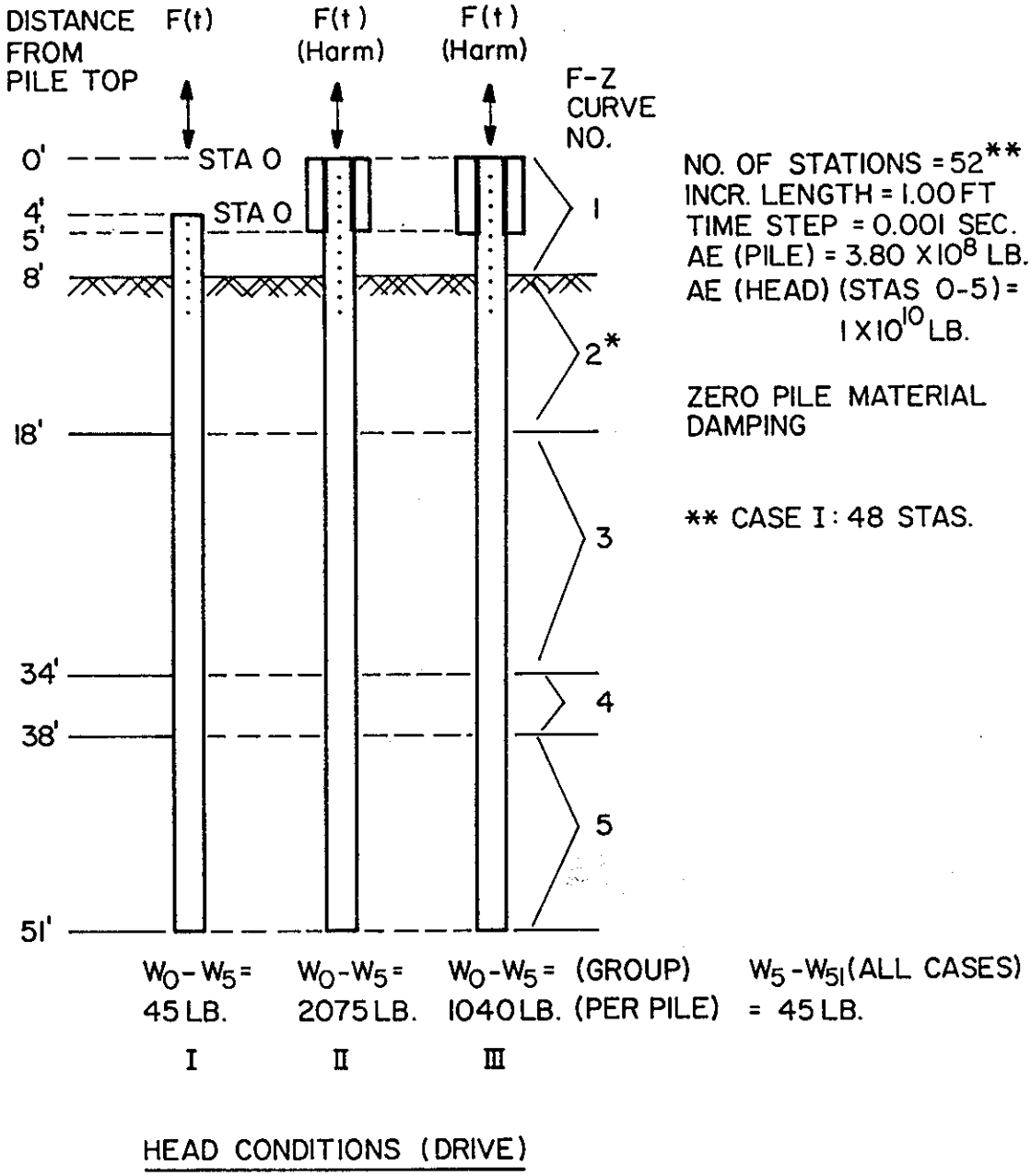

HEAD CONDITIONS (DRIVE)

* F-Z CURVE IN THIS ZONE VARIES LINEARLY FROM FLAT (0 RESISTANCE) AT SURFACE TO CURVE 2 VALUES IN SETS A AND B AT 18 FT. FOR SETS C AND D CURVE 2 VALUES ARE USED THROUGHOUT THIS LAYER.

Fig. 6.7. Pile Properties Used in DRIVE (1 ft = 0.305 m; 1 lb = 4.45 N).

Table 6.1. Soil Response (F-z; Q-z) Curves for DRIVE Analyses
(1 lb = 4.45 N; 1 in. = 25.4 mm; 1 psi = 6.89 kPa)

Set A: As measured statically for single piles. These curves do not explicitly contain residual stress effects.

Curve 1

f(psi)	F(lb)	z(in.)
0	0	0.00
0	0	0.01
0	0	0.02
0	0	0.04
0	0	0.06
0	0	0.10
0	0	5.00

Curve 2

f(psi)	F(lb)	z(in.)
0	0	0.00
1.60	648	0.01
2.60	1053	0.02
3.70	1499	0.04
3.70	1500	0.06
3.70	1500	0.10
3.70	1500	5.00

Curve 3

f(psi)	F(lb)	z(in.)
0	0	0.00
3.00	1215	0.01
6.00	2430	0.02
8.44	3422	0.04
8.84	3584	0.06
8.84	3584	0.10
8.84	3584	5.00

Curve 4

f(psi)	F(lb)	z(in.)
0	0	0.00
5.00	2025	0.01
6.70	2714	0.02
7.70	3119	0.04
7.95	3220	0.06
7.95	3220	0.10
7.95	3220	5.00

Curve 5

f(psi)	F(lb)	z(in.)
0	0	0.00
16.53	6700	0.01
16.53	6700	0.02
16.53	6700	0.04
16.53	6700	0.06
16.53	6700	0.10
16.53	6700	5.00

Q-z (tip) Curve

q(psi)	Q(lb)	z(in.)
0	0	0.00
176	16,000	0.02
273	24,800	0.04
326	29,600	0.08
364	33,000	0.12
386	35,000	0.22
393	35,700	0.32
393	35,700	5.00

Note: Upper case F indicates lumped force used in DRIVE. F-z curves were assumed symmetric. Zero soil degradation assumed for all 3 sets.

Table 6.1.(Cont'd). Soil Response (F-z; Q-z) Curves for DRIVE Analyses

Set B: As measured statically for average group pile. These curves do not explicitly contain residual stress effects.

Curve 1

(per Set A)

Curve 2

f(psi)	F(lb)	z(in.)
0	0	0.00
1.20	486	0.02
2.40	972	0.04
2.60	1053	0.06
2.60	1053	0.10
2.60	1053	0.20
2.60	1053	5.00

Curve 3

f(psi)	F(lb)	z(in.)
0	0	0.00
1.70	690	0.02
3.40	1380	0.04
4.43	1795	0.06
5.45	2209	0.10
8.17	3313	0.20
8.17	3313	5.00

Curve 4

f(psi)	F(lb)	z(in.)
0	0	0.00
2.04	828	0.02
3.29	1335	0.04
4.43	1795	0.06
6.47	2623	0.10
8.29	3360	0.20
8.29	3360	5.00

Curve 5

f(psi)	F(lb)	z(in.)
0	0	0.00
6.36	2578	0.02
11.70	4740	0.04
15.78	6397	0.06
15.78	6397	0.10
15.78	6397	0.20
15.78	6397	5.00

Q-z (tip) Curve

q(psi)	Q(lb)	z(in.)
0	0	0.00
66	6,000	0.02
121	11,000	0.04
165	15,000	0.06
220	20,000	0.10
275	25,000	0.20
275	25,000	5.00

Table 6.1.(Cont'd). Soil Response (F-z; Q-z) Curves for DRIVE Analyses

Set C: As measured statically for single piles but arbitrarily stiffened by a factor of 4. These curves do not explicitly contain residual stress effects.

Curve 1

(per Set A)

Curve 2

f(psi)	F(lb)	z(in.)
0	0	0.00
1.60	648	0.0025
2.60	1053	0.005
3.70	1499	0.010
3.70	1500	0.015
3.70	1500	0.025
3.70	1500	5.00

Curve 3

f(psi)	F(lb)	z(in.)
0	0	0.00
3.00	1215	0.0025
6.00	2430	0.005
8.44	3422	0.010
8.84	3584	0.015
8.84	3584	0.025
8.84	3584	5.00

Curve 4

f(psi)	F(lb)	z(in.)
0	0	0.00
5.00	2025	0.0025
6.70	2714	0.005
7.70	3119	0.010
7.95	3220	0.015
7.95	3220	0.025
7.95	3220	5.00

Curve 5

f(psi)	F(lb)	z(in.)
0	0	0.00
16.53	6700	0.0025
16.53	6700	0.005
16.53	6700	0.010
16.53	6700	0.015
16.53	6700	0.025
16.53	6700	5.00

Q-z (tip) Curve

q(psi)	Q(lb)	z(in.)
0	0	0.00
176	16,000	0.005
273	24,800	0.010
326	29,600	0.020
364	33,000	0.030
386	35,000	0.055
393	35,700	0.080
393	35,700	5.00

Table 6.1.(Cont'd). Soil Response (F-z; Q-z) Curves for DRIVE Analyses

Set D: As measured statically for single piles but arbitrarily stiffened by a factor of 12. These curves do not explicitly contain residual stress effects.

Curve 1
(per Set A)

Curve 2

f(psi)	F(lb)	z(in.)
0	0	0.00
1.60	648	0.00083
2.60	1053	0.0017
3.70	1499	0.0033
3.70	1500	0.0050
3.70	1500	0.0083
3.70	1500	1.670

Curve 3

f(psi)	F(lb)	z(in.)
0	0	0.00
3.00	1215	0.00083
6.00	2430	0.0017
8.44	3422	0.0030
8.84	3584	0.0050
8.84	3584	0.0083
8.84	3584	1.670

Curve 4

f(psi)	F(lb)	z(in.)
0	0	0.00
5.00	2025	0.00083
6.70	2714	0.0017
7.70	3119	0.0033
7.95	3220	0.0050
7.95	3220	0.0083
7.95	3220	1.670

Curve 5

f(psi)	F(lb)	z(in.)
0	0	0.00
16.53	6700	0.00083
16.53	6700	0.0017
16.53	6700	0.0033
16.53	6700	0.0050
16.53	6700	0.0083
16.53	6700	1.670

Q-z (tip) Curve

q(psi)	Q(lb)	z(in.)
0	0	0.00
176	16,000	0.00167
273	24,800	0.00333
326	29,600	0.00667
364	33,000	0.0100
386	35,000	0.0183
393	35,700	0.0267
393	35,700	1.670

Table 6.2 documents the various analyses performed on DRIVE. That table also indicates the reduced field records that are appropriate to the condition modeled. The first analyses were transient response analyses of the restrike, or retap, of Pile No. 1. DE was varied as shown, and the pile stresses and blow counts were compared in order to arrive at an appropriate value (or range of values) for DE. The applied load was the force-time trace recorded by calibrated strain gages located just beneath the pile head at full penetration. Strains (loads) were also monitored during restrike at two other levels below the soil surface, and their time histories were available for comparisons with the output from DRIVE.

The second analyses were preliminary investigations that were carried out to study the sensitivity of DRIVE to the variation of the time step (h_t) that was specified, the soil stiffness properties and pile head displacement magnitudes in terms of the free vibration response of the pile. Free vibration was simulated by releasing the pile after an initial extensional head displacement (i.e., "plucking"). No free vibration tests were actually performed in the field.

Single pile harmonic vibration tests were modeled by applying sinusoidal constant-force-amplitude forcing functions at the top of the pile cap. In the single pile idealization these loads equalled the nominal load values in the tests. In modeling the typical group pile, one-ninth of the total nominal test load was applied. Load functions are generated interally by DRIVE. Only the force amplitude and frequency is required as input. A total of 20 - 30 cycles of load acted on the pile in any one run to pemit damping of initial transients and convergance to steady state. The primary variables in the harmonic test runs were soil set and DE.

A "typical group pile" is defined for purposes of analysis as a group pile that responds to loading in an averge manner among the piles constituting the group. That is, in the real group the stiffness may vary from highest to lowest from the corner piles to the edge piles to the center pile, respectively. A typical group pile might respond more nearly like an edge pile than a center of corner pile. Such a definition is dictated by the fact that DRIVE and SPASM are single-pile

Table 6.2 . Schedule of DRIVE Analyses
(1 lb. = 4.45 N; 1 in. = 25.4 mm)

Pile/Mode	Vibrator/ Force Level (Nominal, Single Amp.)	Head Condition	DE (lb-sec/in.)	f-z, q-z Function Sets	Discrete Frequencies Analyzed (Hz)	Field Record Numbers (Comparisons)
Single/ Retap	N/A. Input measured head force vs. time, Pile 1, 10 April 80 retap.	I	20 40 60 100 180	A	N/A	Analog visicorder force traces and blow count records
Single/ Vertical (Free vibr.)	N/A. Input top displacement = 0.20 in., 0.01 in.	II	Best-fit value from "Single/ Retap" (60 lb-sec/in.)	A C	Natural	-
Single/ Vertical (harmonic)	WES/ 400 lb.	II	Same as above and 3 times that value	A C	28 33 38 40 42 44	602 623

Table 6.2(Cont'd). Schedule of DRIVE Analyses

Pile/Mode	Vibrator/ Force Level (Nominal, Single Amp.)	Head Condition	DE (lb-sec/in.)	f-z, q-z Function Sets	Discrete Frequencies Analyzed (Hz)	Field Record Numbers (Comparisons)
Single/ Vertical (Harmonic)	WES/ 4000 lb. and 8000 lb.	II	Same as previous	A C	28 33 38 40 42 44	616 621
Group/ Vertical (Harmonic)	WES/ 4000 lb. (444 lb./pile)	III	Same as above but use 6 times retap value	A B	30 40 55	633
Group/ Vertical (Harmonic)	WES/ 40,000 lb. (4444 lb./pile)	III	Same as above	A B C D	30 40 50 55 60 70 80	645

algorithms and that simulation of pile response based on the position of the pile within the group with these programs is unrealistic, considering the comments in Chapter 2 on dynamic group action.

Results of the DRIVE analyses are compared with field measurements in the next chapter. The specific outputs from DRIVE that were monitored and evaluated against field performance are listed in Table 6.3.

Preliminary Results. Since the results of the preliminary studies with DRIVE (restrike and free vibration) provided a basis for selection of inputs to model the harmonic field tests, it is appropriate to describe the preliminary results here.

The restrike study is summarized in Figs. 6.8 - 6.11. Figure 6.8 shows the measured force-time trace from a typical blow from the Delmag D-12 hammer at full penetration at the pile head, which was input into DRIVE. Figures 6.9 and 6.10 show the measured and computed force-time histories at 16 ft (4.9 m) and 26 ft (7.9 m) below the ground surface, respectively, for different prescribed values of DE, which were assumed constant over the entire embedded depth of the pile. DI was set at zero throughout. At both levels a DE of 40 - 60 lb-sec/in (7.0 - 10.5 N-sec/MM) appeared to give reasonable results. That value did not yield an accurate value of the pile-head set, however, as indicated in Fig. 6.11. The best agreement with set appeared to occur at DE = 160 lb-sec/in (28.0 N-sec/MM) for the condition of uniform external damping, zero internal damping, and soil resistance from static tests.

Additional modeling of the restrike of Pile 1 was conducted by letting the damping at the pile tip be three times the value for DE along the sides of the pile. This alteration changed the force-time histories in Figs. 6.9 and 6.10 very little but gave a value of DE that matched the measured pile-head set and that was much closer (but not yet equal) to the value that best modeled the force-time histories. An additional run was made in which the tip capacity and static stiffness was increased by 50% relative to the measured static values and where the tip damping remained at three times the side damping, with slightly improved results. Variations of DE along the lengths of the piles were not attempted, nor was the inclusion of added mass, which would have made the pile yield a smaller set per blow with a given DE.

Table 6.3. Output Evaluations For Program DRIVE
(1 in. = 25.4 mm; 1 ft = 0.305 m)

Pile/Mode	Evaluations For Each Combination of Parameters
Single/Retap	1. Force vs. time at pile top and at two levels below soil surface 2. Blows per inch Objective: To ascertain external damping value from retap test.
Single/Vertical (Plucking)	1. Total damping ratio (from log decrement), hysteretic damping ratio from pile force vs. deflection hysteresis curves with zero external damping, and radiation damping ratio (differences between total and hysteretic). Results computed at soil surface and depths of 21 and 36 feet below surface and at pile tip. Objective: To compare relative hysteretic and radiation damping at pile-head displacement typical of retap displacement (0.2 in.) and harmonic loading displacement (0.01 in.).
Single and Group/Vertical (Harmonic)	1. Acceleration, velocity, and displacement vs. time at 5 ft above and 2, 10.5, and 29.5 ft below ground surface. 2. Peak acceleration, velocity, and displacement vs. frequency at each depth denoted above. 3. Phase angle between displacements at 5 ft above ground surface and other depths denoted in 1, above. Objective: To compare with measurements. (In all instrumented piles in group.)

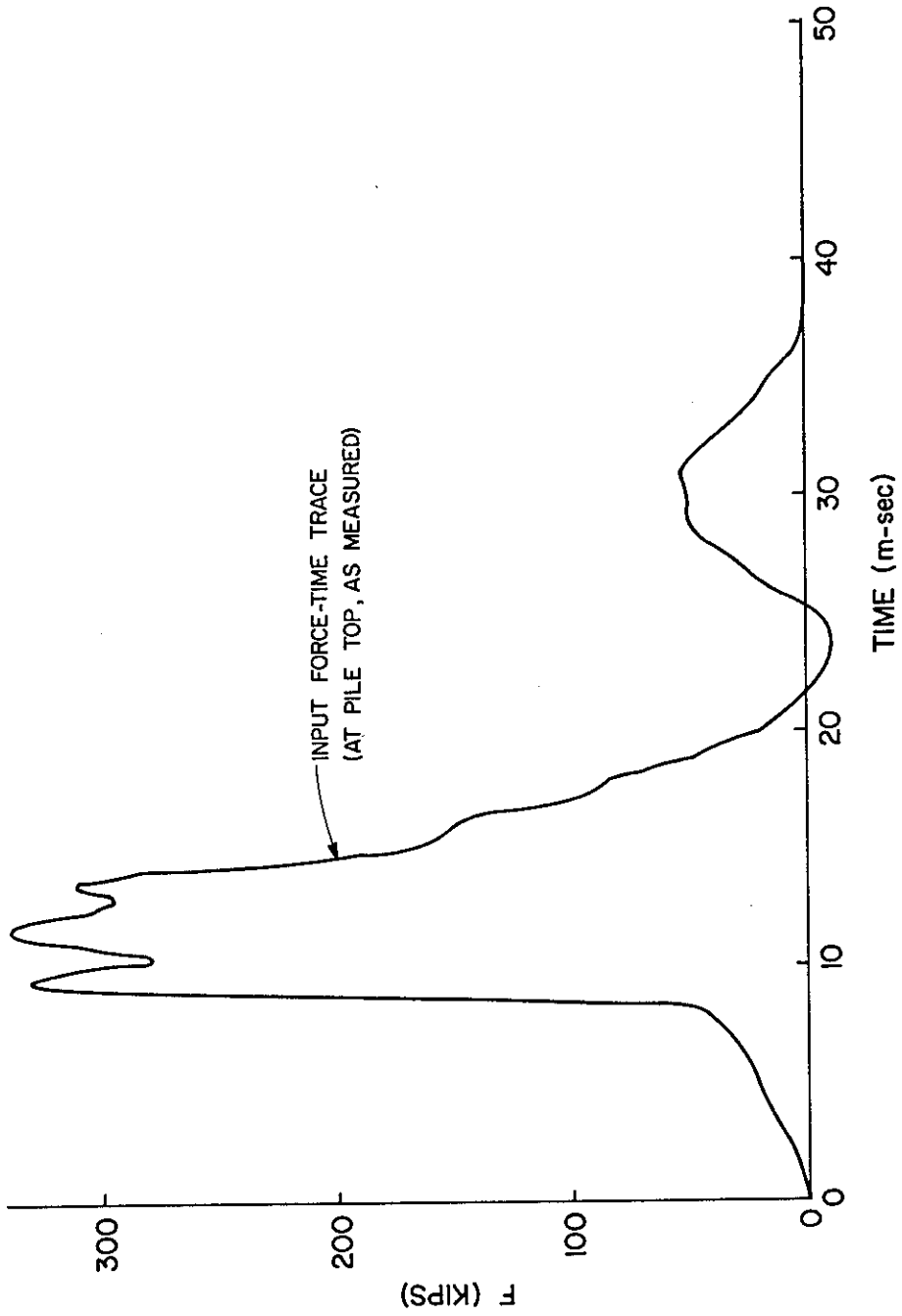

Fig. 6.8. Measured Force-Time History: Pile 1 Restrike; Pile Head (1 k = 4.45 kN).

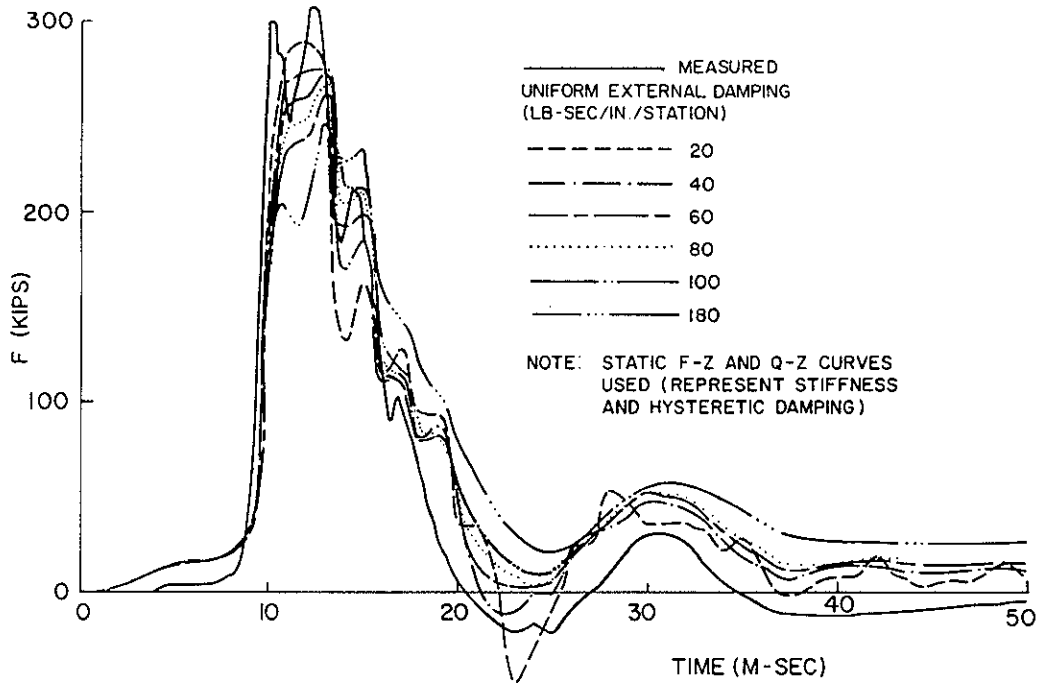

Fig. 6.9. Pile 1 Restrike; 4.9 m Depth (1 lb = 4.45 N; 1 k = 4.45 kN; 1 in. = 25.4 mm).

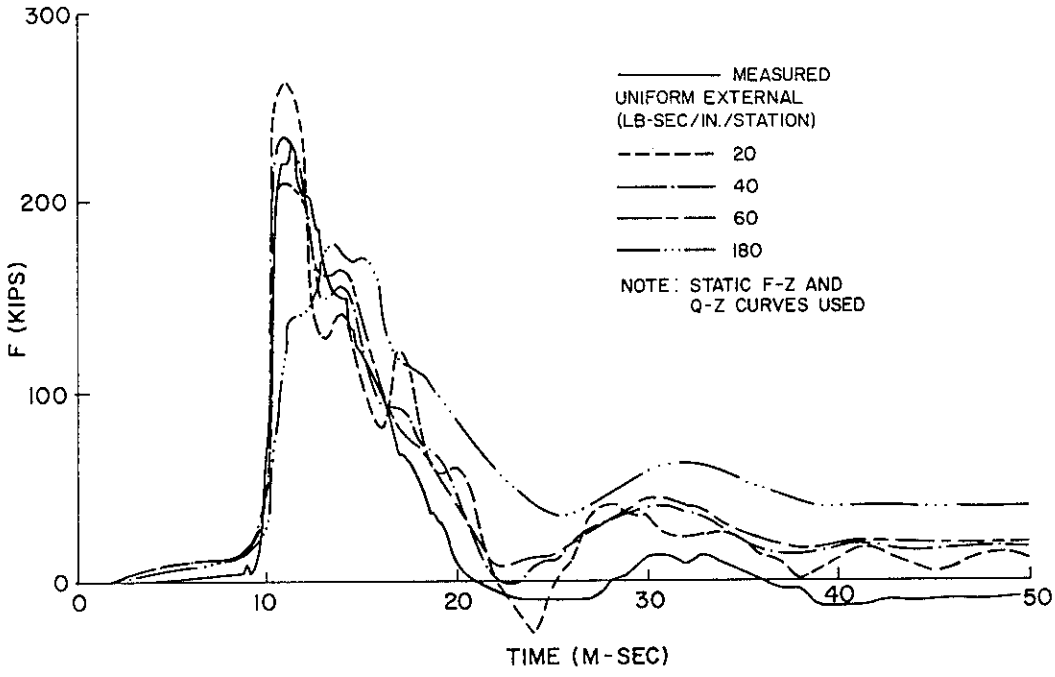

Fig. 6.10. Pile 1 Restrike; 7.9 m Depth (1 lb = 4.45 N; 1 k = 4.45 kN; 1 in. = 25.4 mm).

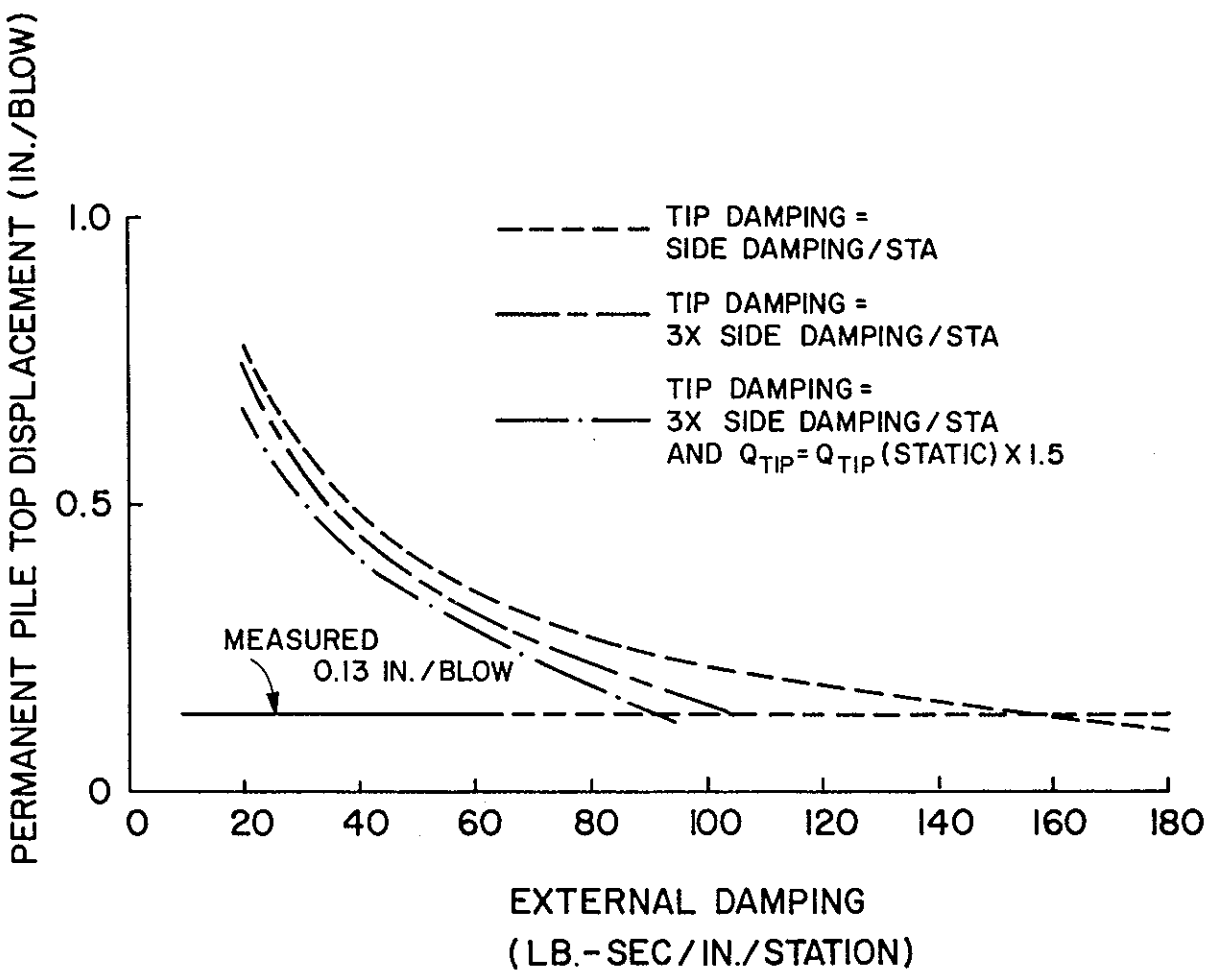

Fig. 6.11. Permanent Set vs. Prescribed External Damping (DRIVE)

The principal conclusion of the study was that a range of uniform DE values of 60 - 180 lb-sec/in. (10.5 - 31.5 N-sec/mm) represented a reasonable range of values to input into the harmonic runs. Further modeling of the restrike was not thought to be warranted because of uncertainties concerning the appropriateness of using the static f-z and Q-z curves (and resultant hysteretic damping) to model pile driving, the absence of any method to evaluate independently the variation of DE along the pile in light of the preceding uncertainty, and the applicability of using transient loading radiation damping to represent harmonic loading.

Typical results of the free vibration analyses are shown in Figs. 6.12, 6.14, and 6.15, and in Tables 6.4 and 6.5. Figure 6.12 summarizes a series of runs conducted to investigate the appropriate time step by plotting pile head displacement versus time for Soil Set A, DE = 60 lb-sec/in. (10.5 N-sec/mm), and an initial head displacement of 0.2 in. (5.1 mm) with zero initial velocity for various time steps. Based on these runs, a time step of 0.001 sec. was chosen for modeling the steady state, forced vibration, field tests, except when the soil was very stiff (Set D), where 0.0005 sec. was employed. This choice was confirmed by conducting steady state, forced vibration analyses of the single pile with time steps of 0.001 and 0.0005 seconds for the conditions shown in Fig. 6.13. Both solutions converged to identical displacement values by the third cycle of applied load.

Analysis of the free vibration data indicates that in general h_t (Δt) should be equal to or less than $1/12f_n$, where f_n is the natural frequency of the pile, in order to obtain a stable solution.

Decay curves from the free vibration runs for soil Sets A and C are shown in Figs. 6.14 and 6.15, respectively. The displacements of the pile at Stations 8 (just below ground surface) and 28 (mid-penetration-depth of the pile) are shown. Soil reaction (lumped force at indicated station) vs. displacement loops are also shown (except for Station 28, Set C). The area of the loop is a reflection of total damping. The total damping ratio was also estimated from the decay curve by the logarithmic decrement method (76). Damping can be seen to decrease with increasing cycle number, with distance along the pile, and with

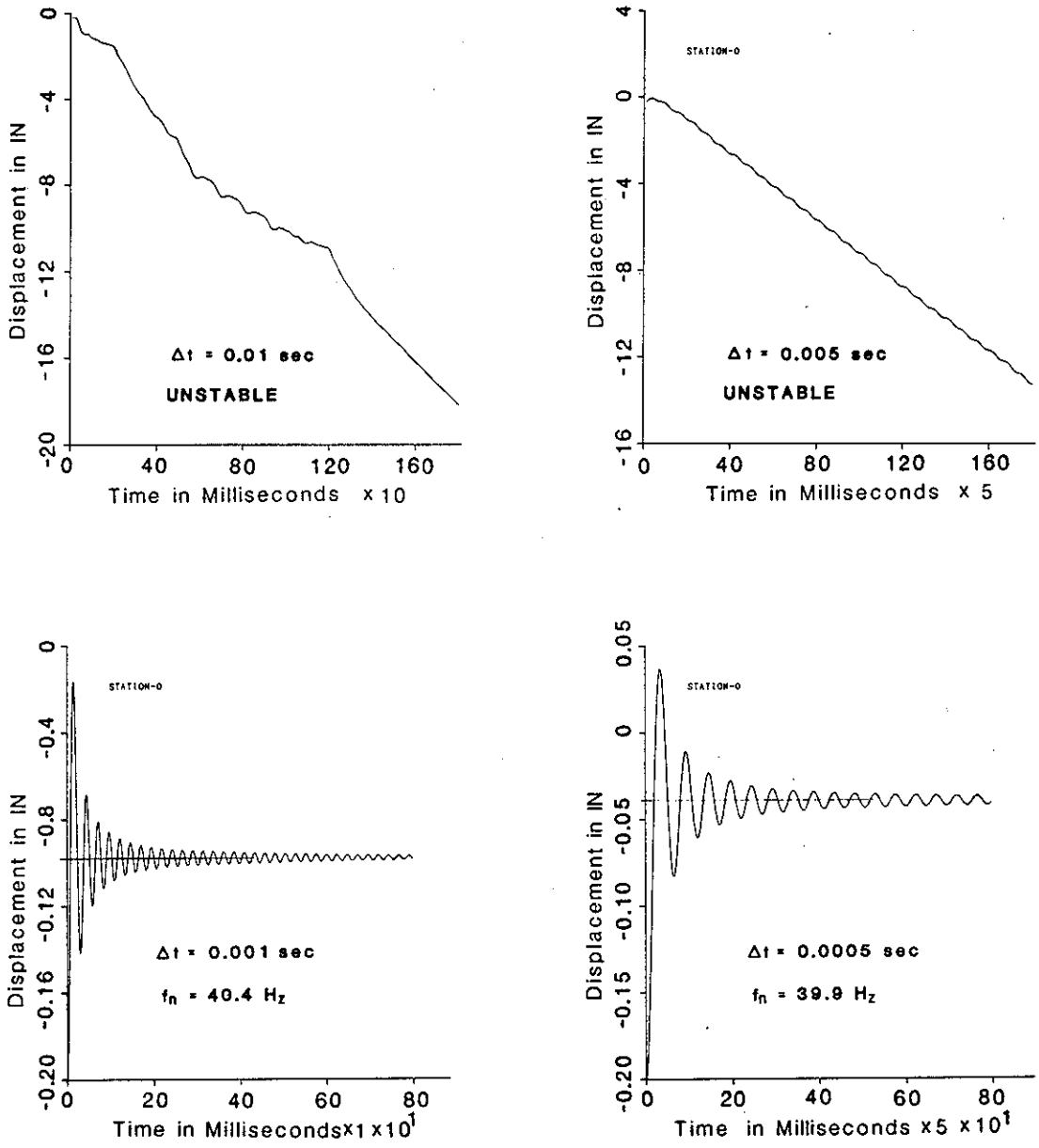

Fig. 6.12. Computed Time Histories of Free Vibration of Head of Single Pile from DRIVE for Different Δt values (1 in. = 25.4 mm).

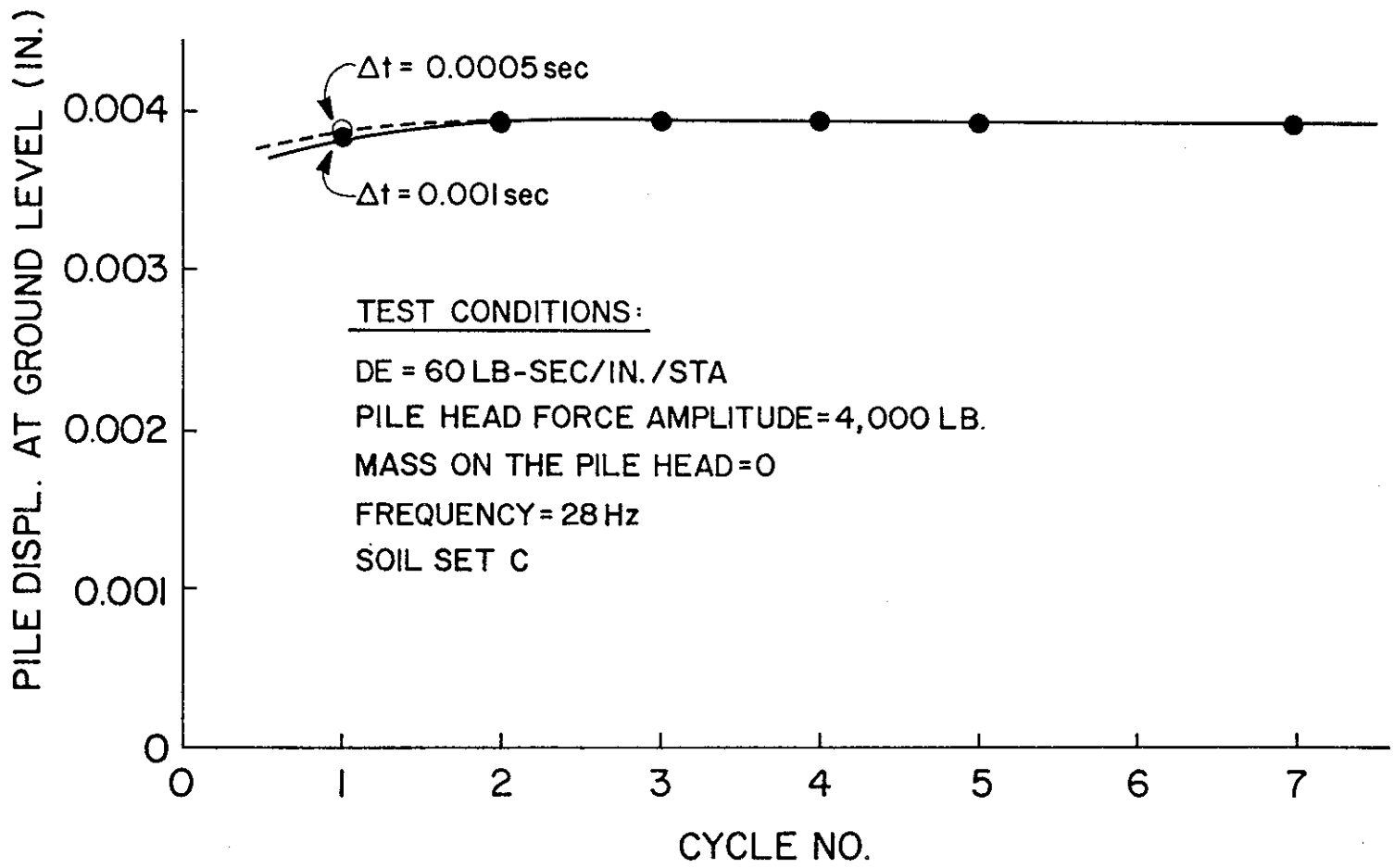

Fig. 6.13. Effect of Δt on Pile Displacement in DRIVE for Steady State Loading (1 in. = 25.4 mm).

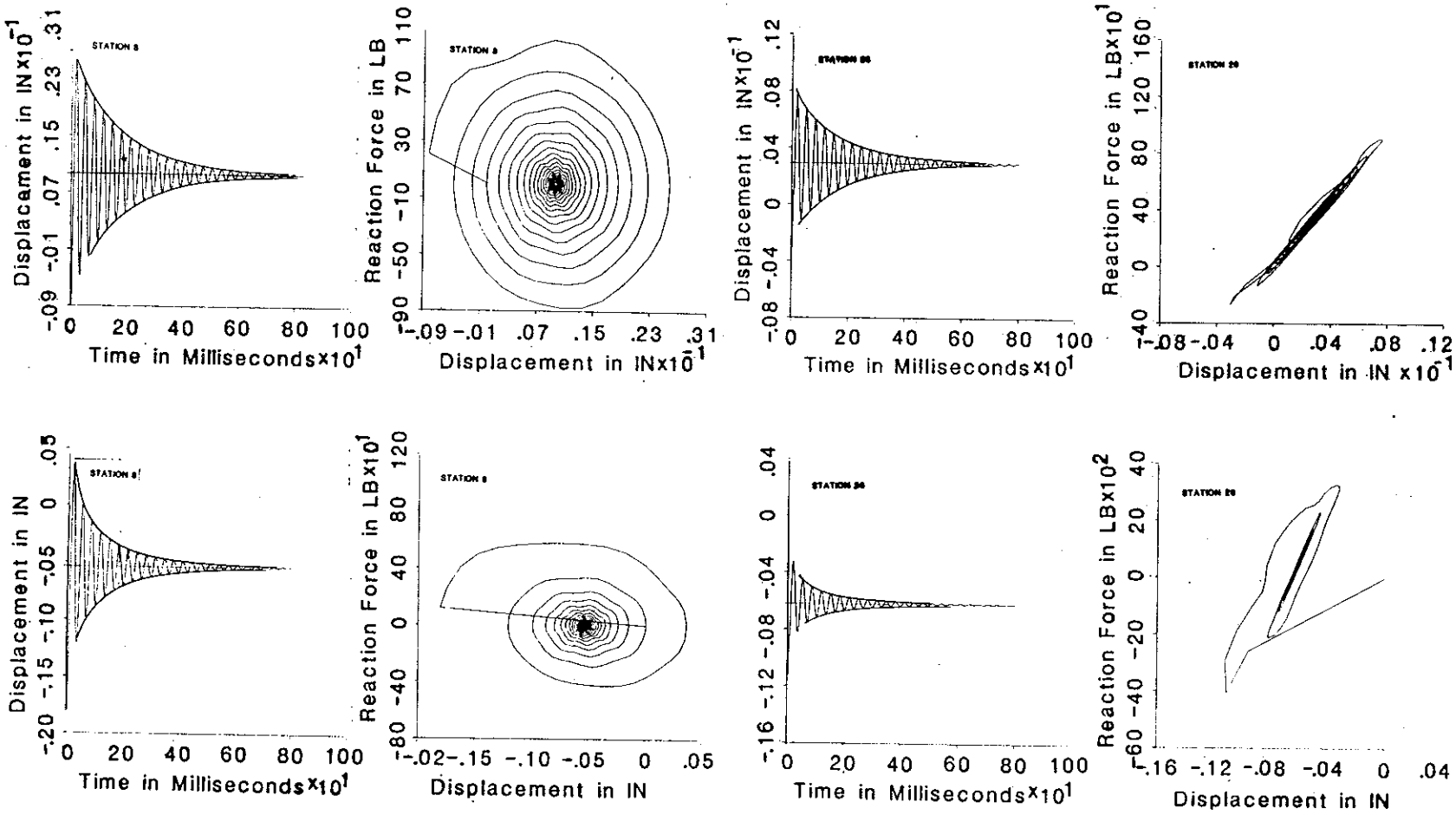

Fig. 6.14. Computed Displacement-Time and Soil Reaction-Time Histories: Soil Set A, δ_u = - 0.01 in. (top), = - 0.2 in. (bottom), Δt = 0.001 sec, C_e = 60 lb-sec/in./sta. (1 in. = 25.4 mm; 1 lb = 4.45 N).

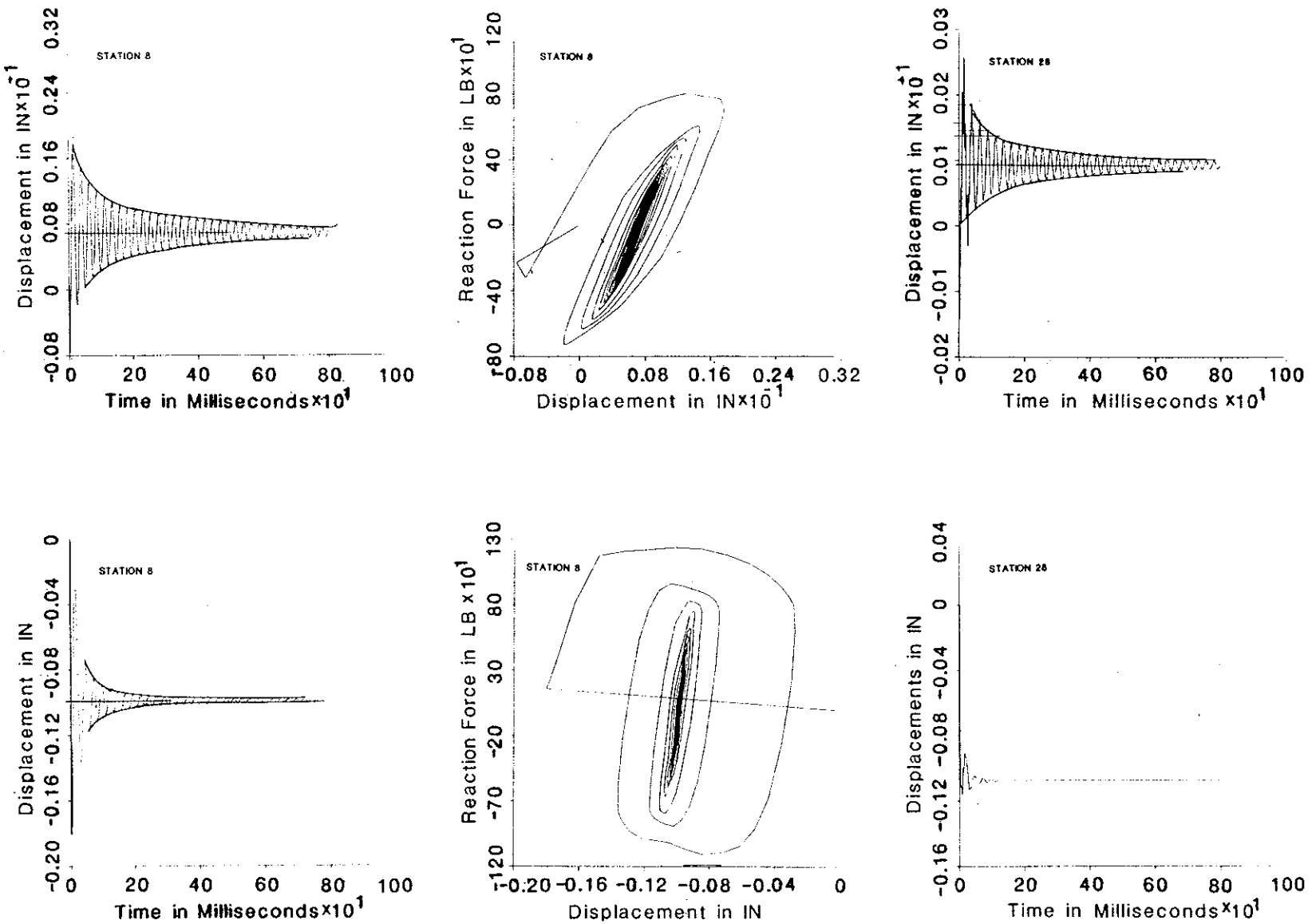

Fig. 6.15. Computed Displacement-Time and Soil Reaction-Time Histories: Soil Set C, δ_u = - 0.01 in. (top) = - 0.2 in. (bottom), Δt = 0.001 sec, C_e = 60 lb-sec/in./sta. (1 in. = 25.4 mm; 1 lb = 4.45 N).

Table6.4. Total Damping for Single Pile Undergoing Free Vibration; Program DRIVE (1 in. = 25.4 mm; 1 lb = 4.45 N)

Pile	Soil Case	Initial Displacement (in.)	Prescribed External Damping (lb-sec/in./sta.)	Damping Ratio
Single (II)	A	0.01	60	0.0330 (2)[a]
				0.0315 (4)[b]
	A	0.2	60	0.0558 (2)
				0.0372 (4)
	C	0.01	60	0.0472 (2)
				0.0257 (4)
	C	0.2	60	0.0910 (2)
				0.0322 (4)

[a]From logarithmic decrement between first and second cycle: Average of Stas. 10, 18 and 37.

[b]From logarithmic decrement between third and fourth and all subsequent cycles: Average of Stas. 10, 18 and 37.

Table6.5. Free Vibration Simulation; Single Pile With Cap; Program DRIVE (1 in. = 25.4 mm; 1 lb = 4.45 N)

Pile Head Condition	Initial Displacement (in.)	Unit Load Transfer Curve Set	Natural Frequency (Hz)
II	0.01	A	30.86
II	0.2	A	30.49
II	0.01	C	40.71
II	0.2	C	39.88

Note: Prescribed external damping = 60 lb-sec/in./sta.

decreasing initial top displacement. Since nonlinear hysteresis and pile flexibility are modeled by DRIVE, these results are not unexpected.

Estimated damping ratios are tabulated in Table 6.4 for Soil Sets A and C at the second and fourth cycles of free vibration. The damping ratio is not constant, because of the influence of hysteretic damping.

When the imposed initial head displacement was 0.01 in. (0.25 mm), displacements all along the piles were below the values that might be described as yield values in Figs. 4.2 and 4.3. Thus, the higher initial (Cycle 2) damping ratios for a 0.01 in. (0.25 mm) head displacement in Set A are probably largely attributable to the manner in which the soil reaction curves were modeled; specifically to the exact displacement values that were input on the f-z curves. That is, in Set A almost no subelements were released (reached yield value), while several were released in Set C during a cycle of displacement. This occurred because the computed displacement values equalled or exceeded the value of the first non-zero point input for f-z only at the top few stations in Set A but exceeded the value of the third or fourth point to a considerable depth in Set C. At least one subelement must be released at any station for hysteretic damping to be simulated. Release of several subelements representing a nonlinear f-z curve signifies larger hysteretic damping than the release of one subelement. This additional subelement release in Set C, coupled with the lower stiffness in Set A, produced the higher initial damping ratios in Set C. A similar explanation can be offered to describe the initial (second cycle) damping ratio variation associated with 0.2 in. (0.51 mm) head displacements. No attempt was made to study the effect of the values of input points on the f-z and Q-z curves directly, but this limitation of the program should be considered. Subelement modeling of hysteretic damping is discussed further as it relates to SPASM.

By the fourth cycle the displacements generally reduced to small values in both soil sets, so that the external (simulated radiation) damping became predominant. The fourth cycle damping ratio was about 3% in all cases. It is of significance to point out that at no time did the estimated free vibration damping ratio ever exceed 9.1%. Damping implied from the field tests was always larger than 9.1%, as will be seen in the next chapter.

The natural frequencies, f_n, from the free vibration simultations are tabulated in Table 6.5. For Set A f_n was about 31 Hz, and for Set C f_n was about 40 Hz, with only minor dependance on displacement amplitude. These natural frequencies bounded the measured range of measured resonant frequencies in the field tests.

It is of interest to note that a fourfold increase in soil stiffness (Set A to Set C) increased the system natrual frequency by only 30%. Had soil stiffness completely controlled the system stiffness, the increase in f_n should have been about 100%. The axial stiffness of the pile itself thus had a strong influence on the pile-soil system response.

Observations. Program DRIVE was designed primarily to model nonlinear, transient response and therefore has many versatile features, including arbitrary force input, hysteretic damping simulation from f-z curves, and provisions for a number of different head restraints. However, it was found to be tedious to use for free vibration and steady state analyses of quasi-linear (low displacement), harmonic vibration problems because of the large amount of data input required. Some of these data require some form of preprocessing (e.g., f-z curves must be derived by some means). Computations and output are in the time domain, requiring considerable computational effort and, in the case of the present study, post-processing of the output was necessary to produce transfer functions.

SPASM

Inputs. The input procedures for SPASM (horizontal excitation) paralleled those for DRIVE: pile and cap idealization, without adding soil mass to the pile elements, soil characterization through p-y curves, and harmonic force application. Several deviations from the procedure described for DRIVE existed, including adoption of independent procedures for calculating p-y curves for the single pile and pile group and for external damping values for lateral motion, since no horizontal static or transient tests that would yield these inputs were available for the piles at the site at the time the analyses were made. (Static pretesting to determine the p-y curves explicitly is destructive and could not have been performed on any of the piles later tested

dynamically. It may be possible to conduct future static lateral load tests of instrumented 10.75 in. (273 mm) diameter piles to measure the p-y curves directly or to deduce p-y curves from the post-test lateral loading described in Chapter 4.) Furthermore, because lateral loading involved coupled lateral translation and rotation about a horizontal axis, special procedures had to be followed to model the caps in a way to allow correct loads and moments to be applied relative to the CG, while maintaining the correct mass moments of inertia.

Separate solutions were obtained for the single pile and for a typical pile in the group. The physical model parameters for the single pile and cap and a typical group pile and cap are shown in Fig. 6.16. The caps (dashed lines), as modeled, are one order of magnitude stiffer in flexure than a single pile and contain approximately the same mass as the real caps they represent. The mass moment of inertia (MMI) of the single pile cap, as modeled, is essentially correct. In order to obtain correct mass and MMI in the single pile cap, it was necessary to change the cap dimensions to those shown in Condition A, Fig. 6.16.

In the cap for the typical group pile (Condition B, Fig. 6.16) one-ninth of the real pile mass was assigned as the modeled mass. The mass was distributed over the top 9 stations to give a close correlation between the positions of the physical CG and modeled CG, but no attempt was made to model the MMI, since it was unclear how the MMI of the group cap should be distributed among the piles when analyzing a typical pile in the group. However, a large, constant rotational restraint was applied at Station 8 to simulate the restraint offered by the vertical stiffness of the piles as the group cap rotated. The rotational restraint was assumed to have a more significant influence on group pile performance than cap inertia. One-ninth of the applied load was assumed to be resisted by the typical group pile (Condition B).

Some errors appear in the location of the load vector relative to the cap CG because the load vector had to be input at station locations, which for convenience and purposes of both computational stability and efficiency were placed at 1 ft (0.305 m) increments.

Other index information, including time step values, numbers of stations, flexural stiffnesses, and pile material damping are shown in Fig. 6.16.

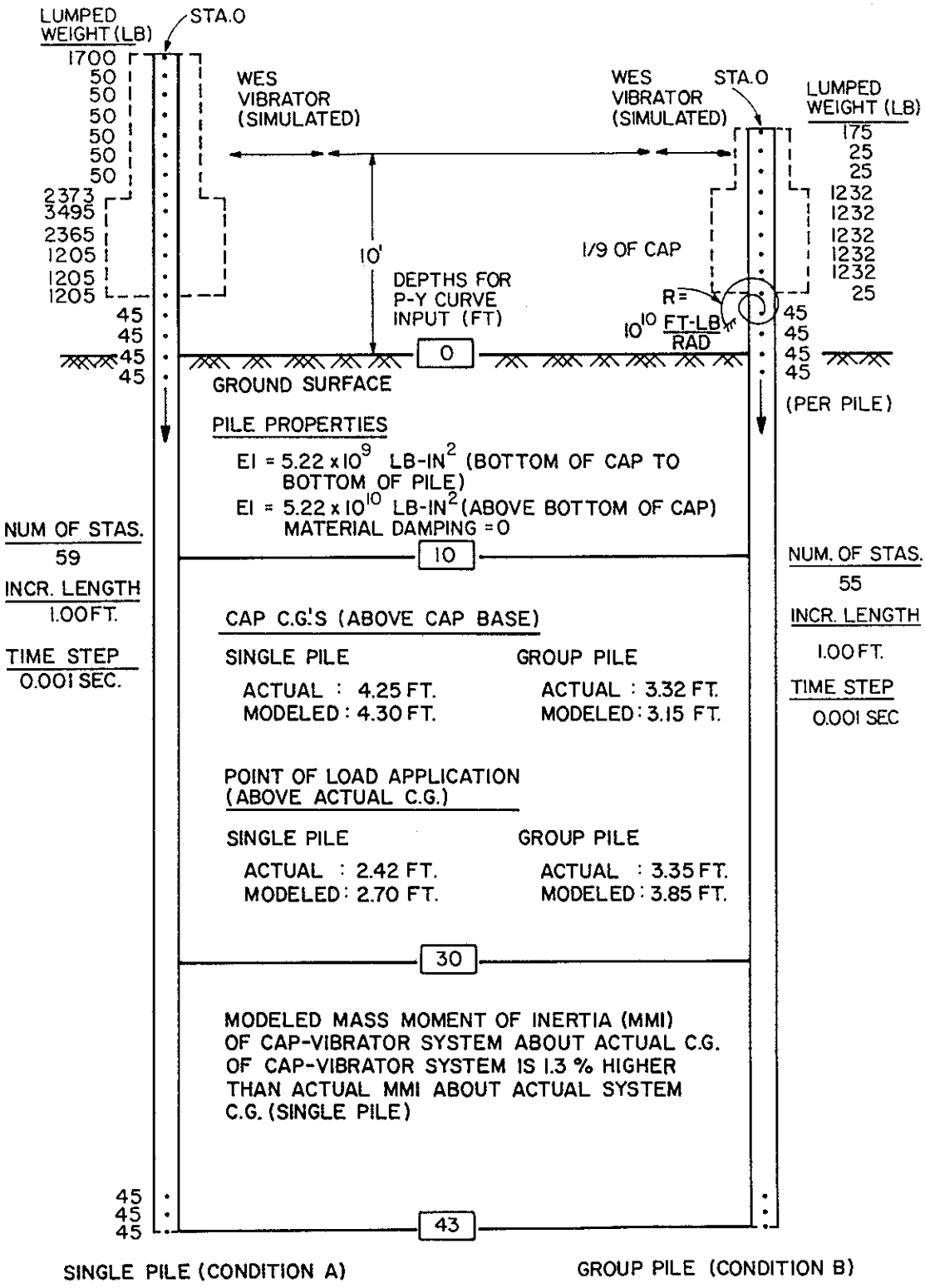

Fig. 6.16. Pile Properties Used in SPASM (1 lb = 4.45 N; 1 ft = 0.305 m; 1 psi = 6.89 kPa).

Discrete-valued soil resistance curves (p-y curves) were input at the depths indicated on Fig. 6.16, and linear interpolation of the curve coordinates was made between input levels.

Four apparently reasonable sets of values of p and y for the soil at the test site all were employed in the study. They are tabulated as Sets I - IV in Table 6.6.

Set I was used to model the single pile (Condition A, Fig. 6.16) and was the Matlock criterion (43) for quasi-static cyclic loading. Matlock's criterion was developed from the analysis of model and full-scale tests of laterally loaded piles in soft to medium stiff clays. The inputs required to represent soil behavior at the various levels where p-y curves are input include

1. ε_{50} = principal strain corresponding to 50% of the peak principal stress difference in triaxial compression,
2. c = undrained cohesion, and
3. γ = unit weight (submerged value below the water table).

Values of ε_{50}, c, and γ obtained from UU triaxial tests and density tests for the site soil (41) were averaged to arrive at the values given in Table 6.6. Ultimate values of p (p_u) were calculated from Eq. (6-12) or Eq. (6-13), depending on whether the soil depth was below the critical depth x_r, determined as indicated in Table 6.6.

$$p_u = 3cb + \gamma xb + \frac{cx}{2} \qquad (x \leq x_r) \qquad (6\text{-}12)$$

$$p_u = 9cb \qquad (x > x_r) \qquad (6\text{-}13)$$

where x = distance below soil surface and b = pile diameter. Values along the backbone (non-degraded) p-y curves were them computed from the cubic equation in Table 6.6, where $y_{50} = 2.5b\varepsilon_{50}$. Matlock's recommendations for cyclic degradation were then applied (43) to arrive at the values tabulated. Two-way symmetric behavior was assumed.

In addition, SPASM subelements were allowed to "gap" (remain disengaged) fully at the ground surface, were not allowed to gap below depth X_r (10 ft (3.05 m)), and partial gapping, as indicated in Table 6.6, was permitted between the ground surface and depth X_r. Additional degradation specifications available in SPASM (44) were not utilized.

Table 6.6. Soil Response (p-y) Curves For SPASM Analyses
(1 ft = 0.305 m; 1 in. = 25.4 mm; 1 lb = 4.45 N; 1 psi = 6.89 kPa)

Set I: (Matlock's Soft Clay Cyclic Criteria, Offshore Technology Conference, 1970)

Soil factors

a. ε_{50}: 0 - 10' 0.010
10 - 30' 0.004
30 - 43' 0.012

(UU triaxial test data, Report No. FHWA/RD-81/005)

b. Undrained cohesion (c): 0' 16.0 psi
30' 16.0 psi
>30' 27.8 psi

(UU triaxial test data, Report No. FHWA/RD-81/005)

c. Unit weight (γ): 0' - 7.5' 133 pcf
>7.5' 66 pcf

$\frac{X_r}{b}$ (depth of wedge zone): $[3 + \frac{\gamma X_r}{C} + \frac{X_r}{2b}] = 9$: X_r = 10 ft
(b = 10.75 in.)

p-y Curves $(p/p_u) = (y/y_{50})^{1/3}$ (Backbone Curve)

1. Depth = 0'		2. Depth = 10'		3. Depth = 30'		4. Depth = 43'	
p (lb/in.)	y (in.)	p (lb/in.)	y (in.)	p (lb/in.)	y (in.)	p (lb/in.)	y (in.)
0	0	0	0	0	0	0	0
147	0.05	440	0.05	599	0.05	722	0.05
212	0.15	637	0.15	773	0.108	1041	0.15
258	0.27	773	0.27	1112	0.15	1234	0.25
371	0.803	1112	0.803	1112	5.00	1344	0.32
0	4.00	1112	4.00			1935	0.97
0	5.00	1112	5.00			1935	5.00

Notes: 1. Linear interpolation between depths specified.

2. Program SPASM permits gap to form at deflections up to 5.0 in. at depths up to 10 ft (X_r). Zero Degradation specified (ie, all subelements are gap-type subelements at soil surface-zero are gap type subelements at depth = 10 ft).

Table 6.6.(Cont'd). Soil Response (p-y) Curves For SPASM Analyses

Set II: (Same as Set I, but with stretching factors (YFACT) from static run of 9-pile group with PILGP1[a], with lateral force and moment corresponding to 12,000 lb force amplitude with WES vibrator, applied to y-values.)

1.	Depth = 0'	YFACT = 1.31
2.	Depth = 10'	YFACT = 1.14
3.	Depth = 30'	YFACT = 1.04
4.	Depth = 43'	YFACT = 1.02

a. PILGP1 is a digital computer program for static analysis of pile groups. (See Report No. FHWA/RD-81/003).

Table 6.6 (Cont'd). Soil Response (p-y) Curves For SPASM Analyses

Set III: (Kagawa-Kraft Procedure for Real Component of Stiffness: Soils and Foundations, Japanese Society of Soil Mechanics and Foundation Engineering, Dec. 1980)

General form: $p = \tilde{\delta}_1 E_{max} \{\frac{\gamma_r}{\frac{0.6}{b} y + \gamma_r}\} y$

Use $\tilde{\delta}_1$ = 1.5 per authors' recommendation

Use ν (soil) = 0.5; b = 10.75 in.

Use $\gamma_r = \tau_{max}/G_{max}$

Soil factors

a. τ_{max}:

0'	16.0 psi
30'	16.0 psi
>30'	27.8 psi

(per undrained cohesion for Set I)

b. G_{max}:

0'	6500 psi	[a]
10'	8400 psi	[b]
30'	18250 psi	[c]
43'	24900 psi	[d]

c. γ_r:

0'	0.0025
10'	0.0019
30'	0.0009
43'	0.0011

d. $E_{max} = 3 G_{max}$

---

a. Based on v_s = 480 ft/sec
b. Based on v_s = 555 ft/sec (avg of v_s at 10'- and at 10'+)
c. Based on v_s = 800 ft/sec
d. Based on v_s = 935 ft/sec (avg of v_s at 42'- and 42'+)

Table 6.6 (Cont'd). Soil Response (p-y) Curves For SPASM Analyses

p-y Curves

1. Depth = 0'		2. Depth = 10'		3. Depth = 30'		4. Depth = 43'	
p (lb/in.)	y (in.)	p (lb/in.)	y (in.)	p (lb/in.)	y (in.)	p (lb/in.)	y(in.)
0	0	0	0	0	0	0	0
28.6	0.001	36.7	0.001	77.3	0.001	106.6	0.001
131.6	0.005	164.8	0.005	313.5	0.005	446.9	0.005
239.1	0.01	292.2	0.01	506.9	0.01	743.4	0.01
691.2	0.05	765.7	0.05	1002	0.05	1584	0.05
905.0	0.10	983.0	0.10	1141	0.10	1845	0.10
1203	0.50	1234	0.50	1283	0.50	2125	0.50
1203	5.00	1234	5.00	1283	5.00	2125	5.00

Notes: 1. Linear interpolation between depths specified.

2. Program SPASM permits gap to form at deflections up to 5.0 in. at depths up to 10 ft (X_r). Zero degradation specified.

Set IV: (Same as Set III, but with stretching factors (YFACT) from static run of 9-pile group with PILGP1, with lateral force and moment corresponding to 12,000 lb force amplitude with WES vibrator, applied to y-values.)

1. Depth = 0' YFACT = 2.50
2. Depth = 10' YFACT = 1.40
3. Depth = 30' YFACT = 1.10
4. Depth = 43' YFACT = 1.06

Set II, which was used to model a typical group pile (Condition B), was identical to Set I except that the deflection (y) values were multiplied by "stretching factors" (YFACT) that represent the average effects among all 9 group piles of static soil offset at the various levels where p-y curves are input due to group action (62). Values of YFACT were obtained by executing a static pile group analysis program entitled PILGP1 (28) for the loading conditions described in Table 6.6. PILGP1 obtains solutions for displacements and moments along piles in a rigidly capped group by softening (or stiffening) p-y curves for isolated pile behavior through the use of elasticity methods that compute the displacements of soil around the various group piles due to soil reactions against all other group piles (i.e., "stretch" the p-y curves). The soil transmitting these reaction effects to any location on any generic pile is assumed to behave elastically. For purposes of developing the Set II curves, the low-strain Young's modulus variation from Fig. 3.9 was approximated in PILGP1 by setting E at the soil surface equal to 18,250 psi (125.7 MPa), E at the pile tips equal to 65,500 psi (451.3 MPa), and assuming a linear variation of E between the two levels. Poisson's ratio for the soil was taken to be 0.5. The process of applying the YFACT multipliers to the p-y curves is equivalent to applying Eq. (6-11). The resulting p-y curves are symmetric and are slightly softer than those for single pile behavior (Set I).

Set III (single pile) was a set of p-y curves derived from an approximation of the dynamic finite element solutions for seismic loading conditions obtained by Kagawa and Kraft (34), assuming that excess pore pressures generated by loading are negligible. The nonlinear equation that was used to compute points on the p-y curves is given in Table 6.6, where E_{max} amd G_{max} are the small-strain Young's modulus and shear modulus, respectively, obtained from Fig. 3.9 (crosshole tests) as confirmed in Fig. 3.8 (resonant column tests); γ_r is a reference strain defined in Table 6.6; τ_{max} is the shear stress on the failure plane at failure in undrained shear; ν is Poisson's ratio of the soil; v_s is shear wave velocity; and δ_1 is a stiffness factor, developed in Ref. 34, equal to 1.5.

Resulting values of p and y are tabulated in Table 6.6. Gapping was specified as in Sets I and II.

Kagawa and Kraft, in deriving a more general version of the p-y equation in Table 6.6, obtained an approximate relationship between y (or u in the notation of the mathematical models) and the average shear strain in the soil, γ:

$$y \text{ (or } u) = \frac{2.5b}{1 + \nu} \gamma \tag{6.14}$$

Equation (6-14) was used to relate the shearing strain amplitudes in Figs. 3.10 - 3.12 to lateral pile displacement and is identical to Eq. (3.2) for b = D = 10.75 in. (273 mm) and ν = 0.5 (incompressible soil).

Finally, Set IV was used to model the typical group pile. It was developed from Set III following the procedure used to develop Set II from Set I. The YFACT values for Set IV are tabulated in Table 6.6. They are larger than those for Set II because the Set III p-y curves are stiffer than the Set I curves and because the same mass soil stiffness was used in PILGP1 to model group action for both situations.

Harmonic load functions must be input pointwise in SPASM. Twelve points per cycle were input to define sine curves, and a total of 5 to 7 load cycles were applied. Generally, this number of cycles was sufficient to reach steady state response.

Representation of Damping. The representation of damping in SPASM requires computation of hysteretic damping from the p-y curves and radiation damping from a viscous dashpot.

The viscous dashpot constants could not be evaluated from experiments, as was the case for the DRIVE analyses. Instead, D^e values were evaluated from p-wave velocities using a modification of a single procedure suggested by Berger, et al. (11), in which energy was assumed to be lost only from the pile by propagation of p-waves in front of and behind the pile. This assumption presumes that any shearing of soil on surfaces parallel to the plane of loading produces negligible seismic waves. The procedure for evaluating D^e from measured shear wave velocity profiles is outlined in Table 6.7, where ρ is the unit mass of the soil. D^e values were varied vertically along the pile but were not

Table 6.7. Damping Inputs For SPASM Analyses
(1 ft = 0.305 m, 1 in. = 25.4 mm, 1 lb = 4.45 N)

1. For all SPASM runs, hysteretic soil damping effects are contained in the p-y curves.

2. External (radiation) damping must be specified. Berger, et al., Offshore Technology Conference, 1977, recommend

$$D^e = 2A\rho v_p = 6.64A\rho v_s \qquad (\nu = 0.45)$$

(p-wave effect only, per Kagawa and Kraft (34))

$$\rho = 2 \times 10^{-4} \frac{\text{lb - sec}^2}{\text{in}^4} \qquad \text{(assume constant)}$$

A = projected lateral area of an element = 129 $\text{in.}^2/\text{ft}$

Where gapping can occur (0 - 10 ft), D^e should be reduced by one-half.

Depth (ft)	v_s (in./sec.)	D^e $\frac{\text{lb - sec}}{\text{in.}}/\text{ft}$
0	5760	493
10	6660	1140
30	9600	1645
43	11220	1922

Use above common values for <u>all</u> runs. Linear variation between depths assumed.

3. Assume material damping in pile is zero.

varied between SPASM runs employing Set I and III p-y curves (single pile) and Set II and IV p-y curves (group pile).

Hysteretic damping, which is contained in the nonlinear p-y curves, is probably more important in the horizontal mode of loading than in the vertical mode. Hence, further consideration of the way in which SPASM models hysteretic damping is in order here. Hysteretic damping D_h as a percentage of critical damping was computed as a function of lateral displacement (y) with full reversal from the hysteresis loops generated by the subelement formulation for the Set III p-y curves (discrete point input) at a depth of 7 ft (2.1 m). The resulting function in shown in Fig. 6.17. No hysteretic damping is simulated as long as the pile displacement is less than the first non-zero y value input (Point 1 in Fig. 6.17), since no subelement is released. Between Points 1 and 2, one subelement is released, and the damping ratio varies as shown. At Point 2 a second subelement is released, with the resulting D_h shown between Points 2 and 3. At Point 3 a third subelement would be released, etc.

The hysteretic damping implied from high amplitude resonant column testing of the sample recovered from a depth of 6.8 ft (2.1 m), from Fig. 3.12, is also shown in Fig. 6.17. The Set III curves appear to provide a good approximation of the laboratory curve in the deflection range shown, with hysteretic damping ratio errors of 1% of critical or less, throughout. However, for Set I the first non-zero y value input is at 0.05 in. (1.3 mm). At that point the implied hysteretic damping ratio from the resonant column test is already 14%. This observation indicates that SPASM could underestimate hysteretic damping significantly at small displacements in Set I, where "small" is defined as a value less than the first non-zero y value input.

Time steps used in all runs were 0.005 sec for $f_n \leq 5$ Hz and 0.001 sec for $f_n > 5$ Hz.

Analyses. Table 6.8 documents the analyses performed on SPASM. Only the WES vibrator was simulated, and only harmonic tests were modeled with SPASM. As with DRIVE, the applied load amplitudes in the single pile idealizations approximated the nominal values used in the load tests. For the typical group pile, one-ninth of the test load amplitudes were applied. The specific outputs from SPASM that were

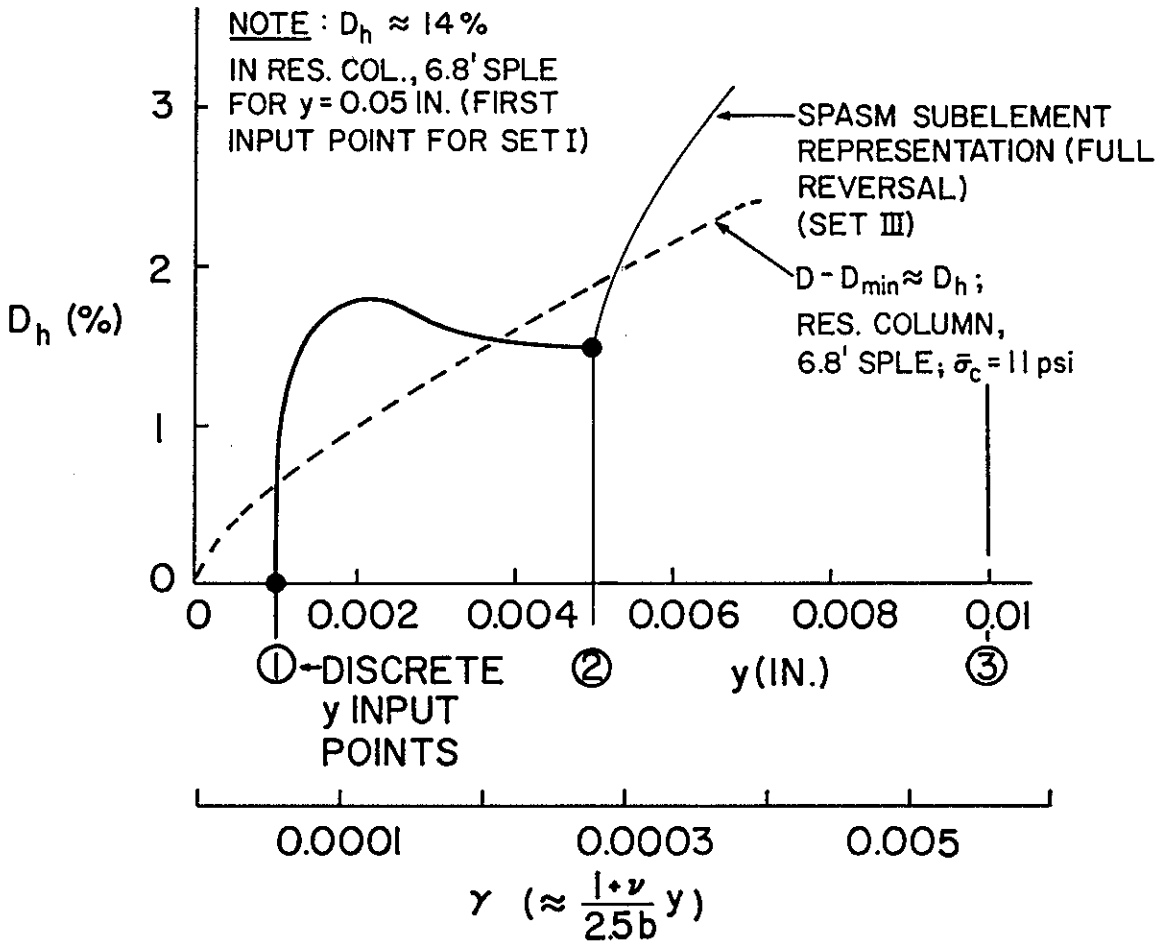

Fig. 6.17. Hysteretic Damping vs. Pile Displacement as Simulated by SPASM (1 in. = 25.4 mm; 1 ft = 0.305 m; 1 psi = 6.89 kPa).

Table 6.8. Schedule of SPASM Analyses (1 lb. = 4.45 N)

Pile/Mode	Vibrator/ Force Level (Nominal, Single Amp.)	Head Condition	D^e Variation (Berger, et. al)	P-Y Function Sets	Discrete Frequencies Analyzed	Field Record Numbers (Comparisons)
Single/ Horizontal	WES/ 400 lb.	A	Common	I, IV	1.5, 2.0, 2.5	832 840
Single/ Horizontal	WES/ 600 lb.	A	Common	I, III	1.5, 2.0, 2.5	835[a] 836[a]
Group/ Horizontal	WES/ 4000 lb. (444 lb./pile)	B	Common	I, II III, IV	4.0, 9.0, 14.0	802[a] 803[a] 804[a] 805[a] 808
Group/ Horizontal	WES/ 8000 lb. (889 lb./pile)	B	Common	I, II III, IV	4.0, 9.0, 14.0	806

a. Discrete frequency records. Remaining records for group are 30-second downsweeps from 50 Hz to 2 Hz and for single pile are 30-second downsweeps from 15 Hz to 0.5 Hz.

monitored and evaluated against field performance are listed in Table 6.9.

Some problems with convergence to steady state were experienced in both DRIVE and SPASM. These problems may be assoicated with input values in some undetermined way. They appear to be related to residual effects of initial transients associated with initiation of motion. In particular, convergence was generally more difficult when the forcing frequency exceeded f_n. Examples of both proper convergence and poor convergence are given in Appendix E for DRIVE AND SPASM.

PILAY/RIGDF

Inputs. PILAY inputs include (1) depthwise variation of soil shear wave velocity (v_s), soil Poisson's ratio (ν_s), total soil unit weight (γ_s) and the physical properties of the pile from the bottom of the pile cap to the pile tip. Unit forces and couples are applied over a specified range of frequencies to develop outputs, which are in the form of pile-head impedance functions and mode shapes along the pile.

A version of PILAY that can account for radial variation of stiffness (60), called PILAY2, was initially considered for use but was not used because CPT probes of the soil immediately adjacent to two of the piles taken after the static tests (41) revealed no detectable softening or strengthening of the soil within one-half a pile radius from the pile surface compared with the undisturbed soil several diameters from the piles.

Five different shear wave velocity, Poisson's ratio, and total unit weight profiles were assumed, shown as Case 1 - Case 5 in Figs. 6.18-6.20. In every case the unit weights were those that were measured. Poisson's ratio was held constant at 0.49. A preliminary study using PILAY revealed essentially no difference in the computed impedance functions in the vertical mode in the frequency range investigated between Poisson's ratios of 0.3 and 0.49. The impedance functions for horizontal translation were found to be 5 to 10% smaller for Poisson's ratio = 0.3 than for Poisson's ratio = 0.49 in the frequency range of interest (0 - 25 Hz for the horizontal tests).

Case 1 used the shear wave velocity profile that was measured in situ. See Fig. 6.18. Case 2 employed shear moduli that were 20% of the

Table 6.9. Output Evaluations for Program SPASM
(1 ft = 0.305 m)

Pile/ Mode	Evaluations For Each Combination of Parameters
Single/ Horizontal Group/ Horizontal	1. Peak displacement vs. frequency at 5 ft above and 0, 2, 4, 7, 10.5, 15, and 29.5 ft below soil surface. 2. Peak displacement and phase lag (wrt forcing function) vs. depth for each frequency analyzed. Objective: To assess whether SPASM, which uses dynamic p-y curves, can replicate measured behavior and to determine which set of p-y curves appears most appropriate. 3. Force vs. deflection (hysteresis loops) and damping ratio at 5 ft above and 2 and 10.5 ft below soil surface for selected tests with ~~and without~~ external damping input. Objective: To assess the effect of the choice of p-y curves on hysteretic damping in the pile-soil system.

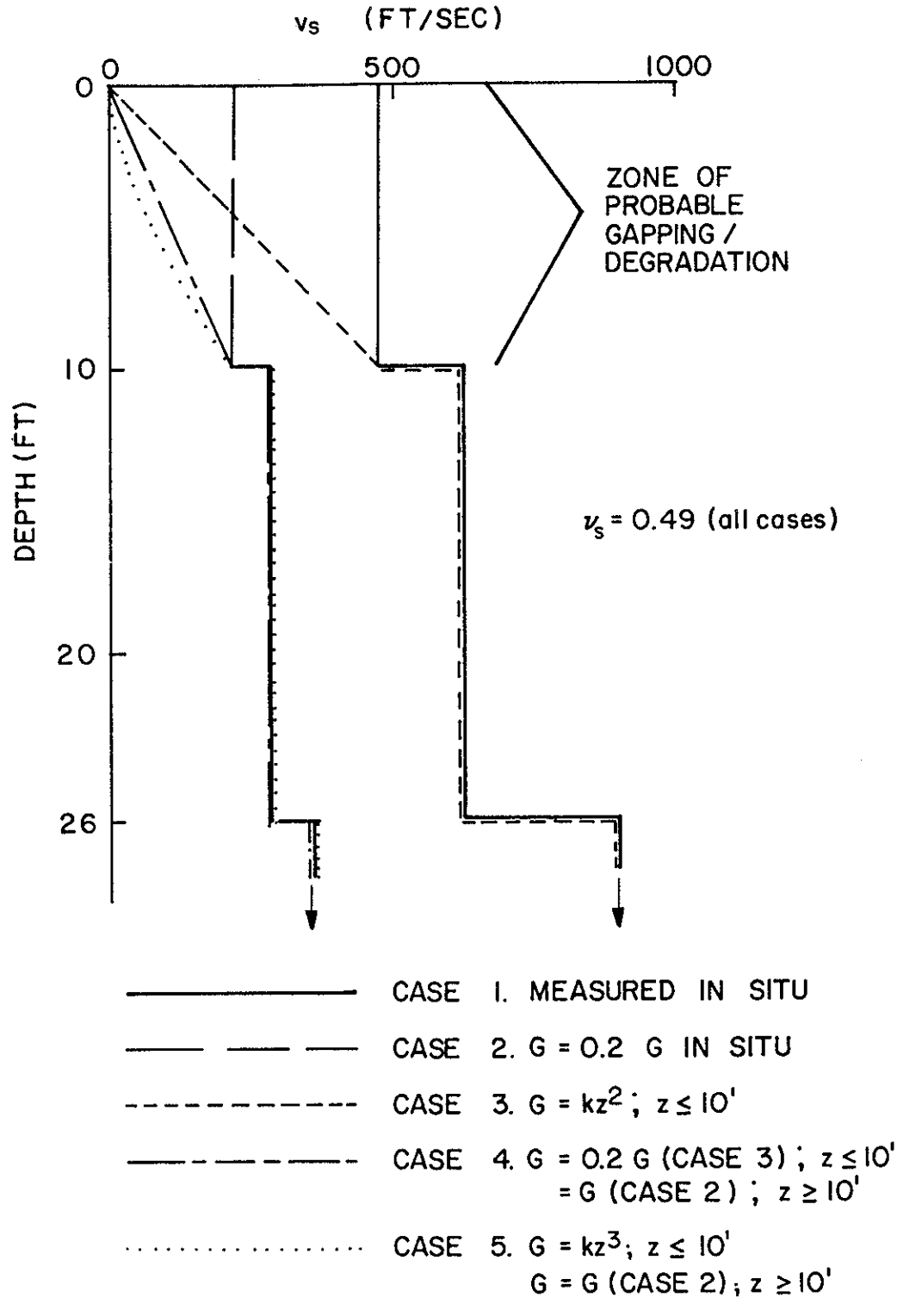

Fig. 6.18. Soil Shear Wave Velocity Profiles Used in PILAY/RIGDF Analyses (1 ft = 0.305 m).

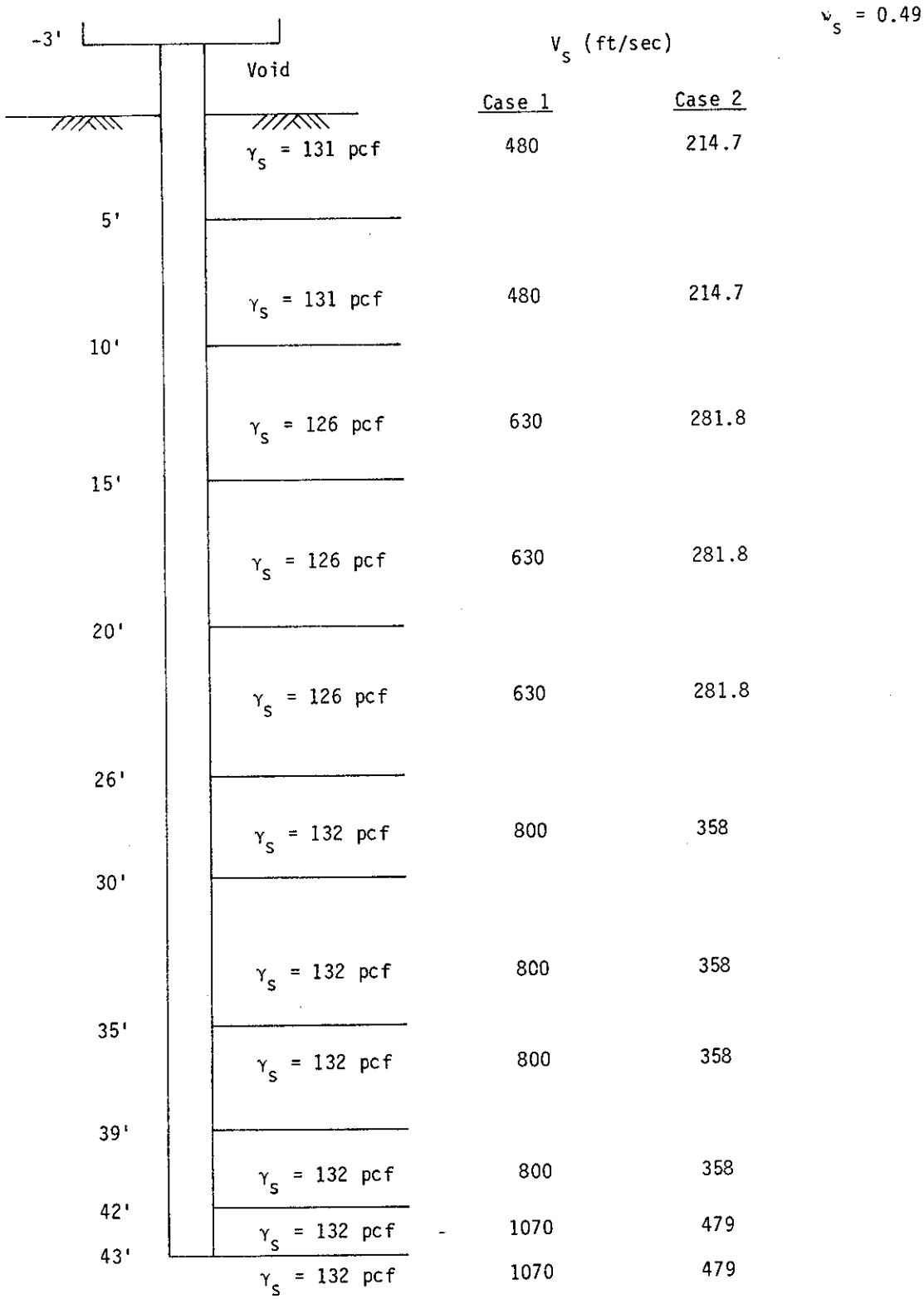

Fig. 6.19. Specific Soil Property Inputs for PILAY: Soil Cases 1 and 2 (1 ft = 0.305 m; 1 lb = 4.45 N).

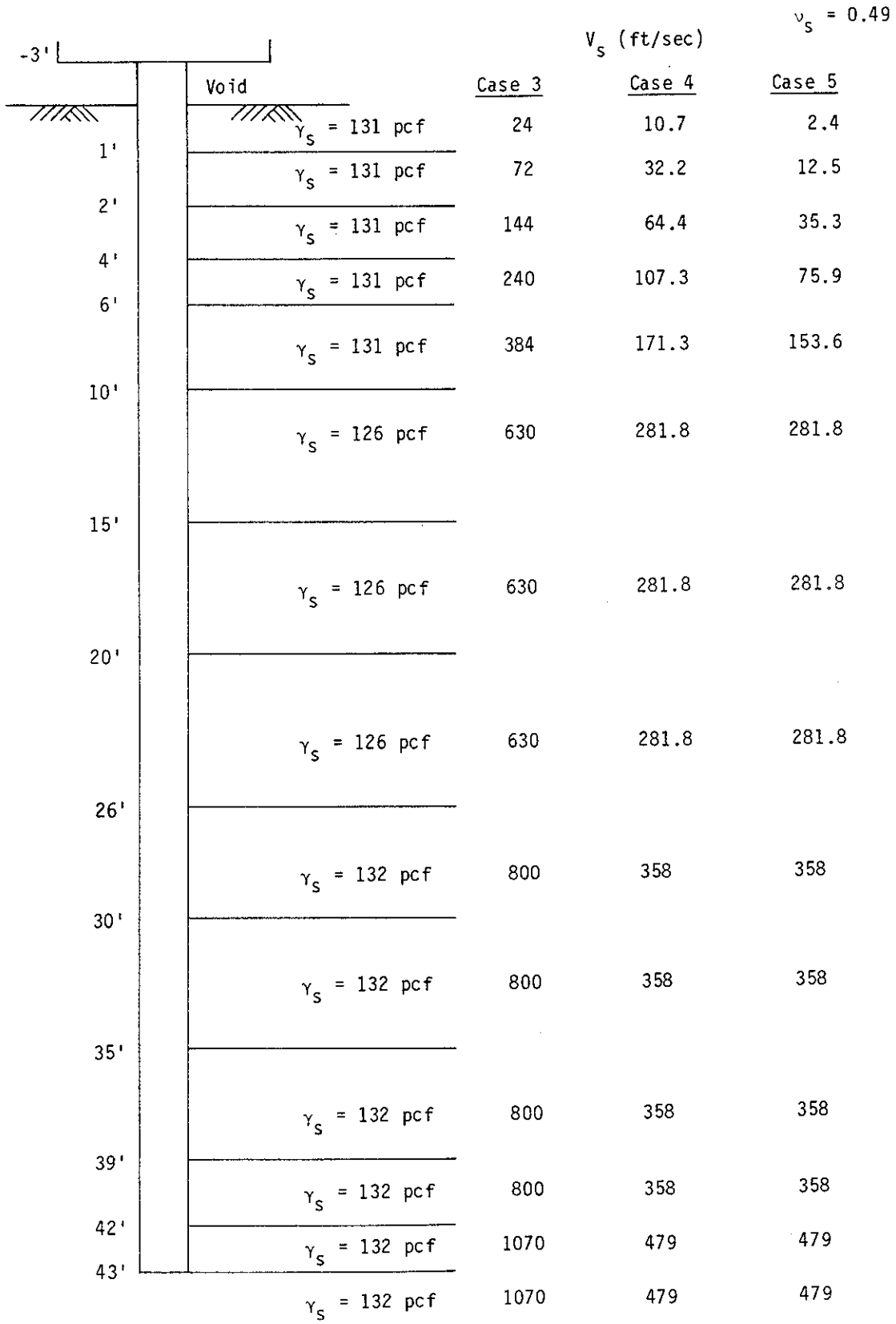

Fig. 6.20. Specific Soil Property Inputs for PILAY: Soil Cases 3-5 (1 ft = 0.305 m; 1 lb = 4.45 N).

in-situ values, resulting in the v_s profile in Fig. 6.18. Case 2 was conceived to represent equivalent linear shear stiffness at operational shear strain amplitudes in excess of the values corresponding to G_{max}, or at $\gamma > 10^{-1}\%$, and thus to apply to either group loading or to equivalent nonlinear response analysis of the single pile.

Case 3 was identical to Case 1 except that gapping and/or degradation was modeled by a parabolically varying shear modulus at depth z less than X_r (10 ft or 3.05 m), as illustrated in Fig. 6.18. Case 4 was identical to Case 2 except for a parabolically decreasing shear modulus above a depth of 10 ft (3.05 m). Case 4 represents highly nonlinear and degraded behavior, that may only be applicable to very large deflections in laterally loaded piles. Finally, Case 5 is identical to Case 4 but with more severe modulus reduction (i.e., degradation) near the ground surface.

Numerical soil property inputs to PILAY are given in Figs. 6.19 and 6.20. Two values of hysteretic damping were also input: 0.2% of critical and 15% of critical, and impedence functions were computed from PILAY for many combinations of the five soil cases and two hysteretic damping ratios at four frequencies: 1.5 Hz, 10 Hz, 35 Hz, and 70 Hz. These frequencies span the range of interest and each is near a known pile system resonance.

Physical properties of the pile that were used are tabulated in Table 6.10. Equivalent (full-section) pile unit weights were used rather than actual unit weights. A preliminary study (described later) showed that use of equivalent unit weights produced very minor differences in impedance functions.

The pile-head impedance functions generated by PILAY were input into RIGDF without modification, except for two analyses, described subsequently. Additional inputs to RIGDF included the mass and inertia properties of the cap (Table 5.2), loads and moments about the cap CG, and the frequency range for which a pile cap response spectrum was desired. For each run (i.e., for each spectrum generated by RIGDF) the impedance functions were invariant over the range of frequencies specified. The input values of k and c were thus to be those that were near the resonant frequencies of the physical system, which were known

Table 6.10. Pile Properties Input For PILAY

Property	Conventional Units	SI Units
Length	46 ft	14,020 mm
Unit Wgt.	68.3 pcf[a]	0.0000107 N/mm^3
Poisson's Ratio	0.30	0.30
Material Damping	0	0
Young's Modulus	4.32×10^9 psf	2.069×10^5 N/mm^2
Radius	0.448 ft	136.5 mm
Cross-Sectional Area	0.0879 ft^2	8166 mm^2
Moment of Inertia of Cross-Sect.	0.00840 ft^4	72,500,000 mm^4
Polar Moment of Inertia of Cross-Sect.	0.0168 ft^4	145,000,000 mm^4
Pile Static Load	0	0

a. Equivalent value for solid section

approximately when the RIGDF runs were made. Variations of the computed impedance functions with frequency are described later.

For purposes of modeling the pile head stiffness and damping of a typical group pile

$$\sum_{i=1}^{N} ((1 + \alpha_{ij}^{A} (i \neq j)/N), \qquad \text{from Eq. (6-10)}$$

was taken to be 1 (no dynamic group action) and 1.7 (factor measured in static tests), and complete pile-head spectra were developed by RIGDF for both conditions. Also, spectra were obtained with

$$\sum_{i=1}^{N} ((1 + \alpha_{ij}^{L} (i \neq j)/N), \qquad \text{from Eq. (6-11)}$$

equal to 1 (no dynamic group action) and 2.56 (factor computed for 9-pile group using chart solutions from Poulos and Davis (68)).

Analyses. Table 6.11 documents the analyses performed on PILAY/RIGDF. Table 6.11 indicates the frequencies for which impedance functions for input into RIGDF were chosen. For the final set of runs (Group/Horizontal), the horizontal, rotational, and cross-stiffness/damping impedances were taken at 10 Hz, near the translational resonance, but the vertical functions were taken at 35 Hz, which was near the resonant frequency for the vertically loaded single pile. The specific outputs from RIGDF that were compared with measured field performance are given in Table 6.12.

Preliminary Studies. In both of the discrete element models (DRIVE and SPASM) and in the continuum model (PILAY/RIGDF), the pile response is theoretically dependent on the static vertical load bias. In DRIVE the solutions were obtained with that bias in place. In SPASM and PILAY, however, the static bias was taken to be zero. The effect in SPASM is insignificant. A preliminary study was made on PILAY to examine the effects of static bias on pile-head impedance up to a static bias of 30 k (133.5 kN). Table 6.13 summarizes the results. Errors in assuming a zero static bias are seen to be small. The errors at 70 Hz in the various lateral modes are of no consequence for this study since the frequencies in excess of about 25 Hz are of little interest.

Table 6.11. Schedule of PILAY/RIGDF Analyses (1 lb. = 4.45 N)

Pile/Mode	Vibrator/ Force Level (Nominal, Single Amp.)	Soil Profiles For Impedance Functions	Frequency Value For Impedance Functions (Hz)	D_h	α (group)	Range Of Frequency Response Spectrum (Hz)	Field Record Numbers (Comparisons)
Single/ Vertical	WES/ 400 lb. 1600 lb. 4000 lb. 8000 lb.	1,3,4	35	0.002 0.15	-	0 - 60 (Incr = 0.5)	602 616 617[a] 618[a] 619[a] 621 623
Single/ Horizontal	FHWA/ 400 lb.	2,3,4,5	1.5	0.002 0.15	-	0 - 12 (Incr = 0.1)	470[b] 476[b]
Single/ Horizontal	WES/ 200 lb. 600 lb.	2,3,4,5	1.5	0.002 0.15	-	0 - 12 (Incr = 0.1)	832 835 836[c] 840

a. Discrete frequencies. Remainder of vertical tests were 30-second, 50 - 2 Hz downsweeps.
b. 16 - 1.8 Hz downsweep.
c. Discrete frequency. Remainder of horizontal tests were 30-second, 15 - 0.5 Hz downsweeps.

Table 6.11 (Cont'd). Schedule of PILAY/RIGDF Analyses

Pile/Mode	Vibrator Force Level (Nominal, Single Amp.)	Soil Profiles For Impedance Functions	Frequency Value For Impedance Functions (Hz)	D_h	α (group)	Range Of Frequency Response Spectrum (Hz)	Field Record Numbers (Comparisons)
Group/ Vertical	FHWA/ 1320 lb.	1, 3, 4	35	0.002 0.15	1.0 1.7	0 - 80 (Incr. = 1)	371
	WES/ 4000 lb. 16,000 lb. 40,000 lb.	1, 2, 3, 4, 5	35	0.002 0.15	1.0 1.7	0 - 80 (Incr. = 1)	633 640 645
Group/ Horizontal	WES/ 400 lb. 4000 lb. 800 lb.	1, 2, 3, 4, 5	10, 35	0.002 0.15	1.0 2.56	0 - 40 (Incr. = 0.25)	802[d] 803[d] 804[d] 805[d] 806 808 815

d. Discrete frequencies. Remainder of group tests (vertical and horizontal) were 30-second, 50 - 2 Hz downsweeps, except for Record 371, which was a 47.5 - 10 Hz downsweep.

Table 6.12. Output Evaluations for Programs PILAY and RIGDF

Pile/Mode	Evaluations For Each Combination Of Parameters
Single/ Vertical Single/ Horizontal Group/ Vertical Group/ Horizontal	1. Pile head frequency response spectrum; resonant frequency and dynamic displacement amplification at pile head; mode shapes. Objective: To compare response spectra to measured transfer functions and mode shapes to measured mode shapes and thereby evaluate the mathematical model and to ascertain the most appropriate soil profile, with respect to surface gapping and degradation and empirical group effect modeling.

Table 6.13. Ratios of Impedance Functions for Zero Static Load (Used in Analyses) to Those for 30,000 lb (133.5 kN) Static Load; Soil Case 2; $D_m = 0.15$

FUNCTION	FREQUENCY (Hz)			
	1.5	10	35	70*
k_{ww}	1.000	1.004	1.032	1.094
k_{uu}	1.004	1.016	1.123	1.590
$k_{\psi\psi}$	1.000	1.003	1.010	1.021
$k_{\psi u}$	1.000	1.006	1.034	1.095
c_{ww}	1.000	0.996	0.967	0.912
c_{uu}	1.001	0.996	0.959	0.882
$c_{\psi\psi}$	0.996	0.992	0.958	0.898
$c_{\psi u}$	0.999	0.995	0.958	0.888

*a_o = 0.412 at pile top

= 0.918 at pile tip

Figures 6.21 and 6.22 report the PILAY solutions and document the frequency dependence of the impedance functions for Case 1, hysteretic damping = 0.002 (stiff soil, minor damping) and Case 4, hysteretic damping = 0.15 (soft soil, major damping). Only small changes occur below 35 Hz for all modes for Case 1. More significant changes occur for Case 4, which implies that more care must be taken in selecting the frequency for which impedance functions are developed in a soft, highly damped soil.

Above 35 Hz in Case 1 changes become more pronounced in the vertical mode (the only mode in which frequencies exceeding 35 Hz are of interest), and pronounced changes in vertical impedance also occur in Case 4 above 35 Hz. All vertical response spectra were generated by RIGDF using PILAY impedance functions corresponding to 35 Hz. Consequently, for systems that resonate at frequencies above 35 Hz, the stiffness modeled is slightly too low and the damping is too high.

Analyses were made using actual and equivalent pile mass. The differences in computed impedance were quite small, except at high frequencies, beyond the range of interest, in Case 4. In fact, the equivalent-mass vertical impedance functions at 35 Hz used in RIGDF are closer to the values using actual mass at 70 Hz than were the actual-mass functions at 35 Hz.

KPILE

Inputs. The program accepts pile and soil properties which vary stepwise within a layered model system. Soil layer properties are layer thickness, unit weight, shear wave velocity, Poisson's ratio and material damping ratio. Pile section properties are pile radius, section length, unit weight and Young's modulus.

The program analyzes end-bearing piles, which may be either fixed or hinged at the tip, and friction piles. The friction pile model is obtained by replacing pile properties with soil properties in a pile section between the friction pile tip and rigid base. Additional pile sections with lumped masses may be added above the ground surface to simulate a pile cap or simple structure.

A unit horizontal load or rocking moment may be applied at the pile head, or a unit horizontal force may be applied to the rigid soil pro-

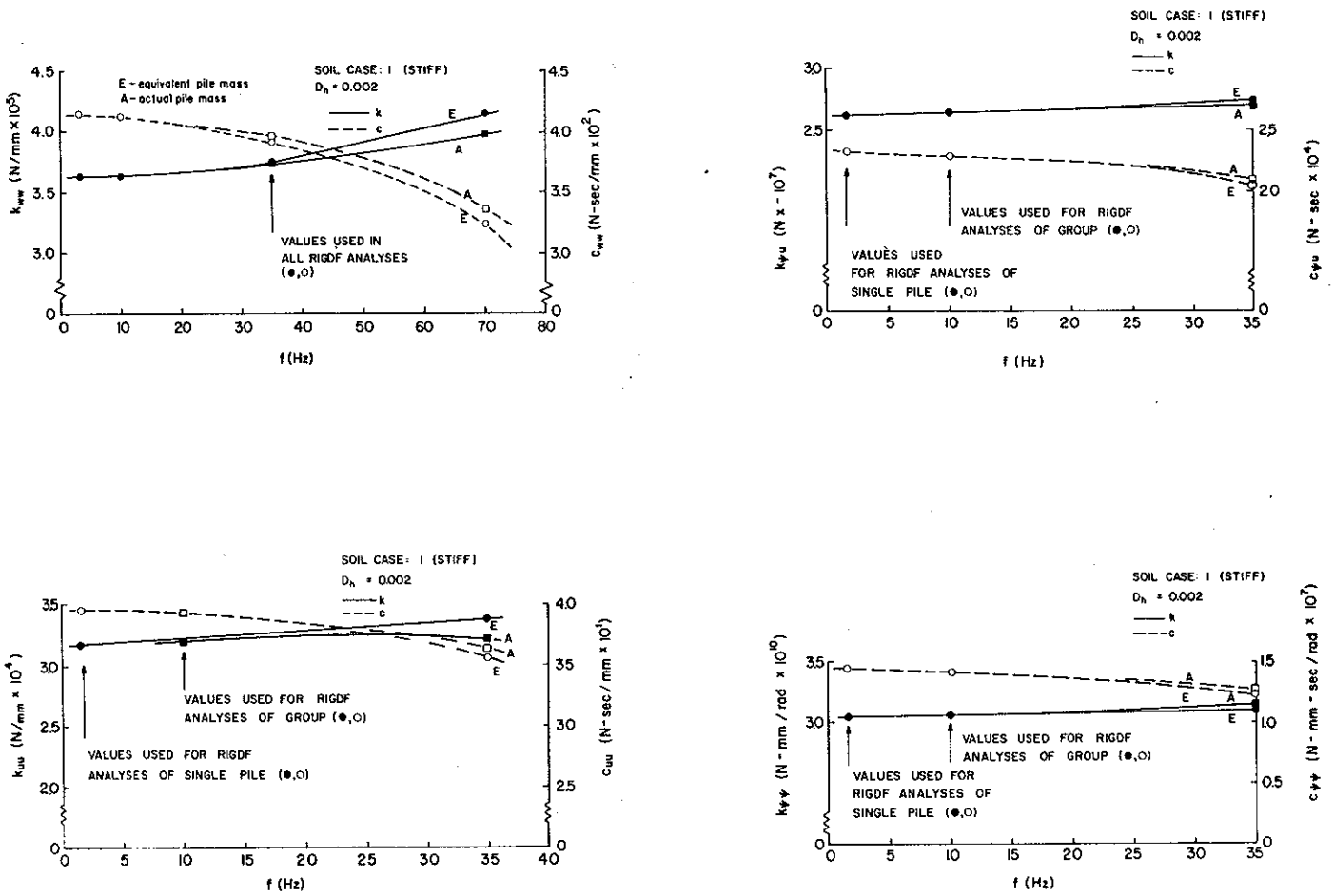

Fig. 6.21. PILAY Impedance Functions vs. Frequency, Case 1, D_m = 0.002.

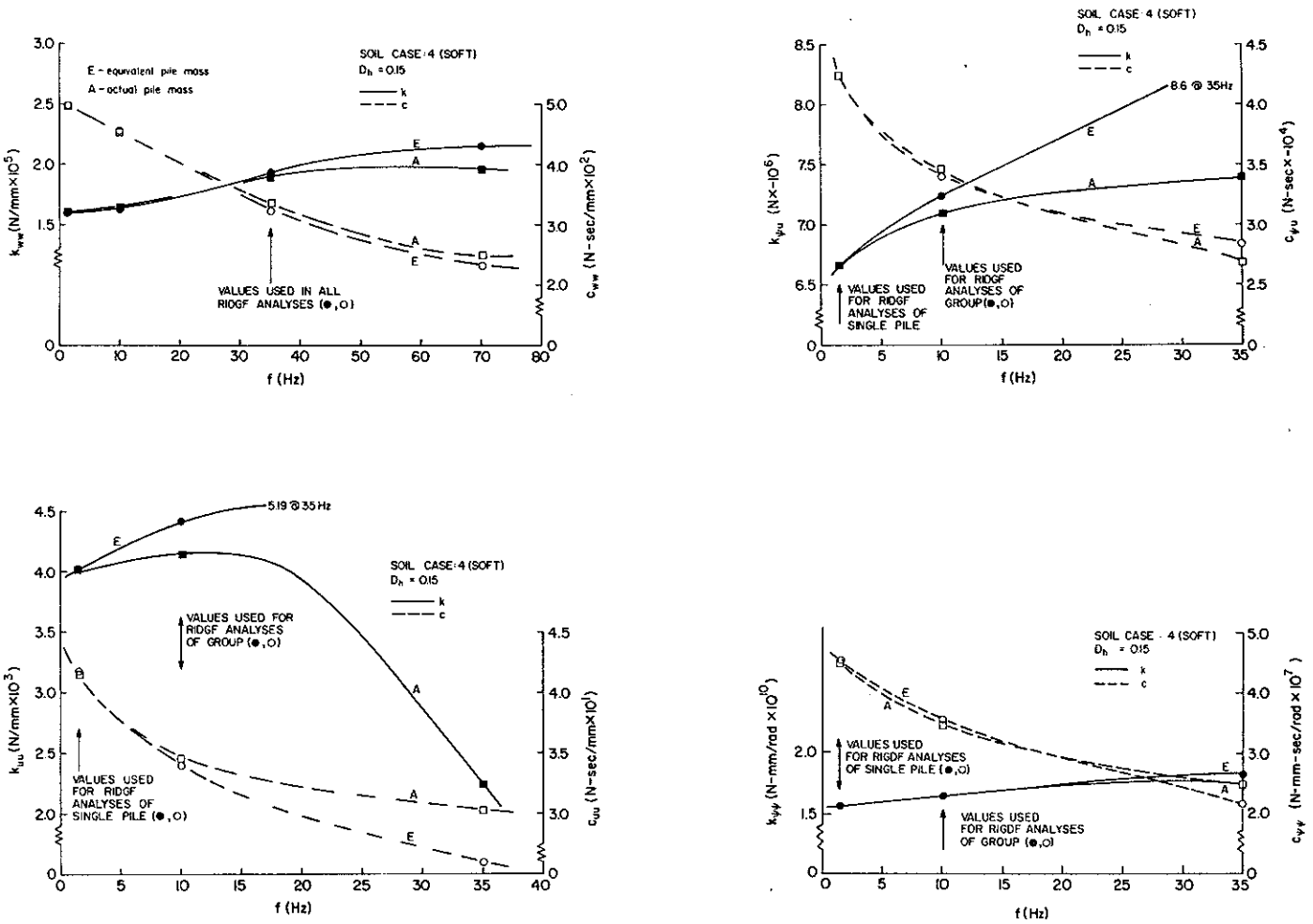

Fig. 6.22. PILAY Impedance Functions vs. Frequency, Case 4, D_m = 0.15.

file base. The computed pile head displacement is then numerically equal to the pile head flexibility.

In addition, equivalent frequency-dependent lateral soil springs may be computed for each layer for comparison with simplified analyses. The soil and pile properties used in the respective horizontal response analyses are shown in Figs. 6.23, 6.24, and 6.25.

Analyses. The individual KPILE analyses are shown in Table 6.14. Response to both pure horizontal and pure rocking unit pile-head loads were computed for comparison with the actual pile-head load, which was a combination of both. The rigid base of the soil stratum was arbitrarily placed at 100 ft (30.5 m) below the soil surface. The single pile cap mass was concentrated at a point 5.0 ft (1.53 m) above the soil surface, while the pile cap bending stiffness was applied to the pile section between 2.5 ft (0.76 m) and 7.5 ft (2.29 m) above the soil surface.

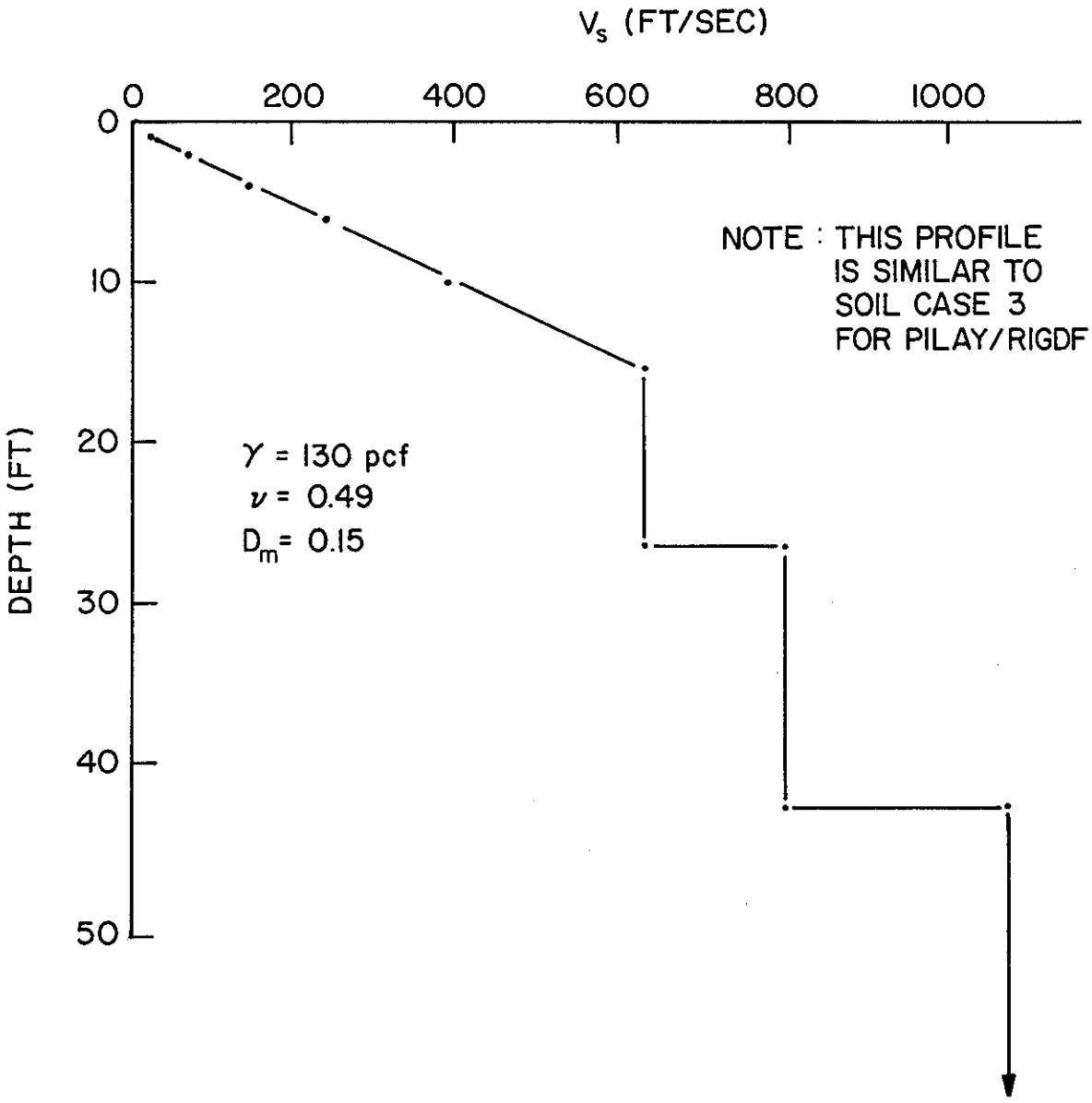

Fig. 6.23. Assumed Soil Properties for Physical System (KPILE).

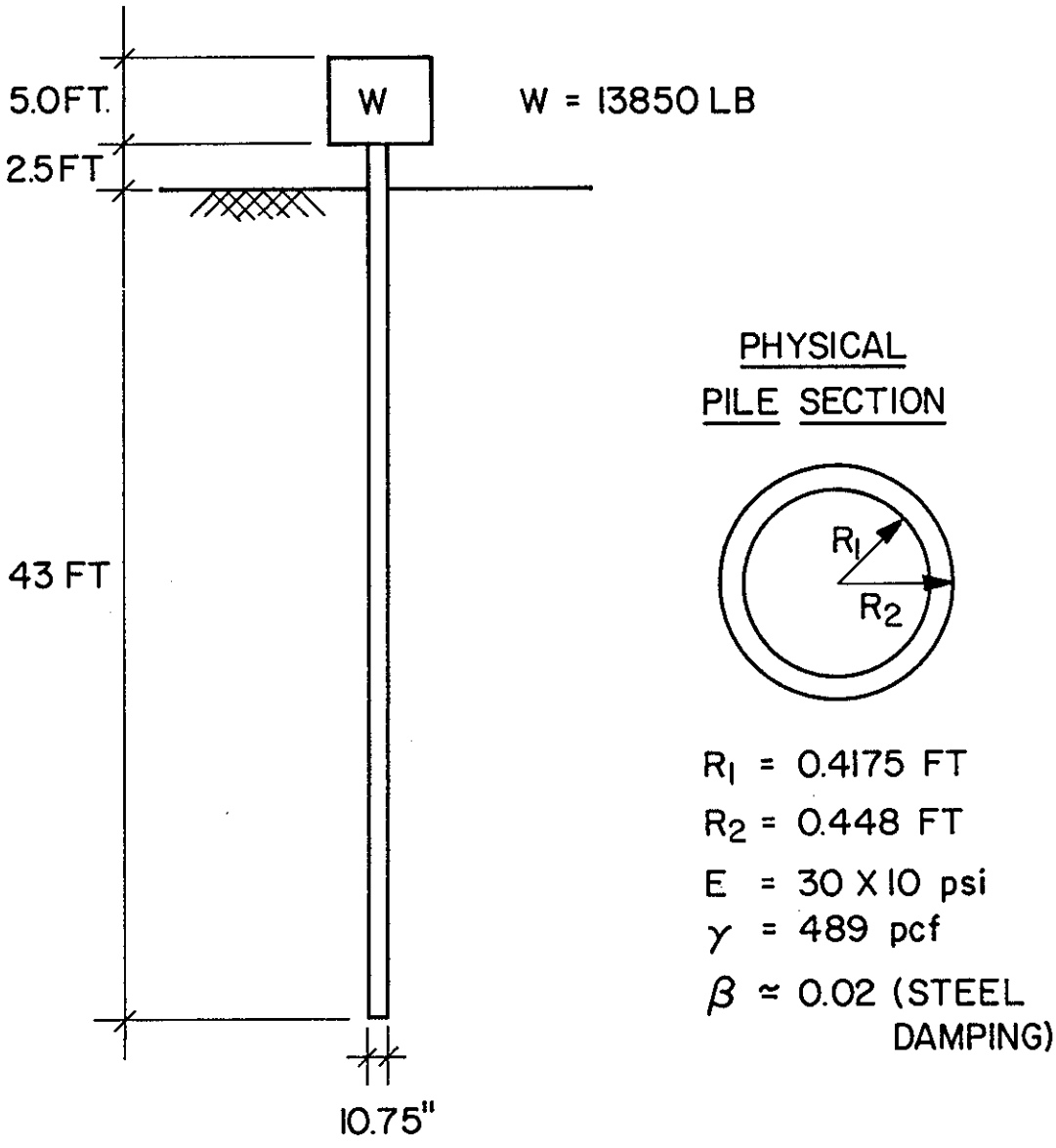

Fig. 6.24. Pile Properties for Physical System (KPILE).

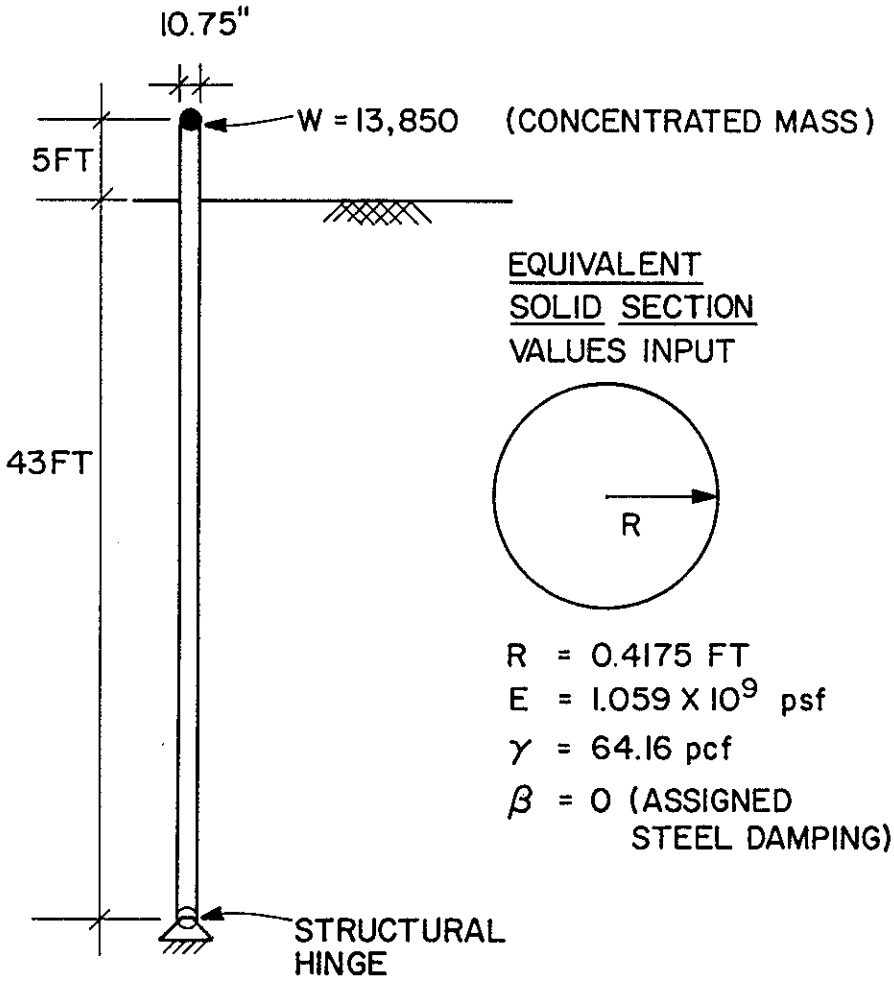

Fig. 6.25. Model Geometry and Properties (KPILE).

CHAPER 7

TEST AND COMPUTATIONAL RESULTS

GENERAL

In order to simplify comparisons between predicted and measured results, the test and representative computational results will be considered simultaneously in this chapter. For each of the four modes of loading analyzed (single pile-vertical, group-vertical, single pile-horizontal, group horizontal), measured performance will be shown first in comparison with performance predicted by DRIVE or SPASM and then with performance predicted by PILAY/RIGDF. In the case of the single pile-horizontal loading, measurements will also be compared with computations from KPILE. Pure rocking behavior is omitted.

Comparisons are made graphically for three basic phenomena: (a) displacement transfer functions between applied load and pile cap displacement, normalized by applied force, (b) normalized deflected shapes of the piles at resonance (hereafter referred to as mode shapes or mode shape envelopes), and (c) phase difference between pile top motion and motion along the pile (computed only for single piles). In addition, soil energy attenuation phenomena are considered in the form of measurements relating applied pile-head loads to soil displacement at various distances away from the piles. Where measured data are not shown for the situations depicted in Chapter 5 for which data were acquired, the coherence of the transfer function was low and the data quality is suspect.

All data are reported for nominal levels of applied load; that is, the amplitude of dynamic load that field personnel attempted to apply. In most instances for tests using the WES vibrator the load amplitude varied, expecially around system resonance, due to the inability of the feedback mechanism to respond to the compliance of the relatively flexible piles. The transfer function analysis performed in the reduction of the data was therefore necessary in order to obtain the true frequency response to the variable amplitude load. However, the reported magnitudes of nominal applied load are not exact and are in fact not meaningful as constant, applied loads. To permit the reader to make

further analyses of the data, measured force versus frequency diagrams are also presented for the test records analyzed.

SINGLE PILE - VERTICAL EXCITATION

Force-Frequency

Figure 7.1 shows the axial force (F_A) vs. frequency (f) relationship measured for the WES vibration tests on the single pile - vertical mode. The variable force amplitude described in the previous section is clearly visible.

Displacement Transfer Function Measurements vs. DRIVE

Figure 7.2 depicts the normalized displacement spectra at several elevations along the single pile as computed by using sets of unit load transfer curves A and C and values of external damping of 60 and 180 lb-sec/in./station (10.8 and 32.4 N-sec/mm/station). Displacements (δ_w) are normalized to a single amplitude applied force (F_A) of 1,000 lb (4.45 kN) for simplicity of comparisons. The predicted curves are identified by Set/External Damping/Force Applied. The measured spectra (transfer functions) for four records, in which the amplitude of nominal force increased in sequence, then decreased, are also shown. DRIVE can be seen to provide a fair prediction of resonant frequency and displacement at and near resonance for Set C input and external damping = 180. The measured curves indicate less dynamic amplification than the Set C predictions over most of the frequency range, such that the prescribed external damping should have been somewhat higher than 180, perhaps as high as 250, in order to better replicate response at frequencies not near resonance. Overall system damping appeared to be in the order of 15% at the cap level. The static load transfer curves (Set A) appear less appropriate for analyzing this particular set of tests.

The measured resonant frequency shift from about 38 Hz at 400 lb (1.8 kN) single amplitude load (Record 602) to about 34 Hz at 8,000 lb (35.6 kN) load suggests that the system responded in a nonlinear manner. That is, the 4 Hz resonant frequency reduction requires an 11 percent system stiffness reduction. This is interpreted to have occurred because of soil nonlinearity. Most of the reduction in stiffness was recovered, however, as evidenced by a 37 Hz resonant frequency when the

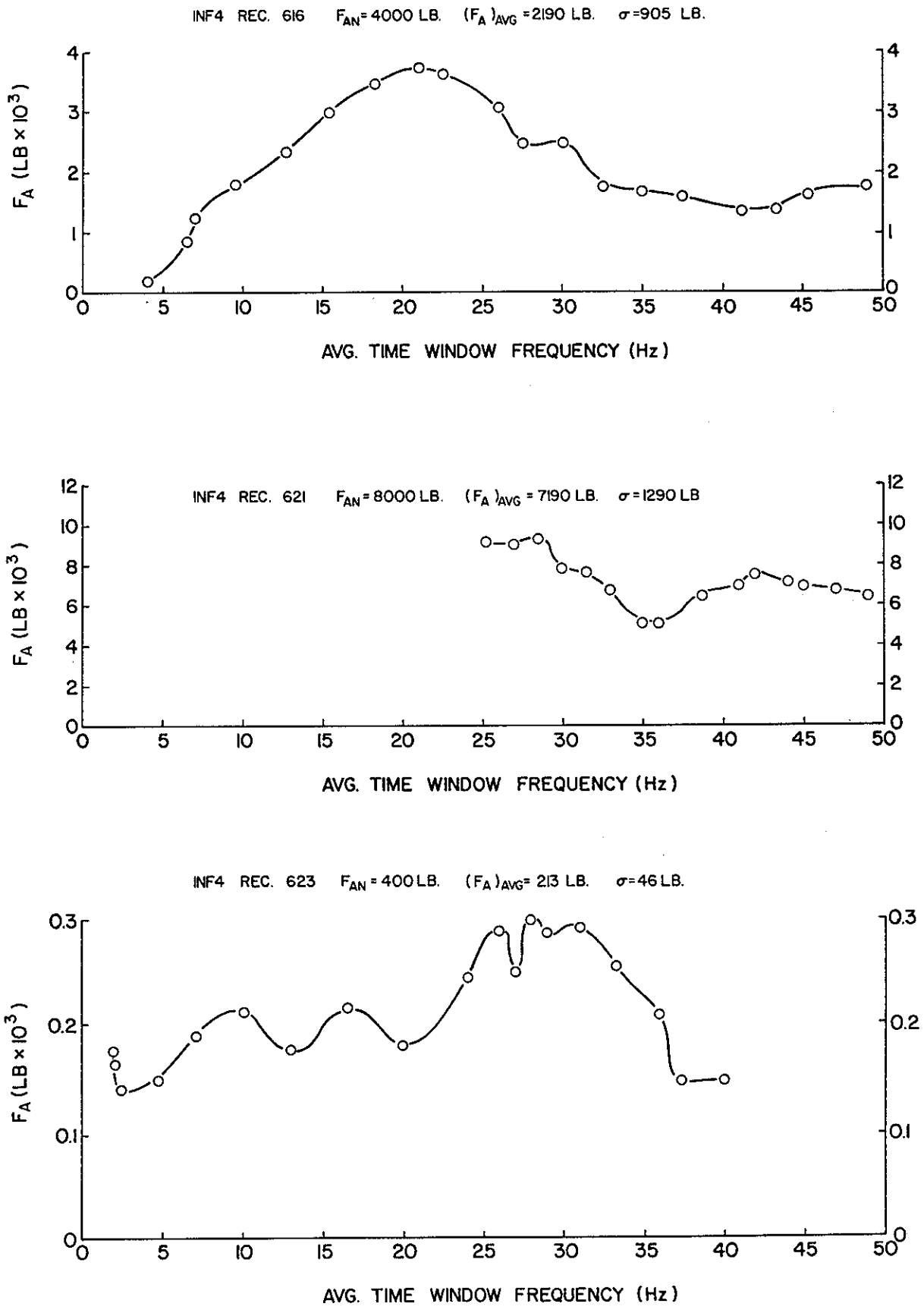

Fig. 7.1. Applied Force vs. Frequency: Single Pile, Vertical Tests (1 lb = 4.45 N).

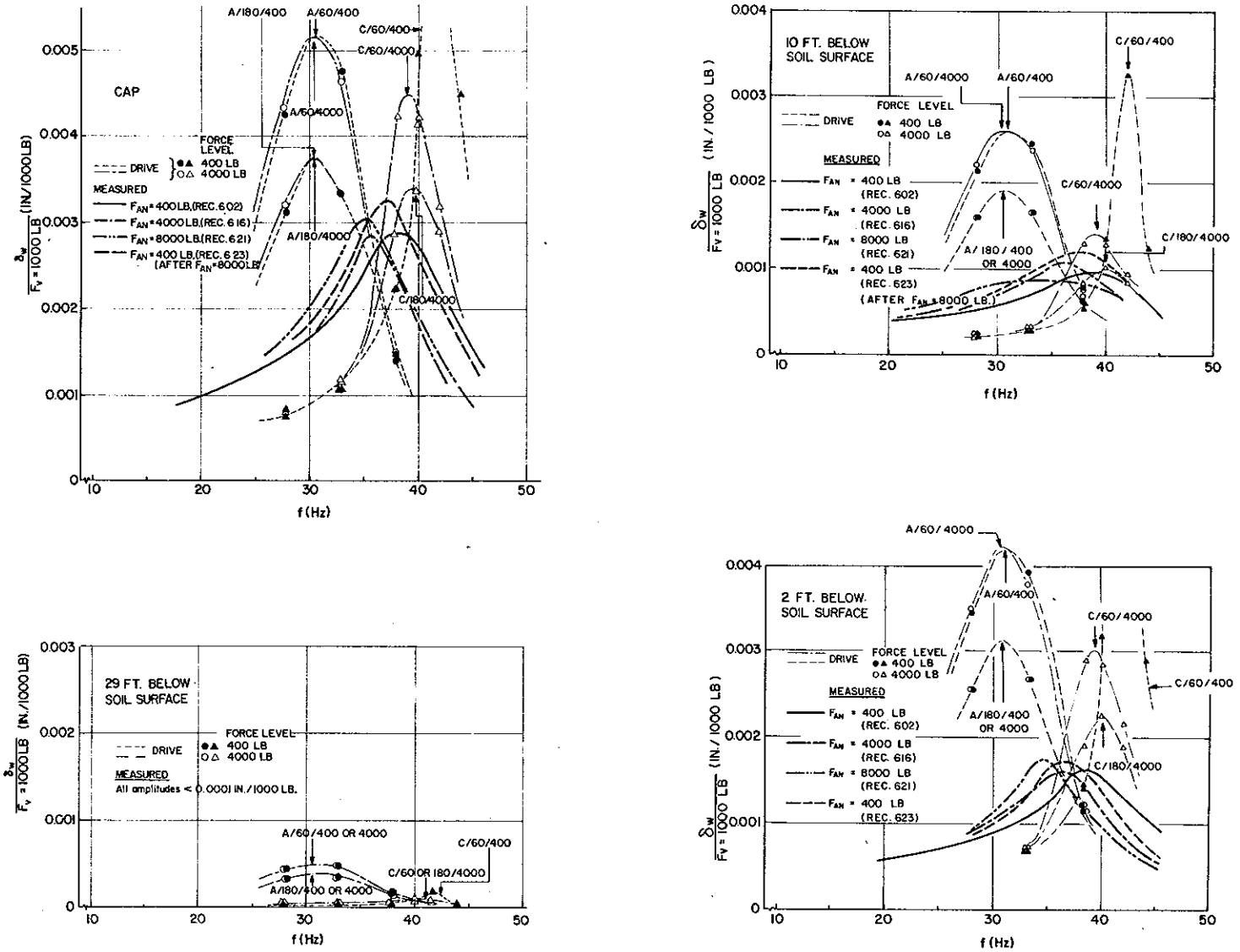

Fig. 7.2. Measured and Computed (DRIVE) Load-Displacement Transfer Functions: Single Pile, Vertical Tests (1 lb = 4.45 N; 1 in. = 25.4 mm).

amplitude of the nominal applied force was reduced from 8,000 to 400 lb (35.6 to 1.8 kN).

The measured and predicted normalized mode shapes (δ_w = vertical displacement/δ_{wb} = vertical displacement at the base of the cap), shown in Fig. 7.3, also suggest better comparisons between the measurements in the down-pile accelerometers and the Set C, rather than the Set A, predictions. Static test data, also superimposed on Fig. 7.3, indicate that load was removed by the soil nearer the surface in the dynamic tests than in the static tests. One-half of the ground line displacement had been dissipated in all dynamic tests at a depth of about 8 ft (2.44 m), although some effect of load amplitude can be seen, again suggesting nonlinearity.

All values shown in Fig. 7.3 are displacements at frequencies at measured or computed resonance. The relative values, however, change very little over a range of frequencies from 20 Hz below resonance to 10 Hz above resonance.

Program DRIVE, as originally written as as used throughout most of this project, does not output forces in the piles. DRIVE was modified to output pile forces for several of the later runs made, however. Normalized force mode shapes for those runs are compared in Fig. 7.4, in which the measured forces were obtained from the strain gages. The measurements again agreed reasonably well with Set C inputs, except for one point at the 22 ft (6.7 m) depth at 8,000 lb (35.67 kN) nominal applied force. The computed forces were for frequencies of 2-10 Hz above resonance, while the measurements were at resonance. Economic considerations prohibited rerunning the modified DRIVE program at resonance to obtain forces, but the relative effects resulting from a small frequency change should be minor.

DRIVE also predicted that some permanent set would be developed with the magnitude of load applied. Table 7.1 reports these predictions. For the "best fit" soil curve set (C/180), the computed permanent set was 0.0058 - 0.0080 in. (0.15 mm - 0.20 mm), depending on frequency. These permanent sets, which were not verified with measurements, result from the application of the pile and cap weights as well as from permanent soil deformations due to hysteresis.

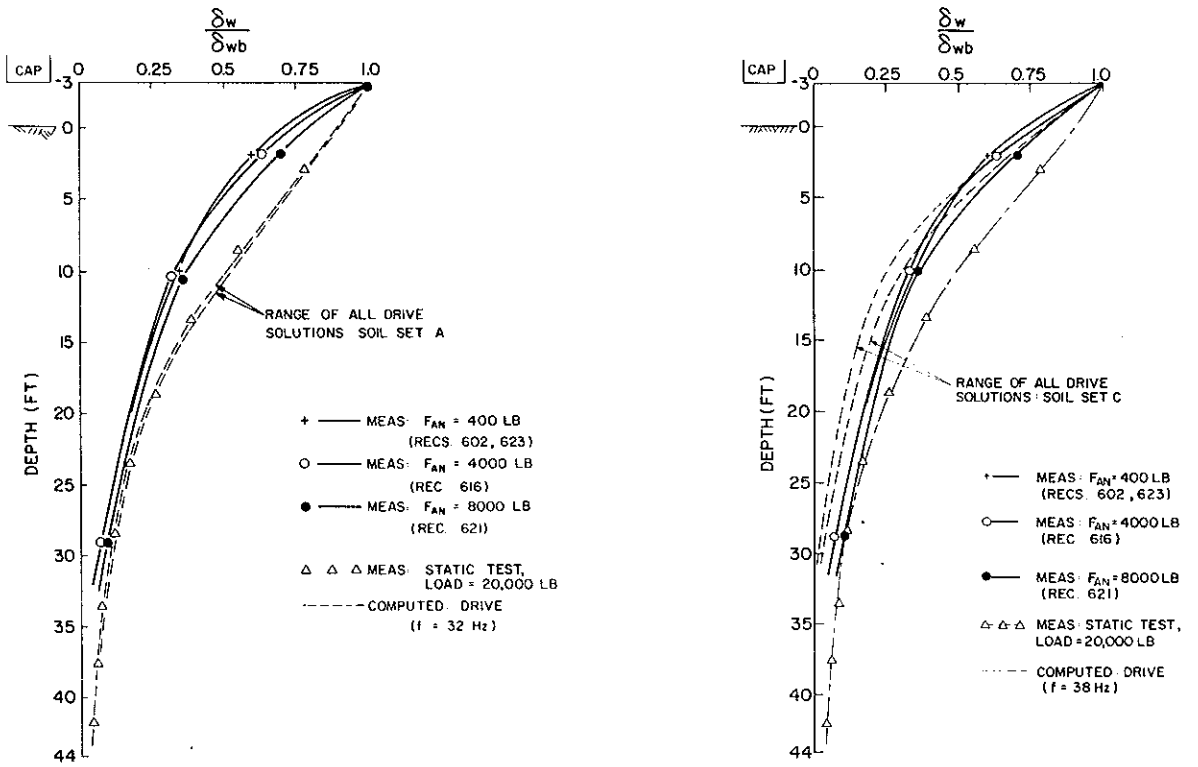

Fig. 7.3. Normalized Displacement Mode Shapes: Single Pile, Vertical Tests (DRIVE) (1 lb = 4.45 N; 1 ft = 0.305 m).

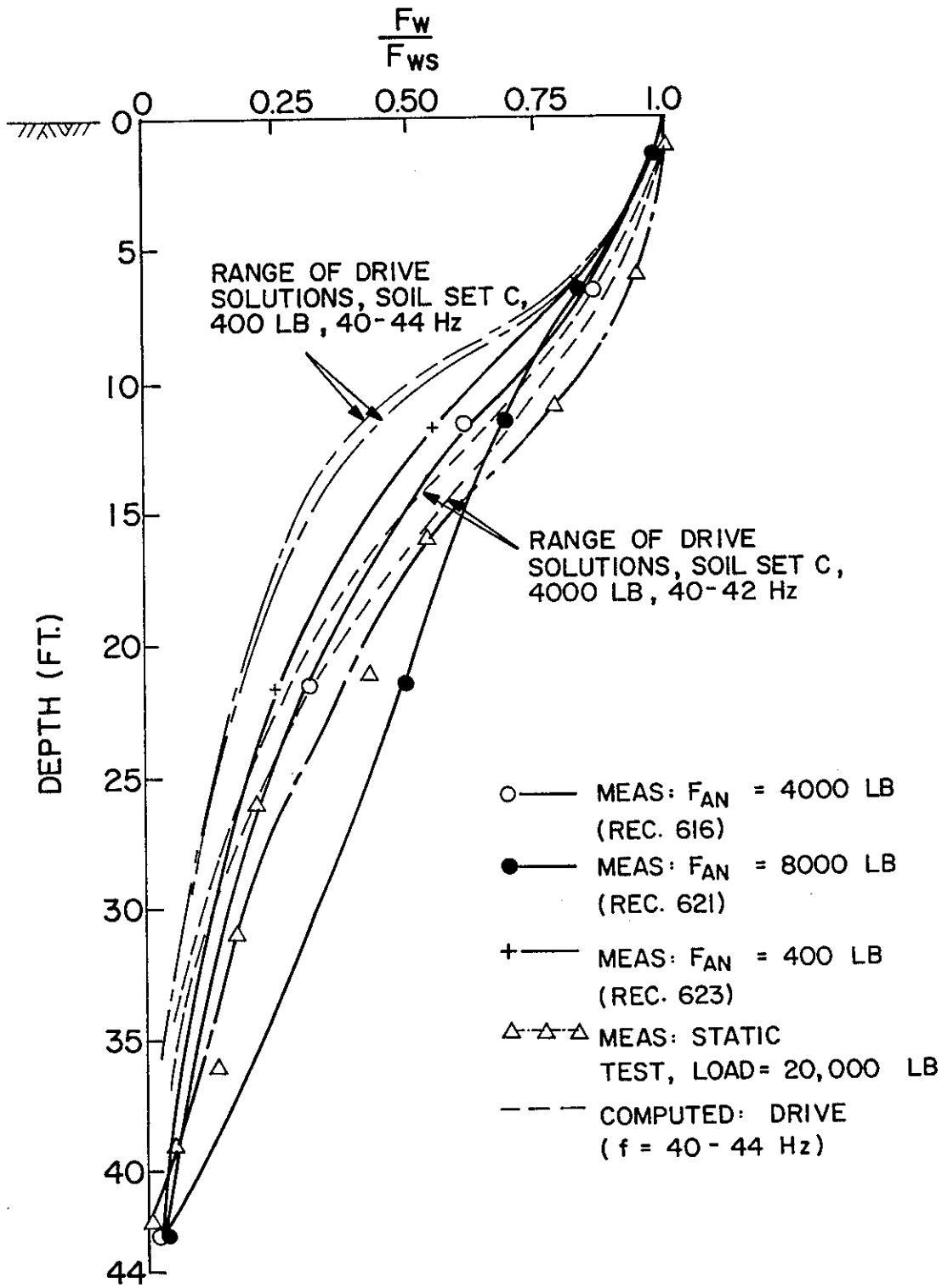

Fig. 7.4. Normalized Pile Thrust Mode Shapes: Single Pile, Vertical Tests (DRIVE) (1 lb = 4.45 N; 1 ft = 0.305 m).

Table 7.1. Mean Displacements for Single Pile at Steady State from DRIVE (1 lb = 4.45 N; 1 in. = 25.4 mm)

Unit Load Transfer Curve Case/ External Damping (lb-sec/in./sta.)	Single Amplitude Unbalanced Force (lb)	f(Hz)	Mean Displacement At Steady State (In.)
A/60	400	28	0.0104
		33	0.0104
		38	0.0104
A/180	400	28	0.0104
		33	0.0104
		38	0.0104
A/60	4000	28	0.0130
		33	0.0118
		38	0.0104
A/180	4000	28	0.0106
		33	0.0105
		38	0.0104
C/60	400	28	0.0058
		33	0.0058
		38	0.0058
		42	0.0060
		44	0.0060
C/180	400	28	0.0058
		33	0.0058
		38	0.0058
C/60	4000	28	0.0064
		32	0.0066
		38	0.0087
		42	0.0082
C/180	4000	28	0.0062
		32	0.0066
		38	0.0080
		42	0.0076

Total damping ratios at several stations along the single pile (with Pile Head Condition II) were computed in DRIVE from the areas of the hysteresis loops of the soil reactions. These damping ratios were compared with those that would exist if the prescribed external damping were removed at several frequencies not near system resonance to obtain a general idea of how much of the damping in DRIVE was hysteretic and how much was external (radiational).

The results are tabulated in Table 7.2. For Set C/180, the external damping provides at least 89 percent of the total damping throughout most of the spectrum. Near resonance (F_A = 4,000 lb (17.8 kN) at 38 Hz), the percentage of damping due to the prescribed external damping factor decreases to 67 percent. These data suggest that, for the load and stiffness conditions described in this test series, it is probably more important to model radiation damping correctly than to model hysteretic damping correctly.

Displacement Transfer Function Measurements vs. PILAY/RIGDF

The transfer functions for PILAY/RIGDF are given in Fig. 7.5, along with the measured transfer functions. Excellent agreement with Soil Case 3, with hystestic damping of 0.002, is noted for the 8,000 lb (35.6 kN) force. (Soil Case 3 assumes linear degradation of soil modulus from the in-situ value at a depth of 10 ft (3.05 m) (11 pile diameters) to zero at the soil surface and in-situ shear wave velocities below 10 ft (0.305 m)).

The f = 0 (static) asymptotes for Soil Case 3 and for the measurements are both observed to be near the static flexibility value for loading in compression.

Figure 7.6 shows the displacement mode shapes for several soil cases studied with PILAY/RIGDF. On the average, the measurements agree well with Case 3/0.002; however, near the surface better agreement with Case 1 (in-situ modulus profile along entire length of pile) is observed, while below about 13 ft (4.0 m) the measurements indicate lower soil stiffness than exists in either Case 1 or Case 3. This is interpreted to imply that a soil case having less degradation than Case 3 above 10 ft (3.05 m) and a somewhat reduced modulus below 10 ft (3.05 m) would be a better model for loads up to the magnitude achieved here.

Table 7.2. Percentages of Total Damping as External Damping; Program DRIVE (1 lb = 4.45 N; 1 in. = 25.4 mm)

Pile	Soil Case	Load Amp. (lb)	Frequency (Hz)	Prescribed External Damping (lb-sec/in./sta.)	Percent of Total Damping[a]
Single (II)	A	400	28	60	99
Single (II)	A	400	28	180	100
Single (II)	A	4000	28	60	96
Single (II)	A	4000	28	180	100
Single (II)	A	4000	38	60	99
Single (II)	A	4000	38	180	100
Single (II)	C	400	33	60	100
Single (II)	C	400	33	180	100
Single (II)	C	4000	33	60	71
Single (II)	C	4000	33	180	89
Single (II)	C	4000	38	60	34
Single (II)	C	4000	38	180	67

[a]Avg. of Computed Total Damping from Hysteresis Loop Areas at Stas. 10, 18 and 37.

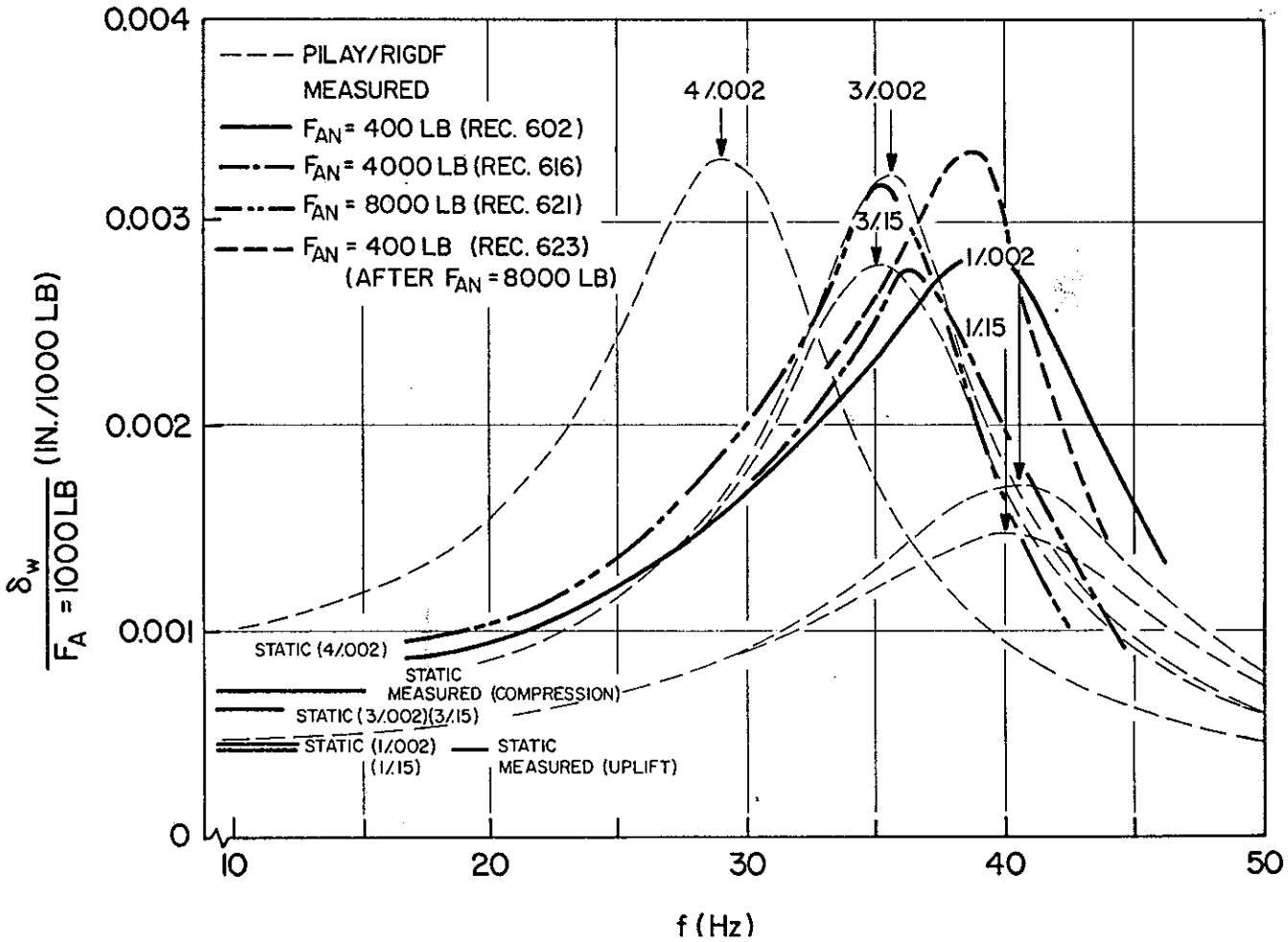

Fig. 7.5. Measured and Computed (PILAY/RIGDF) Load-Displacement Transfer Functions: Single Pile, Vertical Tests (1 lb = 4.45 N; 1 in. = 25.4 mm).

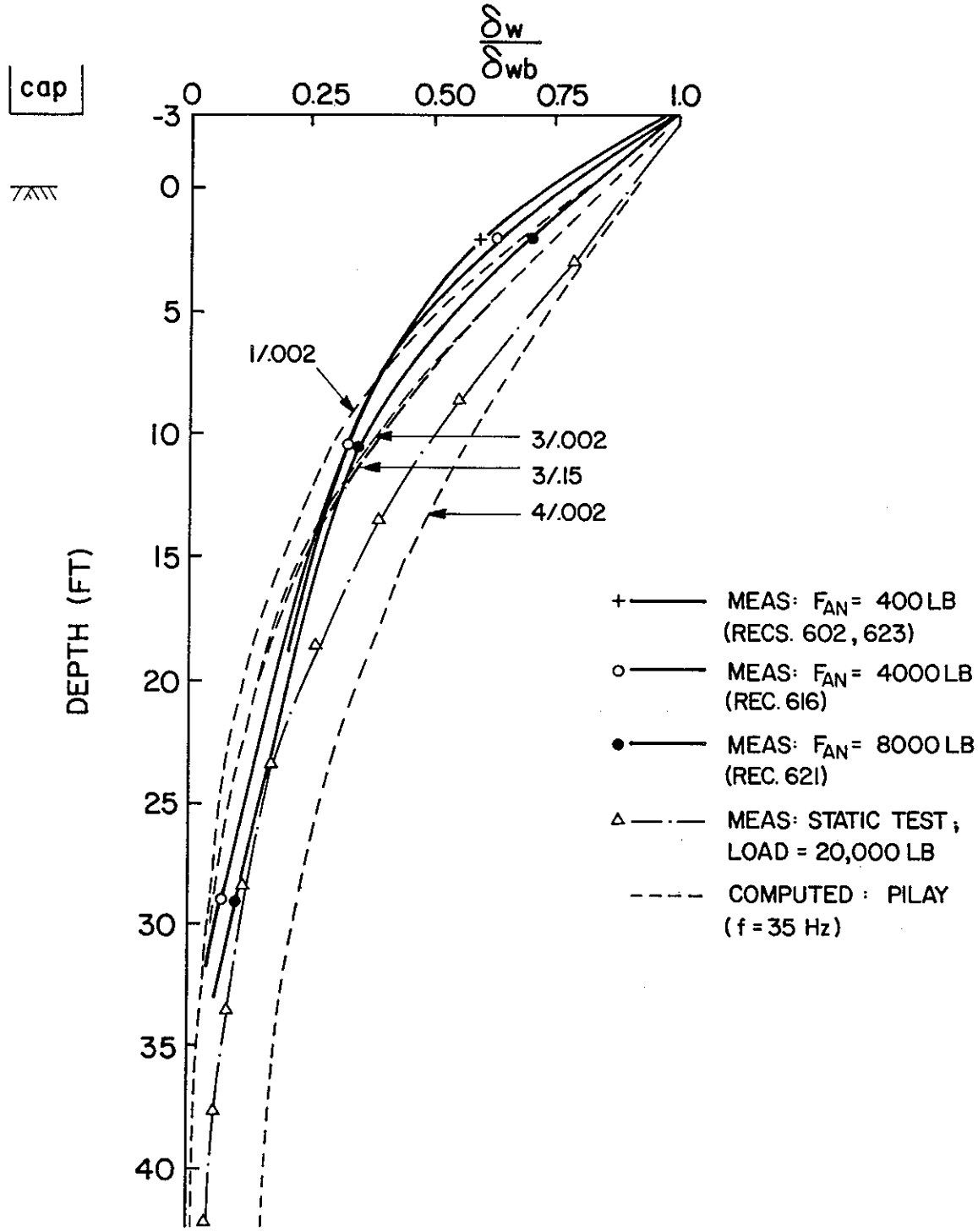

Fig. 7.6. Normalized Displacement Mode Shapes: Single Pile, Vertical Tests (PILAY/RIGDF) (1 lb = 4.45 N; 1 ft = 0.305 m).

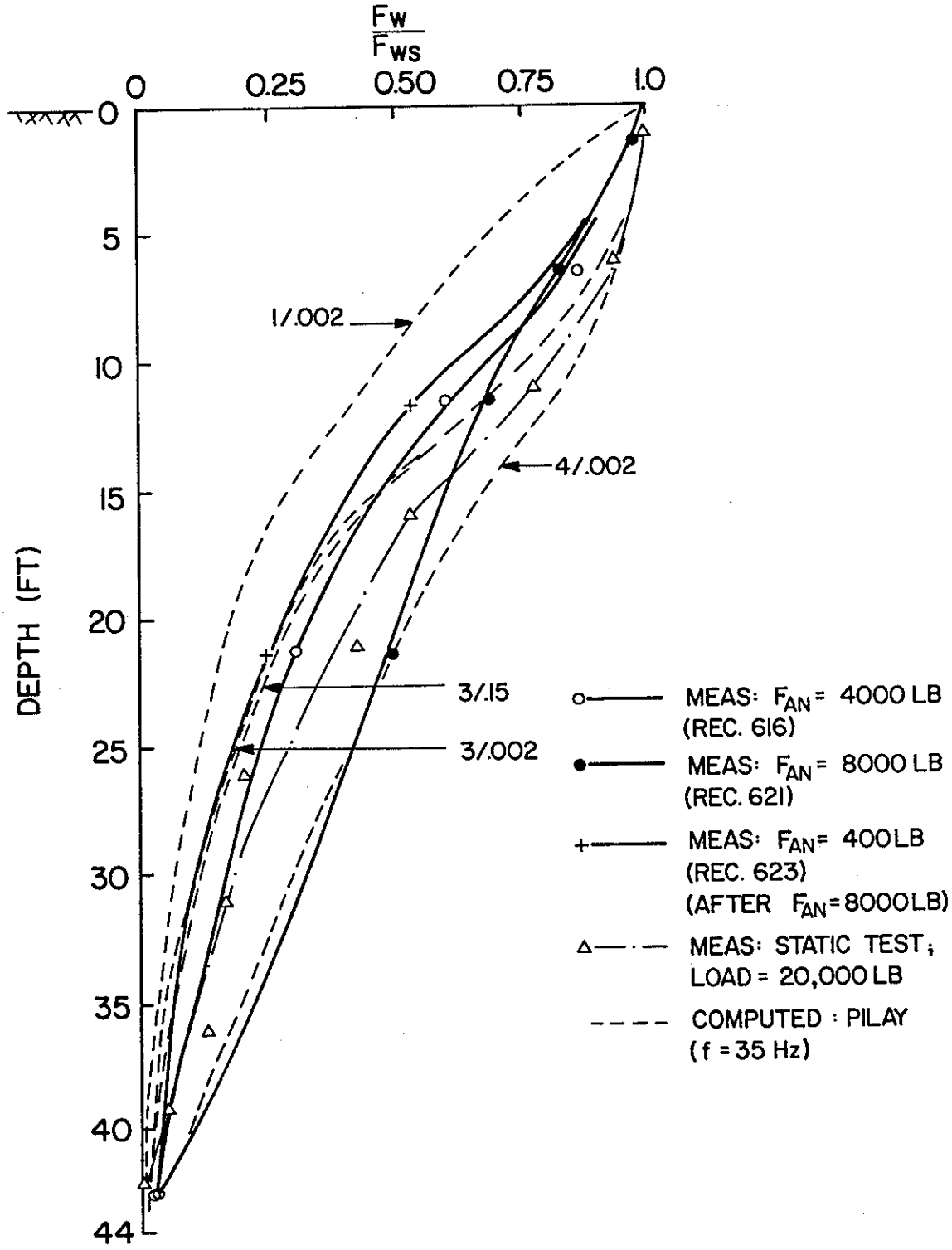

Fig. 7.7. Normalized Pile Thrust Mode Shapes: Single Pile, Vertical Tests (PILAY/RIGDF) (1 lb = 4.45 N; 1 ft = 0.305 m).

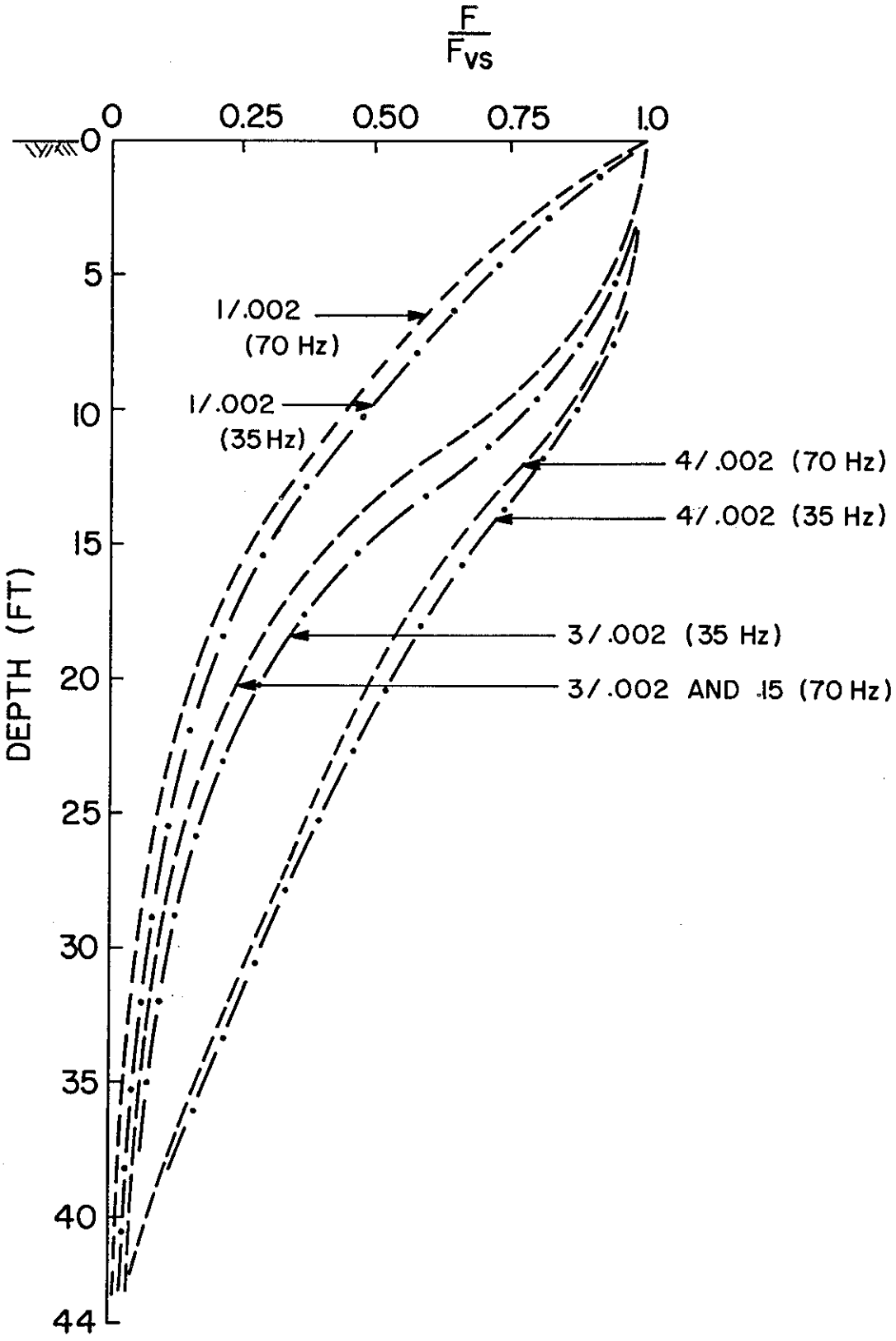

Fig. 7.8. Effect of Frequency on Normalized Pile Thrust Mode Shapes in PILAY/RIGDF (1 ft = 0.305 m).

A similar trend can be observed in Fig. 7.7, which show the axial force mode shapes at resonance. Figure 7.8 is included to show the effect of frequency on force mode shape, where F is the pile force and F_{VS} is the force at the soil surface computed in the mode shape routine of Program PILAY. For the conditions modeled here, a two-fold increase in f has the effect of increasing pile force at any elevation by 10-15%.

Phase

The phase angles between force or motion at the top of the pile and force or motion elsewhere are sensitive to stiffness, damping, and frequency of motion. Therefore, attempts were made to compare measured phase and phase predicted from PILAY. (Phase is not output from DRIVE.) Figures 7.9 and 7.10 compare measured phase with computed phase. The figures indicate a relatively small theoretical dependence of phase on hysteretic damping, but a large dependence on frequency. Although data scatter precludes making any conclusion concerning the appropriateness of either radiation or hysteretic damping, the general trend in phase predicted by PILAY seems correct, so that stiffness and damping are shown to be predicted approximately correctly.

PILE GROUP - VERTICAL EXCITATION

Force-Frequency

F vs. f records for most of the vertical WES vibrator sweeps on the group are shown in Fig. 7.11. Pre-test computations indicated that the resonant vertical frequency of the group would be about 35-40 Hz, and most of the sweeps were conducted in the vicinity of that general frequency range. After the complete suite of tests was conducted at 50-2 Hz, no outstanding resonance peaks were observed. A decision was made to conduct several more frequency sweeps with a nominal force amplitude F_A of 16,000 lb (71.2 kN) between 50 Hz and 100 Hz. The latter value represents an approximate upper limit on the data acquisition resolution. Significant variations of applied force can be observed in the 65-80 Hz range and also in the 5-15 Hz in Fig. 7.11, indicating high system compliance (possible resonance) there. A discrete frequency test was then conducted near the midpoint of the former range (72 Hz). Post-test data processing showed system resonances at 10 Hz and at 68 Hz.

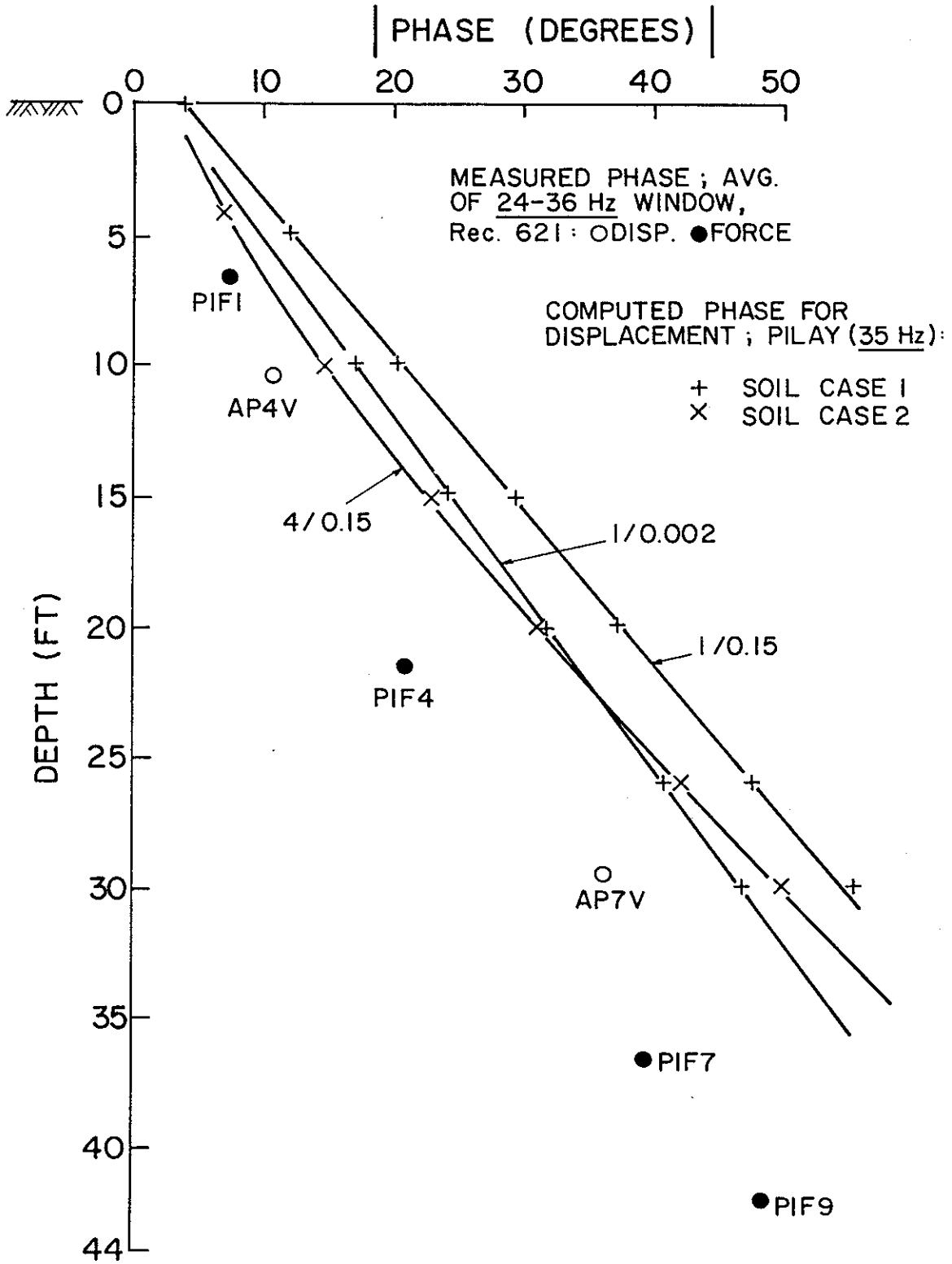

Fig. 7.9. Measured and Computed (PILAY) Phase: Single Pile, Vertical Tests (1 ft = 0.305 m).

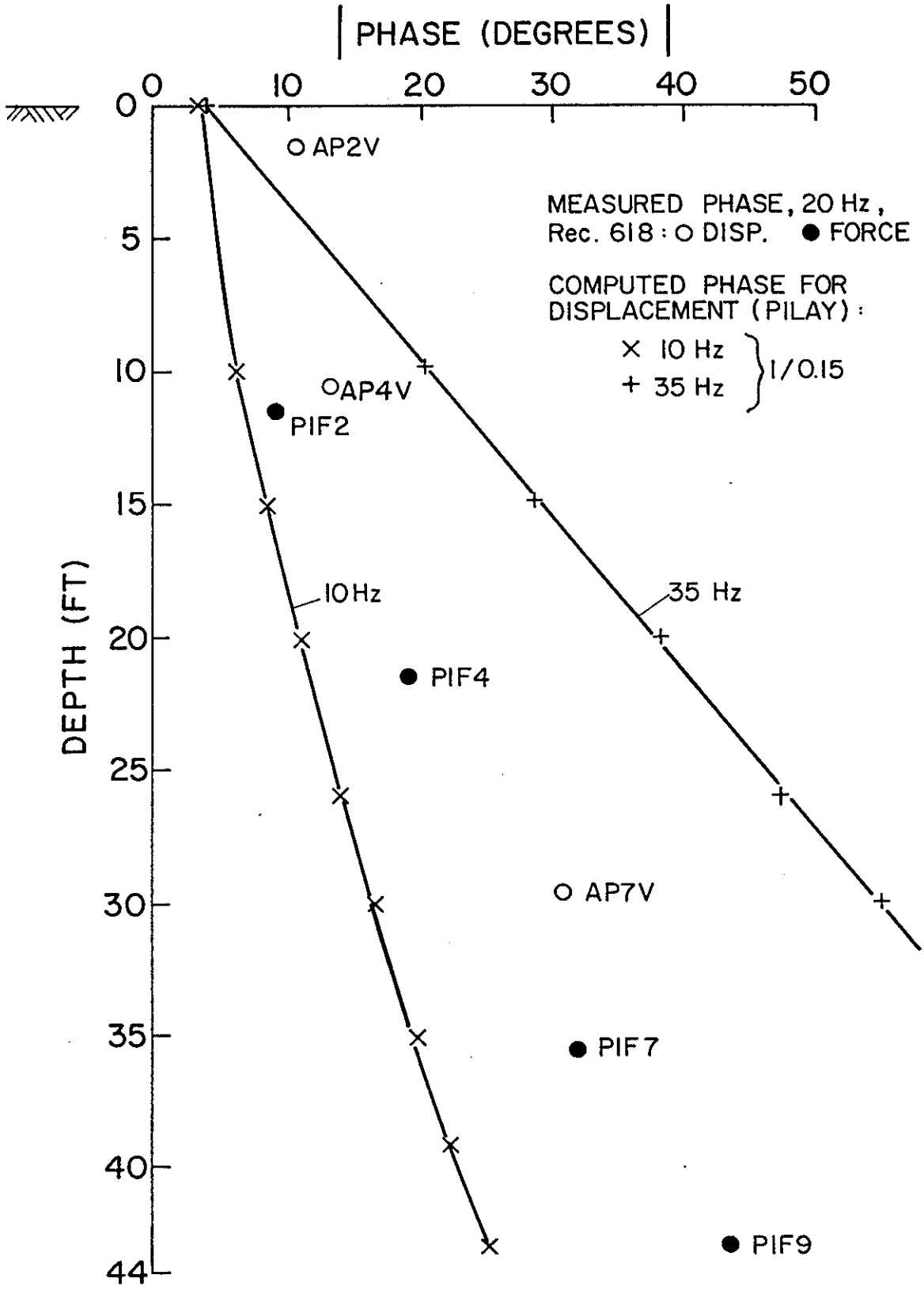

Fig. 7.10. Variation of Computed Phase with Frequency: Single Pile, Vertical Tests (1 ft = 0.305 m).

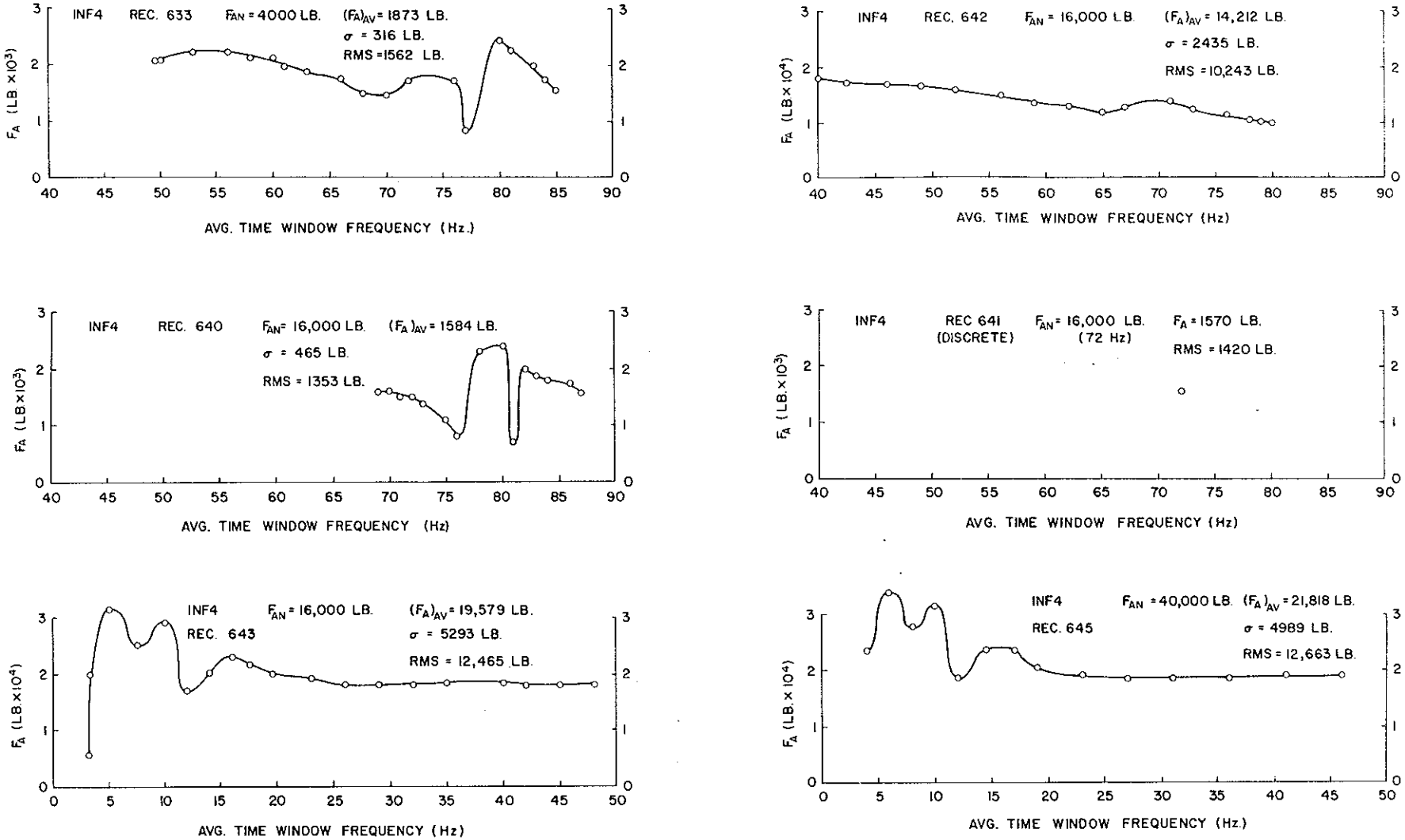

Fig. 7.11. Applied Force vs. Frequency: Group, Vertical Tests (1 lb = 4.45 kN).

Displacement Transfer Function Measurements vs. DRIVE

Figure 7.12 compares the measured pile cap response (synthesized from two frequency sweep records from 4 Hz to 84 Hz) with the DRIVE computations (Chapter 6). The force amplitude F_A refers to the load applied to the entire group and not to one representative pile in the group. Two weak peaks can be seen in the measurements at 10 and 68 Hz; however, there is relatively poor correspondence between the DRIVE predictions and the measured data. The DRIVE algorithm predicts the 68 Hz resonant frequency with Set D inputs, but the predicted displacement are somewhat too large. Since the external (radiation) damping for the Soil Set D spectrum shown is more than twice the value appropriate for the single pile, appropriate damping inputs to DRIVE for analyzing the group would appear to be much higher than those for the single pile. Although no numerical value was established, observation of the test transfer functions suggests that total damping in the physical test was near critical.

The 68 Hz peak could possibly be due to in-phase motion between the piles and p-waves reflected vertically from a soil layer interface. The most obvious of such interfaces occur at depths of 70 ft, 105 ft, and 121 ft (21.4, 32.0 and 36.9 m), respectively (Fig. 3.4). If the equivalent depth of p-wave generation is assumed to be at the mid-depth of the piles, the times required for a p-wave to travel from that level (depth = 22 ft (6.7 m)) to these reflective interfaces and return are 0.019 sec, 0.033 sec, and 0.040 sec, respectively, assuming a nominal p-wave velocity of 5000 ft/sec (1525 m/sec) in the saturated clays, silts, and sands. See Appendix C. These travel times result in approximate in-phase frequencies of 53 Hz, 30 Hz, and 25 Hz, respectively, which do not coincide with the measured peak at 68 Hz. However, reflections from shallower layers and/or depths of equivalent p-wave generation greater than the mid-depth of the piles could conceivably yield in-phase motion at 68 Hz.

It is more plausible that the 68 Hz peak is the result of in-phase motion of the corner piles and incident shear or Rayleigh waves produced by diagonal corner piles. The corner-to-corner pile spacing of 7.5 ft (2.3 m) times a frequency of 68 Hz gives a soil wave velocity of 510

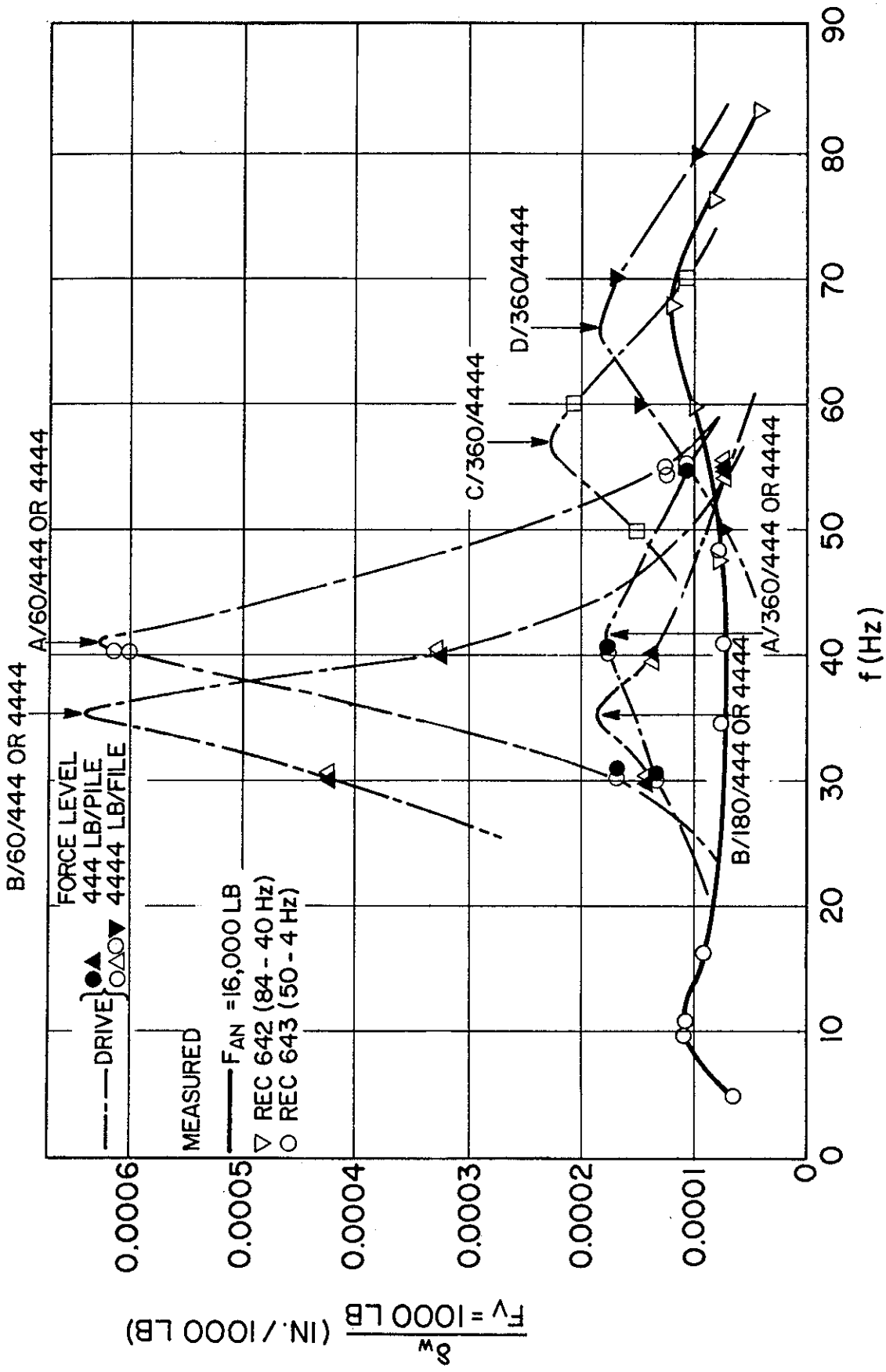

Fig. 7.12. Measured and Computed (DRIVE) Load-Displacement Transfer Functions for Pile Cap: Group, Vertical Tests (1 lb = 4.45 N; 1 in. = 25.4 mm).

ft/sec (156 m/sec), which is very close to the measured shear wave velocity (≈ Rayleigh wave velocity) in the upper 10 ft (3.05 m) at the test site. The effective a_0 (surface) = 0.37 = $\omega r_0/v_s$ (surface) for these piles at this peak. Any other in-phase interactions of piles directly through the soil, as well as harmonics of the corner pile interaction, are likely to be at significantly higher frequencies and therefore were not detectible in these tests.

Figure 7.13 shows the normalized displacement spectra at a depth of 2 ft (0.61 m) below the soil surface. No measurements were made on the piles at that depth during the group tests. Figures 7.14 - 7.16 show computed spectra and transfer functions from the tests at 10 ft (3.05 m) below the soil surface in Piles 2 (center), 8 (corner), and 9 (edge), respectively. About the same displacement occurred in Pile 2 as in Pile 9 at this depth. The accelerometer in Pile 8 malfunctioned so that no usable data were available. The 68 Hz peak is less pronounced at 10.5 ft (3.4 m), suggesting that resonant motion in the piles is seated at a very shallow depth for the 16,000 lb (71.2 kN) nominal force applied to the group. The Set D predictions are seen to be slightly better at this elevation, although, unlike at the cap level, predicted deflections are too small near resonance. This observation suggests that the specified external damping should be highest in the DRIVE elements nearest the ground surface and lower at this depth than the depthwise uniform values used.

Figure 7.17 shows the predicted and measured response at a depth of 29.5 ft (9.0 m). Almost no motion occurred at this level.

The measured normalized mode shapes, Fig. 7.18, are difficult to interpret for this test. The deflection amplitudes in a typical sweep near resonance at 10.5 ft (3.4 m) are almost identical in Piles 2 and 9. (No data are available for Pile 8.) Below 10.5 ft (3.4 m) deflection amplitude decreased more rapidly in Pile 2 than in Pile 9. At 29.5 ft (9.0 m) Pile 8 deflected more than Pile 9, and, although no data were taken in Pile 2 at that level, Pile 9 probably deflected more than Pile 2. The general trend of the data suggest that more load was being transferred in Pile 2 (center pile) than in Piles 8 and 9 (perimeter piles) between 10.5 and 29.5 ft (3.4 and 9.1 m), since the top

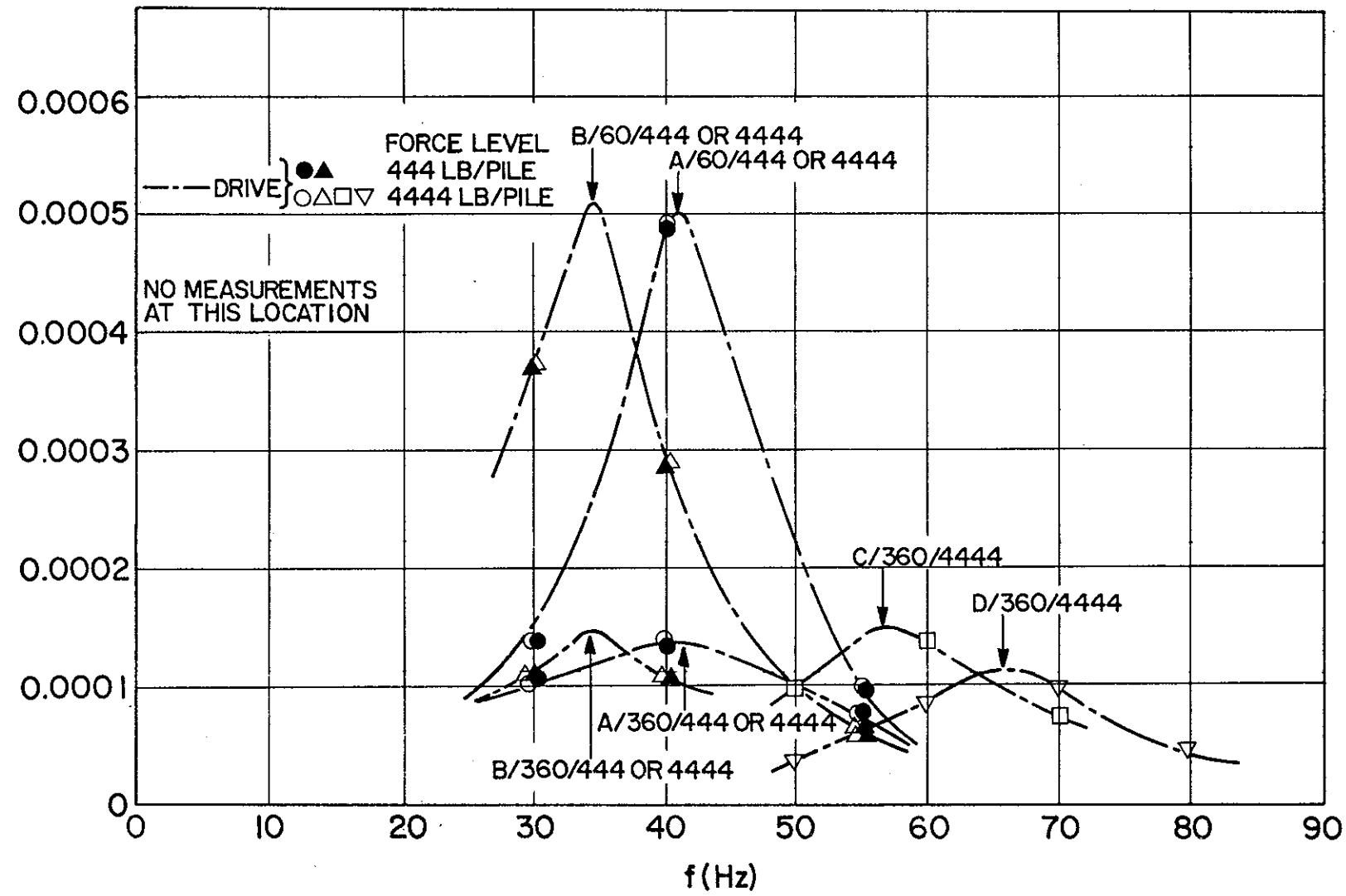

Fig. 7.13. Computed (DRIVE) Load-Displacement Transfer Functions 2 Ft (0.61 m) Below Soil Surface: Group, Vertical Tests (1 lb = 4.45 N; 1 in. = 25.4 mm).

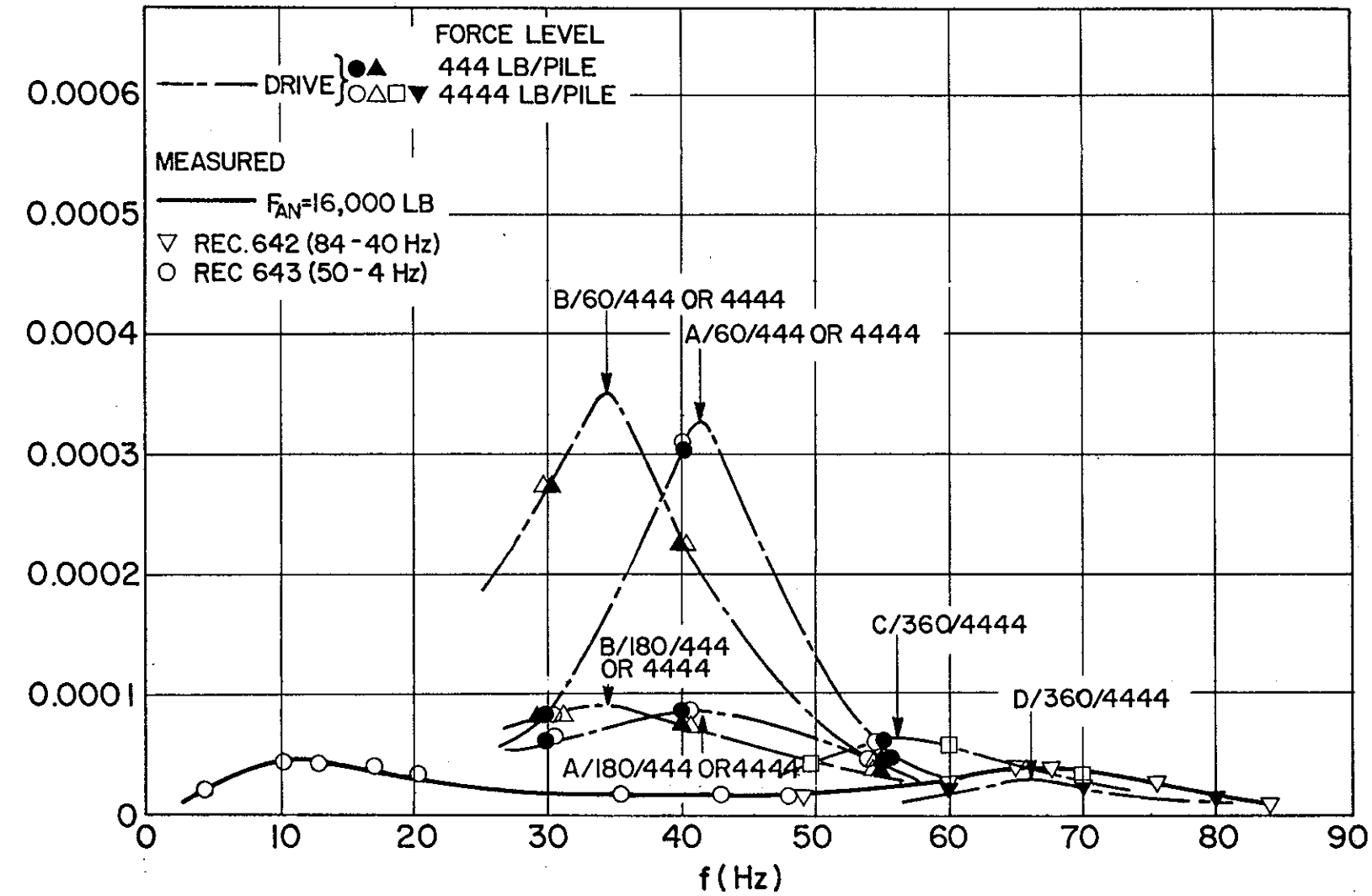

Fig. 7.14. Measured and Computed (DRIVE) Load-Displacement Transfer Functions 10 Ft (3.05 m) Below Soil Surface: Pile 2 of Group, Vertical Tests (1 lb = 4.45 N; 1 in. = 25.4 mm).

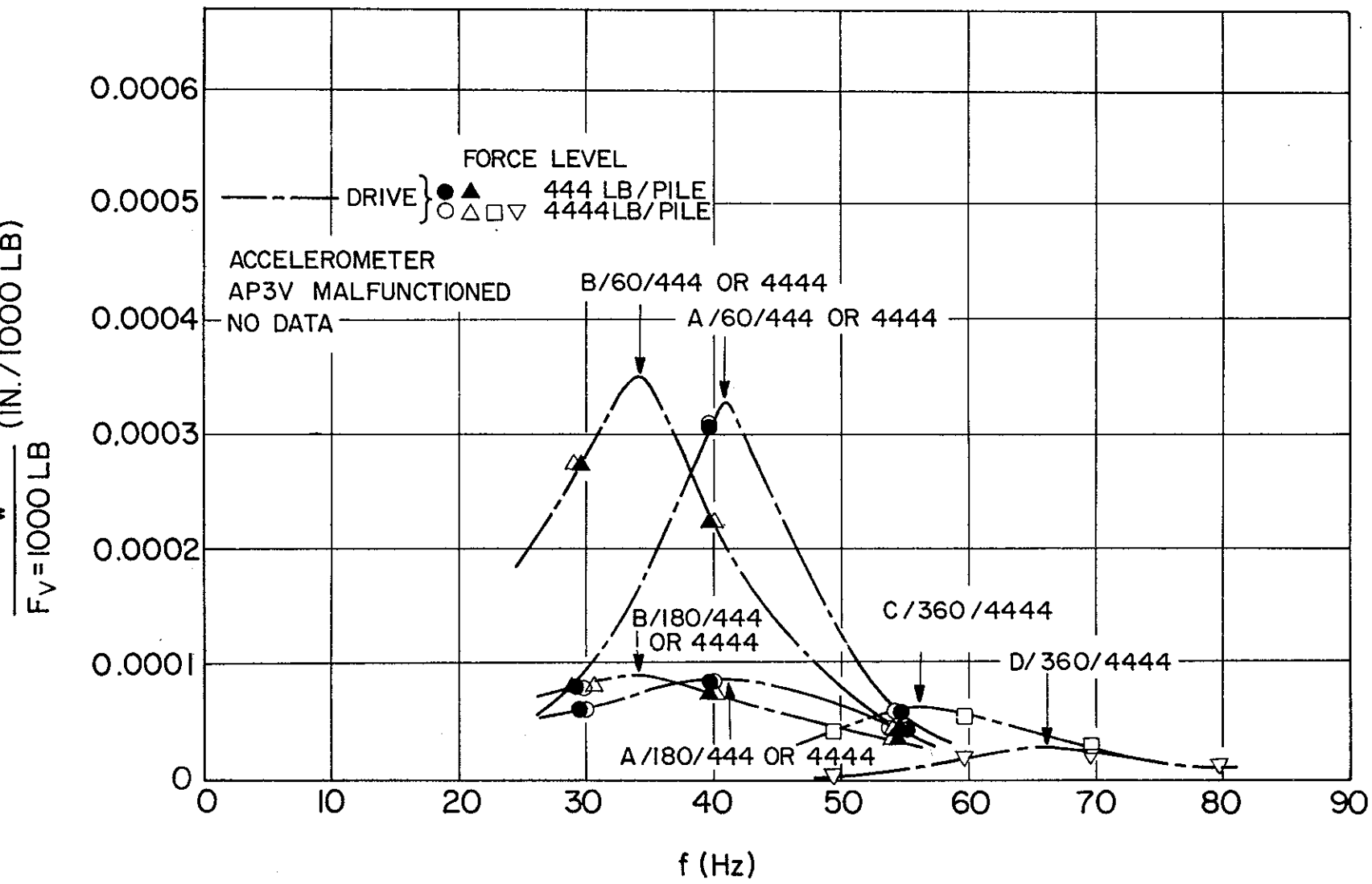

Fig. 7.15. Computed (DRIVE) Load-Displacement Transfer Functions 10 Ft (3.05 m) Below Soil Surface: Pile 8 of Group, Vertical Tests (1 lb = 4.45 N; 1 in. = 25.4 mm).

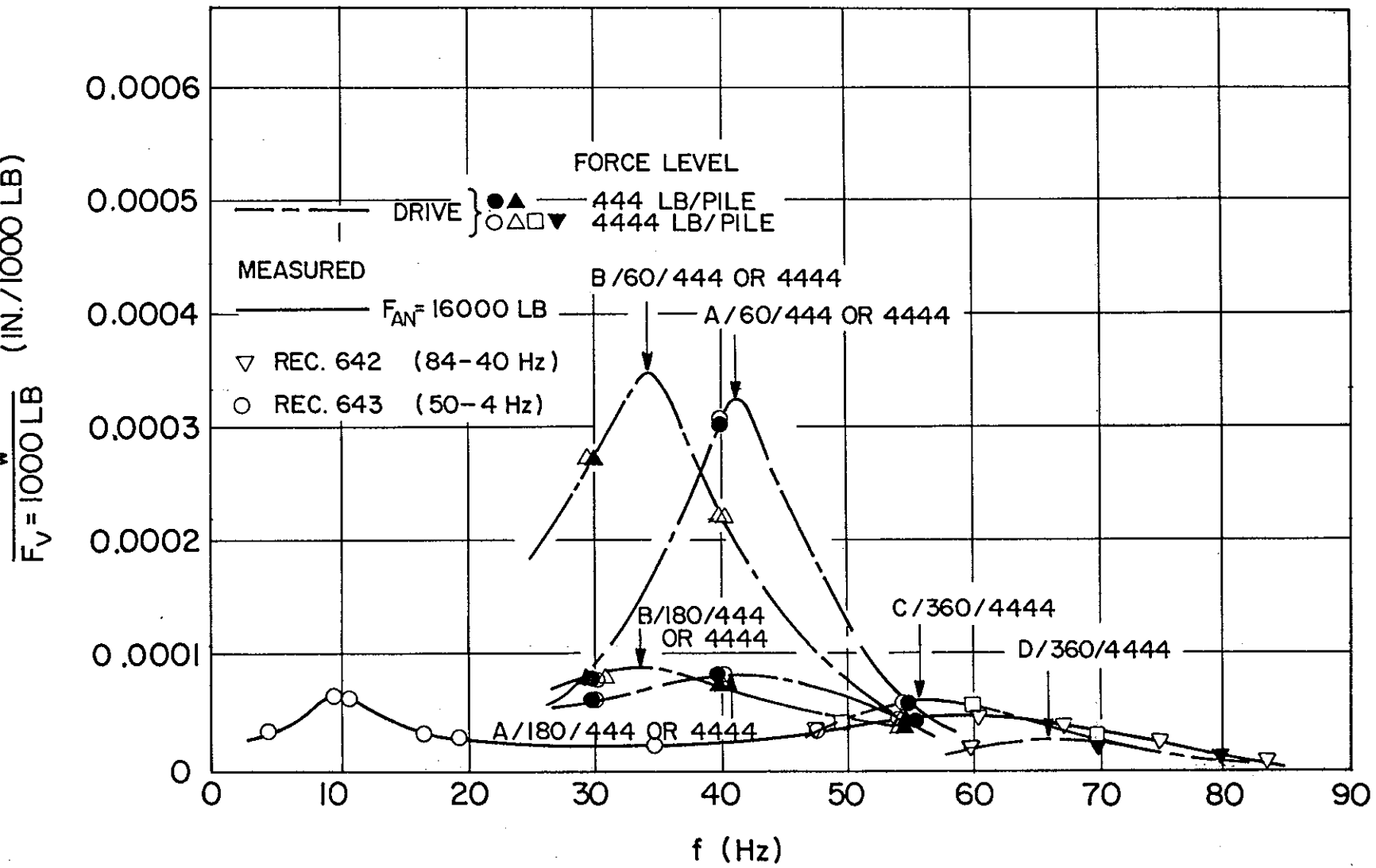

Fig. 7.16. Measured and Computed (DRIVE) Load-Displacement Transfer Functions 10 Ft (3.05 m) Below Soil Surface: Pile 9 of Group, Vertical Tests (1 lb = 4.45 N; 1 in. = 25.4 mm).

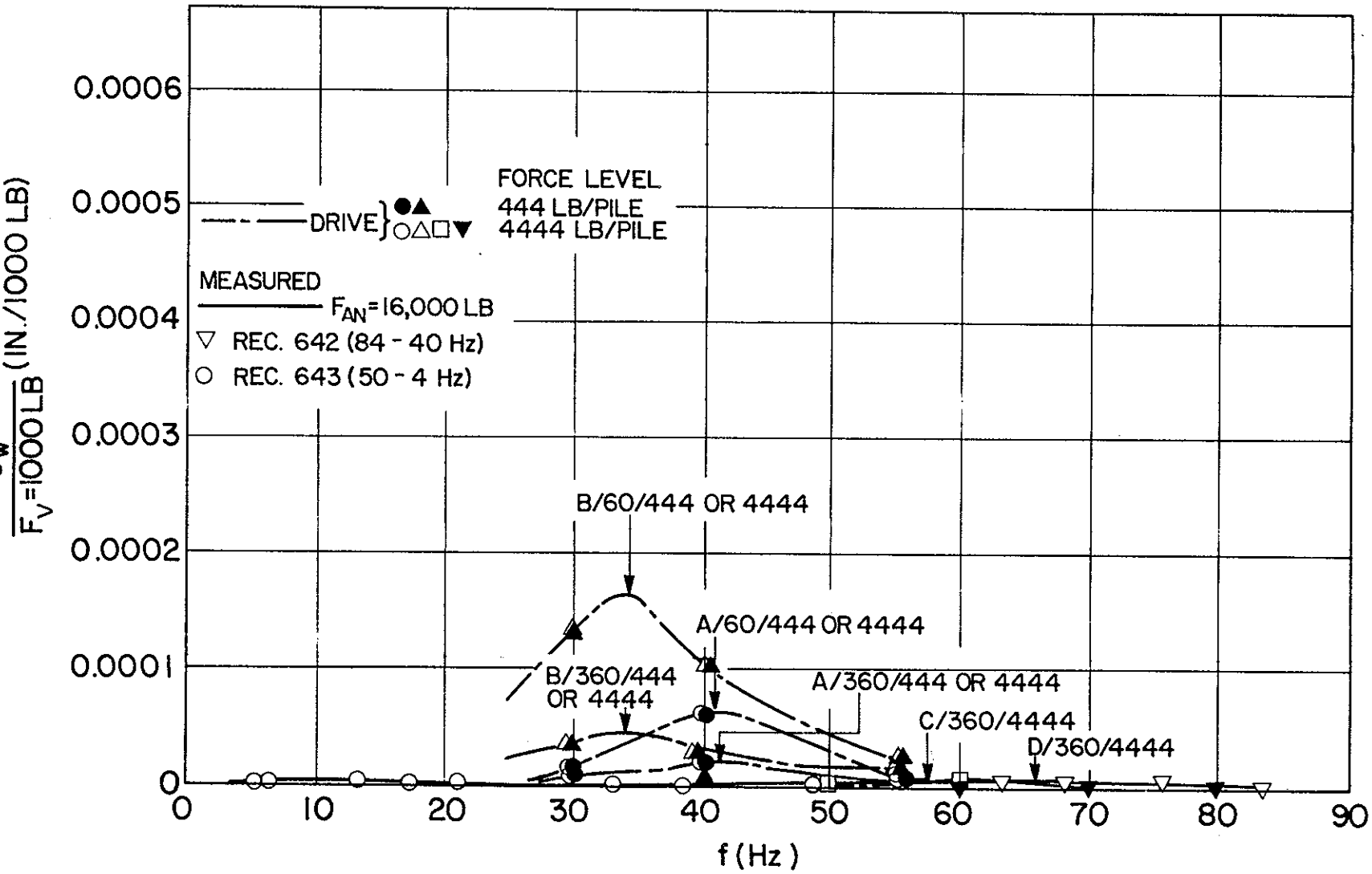

Fig. 7.17. Measured and Computed (DRIVE) Load-Displacement Transfer Functions 29.5 Ft (9.0 m) Below Soil Surface: Pile 9 of Group, Vertical Tests (1 lb = 4.45 N; 1 in. = 25.4 mm).

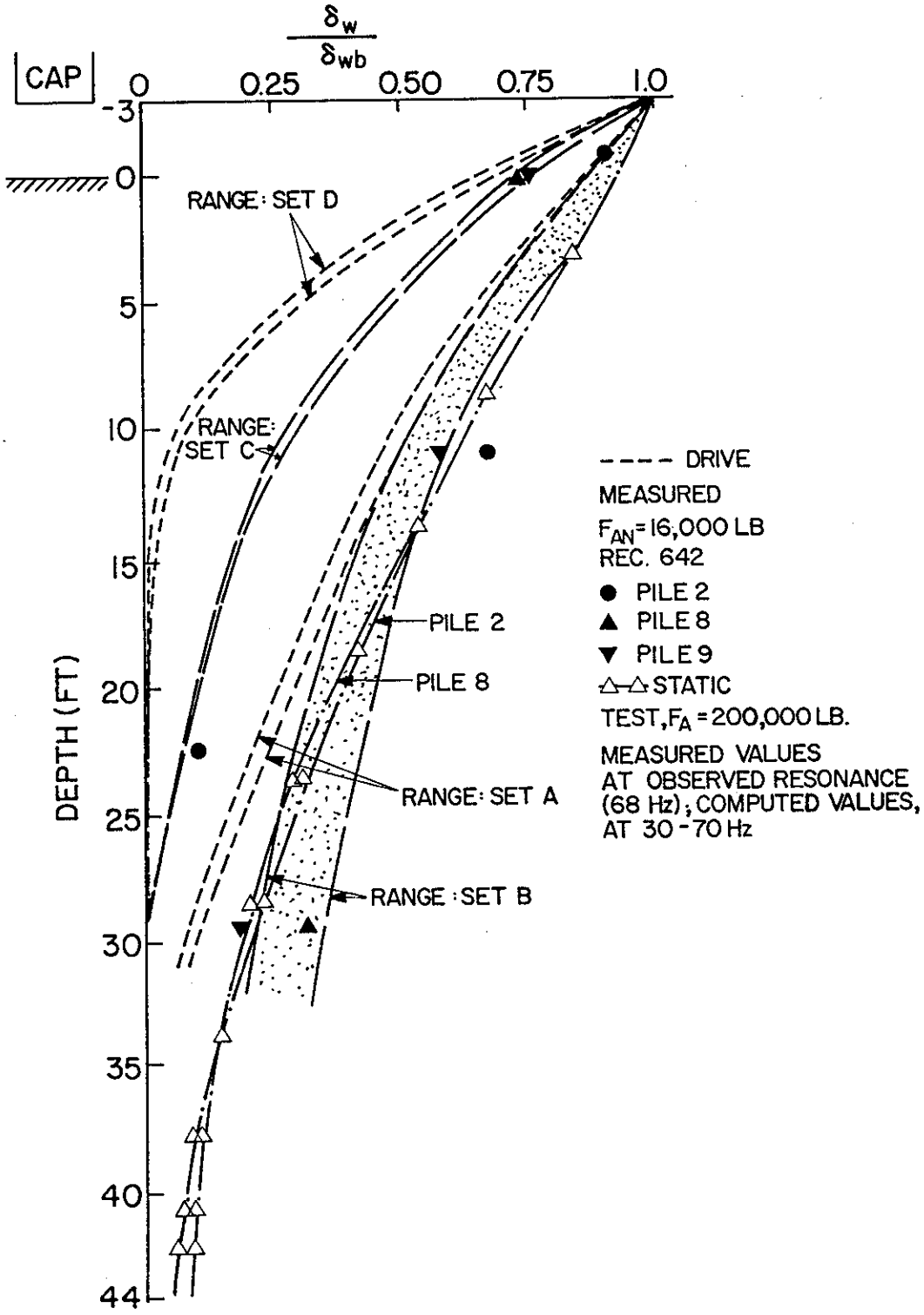

Fig. 7.18. Normalized Displacement Mode Shapes: Group, Vertical Tests (1 lb = 4.45 N; 1 ft = 0.305 m).

displacements, δ_{wb}, were both equal to the displacements of the rigid cap. Above 10.5 ft (3.4 m), somewhat less deflection appears in Pile 2. This behavior is not predicted by any of the soil sets used in the DRIVE analyses. Except for the small displacement at the lowest level in Pile 2, the normalized mode shapes follow those for the static tests relatively closely.

Soil Set D, the set that provided the best estimate of resonant frequency, gave normalized subsurface displacements that were too small, but as already described, absolute displacement amplitude values were slightly too large below 10.5 ft (3.4 m) and slightly too small above 10.5 ft (3.4 m). Hence, in Fig. 7.18, the discrepancies in the actual (non-normalized) measurements and the computed deflection amplitudes are somewhat smaller than implied in Fig. 7.18.

Unit Load Transfer Set C provided the best fit for the single pile, while Set D provided the best fit for the group pile using DRIVE. Since Set D is stiffer than Set C, this effect may be a reflection of the smaller soil strains in the group test than in the single pile test. It is apparent that the need for a stiffer unit load transfer relationship for modeling the group is not consistent with the requirement for softening the single pile relationship to model statically loaded groups.

Load (strain gage) data were acquired, but force amplitudes along the piles were not obtained from DRIVE for the group pile cases. Hence, the force amplitude mode shapes will be displayed when describing comparisons with PILAY/RIGDF.

Displacement Transfer Function Measurements vs. PILAY/RIGDF

Predicted and measured displacement relationships are shown in Fig. 7.19.

The PILAY/RIGDF analyses can be seen to have predicted displacement amplitudes at the pile head somewhat better than did DRIVE. The best match was for Soil Case 1 (in-situ, crosshole wave velocities without degradation) and with $\alpha = 1$ (no flexibility increase of group pile over single pile). However, the resonant frequency was still predicted to be too small. Since displacements were small in the vertical group tests,

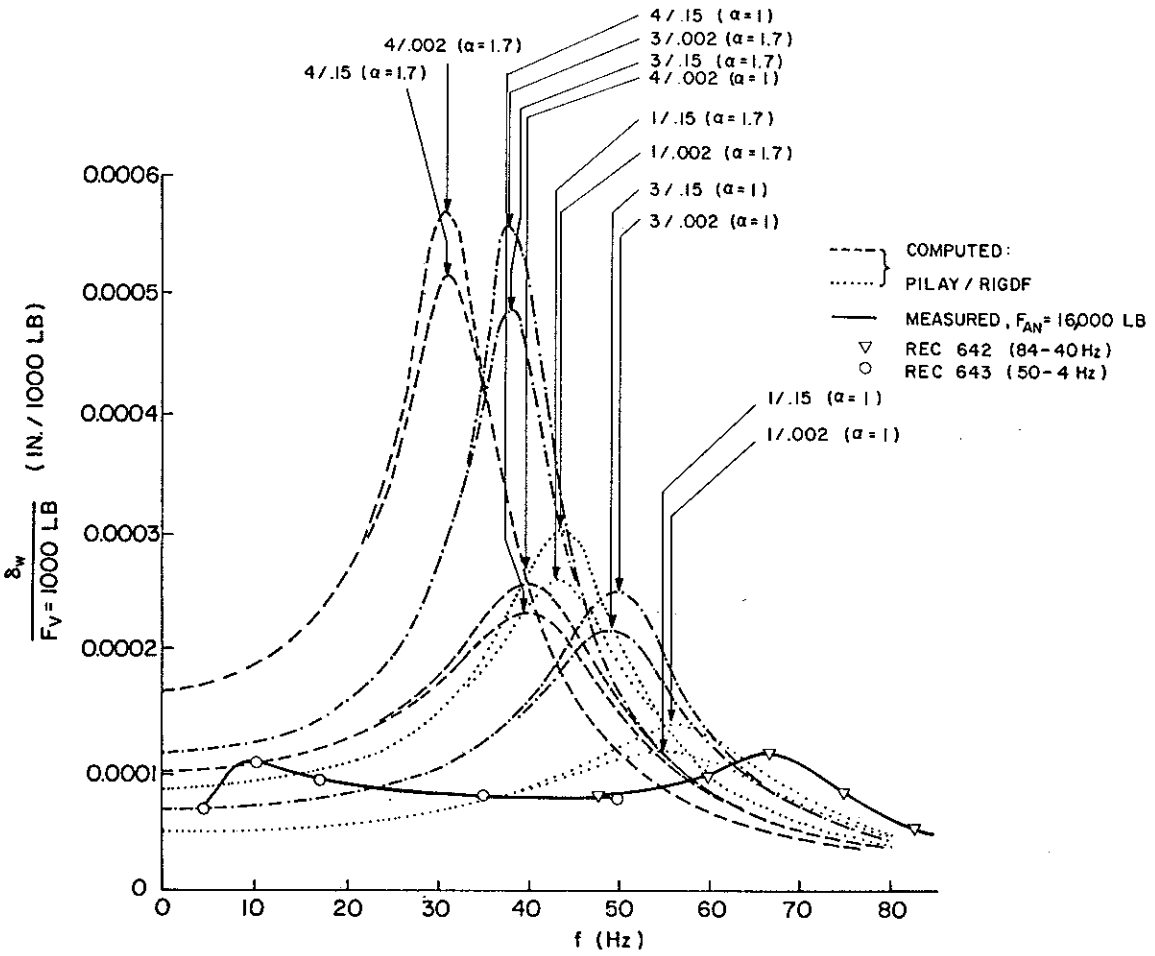

Fig. 7.19. Measured and Computed (PILAY/RIGDF) Load-Displacement Transfer Functions for Pile Cap: Group, Vertical Tests (1 lb = 4.45 N; 1 in. = 25.4 mm).

hysteretic damping was also probably minimal. The relative prositions of the "1/.002 (α = 1)" predicted spectrum and the measured transfer function suggest that effective radiation damping from the single pile PILAY solution was probably nearly correct but that the stiffness was predicted to be too low. The higher implied stiffness in the physical group is speculated to be due to anti-phase interactions between the soil and some of the piles. It should be obvious, as with DRIVE, that $\alpha > 1$ has no validity.

The lower resonance peak ($\approx$ 9.5 Hz) may be due to rocking of the group due to imperfect concentric loading.

Figure 7.20 shows the normalized mode shapes for deflection from Fig. 7.18 superimposed on the predictions from PILAY. Generally better agreement exists here than for DRIVE, although Case 1 (0.2 percent hysteretic damping) tends to predict displacement amplitudes that are too small (in absolute, as well as relative, terms). The computed shapes in Fig. 7.20 were obtained at f = 35 Hz. Reference to Fig. 7.8 shows that little difference exists at 70 Hz for the pile and soil conditions specified.

The data presentation for vertical excitation of the group concludes with Figs. 7.21 and 7.22, which show normalized force mode shapes for Piles 2 and 8, respectively. Unfortunately, excessive noise in the strain gages in Pile 8 prevented comparisons for that pile. Excessive noise also existed in strain gage circuit P2F0 (at soil surface) in Pile 2, so the measured data were normalized with respect to P2F1, at a depth of 6.5 ft (2.0 m). If any load transfer occurred above that depth, the measured curve will shift to the left at every depth and come into better conformity with the computed Soil Case 1 curve (1/.002).

Applied load in Pile 2 was transferred to the soil at a generally higher rate above 30 ft. (9.15 m) than for the indicated load in the static test. Part, but not all, of the difference in the shapes of the normalized static and dynamic force curves can be explained by the fact that the load amplitude was higher in the static test, allowing for deeper transfer of load.

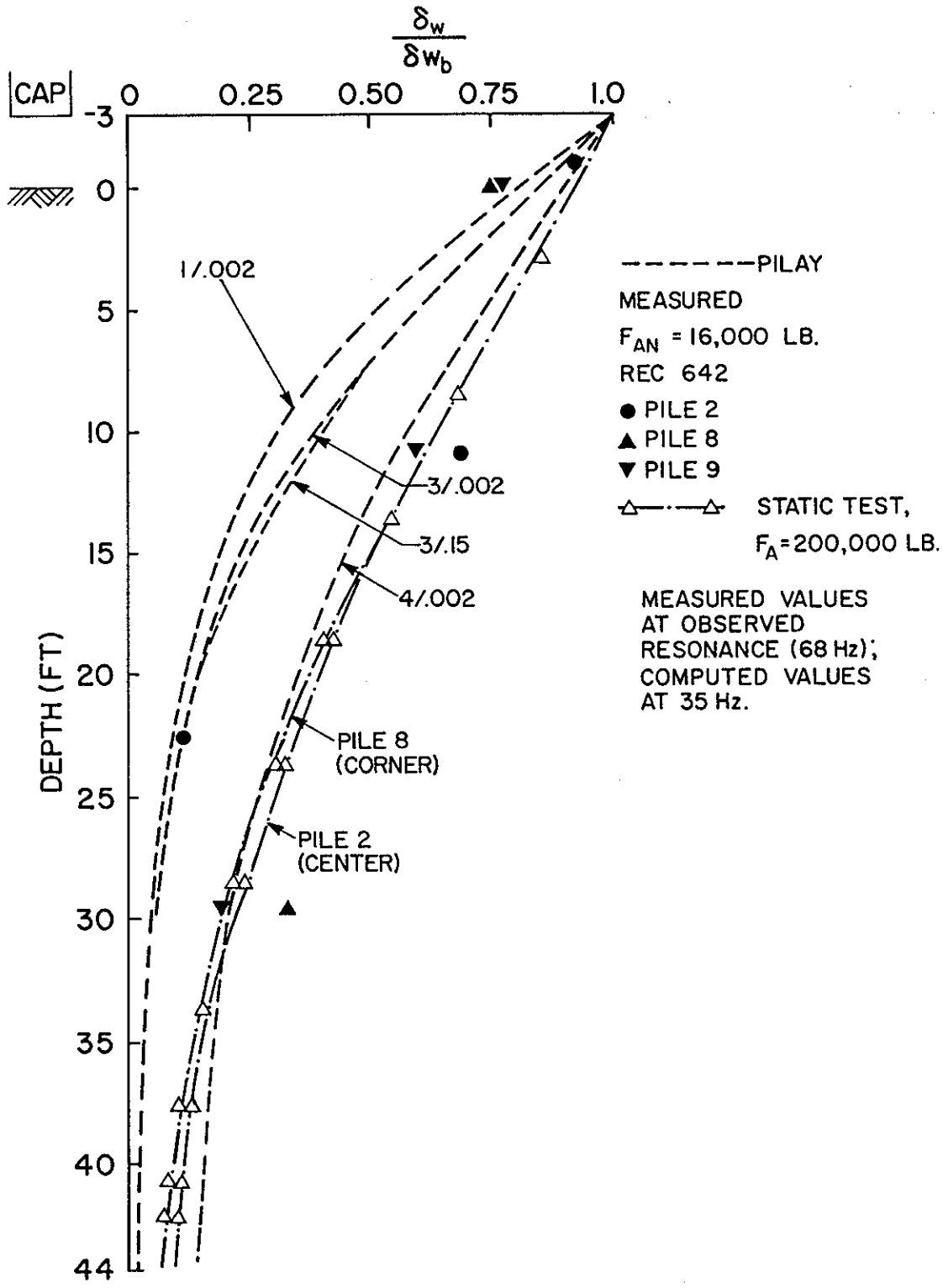

Fig. 7.20. Normalized Displacement Mode Shapes: Group, Vertical Tests (PILAY/RIGDF) (1 lb = 4.45 N; 1 ft = 0.305 m).

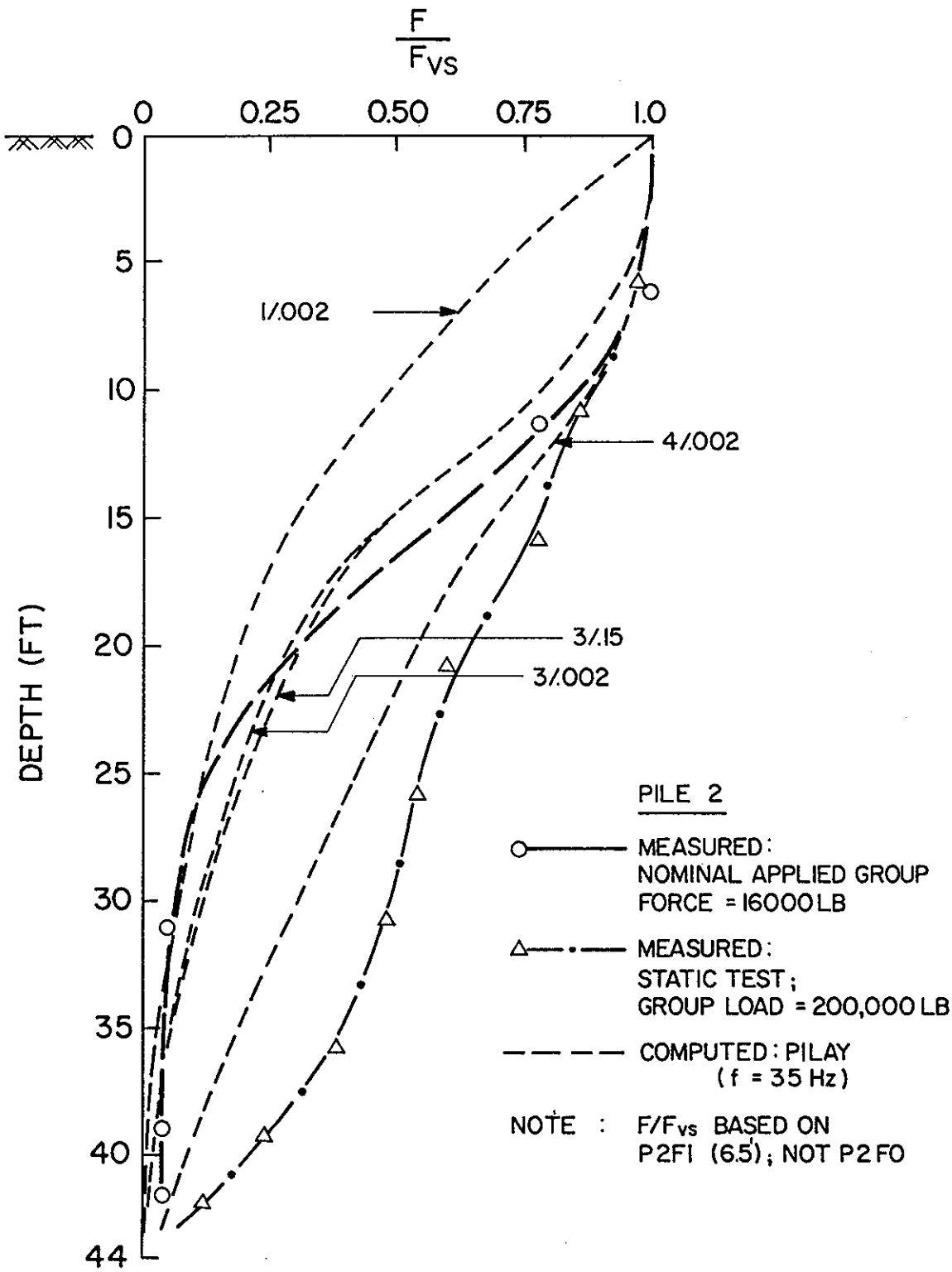

Fig. 7.21. Normalized Pile Thrust Mode Shapes: Group Pile 2, Vertical Tests (PILAY/RIGDF) (1 lb = 4.45 N; 1 ft = 0.305 m).

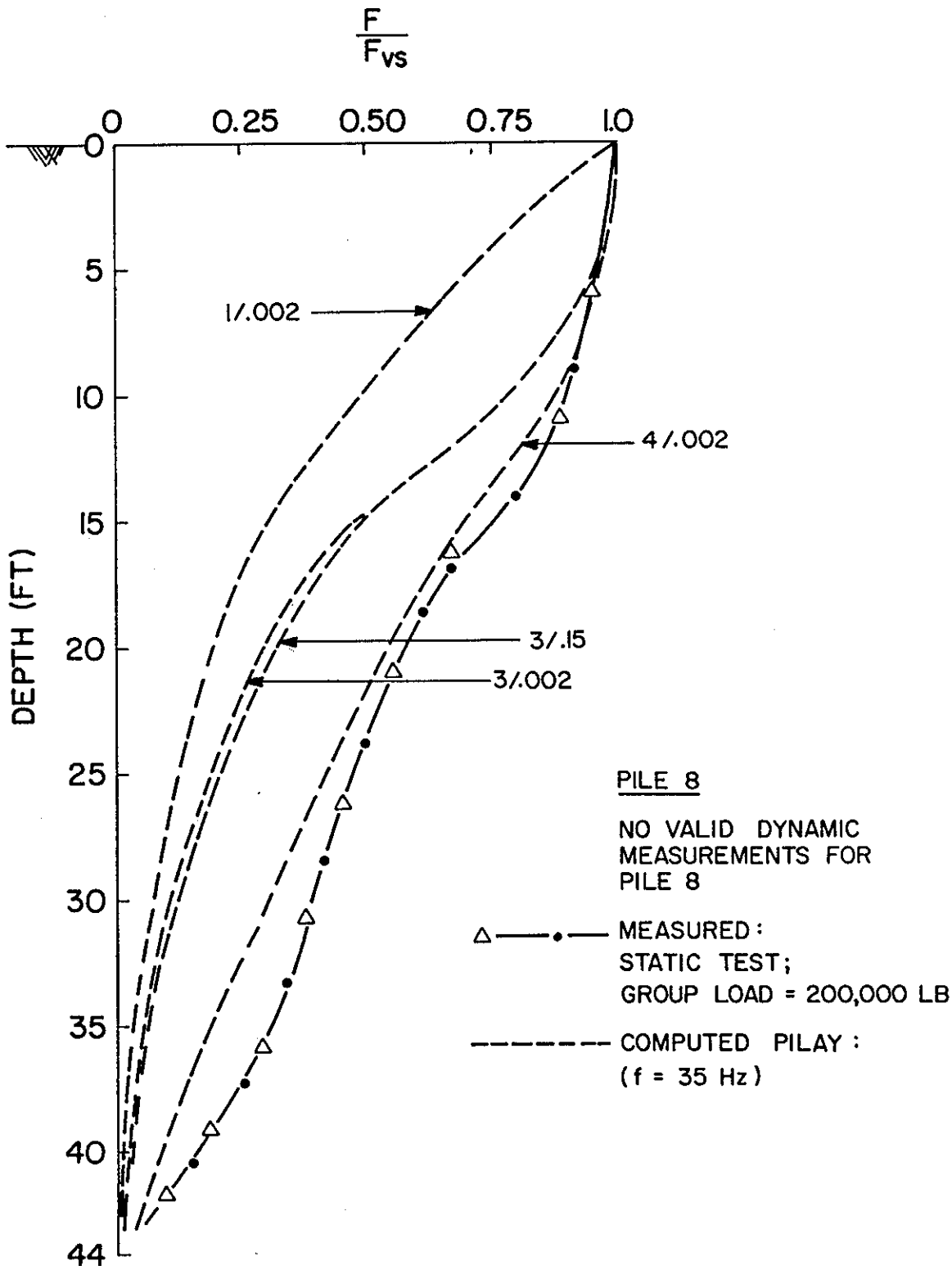

Fig. 7.22. Normalized Pile Thrust Mode Shapes: Group Pile 8, Vertical Tests (PILAY/RIGDF) (1 lb = 4.45 N, 1 ft = 0.305 m).

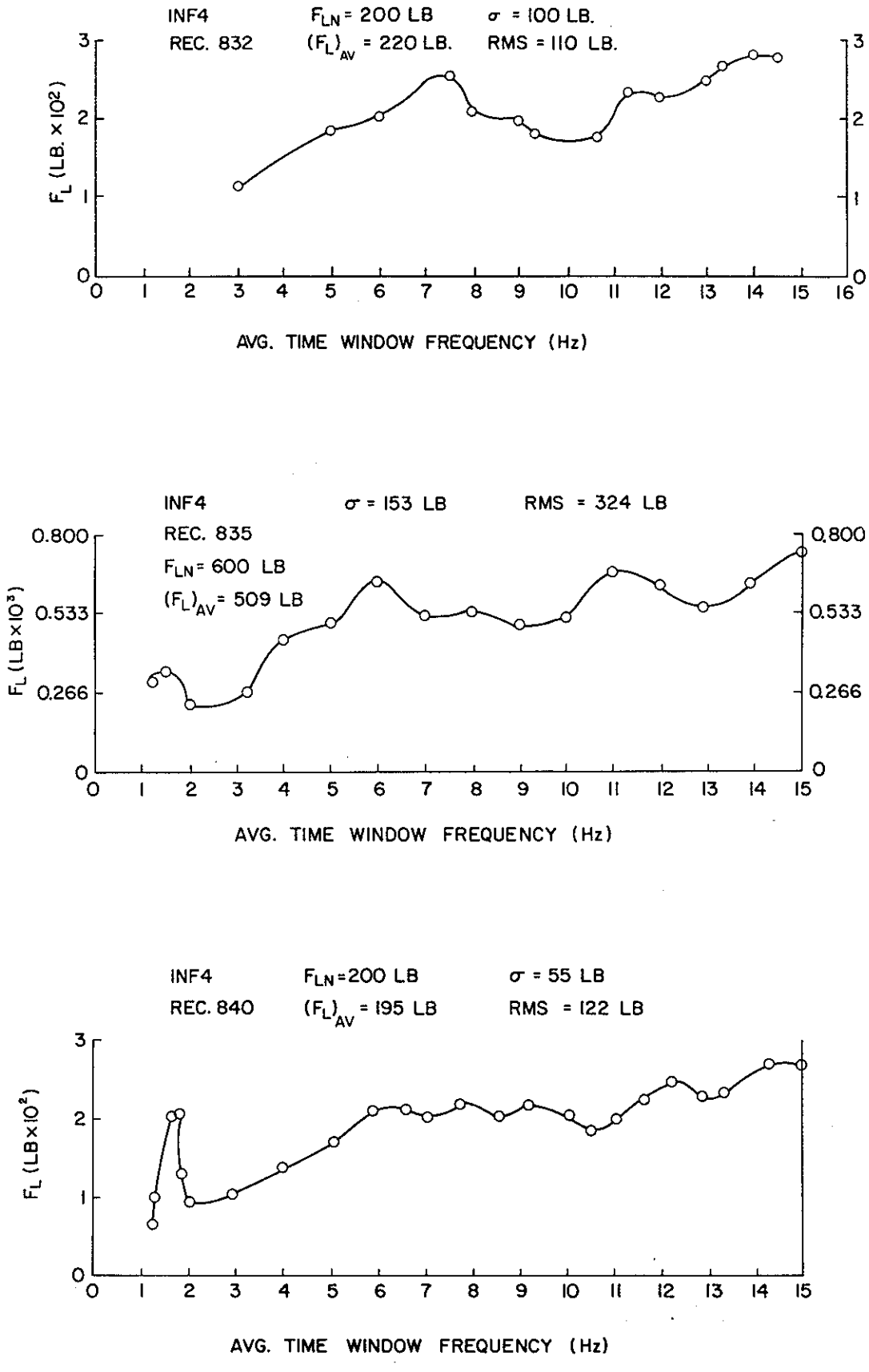

Fig. 7.23. Applied Force vs. Frequency: Single Pile, Horizontal Tests (1 lb = 4.45 N).

SINGLE-PILE - HORIZONTAL EXCITATION

Force-Frequency

Figure 7.23 gives applied lateral force (F_L) vs. frequency (average time window frequency from force-time records) relationships for three frequency sweeps using the WES vibrator on the single pile. It is noted that, because of system compliance, the force applied was generally lowest around 2 Hz, the approximate resonant frequency of the system. The largest force amplitude at resonance was only about 250 lb (1.1 kN) (Rec. 835), while higher forces were delilvered at other frequencies, as may be observed in Fig. 7.23. The normalized transfer functions presented in this section should be interpreted in light of this variable force amplitude. For example, had constant force amplitude been applied, corresponding to the force achieved at frequencies several Hz above resonance, it is likely that the transfer functions would have been less sharply peaked because absolute displacements near resonance would have been higher and hysteretic damping greater. The predicted response curves assume constant force amplitude and so automatically incorporate this effect in their shape at all frequencies. In this respect, matching of predicted and measured frequency-displacement spectra is valid only in the near vicinity of the measured resonant frequency.

Displacement Transfer Function Measurements vs. SPASM

The Matlock p-y criteria curves with the gapping and radiation damping characteristics described in Chapter 6 (p-y Set I) provided a good approximation of the pile head force-displacement measurements at and below system resonance (about 2.10 Hz), as shown in Fig. 7.24. This is consistent with the observation that a small, annular gap existed around the pile after testing. The Set I spectrum appears more sharply peaked than the measurements, but this may be due to the difficulty, described earlier, in determining valid values for pile-head displacement above resonance from SPASM due to convergence problems. Also, however, as discussed in Chapter 5, the accelerometers indicate values of acceleration (and displacment) that are too low by about 19% at 2 Hz, so that the measured displacement values should be increased by a factor of about 1.15 - 1.2 in the range of resonance. Even greater under-registration occurred below 2 Hz.

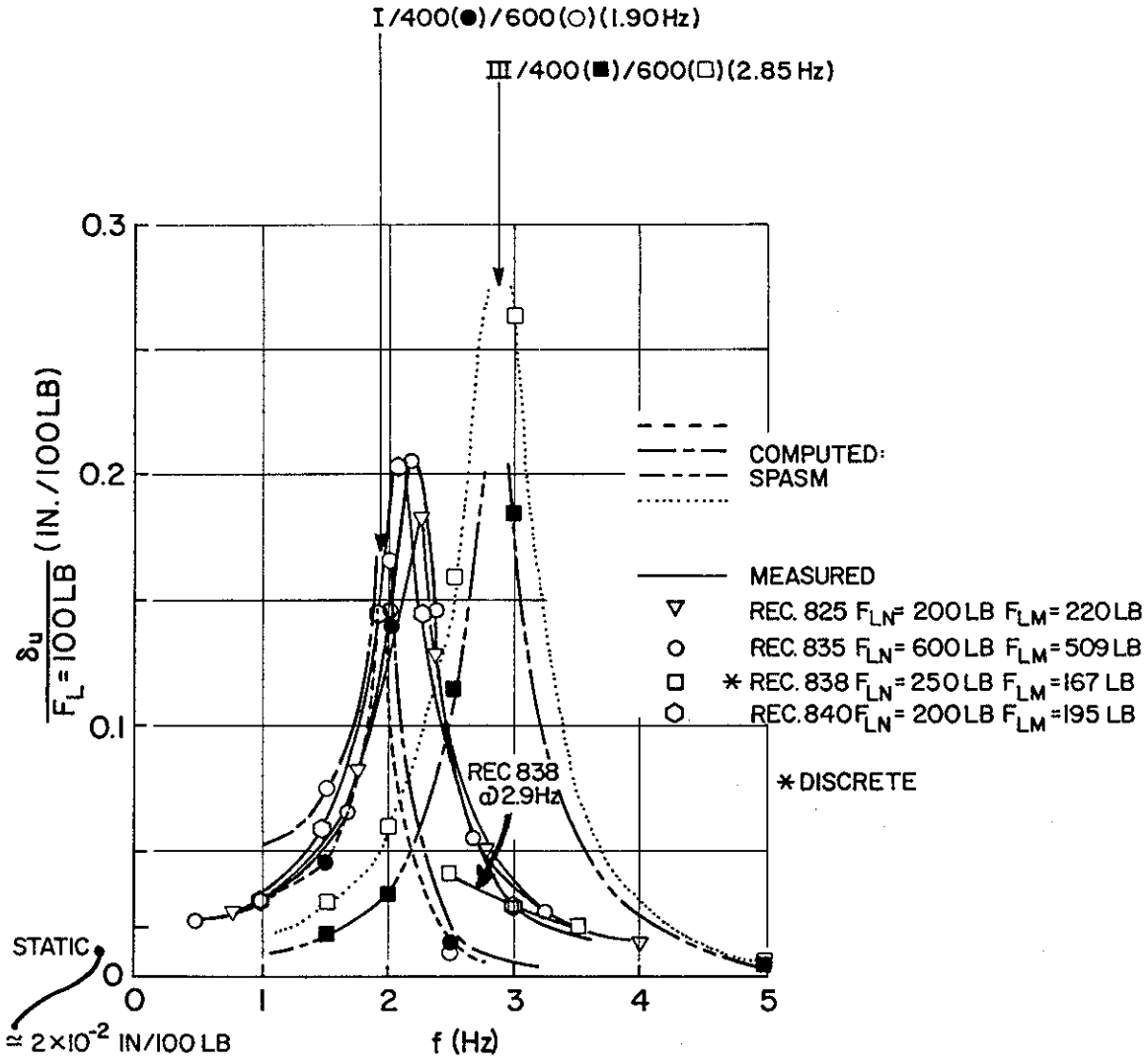

Fig. 7.24. Measured and Computed (SPASM) Load-Displacement Transfer Functions at 2 Ft (0.61 m) Above Cap Base: Single Pile, Horizontal Tests (1 lb = 4.45 N; 1 in. = 25.4 mm).

The Set III p-y curves are somewhat too stiff and are not damped highly enough, probably because the procedure used to derive the basic expressions for these curves considers mainly deep seated soil motion due to upward propagating shear waves, as in a seismic event, and not shallow soil and pile motion, as predominated in these tests. Considering this point, the Case III curves did a fairly accurate job of representing the soil.

The measured transfer functions themselves show a slight softening effect due to repeated loading (with increasing force amplitude), as evidenced by the relative positions of the resonance peaks for Rec. 825 and 835 (taken after 825). Unlike the vertical test, reduction of the force amplitude (Rec. 840) did not indicate recovery of soil stiffness but rather a slightly further increased stiffness reduction (reduced resonant frequency) compared to the earlier sweep record, 835.

The results of a constant force discrete frequency test at f = 2.9 Hz (above resonance), conducted just before the final sweep (Rec. 840) are also included on Fig. 7.24. They show good agreement with the sweep response at 2.9 Hz. Due to imperfect sinusoidal loading, some frequency components were present above and below 2.9 Hz in the records for this test, and these are also shown between 2.5 Hz and 3.5 Hz. Good agreement between the sweep data and discrete data are seen above 2.9 Hz, but the measured displacments at f less than 2.9 Hz were below those measured in the sweeps. This effect may be due to very low energy levels associated with f below 2.9 Hz, such that the effective portion of the system undergoing vibration at 2.5 Hz did not duplicate that part undergoing vibration at the same frequency where force was actually being applied through the vibrator at the frequency. Thus, the technique employed here--developing transfer functions between force in a quasi-discrete frequency test that appear at frequencies other than the discrete shaking frequency and displacements at other than the discrete shaking frequencies--is probably not a valid one for analyzing a laterally vibrating pile.

Figure 7.25 compares the measured lateral normalized displacement mode shape envelopes with those predicted by SPASM, Set I p-y curve input. A favorable comparison can be observed, within the resolution

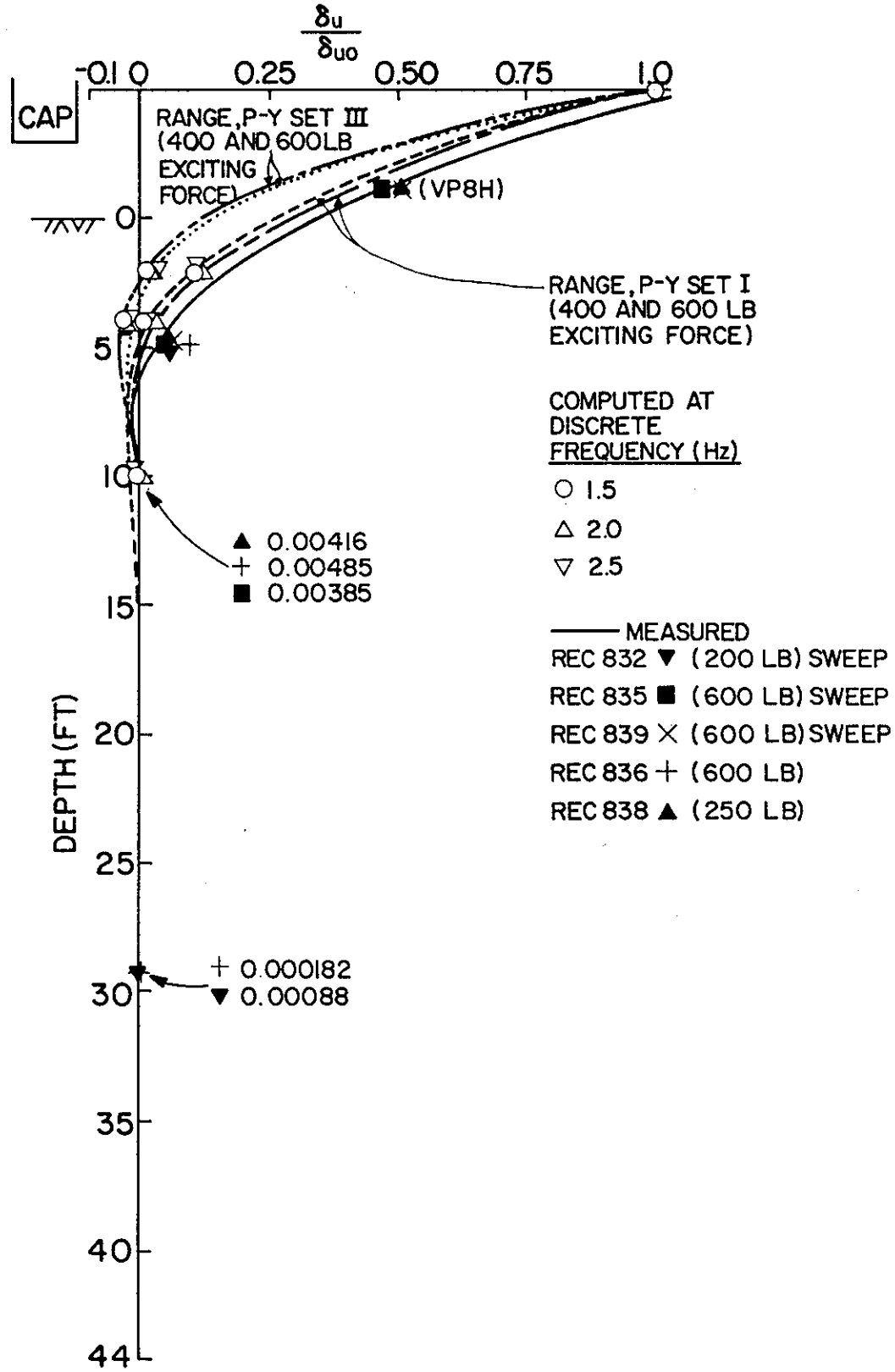

Fig. 7.25. Normalized Displacement Mode Shapes: Single Pile, Horizontal Tests (1 lb = 4.45 N; 1 ft = 0.305 m).

afforded by the number of down-pile instruments that were employed. Phase relationships are not shown in Fig. 7.25 (i.e., all measured displacements are plotted as positive).

Displacement Transfer Function Measurements vs. PILAY/RIGDF

Figure 7.26 compares the measured pile-head transfer functions (without rolloff correction) with response predicted by PILAY/RIGDF. Only Soil Case 2 (reduced soil modulus to full depth of pile) properly reproduced the resonant frequency, but specified hysteretic damping was much too low, as indicated by the sharp peak at resonance. Increasing hysteretic damping in PILAY much above 0.15 (the value for which the functions on Fig. 7.26 are plotted) is inconsistent with Fig. 3.11, as the maximum single amplitude groundline deflections during the test were in the order of 0.10 - 0.15 in. (2.5 - 3.8 mm), and maximum displacement decreased sharply with increasing depth. Thus, increasing hystertic damping to above 0.15 for the Set 3 spectrum in Fig. 7.26 to better replicate measured behavior does not appear to be an appropriate correction, although doing so may give a better solution match than obtained with 2/0.15. The discrepancy in the PILAY/RIGDF soutions and measurements are instead probably due to the fact that surface wave radiation is not considered in PILAY, and that such radiation needs to be included in modeling free-headed laterally loaded piles when the majority of the radiation is near-surface. This may also imply that the choice of damping values for the SPASM analyses was to some extent fortuitous.

The normalized displacement mode shape envelopes computed in PILAY, Fig. 7.27, do not agree as well with the measurments as those computed by SPASM (Fig. 7.25).

The pile-head transfer function measured from one test using the FHWA vibrator is compared with deflections by PILAY/RIGDF in Fig. 7.28. The principal difference between this transfer function and those for the WES vibrator is that the FHWA tests were essentially constant-force-amplitude tests and did not have significant force losses near resonance, as described previously for the WES vibrator in Fig. 7.23. However, the data quality was rather poor because the starting motor frequency of 1.8 Hz was near the resonant frequency of the system.

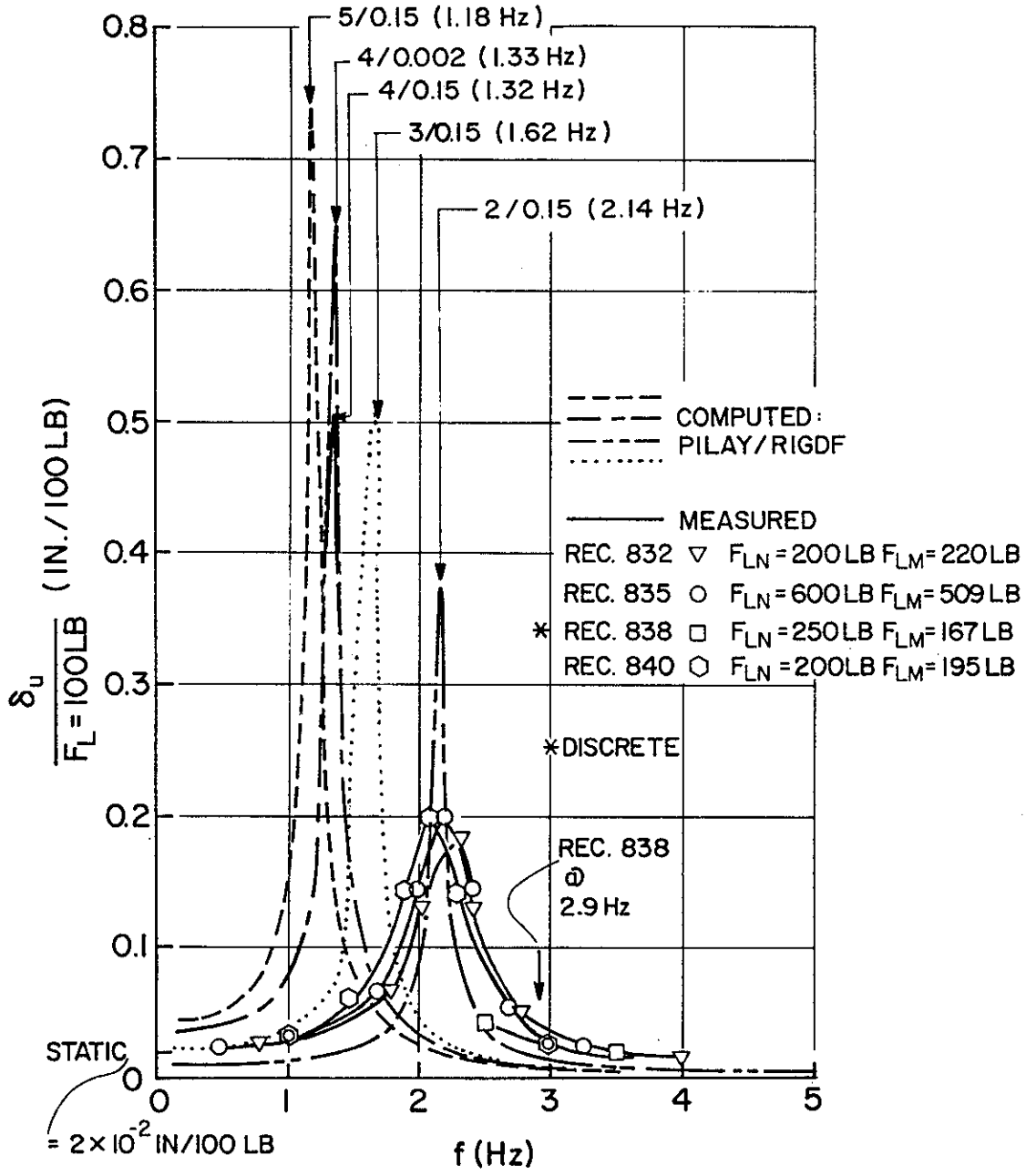

Fig. 7.26. Measured and Computed (PILAY/RIGDF) Load-Displacement Transfer Functions at 2 Ft (0.61 m) Above Cap Base: Single Pile, Horizontal Tests (1 lb = 4.45 N; 1 in. = 25.4 mm).

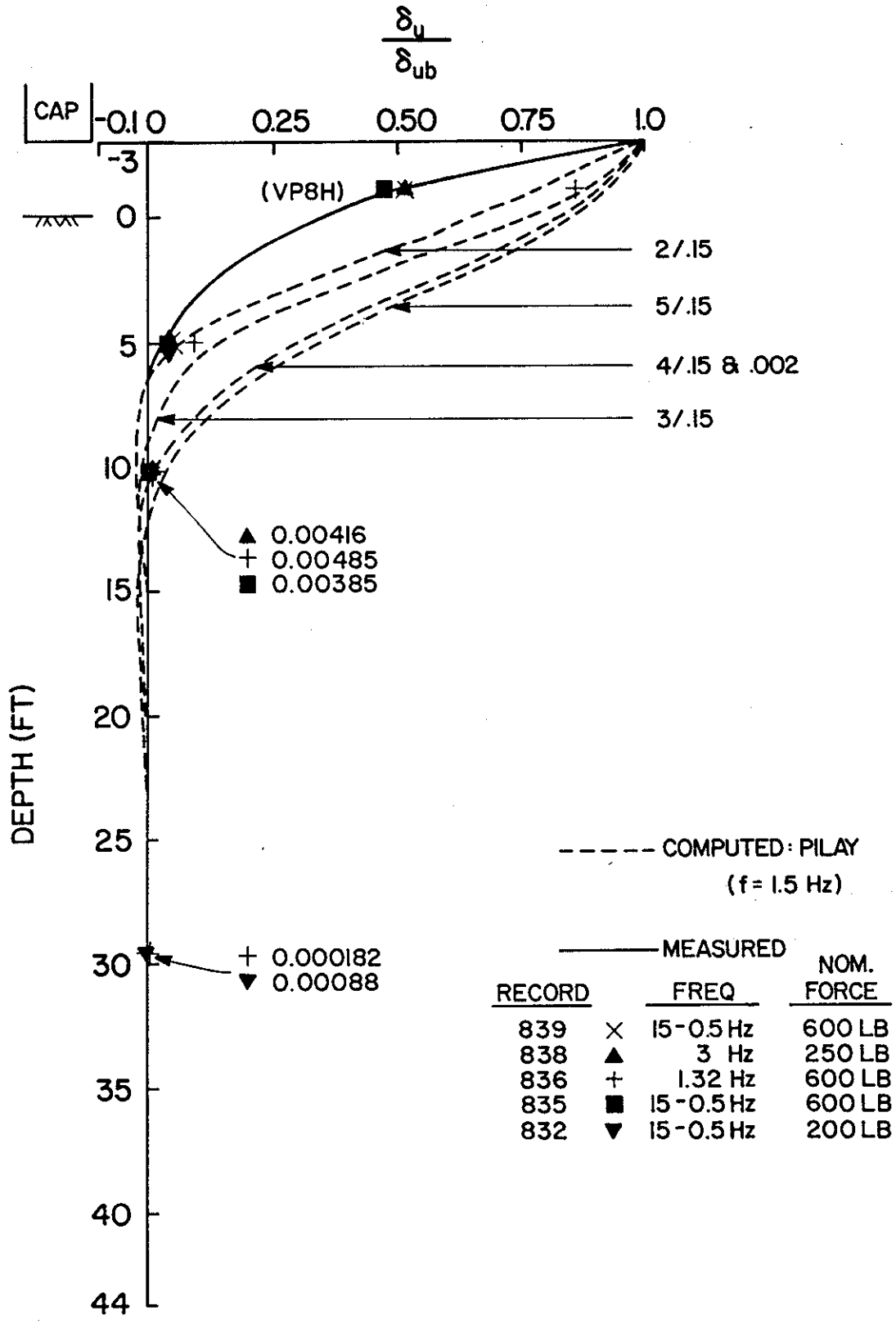

Fig. 7.27. Normalized Displacement Mode Shapes: Single Pile, Horizontal Tests (1 lb = 4.45 N; 1 ft = 0.305 m).

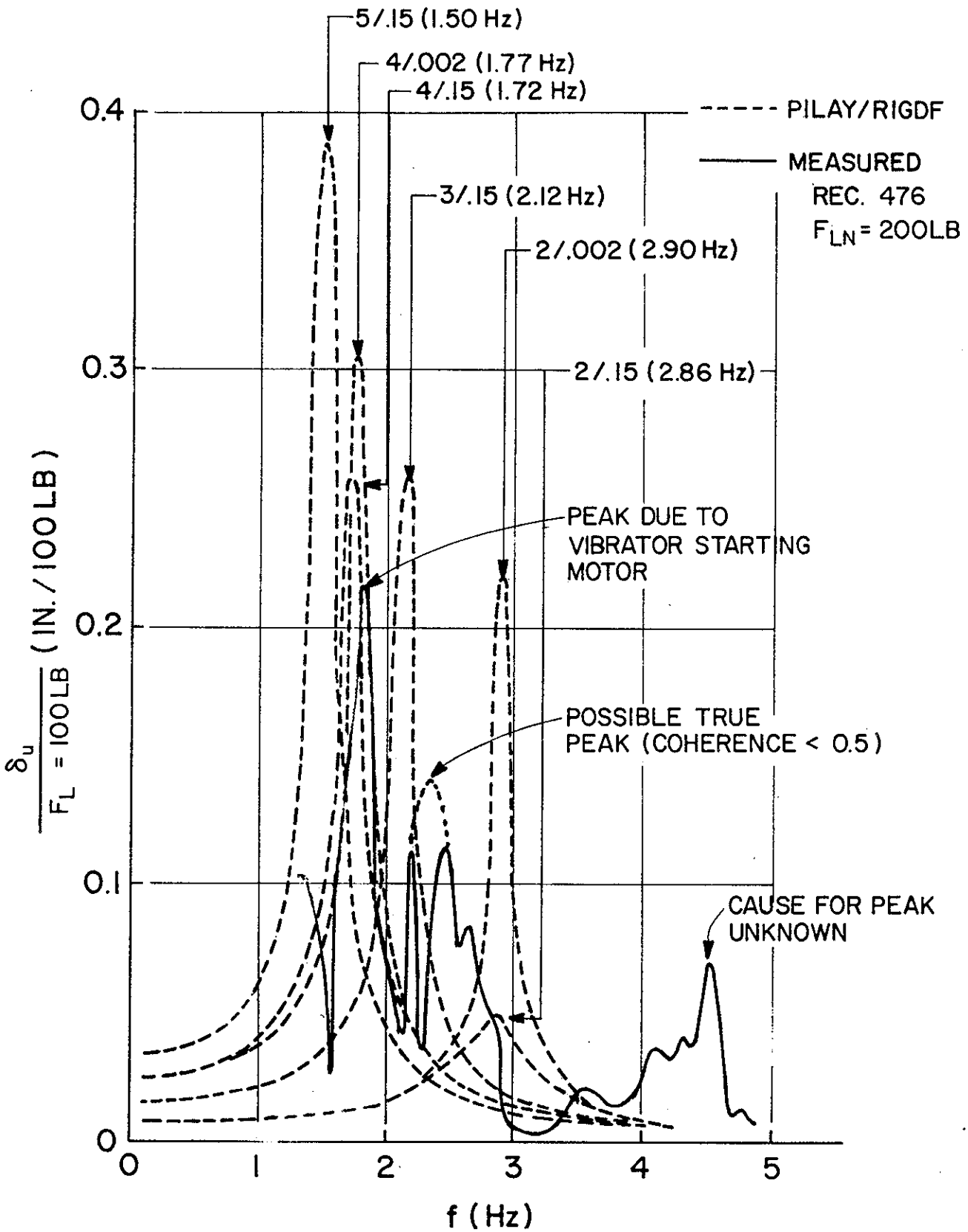

Fig. 7.28. Measured (FHWA Vibrators) and Computed (PILAY/RIGDF) Load-Displacement Transfer Functions at 2 Ft (0.61 m) Above Cap Base: Single Pile, Horizontal Tests (1 lb = 4.45 N; 1 in. = 25.4 mm).

Furthermore, very low coherence was observed at resonance in the FHWA tests for reasons that are not readily determined. The resonant frequency appears to be slightly higher than that for the WES tests due to the lower mass moment of inertia of the cap.

Phase

The measured and computed phase angles for horizontal loading are shown in Figs. 7.29 (SPASM) and 7.30 (PILAY). All measured points shown are for a frequency of 2 Hz (very near resonance) or, in the case of the computed phase, the frequency indicated on the figures, at which computer runs were made. The measured phase is generally consistent with a Case 2 or 3 profile in PILAY/RIGDF.

KPILE

A limited number of runs were made on Program KPILE to simulate the response of the single laterally loaded pile. Unlike PILAY, KPILE models complete coupling of lateral soil response and so should theoretically produce pile displacements that are more nearly correct than does PILAY for this case of loading. The limited KPILE run results are summarized in Table 7.3.

PILE GROUP - HORIZONTAL EXCITATION

Force-Frequency

The force-frequency relationships for six test records analyzed are shown in Fig. 7.31. The sharp reduction in applied force near 7.5 Hz represents the characteristic force drop-off at system resonance.

Displacement Transfer Function Measurements vs. SPASM

Figures 7.32 through 7.36 present measured transfer functions and predicted horizontal translations at the locations of AP1H (2 ft (0.61 m) above the base of the cap), 2 ft (0.61 m) below the soil surface (where no measurements were made), and 10 ft (3.05 m) below the soil surface in Piles 2, 8, and 9, respectively. Displacement responses from all four p-y sets described in Chapter 6 are shown. The normalizing force F_L = 1,000 lb (4.45 kN) is applied to the entire group, not to a pile within the group.

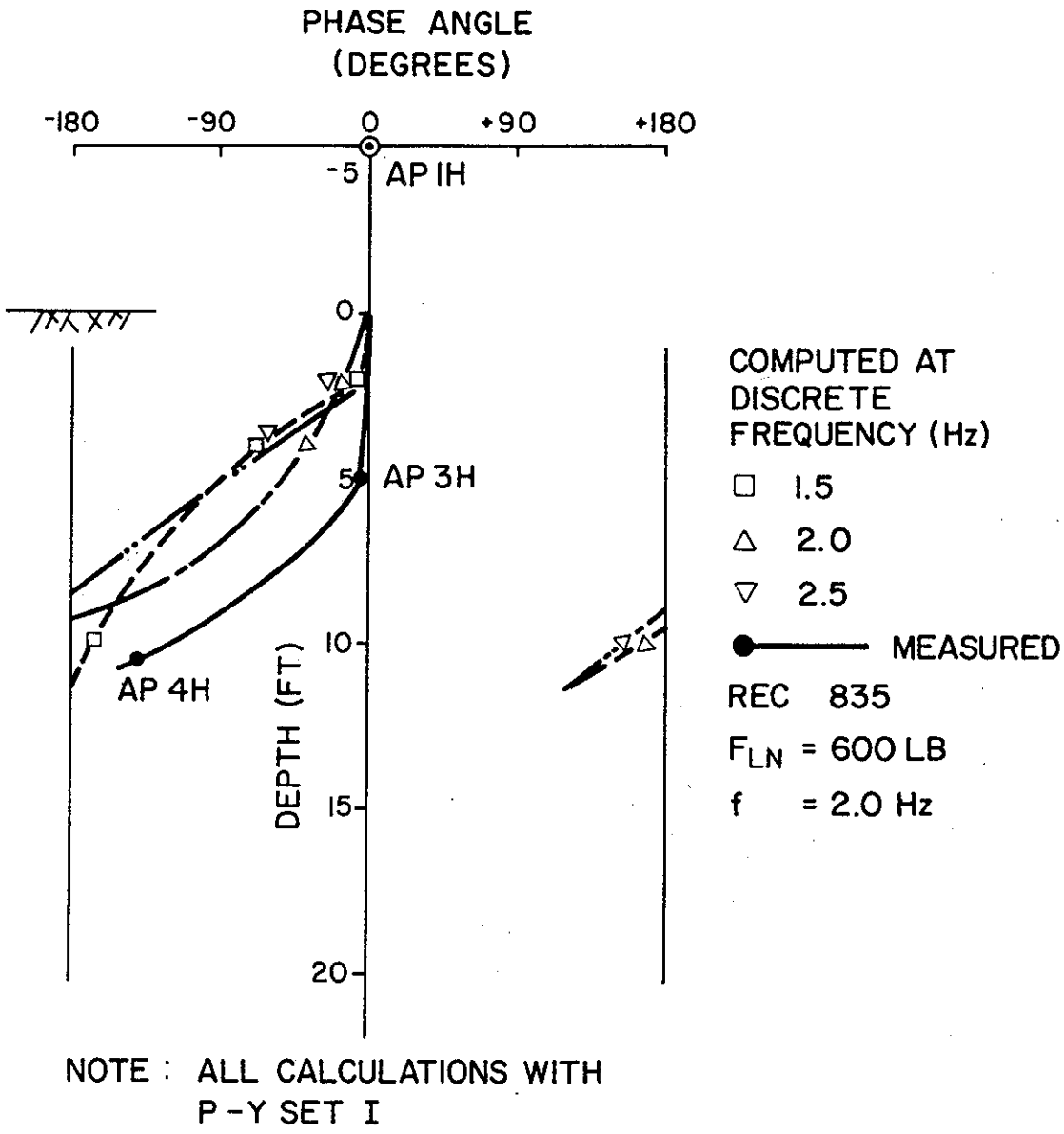

Fig. 7.29. Measured and Computed (SPASM) Phase: Single Pile, Horizontal Tests (1 ft = 0.305 m).

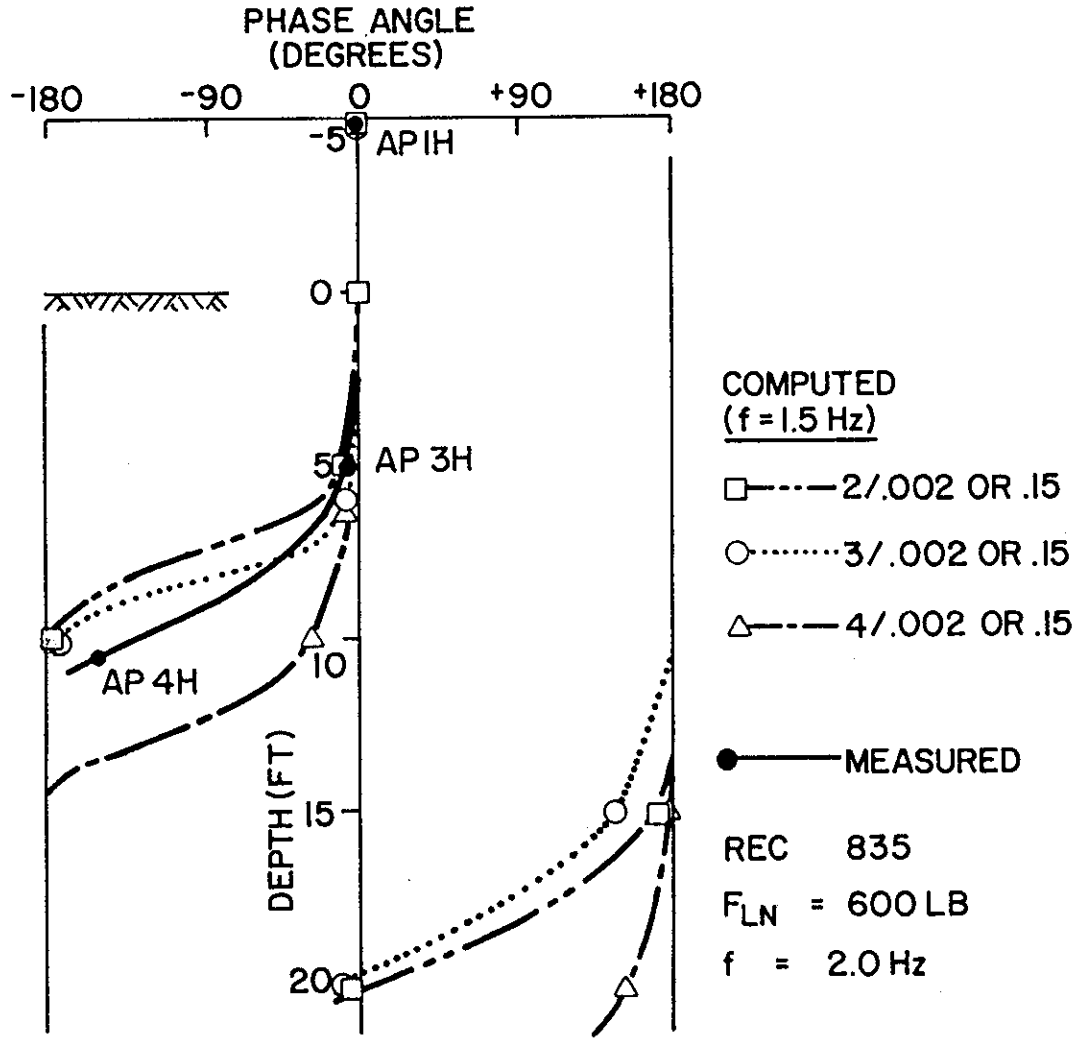

Fig. 7.30. Measured and Computed (PILAY/RIGDF) Phase: Single Pile, Horizontal Tests (1 ft = 0.305 m).

The measured resonant frequency varied from about 7.5 Hz at low force amplitude to about 7.0 Hz at a tenfold increase in nominal force amplitude, as indicated on Fig. 7.32. The same resonant frequencies are observed in Figs. 7.34 - 7.36, 10 ft (3.05 m) below grade. Some displacement amplitude variations can be detected among the 3 piles monitored at that depth, however. The highest resonant amplitude was in Pile 2 at the 4,000 lb and 8,000 lb (17.8 and 35.6 kN) nominal loads, where the amplitudes of the transfer functions are most reliable. Correspondingly, the lowest amplitude was in Pile 8. These data suggest a slightly greater flexibility in Pile 2 and a slightly lower flexibility in Pile 9, compared to Pile 8, the corner pile. This is the same ordering of flexibility that would occur under static loading.

Table 7.3. Comparison of Measurements with KPILE Results: Single Pile, Horizontal Tests (1 lb = 4.45 N; 1 in. = 25.4 mm)

Frequency (Hz)	Transfer Function: Load to Displacement at AP1H (in./100 lb)	
	MEASURED; REC. 835 (WES) F_{LN} = 600 lb	COMPUTED; KPILE
0	-	0.0134
0.50	0.021	0.0140
1.00	0.029	0.0164
1.25	0.039	0.0189
1.50	0.054	0.0232
1.75	0.063	0.0317
2.00	0.141	0.0537
2.25	0.185	0.1390
2.50	0.097	0.0602
2.75	0.045	0.0288
3.00	0.026	0.0182
3.50	0.013	0.0098
4.00	0.012	0.0064
5.00	0.010	0.0035

The spectra developed with SPASM by analyzing several discrete frequencies do not have points corresponding to resonance, but elsewhere they do not match the measured data well, although the modeled and pre-

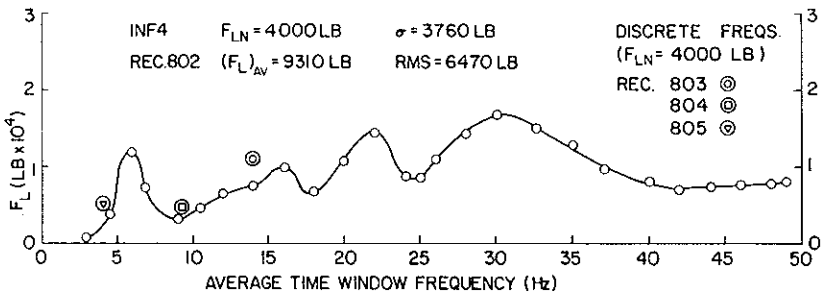

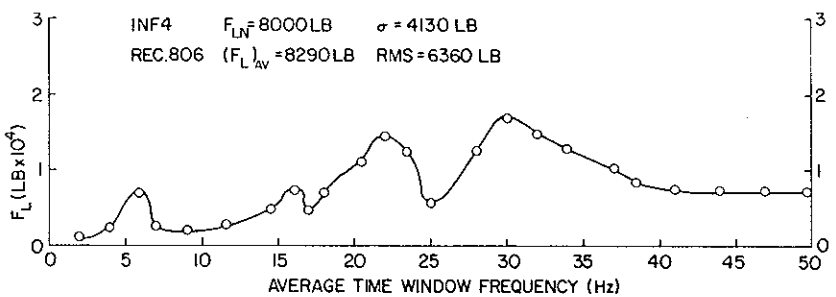

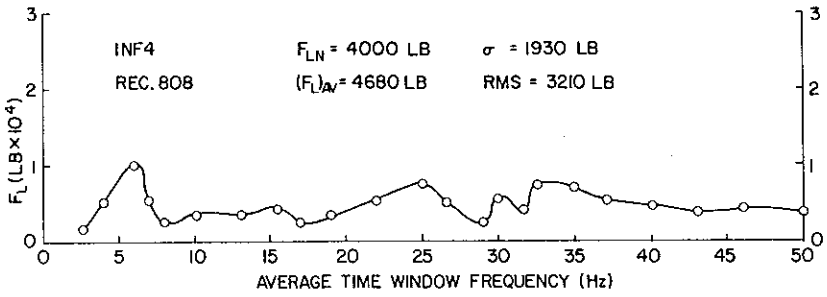

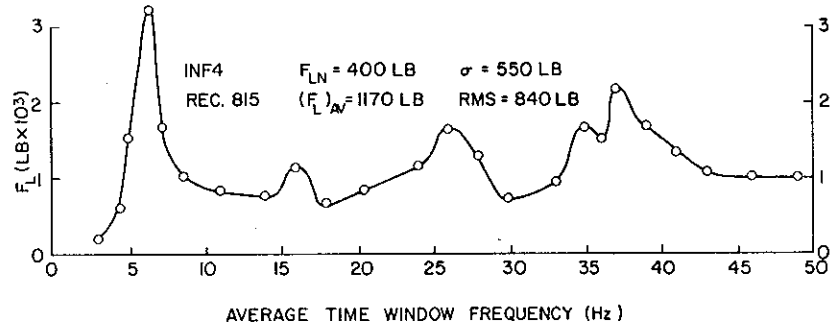

Fig. 7.31. Applied Force vs. Frequency: Group, Horizontal Tests (1 lb = 4.45 N).

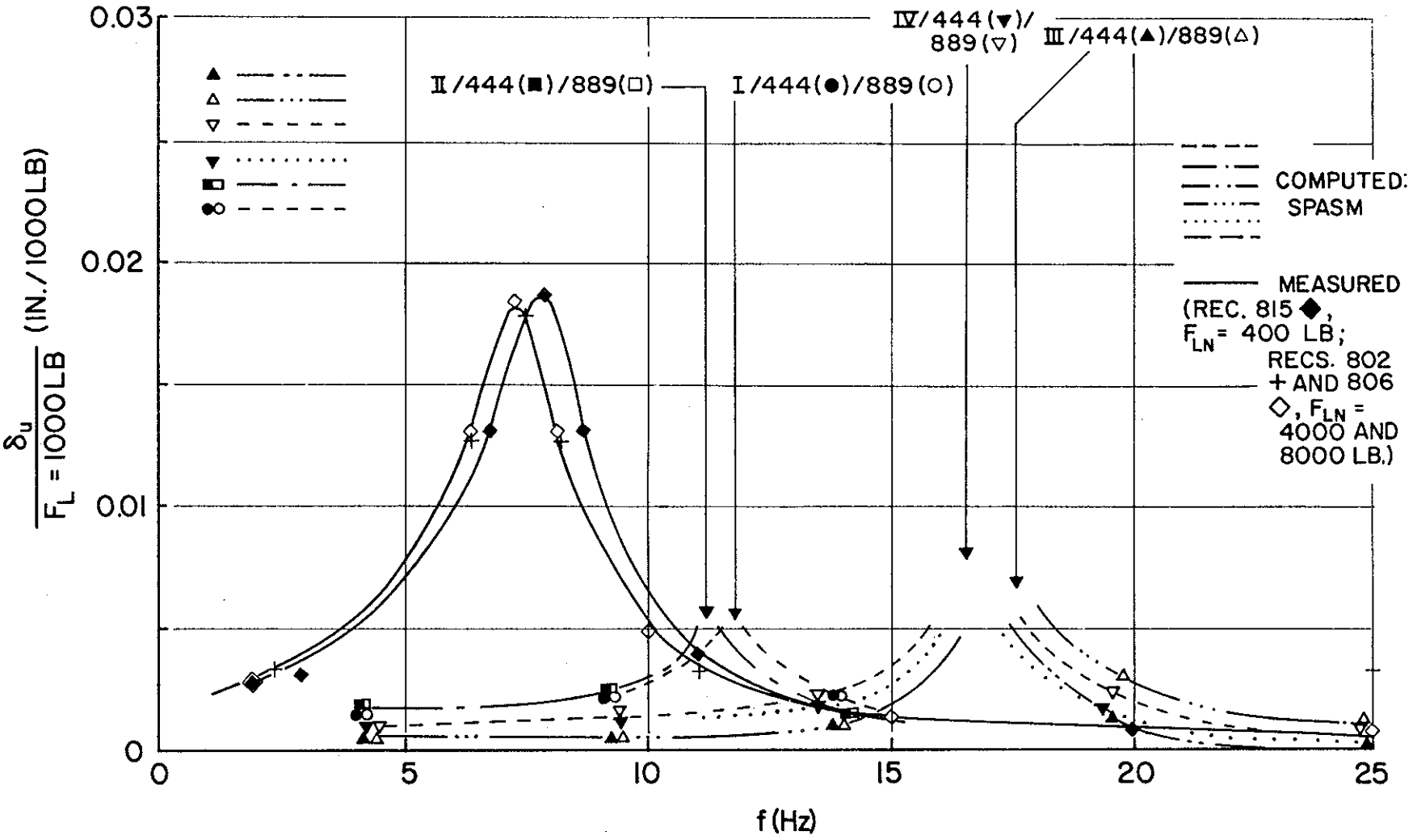

Fig. 7.32. Measured and Predicted (SPASM) Load-Displacement Transfer Functions 2 Ft (0.61 m) Above Cap Base: Group, Horizontal Tests (1 lb = 4.45 N; 1 in. = 25.4 mm).

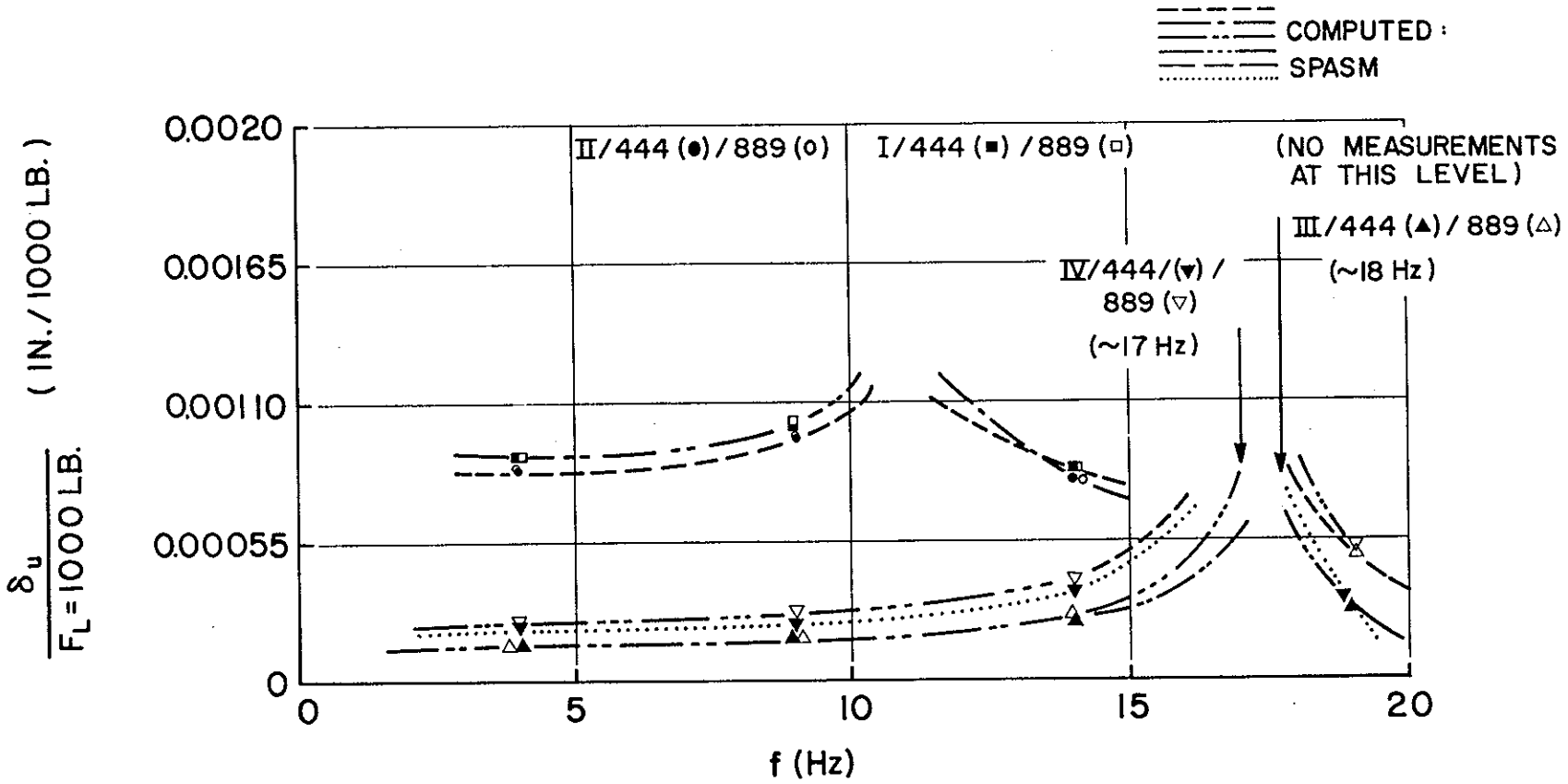

Fig. 7.33. Predicted (SPASM) Load-Displacement Transfer Functions 2 Ft (0.61 m) Below Ground Surface: Group, Horizontal Tests (1 lb = 4.45 N; 1 in. = 25.4 mm).

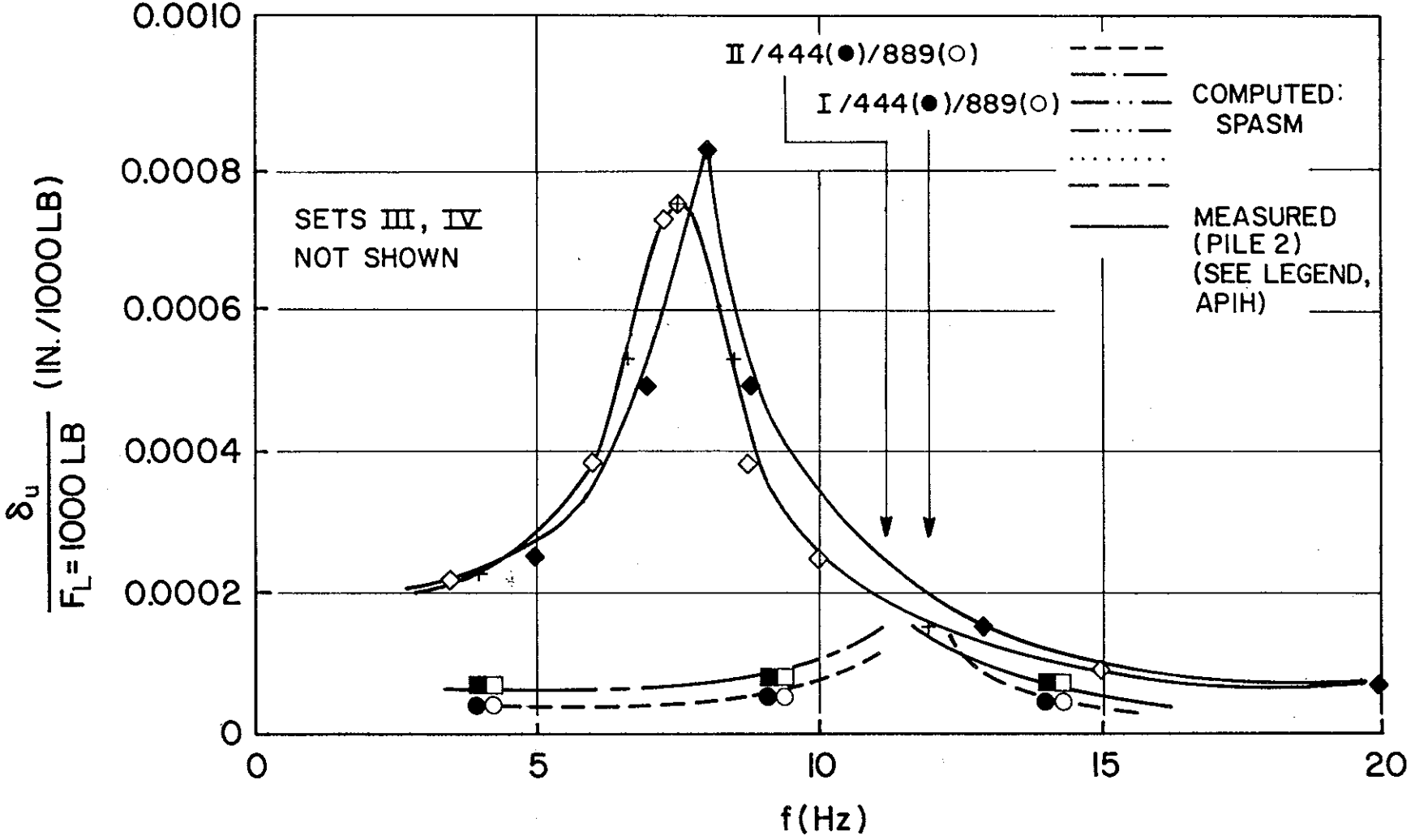

Fig. 7.34. Measured and Predicted (SPASM) Load-Displacement Transfer Functions 10 Ft (3.05 m) Below Ground Surface: Group Pile 2, Horizontal Tests (1 lb = 4.45 N; 1 in. = 25.4 mm).

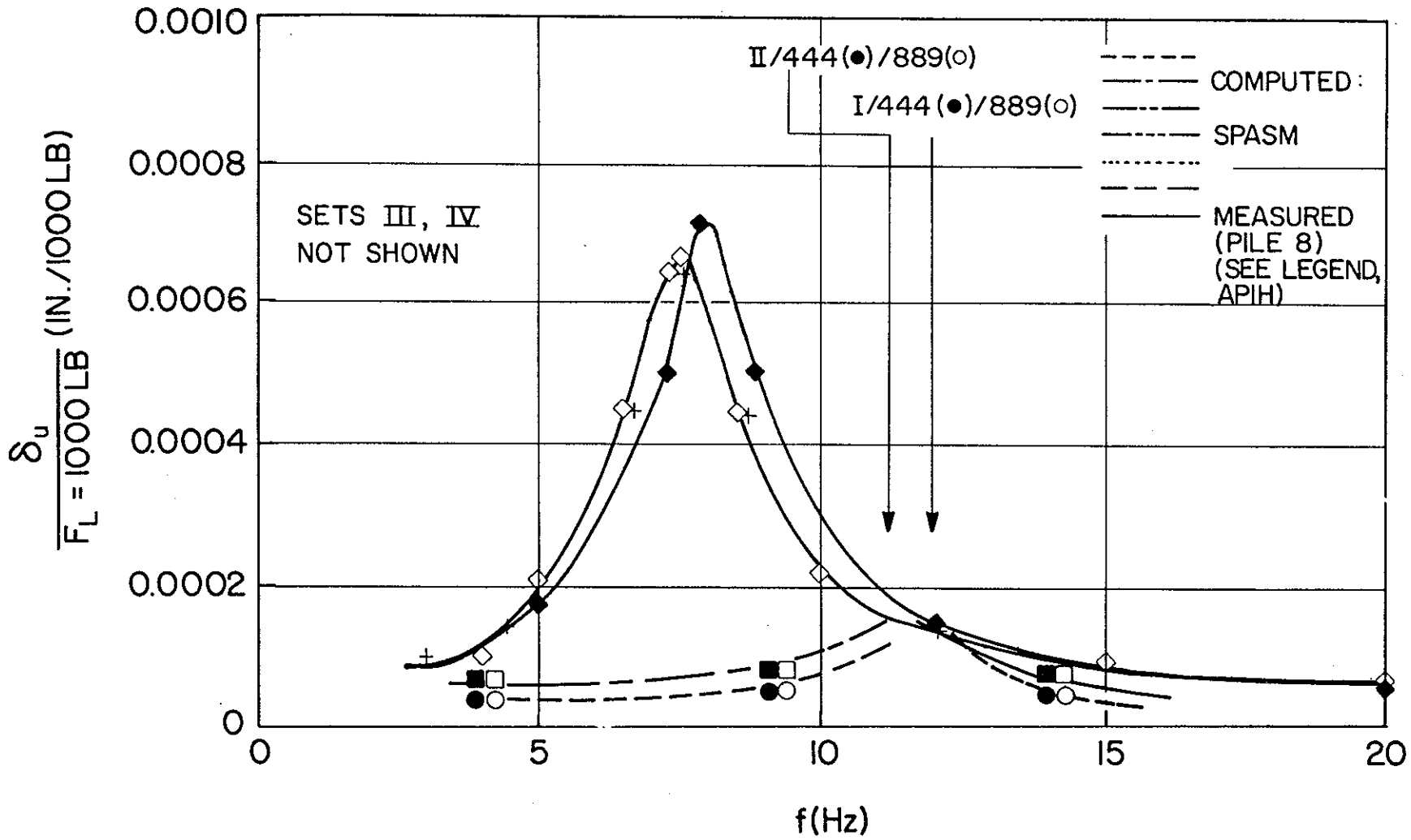

Fig. 7.35. Measured and Predicted (SPASM) Load-Displacement Transfer Functions 10 Ft (3.05 m) Below Ground Surface: Group Pile 8, Horizontal Tests (1 lb = 4.45 N; 1 in. = 25.4 mm).

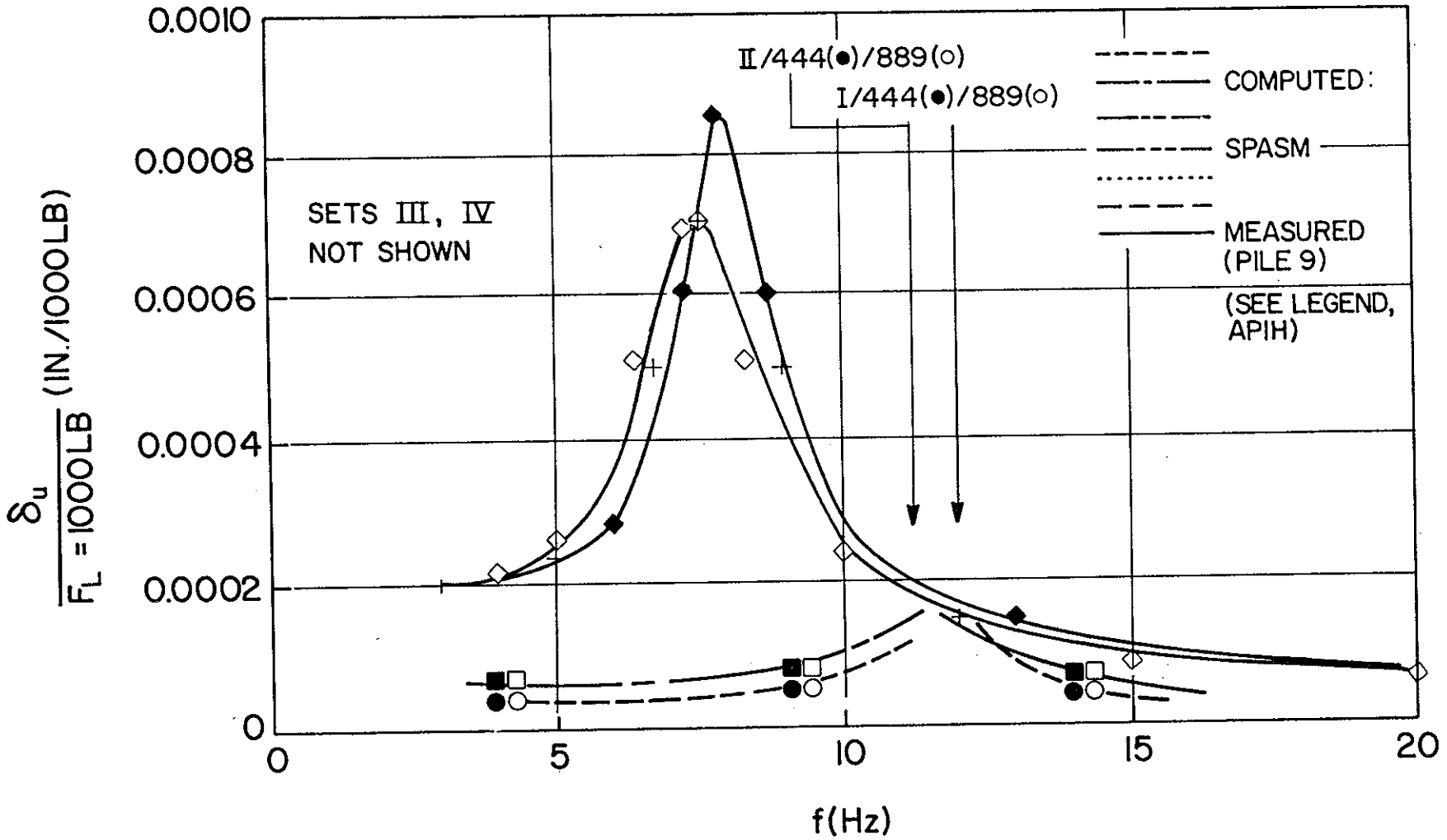

Fig. 7.36. Measured and Predicted (SPASM) Load-Displacement Transfer Functions 10 Ft (3.05 m) Below Ground Surface: Group Pile 9, Horizontal Tests (1 lb = 4.45 N; 1 in. = 25.4 mm).

dicted behavior tend to agree more closely at frequencies far away from resonance at all depth levels. P-y Sets I (unmodified Matlock criterion) and II (Matlock criterion corrected for static group effect), yielded resonant frequencies of about 12 and 11 Hz, respectively, which were much closer to the measured values of 7.0-7.5 Hz than the Set III and IV curves (Kagawa-Kraft and modified Kagawa-Kraft). This observation is consistent with observations made for the single pile. The slightly closer prediction of resonant frequency with Set II does not support an argument for applying static group flexibility to compute displacements for reasons discussed subsequently.

The spectra predicted from Sets I and II suggest that SPASM modeled the pile too stiffly throughout the frequency range considered. This phenomenon is possibly due to the manner in which the representative group pile was assumed to be tied into the group cap, i.e., by using a rotational restraint at the pile head to simulate the restraint of the cap. It is probable that the rotational stiffness was too high, as the value assumed essentially produced a fixed-head condition.

A further source of error in the SPASM model is the prescription that none of the vibrator mass was effective in horizontal translation and that all of the mass was effective in pile head rotation; see Chapter 6. Had part of the vibrator mass been effective in translation a better match would have been achieved between the predictions and measurements, since the added mass would have lowered the resonant frequency and increased pile-head displacements. The prescription of added soil mass vibrating in phase with the pile, particularly near the ground surface, would have a similar effect. Considerable parametric studies with SPASM would therefore need to be conducted before a definitive statement could be made on the desirabiltiy for providing softened p-y curves to model group action.

The normalized mode shape envelopes for Piles 2 and 8 are shown in Figs. 7.37 and 7.38, respectively, for two conditons: the mean of the sweeps reported in the preceding figures, and the mean of the three discrete frequency records referenced on Fig. 7.31. These mode shape envelopes do not indicate phase. The comparisons in Figs. 7.37 and 7.38 suggest that generally good predictions of relative displacements can be made with the SPASM algorithm. The discrete frequency (steady state) vibrations also generally produced slightly higher pile deflections

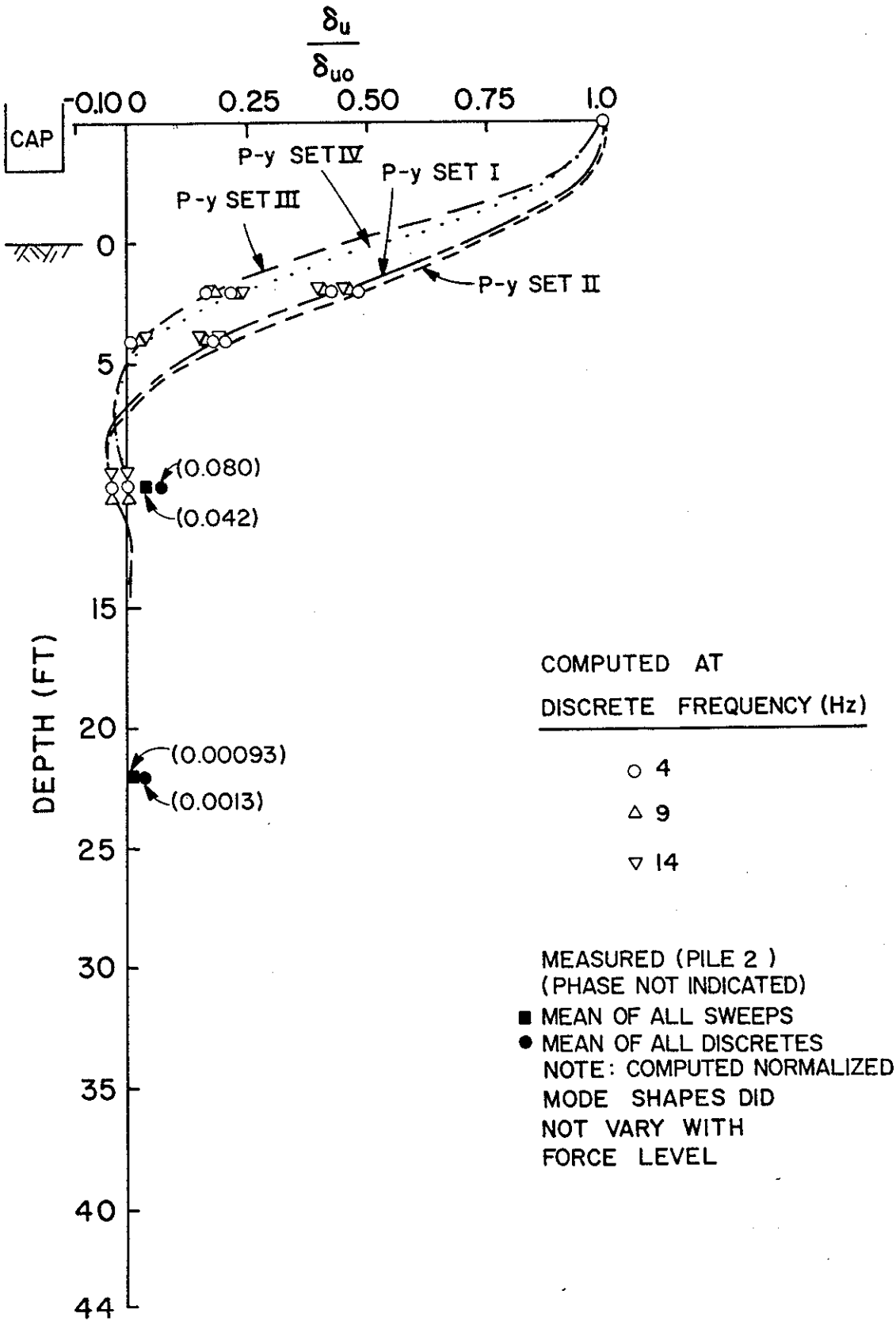

Fig. 7.37. Normalized Displacement Mode Shapes (SPASM): Group Pile 2, Horizontal Tests (1 ft = 0.305 m).

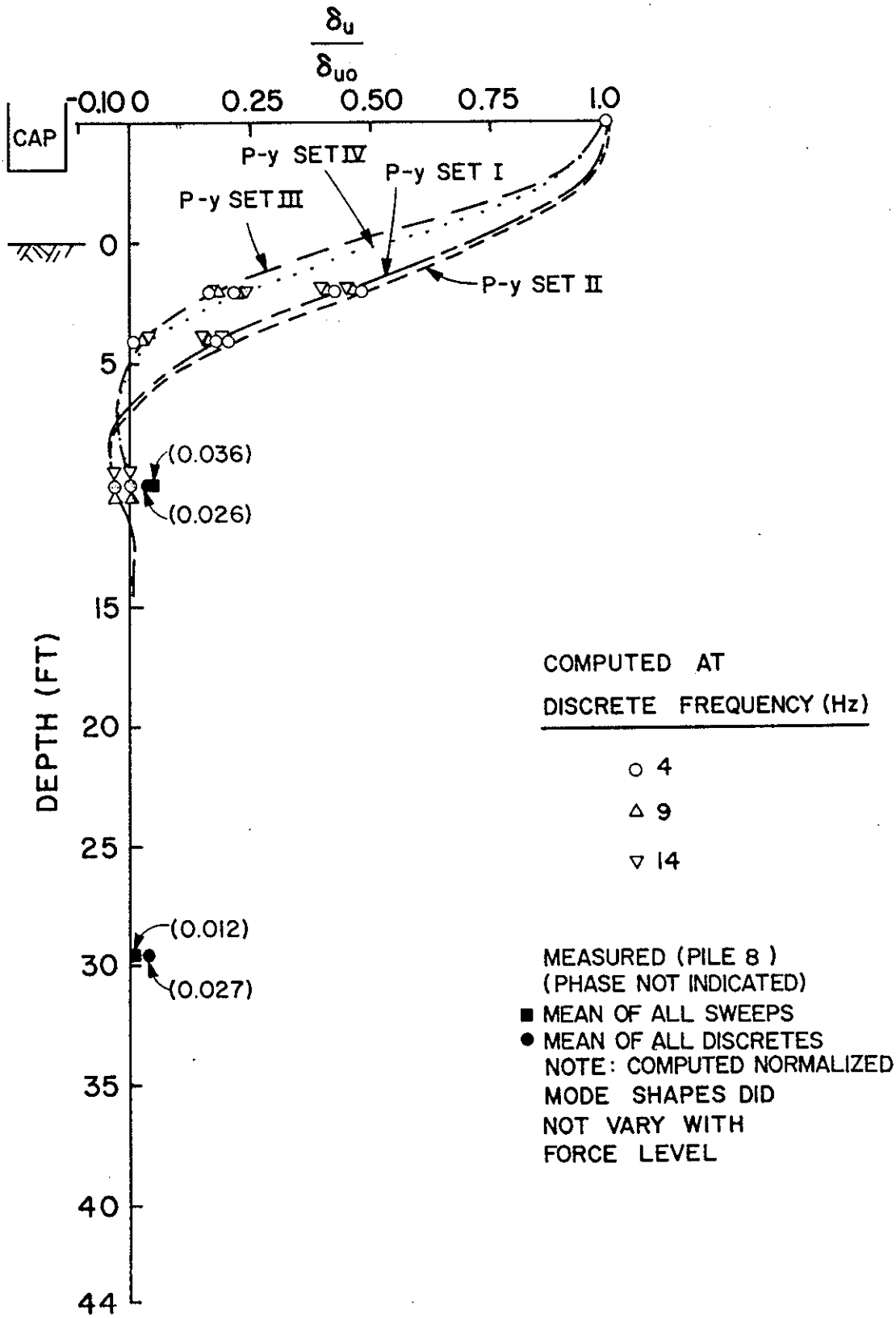

Fig. 7.38. Normalized Displacement Mode Shapes (SPASM): Group Pile 8, Horizontal Tests (1 ft = 0.305 m).

below the soil surface, although slightly greater deflections were produced in the sweeps in Pile 8 at the 10 ft (3.05 m) depth.

Displacement Transfer Function Measurements vs. PILAY/RIGDF

Figure 7.39 compares several RIGDF outputs with the measured transfer functions for Records 802, 806 and 815 at the pile cap (AP1H). Soil Case 3 with 15% hysteretic damping and with no added arbitrary softening for group action agrees well with the results of Records 802 and 806. Figure 7.39 may be contrasted with Fig. 7.36, which shows the spectra computed from RIGDF for the single pile, where the sharp peaks indicate very little radiation damping. The flatter curves produced in Fig. 7.39 are the result of the "push-pull" contributions of the vertically loaded piles produced by rocking which overshadows the damping in horizontal pile-head translation and rotation modes. Unlike SPASM, PILAY/RIGDF considers the entire group structurally, resulting in better matches between measurements and predictions. (If SPASM had been coupled with a cap and a full 9-pile group head been modeled, instead of just one typical pile in the group, it may have also yielded better matches than those shown.)

In PILAY/RIGDF, Soil Case 3 (degraded modulus in top 10 ft (3.05 m), in-situ crosshole modulus below 10 ft (3.05 m)) gave the closest correlations for the group. This is contrasted with Fig. 7.26, for the single pile, in which Case 2 (modulus = 0.2 times in-situ crosshole modulus over the full depth of the pile) gave the best correlation. The reasons for this difference is not clear. It is obvious, however, that neither the in-situ crosshole modulus profile (Case 1) or a highly degraded profile (Case 4 or Case 5) is appropriate for analysis at the force levels produced in this study.

Figure 7.40 compares the mean measured normalized mode shapes (phase considered) for both sweep records for all three piles monitored with the PILAY predictions. Generally good agreement with Case 3 is evident, although the lack of data above 10 ft (3.05 m) precludes any determination of whether a better match may exist with another soil case input.

The PILAY computations for Fig. 7.40 were made at f = 10 Hz, which was not quite at the resonant frequency of the group, which is the

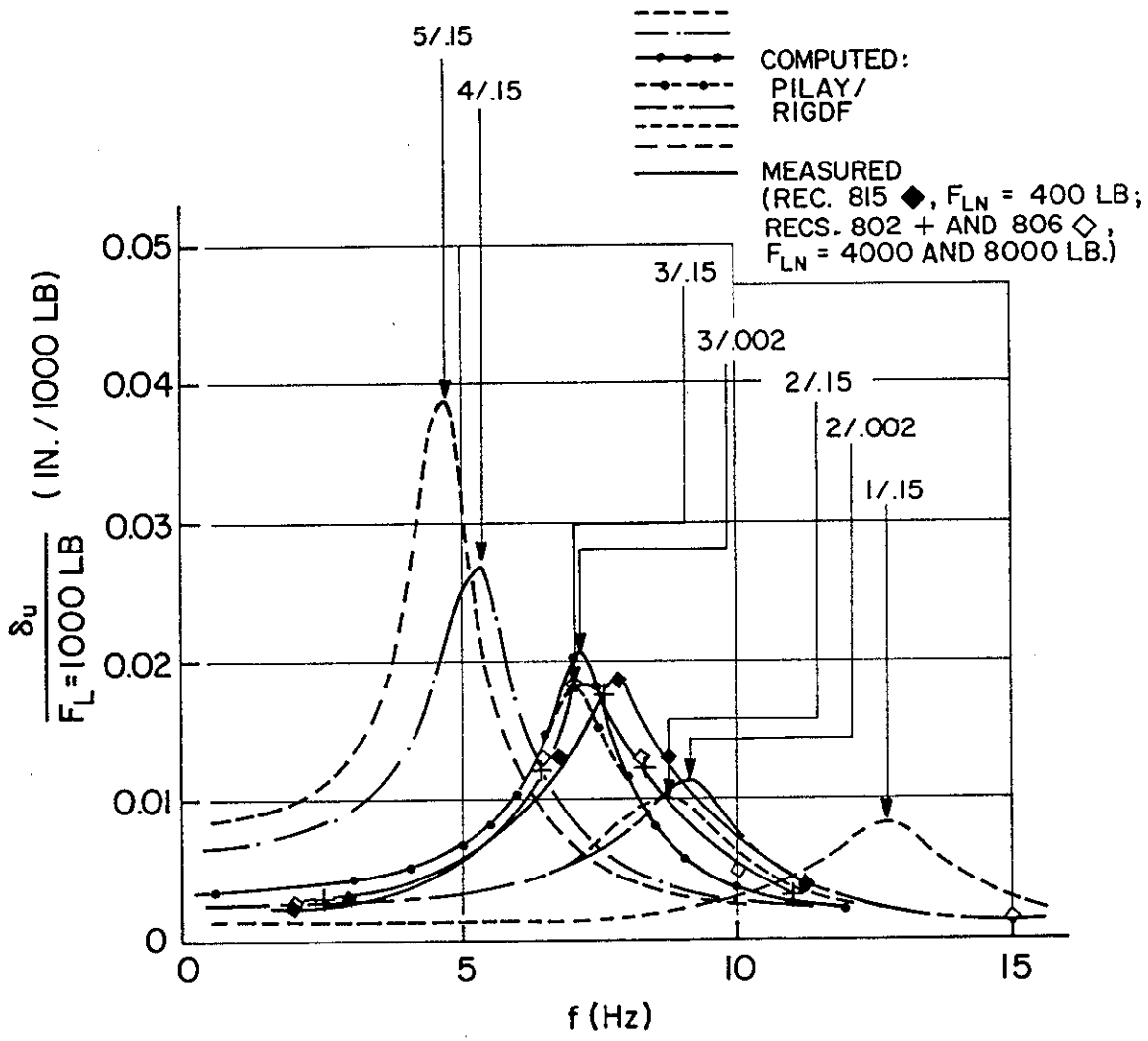

Fig. 7.39. Measured and Predicted (PILAY/RIGDF) Load-Displacement Transfer Functions 2 Ft (0.61 m) Above Cap Base: Group, Horizontal Tests, α = 1 (1 lb = 4.45 N; 1 in. = 25.4 mm).

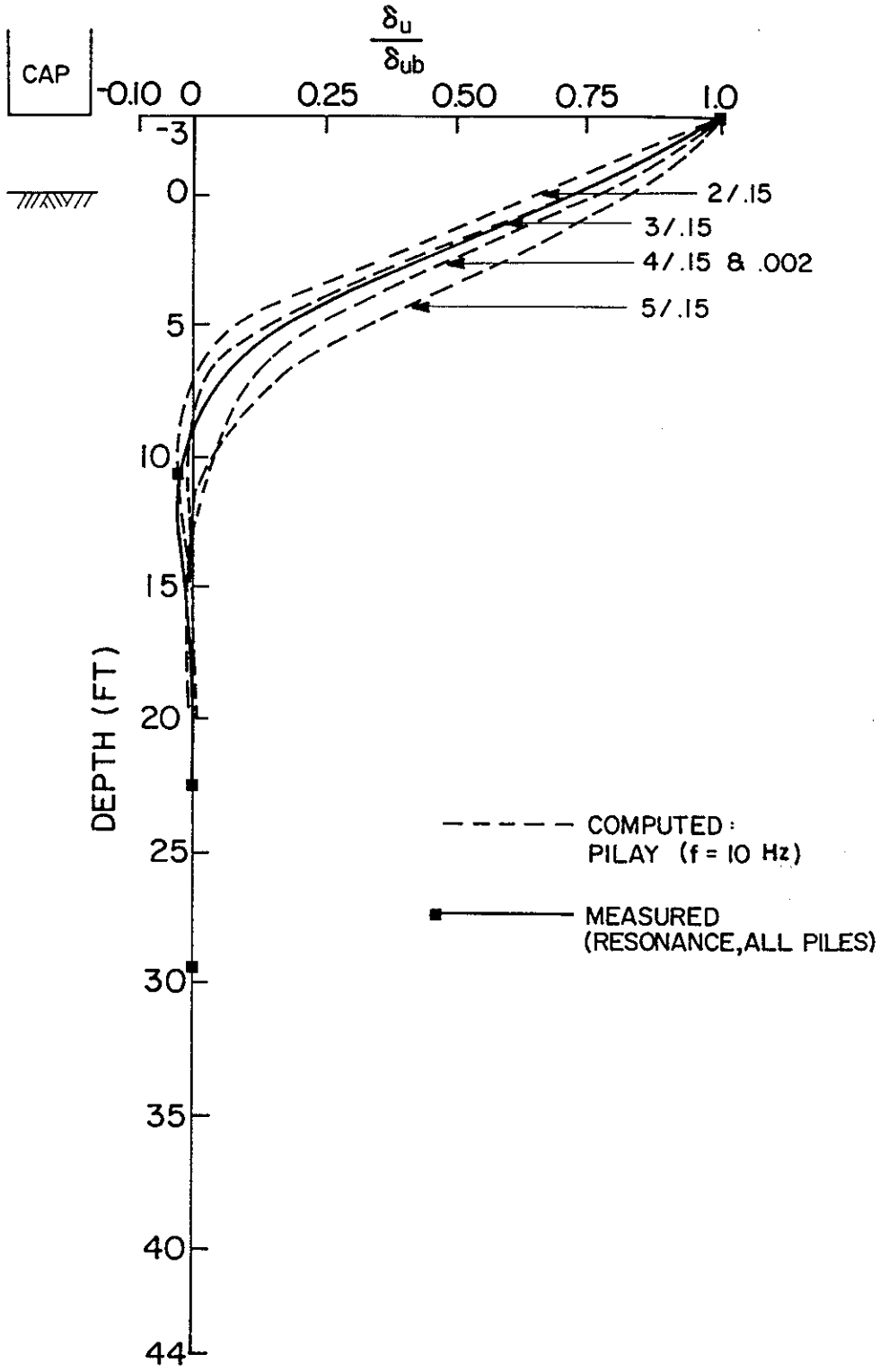

Fig. 7.40. Normalized Displacement Mode Shapes (PILAY/RIGDF): Group, Avg. of all Piles, Horizontal Tests (1 ft = 0.305 m).

frequency for which the measurements are shown. Figure 7.41 is provided to indicate the effect of frequency on normalized mode shape in the frequency range of 1.5 - 10 Hz for a relatively stiff case (Case 2) and for a very soft case (Case 5). Little difference can be observed, so that selection of exactly equal values of frequency for making the comparisons between measurements and predictions in Fig. 7.40 is unnecessary.

Figure 7.42 shows the results of the PILAY/RIGDF analyses considering a static group softening factor of 2.56 in terms of pile cap spectra. Here, Soil Case 1 provides the closest match with measurements (Record 815). Measured resonance is seen to be at a somewhat higher frequency than predicted by the stiffest reasonable soil case (Case 1, in-situ crosshole modulus profile). It is unlikely therefore that the static softening factor should be applied to compute displacements near resonance.

General Observations

For this horizontal group test reasonable predictions of displacement response were obtained with models that did not consider pile-soil-pile interaction, especially with PILAY/RIGDF. It should be noted that a_o (surface) at measured resonance for the cap-soil-pile system investigated was about 0.04. Significant group action, for example in the form of the first in-phase shear wave - vertical corner pile motion (the lowest frequency at which significant dynamic interaction is likely produced by rocking) does not occur at frequencies near measured resonance but does occur theoretically at about 33-34 Hz (a_o (surface) = 0.18). A secondary displacement peak was in fact observed at 23-30 Hz (a_o (surface) = 0.13-0.16) in the horizontal tests, as shown on Fig. 7.43. This peak is associated with rocking, possibly enhanced by wave interference of the type described.

DIFFERENCES IN DISCRETE FREQUENCY AND SWEEP RESULTS

Figures 7.44 - 7.47 compare pile cap displacement amplitudes for typical discrete frequency records to values obtained in the mean of the sweep records that were analyzed in detail. Negative ratios, as in the case of the horizontal group test, indicate that greater amplitudes were obtained at a given frequency in a frequency sweep test than in a

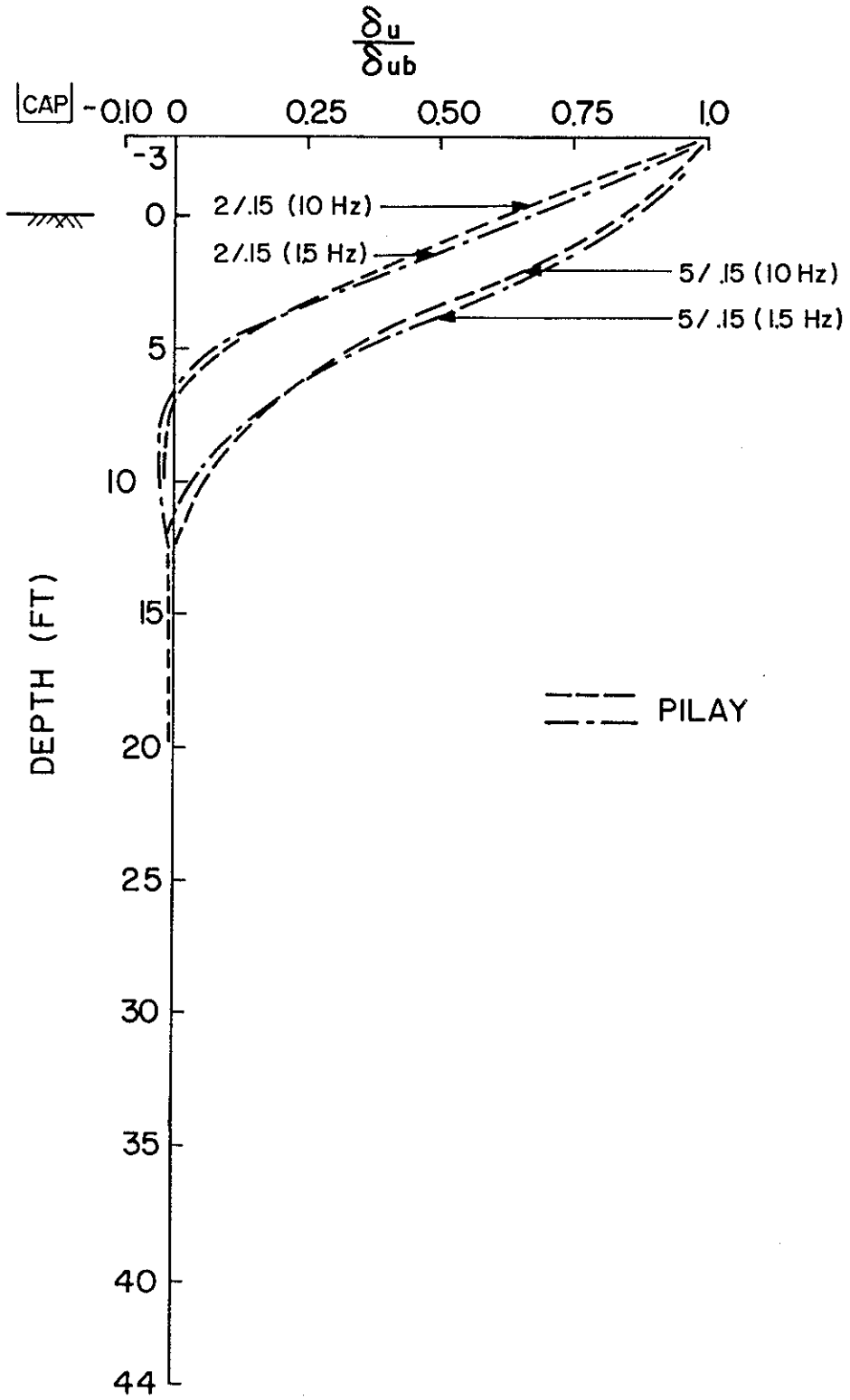

Fig. 7.41. Effect of Frequency on Normalized Displacement Mode Shapes (PILAY/RIGDF): Group, Horizontal Tests (1 ft = 0.305 m).

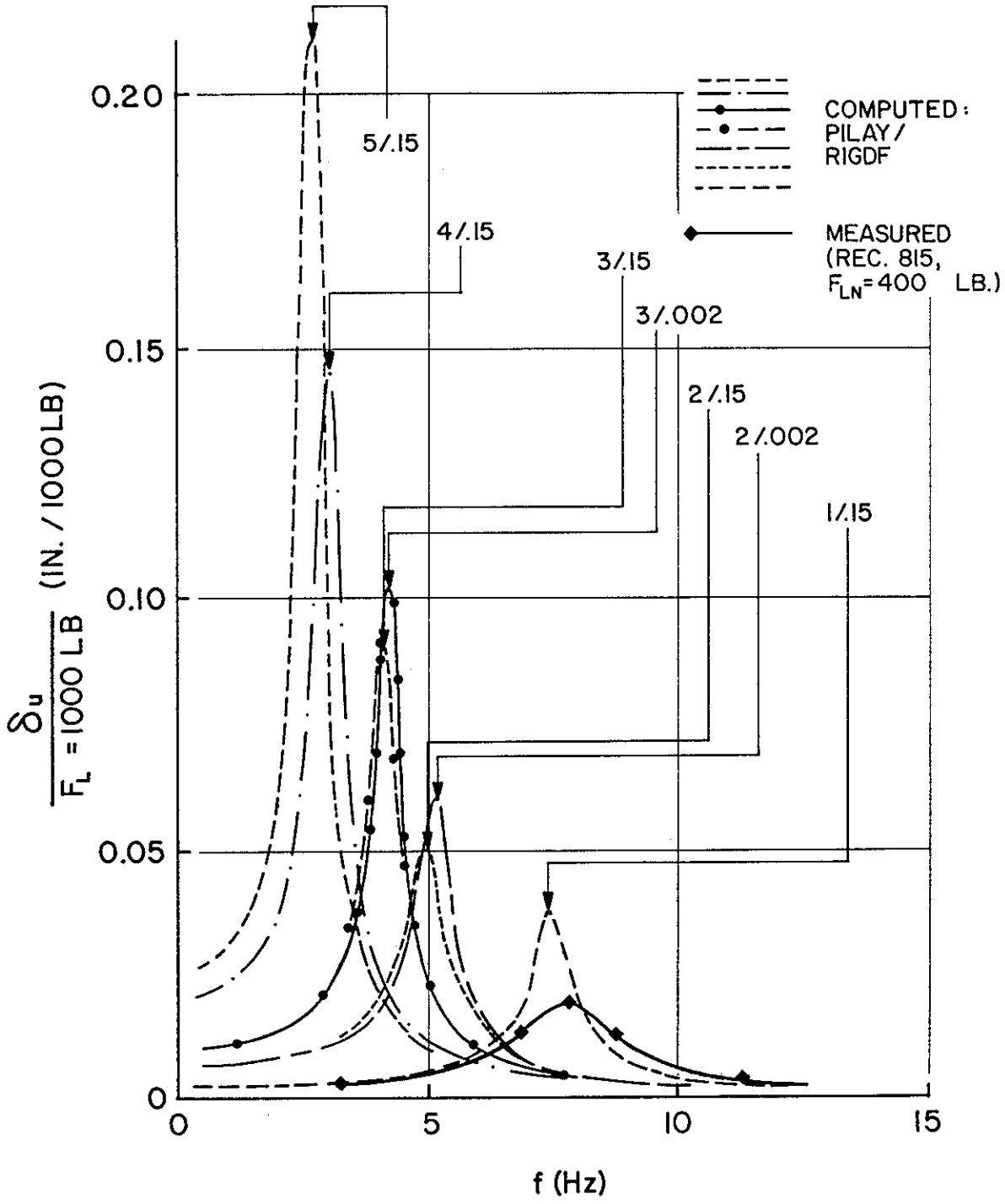

Fig. 7.42. Measured and Predicted (PILAY/RIGDF) Load-Displacement Transfer Functions 2 Ft (0.61 m) Above Cap Base: Group, Horizontal Tests, α = 2.56 (1 lb = 4.45 N; 1 in. = 25.4 mm).

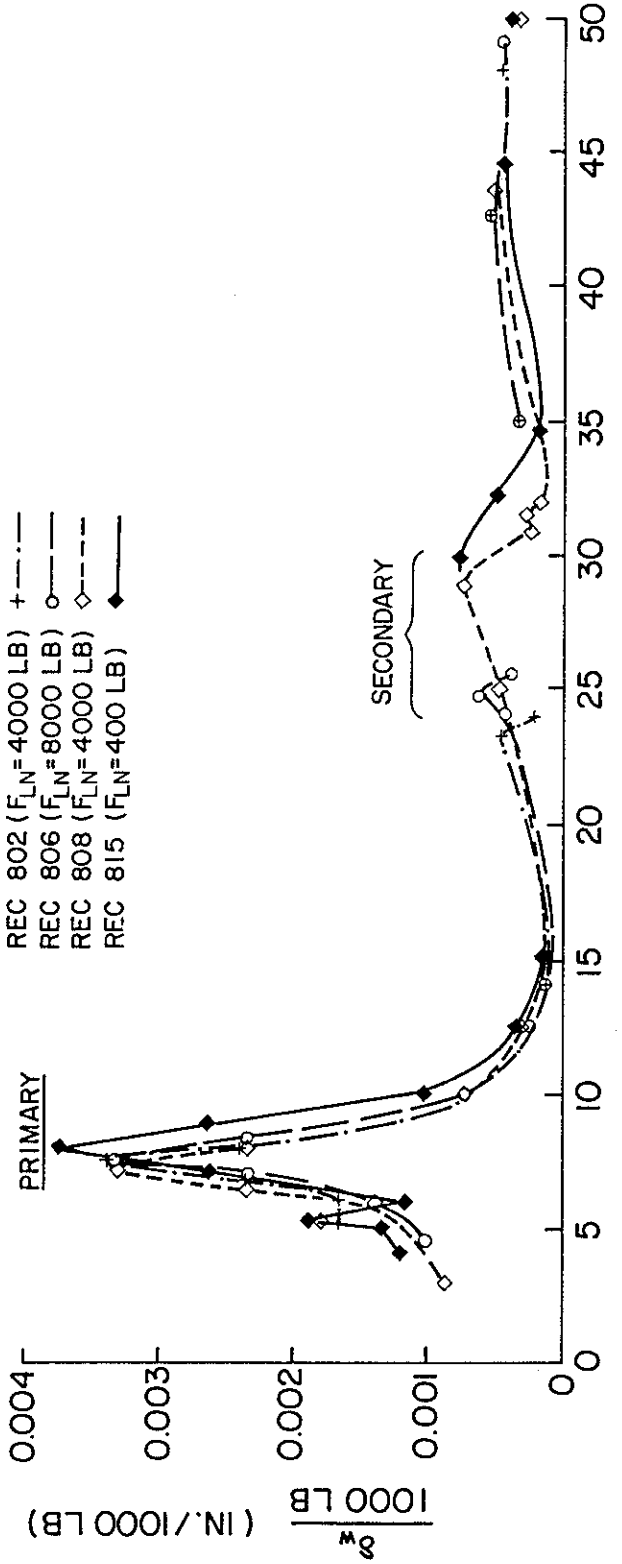

Fig. 7.43. Measured Wide-Band Transfer Functions: Group, Horizontal Tests (1 lb = 4.45 N; 1 in. = 25.4 mm).

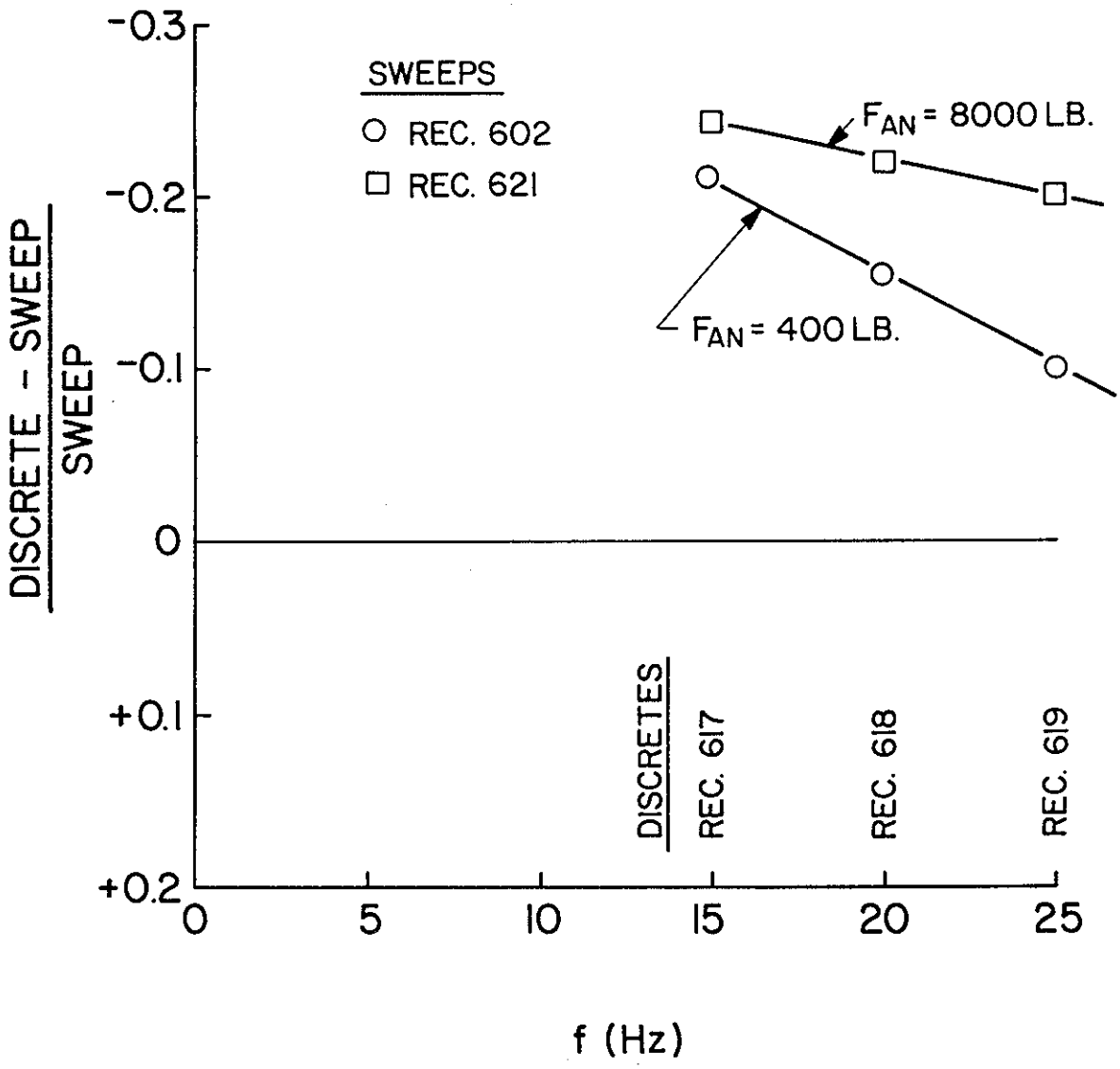

Fig. 7.44. Comparison of Cap Displacement Amplitude for Sweeps and Discrete Frequency Tests: Single Pile, Vertical Tests (1 lb = 4.45 N).

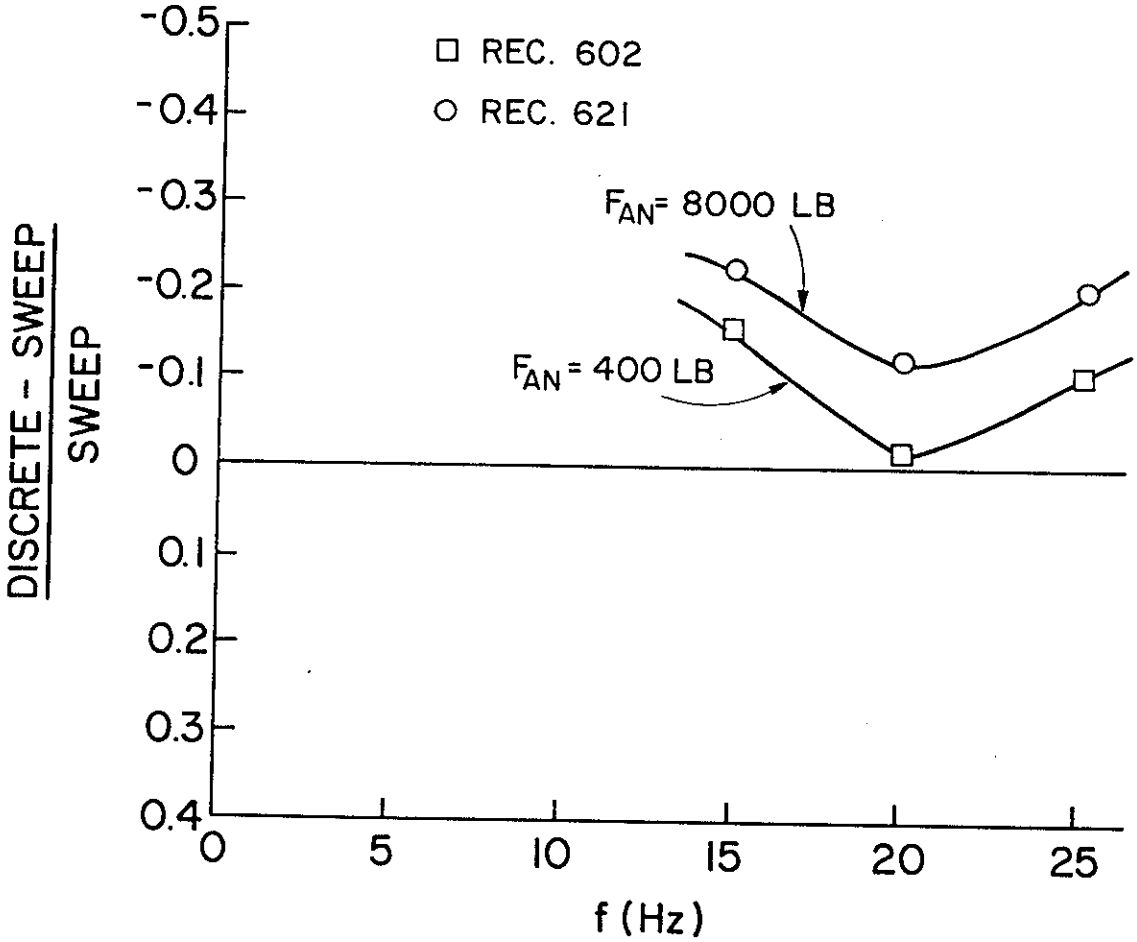

Fig. 7.45. Comparison of Cap Displacement Amplitude for Sweeps and Discrete Frequency Tests: Group, Vertical Tests (1 lb = 4.45 N).

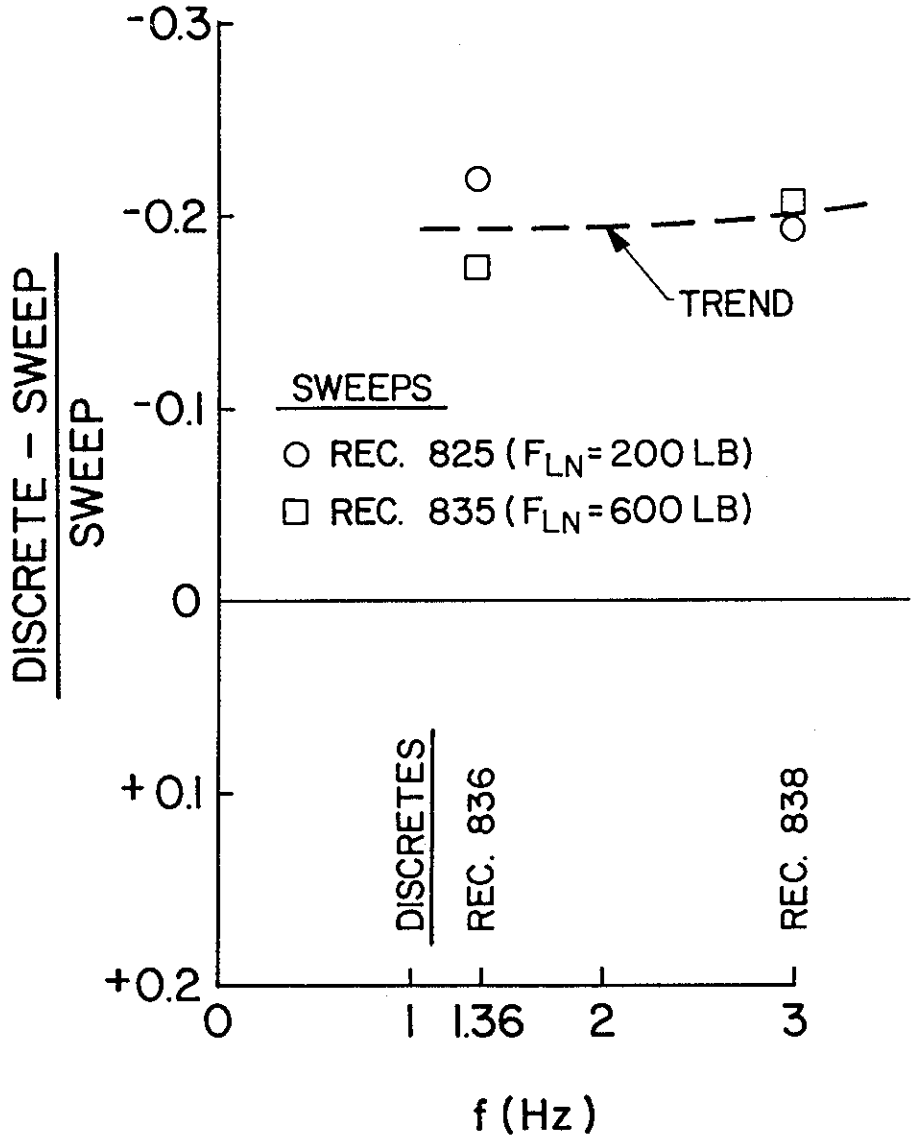

Fig. 7.46. Comparison of Displacement Amplitude 2 Ft (0.61 m) Above Cap Base for Sweeps and Discrete Frequency Tests: Single Pile, Horizontal Tests (1 lb = 4.45 N).

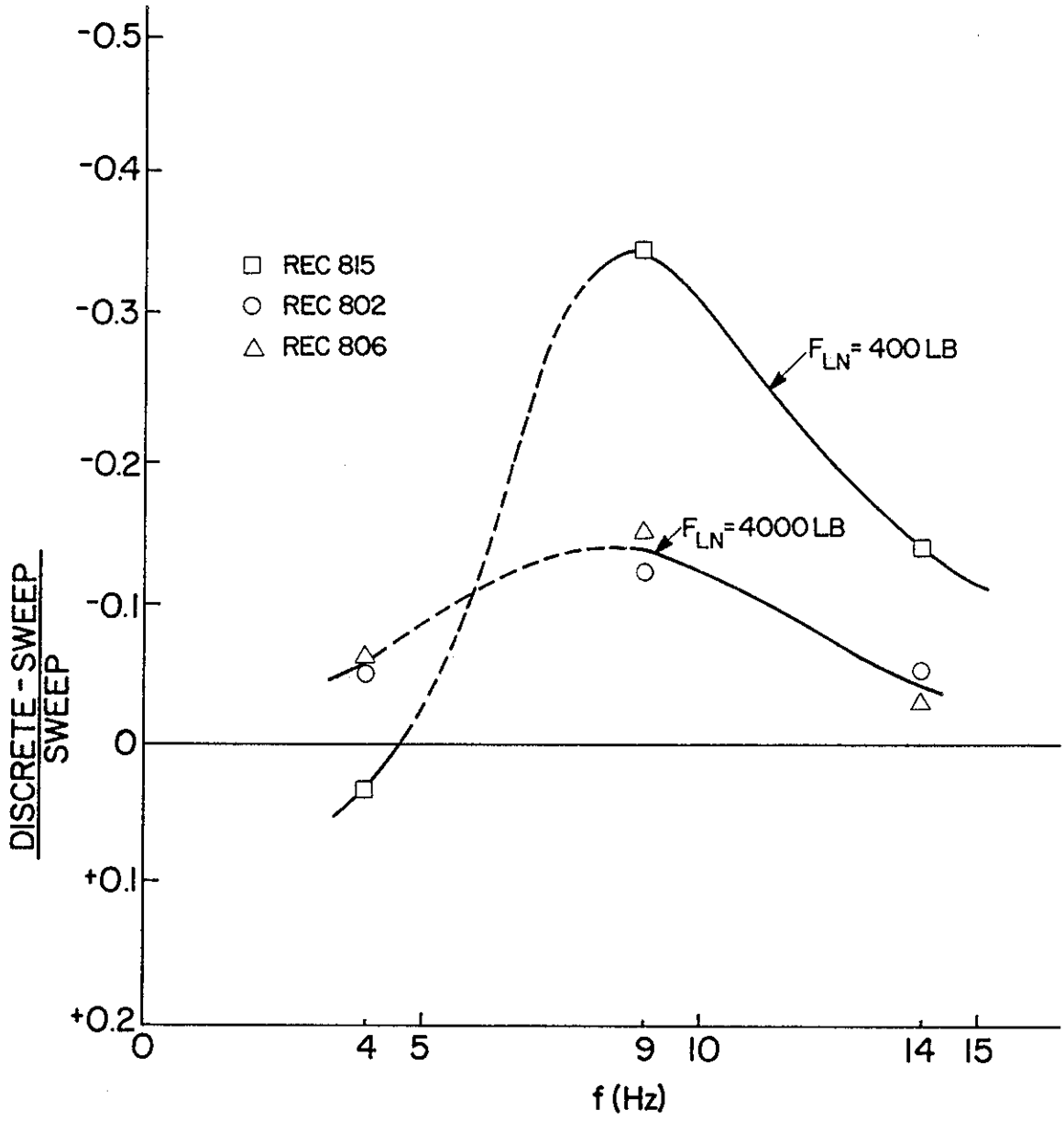

Fig. 7.47. Comparison of Displacement Amplitude 2 Ft (0.61 m) Above Cap Base for Sweeps and Discrete Frequency Tests: Group, Horizontal Tests (1 lb = 4.45 N).

discrete frequency test. In general the differences between the sweep and discrete frequency tests were small, especially at the higher values of nominal applied force (F_{AN} (axial) or F_{LN} (lateral)). This implies that the models that work well for the sweeps would also be appropriate for modeling steady state harmonic loading.

SOIL MOTION ATTENUATION

Figures 7.48 - 7.51 show the amplitudes of soil motion on the ground surface and at depth in the cased holes in selected directions along a line proceeding generally south from the single pile or pile group, as described in Chapter 5. These attenuation patterns, which correspond to resonant conditions in the pile or pile group, were not compared with patterns computed by any of the mathematical models used in this study. It is possible, however, to obtain soil displacements from the PILAY and KPILE algorithms, so that the measurements shown may be of use in further research.

The attenuation of peak soil surface displacement can generally be seen to be quite pronounced with increasing distance from the pile(s). For the vertical tests, the frequencies of ground motion associated with the peak displacements (given in parantheses on the figures) are essentially identical to the frequencies imposed on the piles very near the piles but tend to be altered by soil filtering phenomena at considerable distances from the piles. In the horizontal tests, however, frequency filtering is minimal, possibly because of the low frequencies of applied load that are associated with peak pile response. The patterns of attenuation are seen to vary rather considerably among the various major modes of loading.

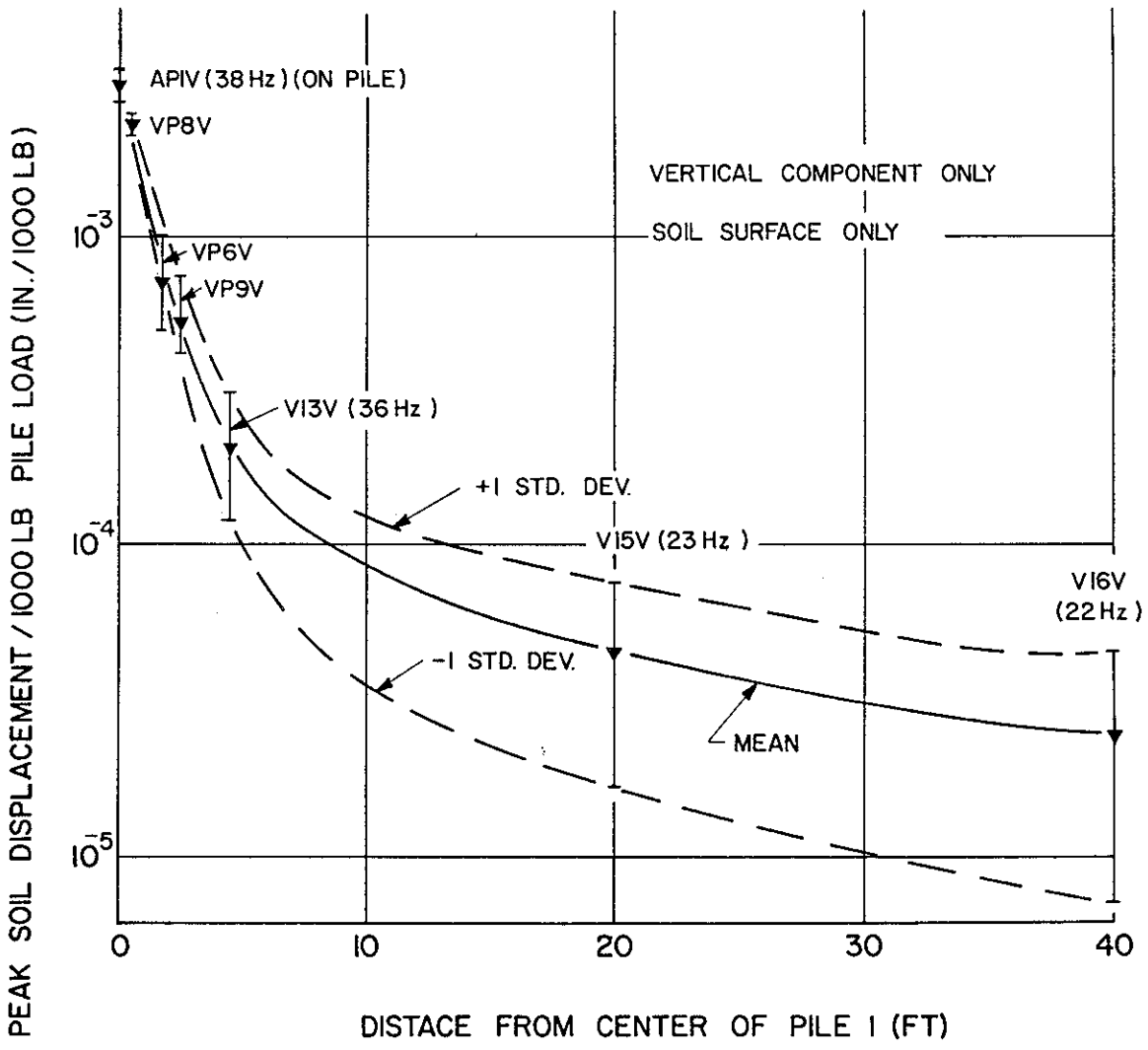

Fig. 7.48. Soil Displacement Attenuation: Single Pile, Vertical Tests (1 lb = 4.45 N; 1 in. = 25.4 mm; 1 ft = 0.305 m).

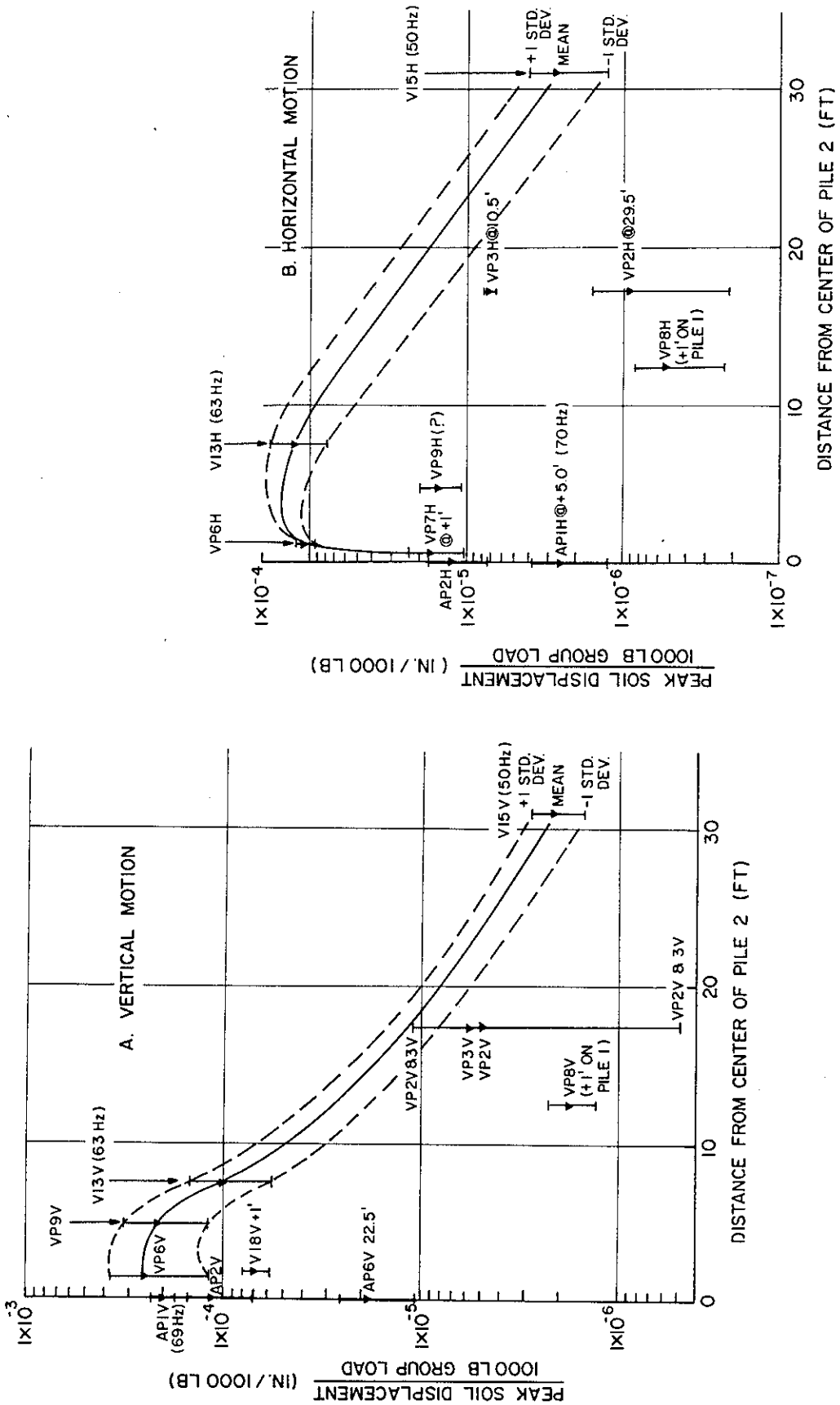

Fig. 7.49. Soil Displacement Attenuation: Group, Vertical Tests (1 lb = 4.45 N; 1 in. = 25.4 mm; 1 ft = 0.305 m).

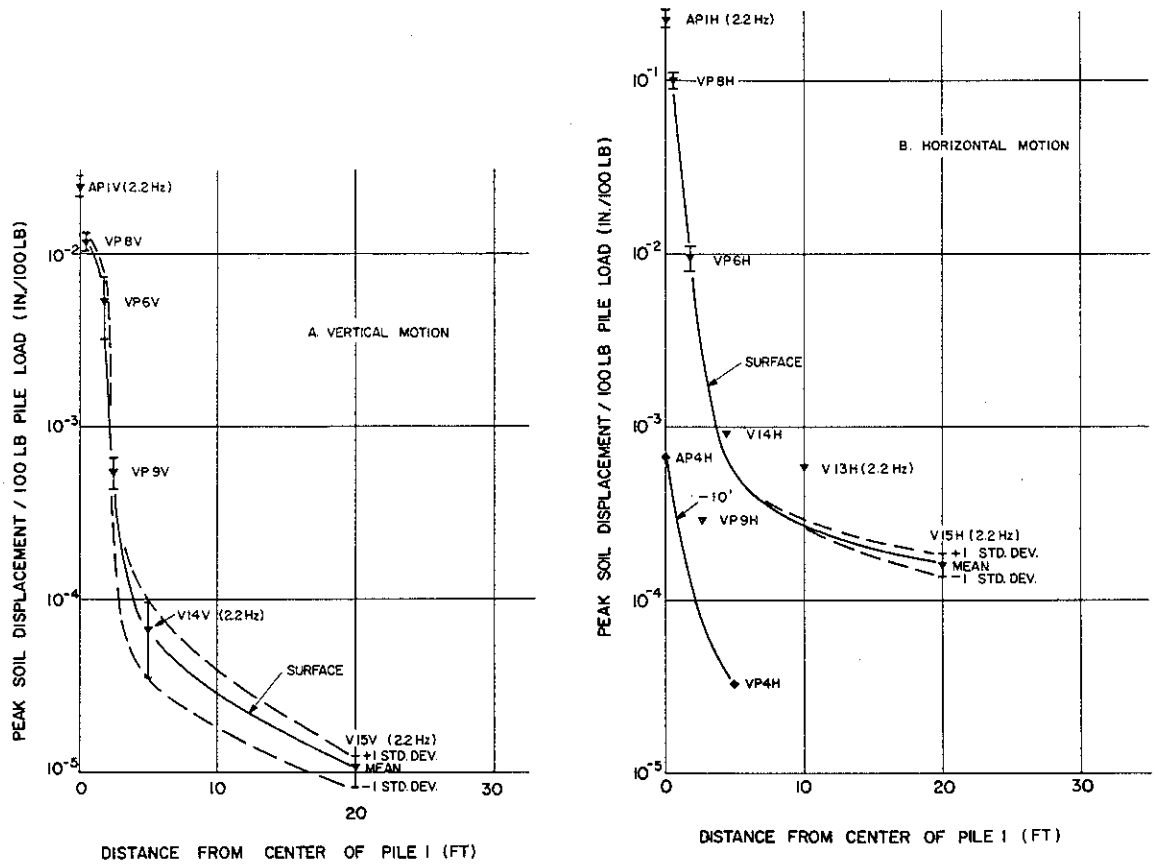

Fig. 7.50. Soil Displacement Attenuation: Single Pile, Horizontal Tests (1 lb = 4.45 N; 1 in. = 25.4 mm; 1 ft = 0.305 m).

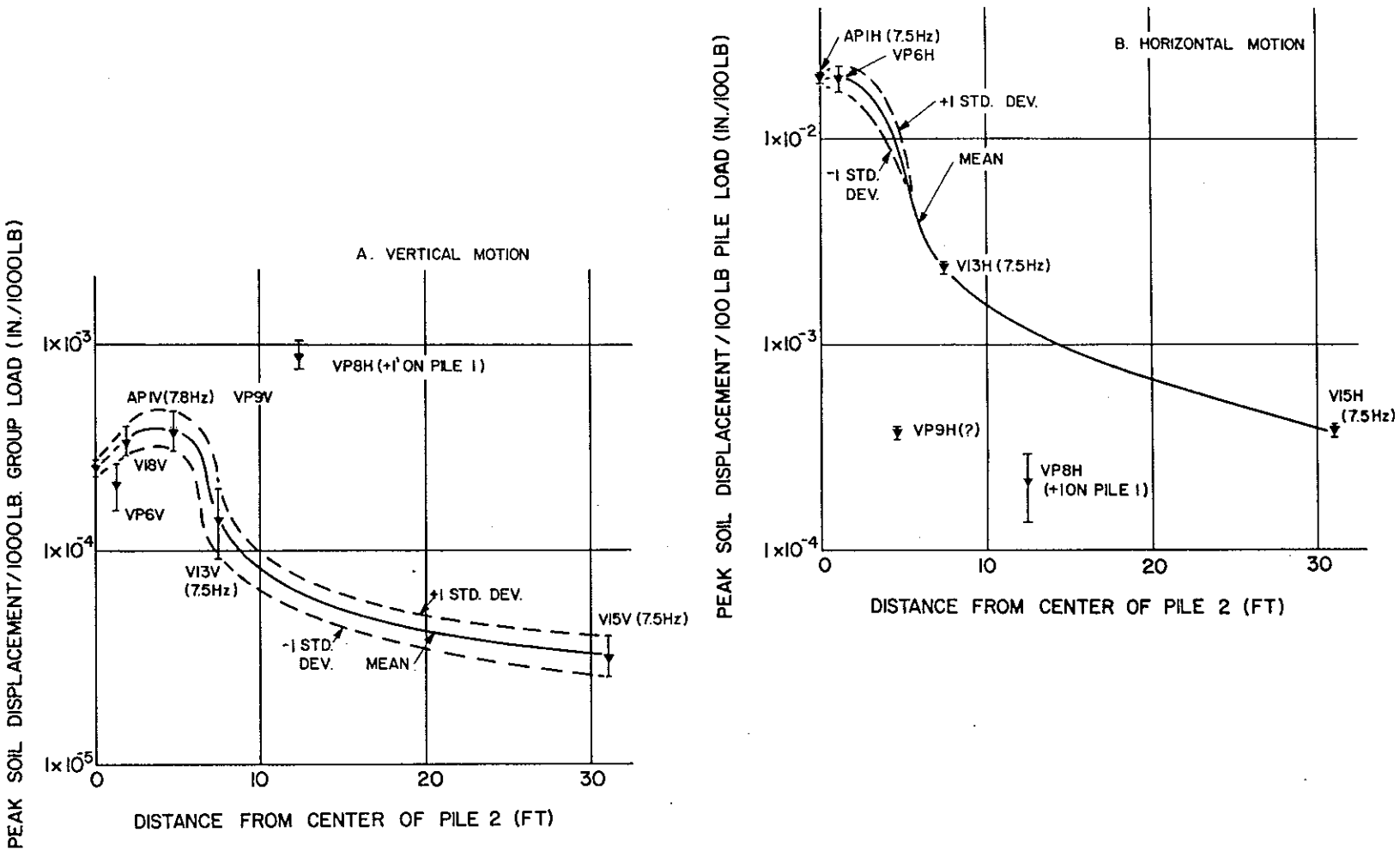

Fig. 7.51. Soil Displacement Attenuation: Group, Horizontal Tests (1 lb = 4.45 N; 1 in. = 25.4 mm; 1 ft = 0.305 m).

CHAPTER 8

CONCLUSIONS AND RECOMMENDATIONS

CONCLUSIONS

The following conclusions and observations are made for the study described in this report:

Experimental Data

1. The data that were obtained appear to be reliable, based upon observations of (a) high coherence between the forcing functions and individual instrument response, (b) reasonable relationships between the response of the various instruments, and (c) low frequency convergence to measured static flexibilities. Some transducers (such as AP3V) malfunctioned.

2. The seismic instrumentation used in the tests was somewhat difficult to interpret for the horizontal test of the single pile because the resonant condition for the system was near the rolloff frequencies of the instruments.

3. The instruments were geometrically positioned for optimum information recovery in the vertical tests. In the horizontal loading case, the down-pile accelerometers were apparently situated too far below the ground surface to permit accurate definition of mode shapes.

4. The primary high-force-amplitude vibrator produced nonuniform loads as the frequency varied in the sweeping mode used as the primary loading procedure. Better load control was obtained in the discrete frequency tests, however. Resonant frequencies could not be readily determined during the field operations with the seismic data acquisition equipment that was employed; therefore, most of the discrete frequency tests were not conducted at or adequately near resonance for use in the analyses. The consequences of this problem were (a) forces near resonance in the frequency sweeps were lower than programmed, such that the induced nonlinearities were less than had been planned, and (b) sophisticatd signal processing techniques had to be employed in order to develop usable processed data.

5. The effort required to process the data made it unfeasible to analyze more than a small percentage of the digital test records made. All test records are stored on magnetic tape and archived at the University of Houston. Chapter 6 and Appendix G describe procedures for processing the data so that further analyses may be undertaken at a later date.

Pile Response

1. Maximum relative pile-soil displacements achieved were approximately 0.02 in. (0.5 mm, or 0.2% of pile diameter) in the vertical mode and 0.10 in. (2.5 mm, or 1% of the pile diameter) in the horizontal mode. These displacements were sufficient to affect a degree of nonlinear response, as evidenced primarily by downshifts in the measured resonant frequencies. In the case of the laterally excited single pile, where nonlinearity is of most concern, pile displacements at the ground surface were about 0.1 in. (2.5 mm), which produced some observable gapping and resultant nonlinearity. However, the depth of the zone of significant lateral displacement was quite shallow (Fig. 7.25), so that the overall response of the pile-system was not highly nonlinear.

2. DRIVE was capable of predicting reasonably closely the resonant frequencies of the vertically loaded single pile where the static f-z curves, which had been measured in an earlier series of static load tests, were stiffened by dividing the static displacements by a factor of 4 (C/180, Fig. 7.2).

4. DRIVE predicted values of vertical displacement at resonance in the single pile that were slightly too large when the upper limit external damping value that was back-calculated from analysis of the driving record of the single pile (180 lb-sec/in./station) (31.5 N-sec/mm/station) was input. At frequencies not near resonance DRIVE predicted displacements that were too small. See Fig. 7.2. These observations indicate that, under quasi-harmonic loading, the radiation (external) damping value should have been somewhat higher than the upper limit assessed from pile driving, perhaps in the order of 250 lb-sec/in./station (44 N-sec/mm/station).

5. PILAY/RIGDF predicted the displacement response of the single pile under vertical loading well over a wide range of frequencies (Fig. 7.5) when "Profile 3" (Fig. 6.18) was used to characterize the soil

stiffness and hysteretic damping was prescribed to be 0.2%. The somewhat improved predictions of PILAY/RIGDF, as compared to DRIVE, suggested that accurate modeling of radiation damping (done analytically in PILAY) is more important than accurate modeling of hysteretic damping (done analytically in DRIVE) for loadings of the type and magnitude achieved here.

6. In both DRIVE and PILAY/RIGDF the measured force and displacement mode shapes for the single pile under vertical loading were predicted reasonably well with the same inputs that produced good matches in the measured and predicted pile-head response. This observation attests to the fundamental adequacy of both programs.

7. Vertical loading of the 9-pile group produced a near-flat response but with discernable peaks in the load-cap displacement transfer funciton at 10 Hz and 68 Hz. The former frequency is probably associated with rocking, while the latter frequency probably represents the lowest frequency of in-phase vertical motion between the corner piles and propagating shear waves produced by diagonally opposite corner piles. The near-flat response suggests that damping was near critical.

8. Neither DRIVE nor PILAY/RIGDF produced close matches with the measured vertical response of the group under vertical loading. The group responded more stiffly above 2 Hz than either a single pile or as predicted by static group action analogy (Eqs. (2-5) and (2-6)). Soil stiffness and damping could have been arbitrarily increased in both models to replicate the response in the neighborhood of the 68 Hz peak, but the rational extension of that increase to other groups cannot be established. It is concluded therefore that the single pile models are inadequate to model complex groups of piles in the vertical mode.

9. SPASM predicted the forced horizontal response of the single pile with reasonable accuracy at and below resonance (Fig. 7.24) when p-y curves were computed from the UU triaxial shear strength profile at the test site and when radiation damping associated with halfspace p-wave generation (Table 7.7) was input. The p-y curves computed from the finite element analyses of Kagawa and Kraft were somewhat too stiff, as evidenced by the prediction of a resonant frequency that was about 34% too high (Fig. 7.24).

10. PILAY/RIGDF predicted the horizontal motion of the single pile, but less precisely than did SPASM, when "Profile 2" (Fig. 6.18) was used. In particular PILAY/RIGDF underestimated damping, as indicated by the sharp displacement response peaks near resonance in Fig. 7.26. Pile displacements during dynamic load testing should not have produced hystertic damping in the soil in excess of about 15%, as evidenced by the measured hysteretic damping in the range of maximum lateral displacement (u) experienced by the soil (≈ 0.1 in, or 2.5 mm) in Fig. 3.12. Since, in Fig. 7.26, the prescription of hysteretic damping results in too little overall damping, it appears that PILAY, which is a plane strain radiation model, failed to model properly the dissipation of energy through radiational damping. Since most of the soil motion was near-surface (Fig. 7.50) and therefore probably did not occur under plane strain conditions, the discrepancies in PILAY/RIGDF are believed to be due its inability to model surface wave propagation.

11. KPILE predicted the response of the single pile reasonably well, although an extensive analysis of the KPILE solution were not made.

12. The 9-pile group behaved in a much more predictable manner under horizontal loading than under vertical loading. No evidence of in-phase motion between piles and body or surface waves in the soil was evident near system resonance, although such effects appear in rocking at a frequency of about four times the primary frequency (Fig. 7.43). "Dynamic group effects" in the case of horizontal loading were unimportant in this system because the cap (structure) mass and rotational and translational stiffnesses combined to produce a very low primary dimensionless resonant frequency (0.04). In pile group systems in the soil system tested that contain lighter structural masses, stiffer piles, more widely spaced piles, or piles with less freestanding length (factors that produce mass reduction or stiffness increase), dynamic group effects, such as observed for the vertically loaded group, may become significant.

13. SPASM predicted pile-head stiffnesses of the horizontally loaded group that were too high for all soil conditions tested, even when single pile p-y curves were input (Fig. 7.32). This phenomenon may

have been due to the provision of essentially a fixed-head restraint at the head of the single pile that is modeled by SPASM in order to model that pile as one in a rigidly capped group. Physically, some rotation of the cap did occur, thus "softening" the response.

14. PILAY/RIGDF produced good matches with the measured load to pile cap displacement transfer function for the horizontally loaded group when "Profile 3" (Fig. 6.18) was used to characterize the soil, but when static interaction (softening) factors were omitted.

Soil Response

1. No excess pore water pressures were detected in the soil or at the pile-soil interface during any of the tests using a slow-response static pore pressure measurement system.

2. Displacements in the soil attenuated with distance from the piles in an approximate "log displacement-linear distance" form, as indicated in Figs. 7.48 - 7.51, but the patterns were complex and varied with mode of loading. Frequency filtering occurred in the soil near resonance in the vertical tests, but not in the horizontal tests, where induced frequencies were very low in comparison with the vertical tests.

Computations

1. PILAY/RIGDF required the least computational and human effort. DRIVE and SPASM required much more effort, since they are time-domain solutions, and KPILE, which is a research-oriented program, required the greatest effort to execute on a per-run basis.

2. DRIVE and SPASM experienced problems with convergence at frequencies above system resonance for some combinations of input. These problems were believed to be due to the failure of initial transients to become sufficiently damped.

RECOMMENDATINS FOR FURTHER STUDY

Based on the lessons learned in this study the following recommendations for future work are given to further the understanding of dynamic pile behavior:

1. The tests conducted here should be repeated in other soils, most notably loose sands or sensitive clays, whose properties may change substantially under dynamic, pile head loading.

2. Higher amplitudes of load, relative to capacity, should be applied, especially near resonance, in future full-scale tests. This may require vibrations to be conducted at discrete frequencies rather than under sweep conditions. Field-type spectrum analyzers would be necessary in such tests to define resonant frequencies from preliminary sweep data.

3. Dynamic group action of the type described for the vertically loaded group should be studied more thoroughly experimentally, perhaps at a smaller scale than employed here, by conducting vertical and horizontal tests on a series of groups with variable pile spacings and very light pile cap masses.

4. The problem of pile response to soil loading should be studied to assess the possible uniqueness of the transfer functions between pile-head and soil response. Such a study should also include pile-head loading. It would provide useful insights into whether data of the type developed in this study could be applied to problems involving seismic loading.

5. In future horizontal tests more pile instrumentation should be provided near the soil surface than was used here. If seismic equipment is used to monitor pile and/or soil response, such equipment should have lower rolloff frequencies than the equipment used in this study.

6. Additional investigations should be made into the performance of DRIVE and SPASM at frequencies above system resonance for cases where the applied load is harmonic.

7. The p-y curves that were developed for input into SPASM are specific to the UU triaxial strength profile. It would be instructive to correlate those p-y curves with the static cone strength profile and also to the pressuremeter pressure-volume relationships.

ACKNOWLEDGMENTS

The authors are indebted to the following individuals and organizations for their assistance:

University of Houston Allied Geophysical Laboratories for use of their data acquisition truck and VAX 11/780 computer; Federal Highway Administration for use of the test piles and vibrators; Real Time Data Processing Laboratory of the Department of Electrical Engineering, University of Houston, for the use of the PDP 11/70 minicomputer used to make the PILAY/RIGDF runs; H-L Chen, L.J. Mahar, and Gary Chow for making the DRIVE and SPASM runs; Kenneth Stokoe, II, The University of Texas at Austin, for conducting the high-amplitude resonant column tests; Pileco, Inc., for restriking the piles; U.S.A.E. Waterways Experiment Station for providing their vibrator and advice on conducting the tests; University of Western Ontario (SACDA) for copies of PILAY and RIGDF; the Department of Civil Engineering of the University of Houston for providing the services of Roy Henson and Brad Gana, engineering technicians, and Mary DeCou, who painstakingly typed the text; and the several undergraduate students at the University of Houston who performed many of the routine calculations.

APPENDIX A - References

1. Alpan, I., "Dynamic Response of Pile Foundations to Lateral Forces," Proceedings, Fifth World Conference on Earthquake Engineering, Paper No. 229, Rome, Italy, June 1973.

2. Angelides, D.C., and J.M. Roesset, "Nonlinear Lateral Dynamic Stiffness of Piles," Journal of the Geotechnical Engineering Division, A.S.C.E., Vol. 107, No. GTII, Nov. 1981, pp. 1443-1460.

3. Arnold, P., R.G. Bea, I.M. Idriss, R.B. Riemer, K.E. Beebe, and P.W. Marshall, "A Study of Soil-Pile-Structure Systems in Severe Earthquakes," Proceedings, Ninth Offshore Technology Conference, Vol. I, 1977, pp. 189-202.

4. Arya, S., M.W. O'Neill, and G. Pincus, Design of Structures and Founations for Vibrating Machines, Gulf Publishing Company, Houston, 1979.

5. Baka, J., and K.H. Stokoe, II, "Dynamic Response in Vertical Motion of Small-Scale Piles in Sand," Report to the National Science Foundation, Aug. 1982.

6. Barkan, D.D., "Dynamics of Bases and Foundations, Translated from the Russian by G.P. Tschebotarioff, McGraw-Hill, New York, 1962.

7. Bea, R.G., "Dynamic Response of Piles in Offshore Platforms," Dynamic Response of Pile Foundations: Analytical Aspects, M.W. O'Neill and R. Dobry, Eds., A.S.C.E., Oct. 1980, pp. 80-109.

8. Bea, R.G., J.M.E. Audibert, and A.R. Dover, "Dynamic Response of Axially and Laterally Loaded Piles," Proceedings, Twelfth Offshore Technology Conference, Vol. II, 1980, pp. 129-139.

9. Bendat, J.S., and A.G. Piersol, Measurement and Analysis of Random Data, John Wiley and Sons, New York, 1966.

10. Beredugo, Y.O., and M. Novak, "Coupled Horizontal and Rocking Vibration of Embedded Footings," Canadian Geotechnical Journal, Vol. 9, 1972, pp. 477-497.

11. Berger, E., S.A. Mahin, and R. Pyke, "Simplified Method for Evaluating Soil-Pile-Structure Interaction Effects," Proceedings, Ninth Offshore Technology Conference, Vol. III, 1977, pp. 589-598.

12. Bingham, G., M.D. Godfrey, and J.W. Tukey, "Modern Techniques of Power Spectrum Estimation," Transactions on Audio and Electroacoustics, I.E.E.E., Vol. AU-15, June 1967, pp. 56-66.

13. Blaney, G.W., E. Kausel, and J.M. Roesset, "Dynamic Stiffness of Piles," Proceedings, Second International Conference in Geomechanics, Vol. II, A.S.C.E., 1976, pp. 1001-1012.

14. Boutwell, G.P. Jr., and D.S. Saxena, "Design Method: Dynamically Loaded Pile Foundations," Paper Presented Before A.S.C.E. Annual Meeting, Houston, Texas, Preprint No. 1833, Oct. 1972.

15. Chichy, W., E. Dembicki, and W. Odrobinski, "Analysis of Pile-Soil System Loaded By Horizontal Force, Cyclic or Dynamic," Soils Under Cyclic and Transient Loading, Ed. by G.N. Pande and O.C. Zienkiewicz, II, Balkema, Rotterdam, 1980, pp. 645-652.

16. Chon, C-S, "Dynamic Response of Friction Piles," Thesis submitted in partial fulfillment of the degree of Doctor of Philosophy, Department of Civil Engineering, University of Michigan, 1977.

17. Chung, K.Y.C., and R.D. Stoll, "Dynamic Pile Interaction," paper presented before A.S.C.E. Convention and Exposition, Portland, Oregon, Preprint No. 80-038, April 1980.

18. Cook, M.F., and J.K. Vandiver, "Measured and Predicted Dynamic Response of a Single Pile Platform to Random Wave Motion," Proceedings, Fourteenth Offshore Technology Conference, Vol. 2, 1982, pp. 637-646.

19. de Mello, C.E., "Dynamic Response of Foundations Under Rotating Machines on Piles," Soils Under Cyclic and Transient Loading, Ed. by G.N. Pande and O.C. Zienkiewicz, II, Balkema, Rotterdam, 1980, pp. 665-672.

20. Diaz, G.M., "Measured Response of Pile Supported Machines," Proceedings, Symposium on Deep Foundations, A.S.C.E., 1979, pp. 75-100.

21. Dobry, R., E. Vicente, M.J. O'Rouke, and J.M. Roesset, "Horizontal Stiffness and Damping of Single Piles," Journal of the Geotechnical Engineering Division, A.S.C.E., Vol. 108, No. GT3, March 1982, pp. 439-460.

22. Dodge, C.F., and W.F. Swiger, "Vibration Testing of Friction Piles," Engineering News-Record, May 13, 1948.

23. Ettouney, M.M., and J.S. Janover, "Dynamic Behavior of Battered Piles," Proceedings, Second International Conference on Numerical Methods in Offshore Piling, I.C.E., April 1982.

24. Flores-Berrones, R., and R.V. Whitman, "Seismic Response of End-Bearing Piles," Journal of the Geotechnical Engineering Division, A.S.C.E., Vol. 108, No. GT4, April 1982, pp. 554-569.

25. Foo, S.H.C., H. Matlock, and P.L. Meyer, "Analysis of Driving of Foundation Piles," Proceedings, Ninth Offshore Technology Conference, Vol. II, 1977, pp. 281-290.

26. Gaul, R.D., "Model Study of a Dynamically Laterally Loaded Pile," Journal of the Soil Mechanics and Foundations Division, A.S.C.E., Vol. 84, No. SM1, Feb. 1958.

27. Ghazzaly, O.I., S.T. Hwong, and M.W. O'Neill, "Approximate Analysis of a Pile Under Dynamic, Lateral Loading," Computers and Structures, Vol. 6, No. 4, 1976, pp. 363-368.

28. Ha, H.B., and M.W. O'Neill, "Field Study of Pile Group Action; Appendix A; PILGP1 Users' Guide," Report No. FHWA/RD-81/003, Federal Highway Administration, March 1981.

29. Hardin, B.O., and V.P.Drnevich, "Shear Modulus and Damping in Soils: Design Equations and Curves," Journal of the Soil Mechanics and Foundations Division, A.S.C.E., Vol. 98, No. SM7, July 1972, pp. 667-692.

30. Hwong, S.T., O.I. Ghazzaly, and M.W. O'Neill, "Pile Response to Dynamic Lateral Loading," Proceedings, Tenth Offshore Technology Conference, Vol. IV, 1978, pp. 2255-2259.

31. Isenhower, W.M., "Torsional Simple Shear/Resonant Column Properties of San Francisco Bay Mud," Thesis presented in partial fulfullment of the degree of Master of Science, Department of Civil Engineering, The University of Texas at Austin, 1979, 307 pp.

32. Kagawa, T., "Soil-Pile-Structure Interaction of Offshore Structures During an Earthquake," Proceedings, Twelfth Offshore Technology Conference, Vol. III, 1980, pp. 237-245.

33. Kagawa, T., and L.M. Kraft, Jr., "Seismic p-y Responses of Flexible Piles," Journal of the Geotechnical Engineering Division, A.S.C.E., Vol. 106, No. 658, Aug. 1980, pp. 899-918.

34. Kagawa, T., and L.M. Kraft, Jr., "Lateral Load-Deflection Relationships for Piles Subjected to Dynamic Loadings," Soils and Foundations, Japanese Soc. of Soil Mech. and Foundation Engineering, Vol. 20, No. 4, December 1980, pp. 19-36.

35. Kagawa, T., and L.M. Kraft, Jr., "Lateral Pile Response During Earthquakes," Journal of the Geotechnical Engineering Division, A.S.C.E., Vol. 107, No. GT12, December 1981, pp. 1713-1731.

36. Kaynia, A.M.,and E. Kausel, "Dynamic Behavior of Pile Groups," Proceedings, Second International Conference on Numerical Methods in Offshore Piling, I.C.E., April 1982.

37. Kuhlemeyer, R.L., "Vertical Vibration of Piles," Journal of the Geotechnical Engineering Division, A.S.C.E., Vol. 105, No. GT2, Feb. 1979, pp. 273-287.

38. Kuhlemeyer, R.L., "Static and Dynamic Laterally Loaded Floating Piles," Journal of the Geotechnical Engineering Division, A.S.C.E., Vol. 105, No. GT2, Feb. 1979, pp. 289-304.

39. Kuhlemeyer, R.L., "Dynamic Response Curves for Vertically Loaded Floating Pile Foundations," Canadian Geotechnical Journal, Vol. 18, 1981, pp. 300-312.

40. Liou, D.D., and J. Penzien, "Seismic Analysis of an Offshore Structure Supported on Pile Foundations," Report No. EERC 77-25, University of California at Berkeley, 1977.

41. Mahar, L.J., and M.W. O'Neill, "Field Study of Pile Group Action; Appendix C," Report No. FHWA/RD-81/005, Federal Highway Administration, March 1981.

42. Mahar, L.J., and M.W. O'Neill, "Geotechnical Characterization of Desiccated Clay," Journal of the Geotechnical Engineering Division, A.S.C.E., Vol. 108 (to appear), 1982.

43. Matlock, H., "Correlations for the Design of Laterally Loaded Piles in Soft Clay," Preprints, Second Offshore Technology Conference, Paper No. OTC 1204, 1970.

44. Matlock, H., S.H.C. Foo, and L.M. Bryant, "Simulation of Lateral Pile Behavior Under Earthquake Motion," Proceedings, A.S.C.E. Specialty Conference on Earthquake Engineering and Soil Dynamics, Vol. II, 1978, pp. 600-619.

45. Matlock, H., S.H.C. Foo, and L.C.C. Cheang, "Example of Soil-Pile Coupling Under Seismic Loading," Proceedings, Tenth Offshore Technology Conference, Vol. IV, 1978, pp. 2261-2269.

46. Maxwell, A.A., Z.B. Fry, and J.K. Poplin, "Vibratory Loading of Pile Foundations," Performance of Deep Foundations, A.S.T.M. STP 444 1969, pp. 338-361.

47. Nogami, T., "Dynamic Group Effect of Multiple Piles Under Vertical Vibration," Proceedings, Engineering Mechanics Specialty Conference, Austin, Texas, A.S.C.E., 1979, pp. 750-754.

48. Nogami, T., "Dynamic Stiffness and Damping of Pile Groups in Inhomogeneous Soil," Dynamic Response of Pile Foundations: Analytical Aspects, M.W. O'Neill and R. Dobry, Eds., A.S.C.E., Ootober 1980, pp. 31-52.

49. Nogami, T., and M. Novak, "Coefficient of Soil Reaction to Pile Vibration," Journal of the Geotechnical Engineering Division, A.S.C.E., Vol. 106, No. GT5, May 1980, pp. 565-570.

50. Novak, M., "Dynamic Stiffness and Damping of Piles," Canadian Geotechnical Journal, Vol. 11, 1974, pp. 574-598.

51. Novak, M., "Vertical Vibration of Floating Piles," Journal of the Engineering Mechanics Division, A.S.C.E., Vol. 103, No. EM1, Feb. 1977, pp. 153-168.

52. Novak, M., "Soil-Pile Interaction Under Dynamic Loads," Numerical Methods in Offshore Piling, I.C.E., 1980, pp. 59-68.

53. Novak, M., and F. Aboul-Ella, RIGDF: A Computer Program for Calculation of Response of Footings to Harmonic Loads; S.A.C.D.A., The Univeristy of Western Ontario, London, June 1978.

54. Novak, M., and F. Aboul-Ella, "Stiffness and Damping of Piles in Layered Media," Proceedings, A.S.C.E. Specialty Conference on Earthquake Engineering and Soil Dynamics, Vol. II, 1978, pp. 704-719.

55. Novak, M., and F. Aboul-Ella, PILAY: A Computer Program for Calculation of Stiffness and Damping of Piles in Layered Media, S.A.C.D.A., The University of Western Ontario, London, June 1979.

56. Novak, M., and Y.O. Beredugo, "Vertical Vibration of Embedded Footings," Journal of the Soil Mechanics and Foundations Division, A.S.C.E., Vol. 98, No. GT12, December 1972, pp. 1291-1310.

57. Novak, M., and R.F. Grigg, "Dynamic Experiments with Small Foundations," Canadian Geotechnical Journal, Vol. 13, 1976, pp. 372-385.

58. Novak, M., and J.F. Howell, "Torsional Vibration of Pile Foundations," Journal of the Geotechnical Engineering Division, A.S.C.E., Vol. 103, No. GT4, April 1977, pp. 271-286.

59. Novak, M., and J.F. Howell, "Dynamic Response of Pile Foundations in Torsion," Journal of the Geotechnical Engineering Division, A.S.C.E., Vol. 104, No. GT5, May 1978, pp. 535-552.

60. Novak, M., and M. Sheta, "Approximate Approach to Contact Effects of Piles," Dynamic Response of Pile Foundations: Analytical Aspects, M.W. O'Neill and R. Dobry, Eds., A.S.C.E., Oct. 1980, pp. 53-79.

61. Novak, M., and M. Sheta, "Dynamic Response of Piles and Pile Groups," Proceedings, Second International Conference on Numerical Methods in Offshore Piling, I.C.E., April 1982.

62. O'Neill, M.W., O.I. Ghazzaly, and H.B. Ha, "Analysis of Three-Dimensional Pile Groups with Nonlinear Soil Response and Pile-Soil-Pile Interaction," Proceedings, Ninth Offshore Technology Conference, Vol. II, 1977, pp. 245-256.

63. O'Neill, M.W., R.A. Hawkins, and L.J. Mahar, "Field Study of Pile Group Action," Report No. FHWA/RD-81/002, Federal Highway Administration, March 1981.

64. Oppenheim, A.V., and R.W. Shafer, Digital Signal Processing, Prentice-Hall, Inc., Englewood Cliffs, N.J., 1975.

65. Oweis, I.S., "Response of Piles to Vibratory Loads," Journal of the Geotechnical Engineering Division, A.S.C.E., Vol. 103, No. GT2, Feb. 1977, pp. 136-142.

66. Penzien, J., C.F. Scheffey, and R.A. Parmelee, "Seismic Analysis of Bridges on Long Piles," Journal of the Engineering Mechanics Division, A.S.C.E., Vol. 90, No. EM3, June 1964, pp. 223-254.

67. Petrovski, J., and D. Jurukovski, "Static and Dynamic Tests of Piles Under Horizontal Load," Proceedings, Fifth European Conference on Earthquake Engineering, Istanbul, Sep. 1975.

68. Poulos, H.G., and E.H. Davis, Pile Foundation Analysis and Design, John Wiley and Sons, New York, 1980.

69. Prakash, S., Soil Dynamics, McGraw-Hill, New York, 1981.

70. Prakash, S., and S.L. Aggawal, "Study of a Vertical Pile Under Dynamic Lateral Load," Proceedings, Third World Conference on Earthquake Engineering, Vol. I., 1965.

71. Prakash, S., and V. Chandrasekaran, "Analysis of Piles in Clay Against Earthquakes," Paper Presented Before A.S.C.E. Convention and Exposition, Portland, Oregon, Preprint No. 80-109, April 1980.

72. Prevost, J.H., and A.M. Abdel-Ghaffar, "Centrifugal Modeling of the Dynamic Response of Piles," Proceedings, Second International Conference on Numerical Methods in Offshore Piling, I.C.E., April 1982.

73. Prevost, J.H., J.D. Romano, A.H. Abdel-Ghaffar, and R. Rowland, "Dynamic Response of Laterally Loaded Piles in Centrifuge," Proceedings, Second Specially Conference on Dynamic Response of Structures: Experimentation, Observation, Prediction, and Control, A.S.C.E., Jan. 1981, pp. 386-400.

74. Richart, F.E., "Foundations for Dynamic Machine Loadings," Paper Presented to the American Concrete Institute, Houston, Tex., Oct. 1978, 50 pp.

75. Richart, F.E., Jr., and C.S. Chon, "Notes on Stiffness and Damping of Pile Systems," Specialty Session No. 10, Effects of Horizontal Loads on Piles Due to Surcharge or Seismic Effects," Ninth International Conference on Soil Mechanics and Foundation Engineering, 1977.

76. Richart, F.E., Jr., J.R. Hall, Jr., and R.D. Woods, Vibrations of Soils and Foundations, Prentice-Hall, Inc., Englewood Cliffs, N.J., 1970.

77. Richart, F.E., Jr., and R.D. Woods, "Foundations for Auto Shredders," Paper Presented to the American Concete Institute, Houston, Tex., Oct. 1978, 20 pp.

78. Rodriquez Ortiz, J.M., and J. Castanedo, "Dynamic Behavior of Piles in Nonlinear Stratified Soil," Proceedings, Ninth International Conference on Soil Mechanics and Foundation Engineering, Vol. 2, 1977, pp. 355-358.

79. Roesset, J.M., "Stiffness and Damping Coefficients of Foundations," Dynamic Response of Pile Foundations: Analytical Aspects, M. W. O'Neill and R. Dobry, Eds., A.S.C.E., Oct. 1980, pp. 1-30.

80. Roesset, J.M., and D. Angelides, "Dynamic Stiffness of Piles," Numerical Methods in Offshore Piling, I.C.E., 1980, pp. 75-81.

81. Ross, H.E., Jr., "Dynamic Response of Laterally Loaded Offshore Piling," Sea Grant Report 70-224, Texas A and M University, 1970.

82. Satter, M.A., "Dynamic Behavior of Partially Embedded Pile," Journal of the Geotechnical Engineering Division, A.S.C.E., Vol. 102, No. GT7, July 1976, pp. 775-785.

83. Saul, W.E., "Static and Dynamic Analysis of Pile Foundations," Journal of the Structural Division, A.S.C.E., Vol. 94, No. ST5, May 1968, pp. 1077-1100.

84. Scott, R.F., C-F Tsai, D. Steussy, and J.M. Ting, "Full-Scale Dynamic Lateral Pile Tests," Proceedings, Fourteenth Offshore Technology Conference, Vol. 1, 1982, pp. 435-450.

85. Seed, H.B., and I.M. Idriss, "Soil Moduli and Damping Factors for Dynamic Response Analyses," Report No. EERC 70-10, University of California at Berkeley, 1970.

86. Sheta, M., and M. Novak, "Vertical Vibration of Pile Groups," Journal of the Geotechnical Engineering Division, A.S.C.E., Vol. 108, No. GT4, April 1982, pp. 570-590.

87. Singh, J.P., N.C. Donovan, and A.C. Jobsis, "Design of Machine Foundations on Piles," Journal of the Geotechnical Engineering Division, A.S.C.E., Vol. 103, No. GT8, Aug. 1977, pp. 863-877.

88. Skipp, B.O., "Ground Vibration Instrumentation--A General Review," Instrumentation for Ground Vibration and Earthquakes, I.C.E., 1978, pp. 11-34.

89. Stevens, J. "Prediction of Pile Response to Vibratory Loads," Proceedings, Tenth Offshore Technology Conference, Vol. IV, 1978, pp. 2213-2223.

90. Stokoe, K.H., II, and P.F. Lodde, "Dynamic Response of San Francisco Bay Mud," Proceedings, A.S.C.E. Specialty Conference on Earthquake Engineering and Soil Dynamics, Vol. II, 1978, pp. 940-959.

91. Stokoe, K.H., II, and R.J. Hoar, "Field Measurement of Shear Wave Velocity By Crosshole and Downhole Seismic Methods," Dynamical Methods in Soil and Rock Mechanics, 3, Rock Dynamics and Geophysical Aspects, Ed. by G.W. Borm, Balkema, Rotterdam, 1978, pp. 115-137.

92. Tschebotarioff, G.P., and E.R. Ward "The Resonance of Machine Foundations and the Soil Coefficients Which Affect It., Proceedings, Second International Conference on Soil Mechanics and Foundation Engineering, Vol. I, 1948, pp. 309-313.

93. Tucker, R.L., "Lateral Analysis of Piles with Dynamic Behavior," Proceedings, Conference on Deep Foundations, Mexican Society of Soil Mechanics, Mexico City, Vol. I, 1964, pp. 156-167.

94. Ueda, S., and S. Shirashi, "Observation and Analysis of Earthquake Response of a Coupled Pile Offshore Platform," Proceedings, Fourteenth Offshore Technology Conference, Vol. 1, 1982, pp. 511-531.

95. Valeria, J., and C. Oteo, "Dynamic Behavior of a Group of Free-Standing Piles," Soils Under Cyclic and Transient Loading, Ed. by G.N. Pande and O.C. Zienkiewicz, II, Balkema, Rotterdam, 1980, pp. 627-638.

96. Veletsos, A.S., and V.V.D. Nair, "Torsional Vibration of Viscoelastic Foundations," Journal of the Geotechnical Engineering Division, A.S.C.E., Vol. 100, No. GT3, March 1974, pp. 225-246.

97. Veletsos, A.S., and Y.T. Wei, "Lateral and Rocking Vibration of Footings," Journal of the Soil Mechanics and Foundations Division, A.S.C.E., Vol. 97, No. SM9, Sep. 1971, pp. 1227-1248.

98. Waas, G., and H.G. Hartmann, "Pile Foundations Subjected to Dynamic Horizontal Loads," Symposium on Modeling and Simulation of Large-Scale Structural Systems, Capri, Italy, Sep. 1981, 17 pp.

99. Whitman, R.V., "Analysis of Soil-Structure Interaction: A State-of-the-Art Review," Soils Publication No. 300, Massachussets Institute of Technology, April 1972, 19 pp.

100. Wolf, J.P., "Dynamic Stiffness of Group of Battered Piles," Journal of the Geotechnical Engineering Division, A.S.C.E., Vol. 106, No. GT2, Feb. 1980, pp. 198-202.

101. Wolf, J.P., and G.A. Von Arx, "Impedance Function of a Group of Vertical Piles," Proceedings, A.S.C.E. Specialty Conference on Earthquake Engineering and Soil Dynamics, Vol. II, 1978, pp. 1024-1041.

102. Wu, T.H., Soil Dynamics, Allyn and Bacon, Inc., Boston, 1971.

APPENDIX B

NOTATION

A	=	Projected lateral area of a pile element;
AE	=	Product of cross-sectional area and Young's modulus of pile;
a-d	=	Coefficients defined in Eq. (6-1);
a-f	=	Coefficients defined in Eq. (6-2);
a_o	=	Dimensionless frequency;
b	=	Pile diameter;
C^e	=	External dashpot coefficient (general);
C_G	=	Group damping;
CG	=	Center of mass;
CU	=	Consolidated - undrained test;
c	=	Cohesion;
c	=	Damping constant;
D	=	Pile diameter, damping ratio;
D^e	=	External dashpot coefficient (SPASM);
D_h	=	Hysteretic damping;
D^i	=	Internal dashpot coefficient (SPASM);
D_m	=	Material damping;
DE	=	External dashpot coefficient (DRIVE);
DI	=	Internal dashpot coefficient (DRIVE);
d	=	Depth;
E_s	=	Young's modulus of soil;
E_p	=	Young's modulus of pile;
F	=	Force;
F_A	=	Applied axial force;

F_{AN} = Nominal axial applied force;

F_L = Applied lateral force;

F_{LN} = Nominal lateral applied force;

F_o = Force applied to pile head in Eq. (2-4);

F_W = Axial force;

F_{WS} = Axial force at ground level;

F_{VS} = Axial force at ground level;

f = Frequency; Unit side resistance;

f_n = Natural frequency;

f_{nr} = Reduced natural frequency defined by Eq. (2-2);

f_r = Resonant frequency;

G = Group designator;

G_o = Shear modulus of soil;

g = Acceleration due to gravity;

$H_n^{(m)}( )$ = Hankel function of kind M and order n;

h = Increment length;

h_t = Time increment;

I = Moment of inertia;

I_δ = Dynamic interaction factor;

i,j = Finite node or pile indicators;

$J_o(a_o)$ = Bessel function of first kind, order zero;

$J_1(a_o)$ = Bessel function of first kind, order one;

K_o = Coefficient of earth pressure at rest;

K^* = Complex stiffness;

k = Stiffness; Time station designator;

k_G = Group stiffness;

k_i = Imaginary component of stiffness;

k_r = Real component of stiffness;

k_1 = Stiffness of embedded protion of pile;

k_2 = Stiffness of freestanding portion of pile;

L = Pile length;

M = Lumped mass (DRIVE, SPASM);

m = Structural mass vibrating in phase;

N = Number of piles;

OCR = Overconsolidation ratio;

P_o = Amplitude of (magnified) dynamic force;

p = Equivalent contact pressure; Lateral soil reaction per unit length of pile;

Q = End-bearing load; Soil reaction force;

R = Rotational restraint (SPASM);

r_p = Radius of pile;

S = Soil spring support;

SP = Single pile designator;

T = Axial thrust (SPASM);

t = Time; Stratum thickness;

u = Lateral deflection;

ub = U-direction, base of cap (subscript);

uo = U-direction, CG of cap (subscript);

UU = Unconsolidated-undrained test;

uu = Response in lateral direction to lateral loading (subscript);

v_s = Shear wave velocity;

W = Element weight;

w = Axial displacement;

W_s = Weight of vibrating mass, piles and pile cap;

W_v = Weight of soil vibrating in phase with piles;

wb = W-direction, cap base (subscript);

ws = W-direction, soil surface (subscript);

ww = Response in axial direction to axial loading (subscript);

x = Depth in Eq. (6-12);

x_r = Depth to plane strain failure;

$Y_o(a_o)$ = Bessel function of second kind, order zero;

$Y_1(a_o)$ = Bessel function of second kind, order one;

y = Lateral deflection;

z = Depth; Relative pile-soil movement;

z_a = Distance (vertical) from CG to cap accelerometer;

z_c = Distance (vertical) from base of cap to CG;

α = Interaction factor;

γ = Unit weight; Shear strain amplitude;

δ = Deflection;

$\tilde{\delta}$ = Stiffness factor;

ε_{50} = Major principal strain at one-half peak principal stress difference;

μ^G = Impedance function (general term);

ν_s = Poisson's ratio of soil;

$\tilde{\rho}$ = Mass per unit length of pile;

ρ_p = Pile mass density;

ρ_s = Soil mass density;

ψ^u = Response in rotation due to lateral load or vice-versa (subscript);

$\psi\psi$ = Response in rotation due to rotational load (subscript);

ω = Circular frequency;

$\bar{}$ (overbar) = Effective stress condition.